# SEISMIC DAMAGE AVOIDANCE DESIGN OF WAREHOUSE BUILDINGS CONSTRUCTED USING PRECAST HOLLOW CORE PANELS

---

A thesis submitted in partial fulfilment of the
requirements for the Degree
of Doctor of Philosophy in Civil Engineering
in the University of Canterbury
by N.H. Abdul Hamid

**University of Canterbury**

**2006**

---

# ABSTRACT

Precast prestressed hollow core units are commonly used in the construction of the flooring system in precast buildings. These units without transverse reinforcement bars are designed to resist seismic loading as replacement for fixed-base precast wall panels in the construction of warehouse buildings. Thus, this research seeks to investigate the seismic performance of the units constructed as a subassemblage (single wall) subjected to biaxial loading and as a superassemblage (multi-panel) subjected to quasi-static lateral loading. A design procedure for warehouse building using precast hollow core walls under Damage Avoidance Design (DAD) is proposed. In addition, a risk assessment under Performance-Based Earthquake Engineering (PBEE) is evaluated using the latest computational tool known as Incremental Dynamic Analysis (IDA). A comparative risk assessment between precast hollow core walls and fixed-base monolithic precast wall panels is also performed.

Experimental results demonstrate that rocking precast hollow core walls with steel-armouring do not suffer any non-structural damage up to 2.0% drift and minor structural damage at 4.0% drift. Results revealed that the wall with unbonded fuse-bars and 50% initial prestressing of unbonded tendons performed the best compared with other types of energy dissipators. Furthermore, 12mm diameter of fuse-bar is recommended as there is no uplifting of the foundation beam during ground shaking. Hence, this type of energy dissipator is used for the construction of seismic wall panels in warehouse buildings.

One of the significant findings is that the capacity reduction factor $(\phi)$ which relates to global uncertainty of seismic performance is approximately equal to 0.6. This value can be used to estimate the $90^{th}$ percentile of the structures without performing IDA. Therefore, the structural engineers are only required to compute Rapid-IDA curve along with the proposed design procedure.

# ACKNOWLEDGEMENTS

First and foremost, I thank God for giving me blessings, strength and the perseverance to complete my study. This research would neither have been started, nor completed without the generous support from the MARA University of Technology (UiTM) who awarded a scholarship as well as allowing me to pursue doctoral study at the University of Canterbury, Christchurch, New Zealand.

My sincere appreciation and thanks goes to my supervisor Professor J.B. Mander. Being a student of Professor Mander for the past four years has been most instrumental in the progress of my doctoral studies and he helped in developing my professional interests and research skills. With his guidance and ungrudging generosity with time and resources I was able to complete this thesis of which I feel proud. He is nurturing and demanding, a “bipolar" quality I will adopt in my academic career as a faculty member and advisor in the Department of Civil Engineering, MARA University of Technology. Similarly, a special thank you goes to Dr. Stefano Pampanin for his advice, comments and suggestions particularly at the initial stage of shaping this research.

I further gratefully acknowledge the assistance of the technicians, academic staffs and colleagues of the Civil Engineering Department, University of Canterbury who have made tremendous efforts during the experimental work. Thanks particularly go to the following individuals:

| | | |
|---|---|---|
| Mr. Nigel Dixon | Mr. John Chaby | Asmalini |
| Mr. Russell | Mr. Stuart | Nastein |
| Mr. Alan Pointer | Hamdan | Lionel Liyanage |
| Assoc. Prof. Dr. Athol Carr | Mr. Kevin | Iwan Surdano |

I also wish to thank my parents and immediate family for their influence in shaping my educational goals and their moral support. Finally, I deeply thank my husband, Dr. Salehuddin for all his support, prayers, patience, love and encouragement. To my children, Myra, Irfan and Nouha, mama acknowledges your love, joy and trusts that you will each take home something good from the Kiwi experience.

# TABLE OF CONTENTS

# LIST OF TABLES

# LIST OF FIGURES

# LIST OF SYMBOLS

| | |
|---|---|
| $a$ | coefficient of non-linear time history analyses |
| $\sum A_f$ | summation of area for fuse-bars |
| $\sum A_p$ | summation of area for unbonded tendons |
| $A$ | cross-sectional area of rubber block |
| $A_i$ | median spectral acceleration to cause the $i^{th}$ damage state to occur |
| $A_g$ | gross bottom cross-section of the wall |
| $B_a$ | reduction damping factor for constant acceleration |
| $B_d$ | reduction damping factor for constant displacement |
| $B_v$ | reduction damping factor for constant velocity |
| $B_r$ | in-plane contact base width of compressed concrete (immediately above any steel armouring) |
| $b_w$ | wall thickness |
| $B$ | wall width |
| $C_c$ | base shear capacity |
| $C_d$ | seismic demand spectrum |
| $C_c^{DBE}$ | base shear capacity under Design Basis Earthquake |
| $C_c^{MCE}$ | base shear capacity under Maximum Considered Earthquake |
| $\hat{D}$ | median drift demand |
| $DBE$ | Design Basis Earthquake |
| $DS$ | Damage State |
| $e_p$ | eccentricity between unbonded post-tensioned tendons |
| $e$ | eccentricity underneath foundation beam |
| $E_c$ | Young's modulus of concrete |
| $E_h$ | absorbed hysteretic energy observed during experiment |
| $E_{EPP}$ | energy dissipated using theoretical elasto-perfectly plastic system |

| | |
|---|---|
| $E_D$ | theoretical cyclic pushover curve area under flag-shape loops |
| $E_p$ | potential energy |
| $E_{sp}$ | Young's Modulus for unbonded tendons |
| $E_s$ | Young's modulus of steel |
| $E_{SO}$ | average energy absorption |
| $E_s^{'}$ | secant Young's modulus of steel |
| $E_{sd}$ | Young's modulus of energy dissipator |
| $F$ | in-plane lateral force |
| $F_{pad}$ | lateral force on rubber block |
| $F_{sealant}$ | lateral force on the silicone sealant |
| $F_y$ | yield force of the bar |
| $F_{out}$ | out-of-plane lateral force |
| $F_H$ | total lateral force applied at eaves level |
| $F_{sw}$ | resistance provided by post-tensioned seismic wall and energy dissipator |
| $F_{NS}$ | resistance arising from self-weight non-seismic walls |
| $F_V$ | shear resistance from sealant |
| $F_{CH}$ | contribution of plastic mechanism of steel channel |
| $F_{\max}$ | average maximum strength in forward and reverse direction |
| $F_1$ | lateral load at Point 1 |
| $F_2$ | lateral load at Point 2 |
| $F_3$ | lateral load at Point 3 |
| $F_4$ | lateral load at Point 4 |
| $F_5$ | lateral load at Point 5 |
| $F_{out}$ | out-of-plane displacement |
| $f_y$ | yield strength of reinforcement bar |
| $F_{ydis}$ | energy dissipator force depending on cross-section and yield strength |

| | |
|---|---|
| $F_a$ | adjustment on spectral acceleration for short period at different site |
| $f_b$ | base flexibility |
| $f_g$ | full gross flexibility |
| $f_c$ | maximum concrete compressive stress |
| $f_c^{'}$ | characteristic strength of concrete |
| $f_{su}$ | fuse-bars ultimate strength |
| $G$ | shear modulus of rubber pad |
| $g$ | gravitational acceleration |
| $H$ | wall height |
| $H_{eff}$ | effective height of wall |
| $I_g$ | gross moment of inertia |
| $I_{re}$ | reduce moment of inertia |
| $I_o$ | moment of inertia for rigid block |
| $I_t$ | moment of inertia for top block |
| $I_{eff}$ | effective moment of inertia |
| $K_p$ | the stiffness of unbonded tendons |
| $K_{ed}$ | stiffness of energy dissipator |
| $K_{ed}^{'}$ | stiffness of energy dissipator at strain-hardening region |
| $K$ | slope of IDA curve in the initial proportional range |
| $L_p$ | length of unbonded tendons |
| $L_f$ | length of fuse-bars |
| $L_s$ | total length of strip footing |
| $M_p$ | plastic capacity of reduced channel section |
| $M_{rpad}$ | moment resistance provided by rubber block |
| $M_{rsealant}$ | moment resistance provided by silicone sealant |
| $M$ | maximum moment at the base of the wall |
| $MCE$ | Maximum Considered Earthquake |

| | |
|---|---|
| $m$ | mass of rigid body |
| $m_{eff}$ | effective mass of rigid block |
| $m_r$ | mass of top block |
| $m_w$ | mass of wall panel |
| $\eta$ | energy absorption efficiency factor |
| $n_j$ | number of vertical joints containing sealant |
| $n_s$ | number of seismic walls |
| $n_{ns}$ | number of non-seismic walls |
| $p_a$ | annual frequency |
| $P$ | total compression forces |
| $P_p$ | prestressing unbonded tendons |
| $P_{py}$ | forces in unbonded tendons when they are yielded |
| $P_o$ | initial prestressing of unbonded tendons |
| $P_d$ | fuse-bar force |
| $P_d^{'}$ | ultimate force in fuse-bars |
| $q$ | an exponent based on local seismic hazard-recurrence relations |
| $r$ | kinetic energy ratio after and before impact |
| $R$ | distance from the pivot point to the center of gravity |
| $S_s$ | spectral acceleration at short period |
| $S_1$ | spectral acceleration at one-second period |
| $S_{PGA}$ | spectral peak ground acceleration |
| $S_{dv}$ | spectral displacement within medium period |
| $S_{da}$ | spectral displacement at short period |
| $S_{dd}$ | spectral displacement at long period |
| $S_{PGA}^{(T=Tr)}$ | PGA relevant to its return period |
| $S_{PGA}^{(T=475)}$ | PGA at a return period of 475 years |
| $S_c$ | “critical” earthquake acceleration |

| | |
|---|---|
| $S_a$ | the spectral amplitude (for a period of $T = 1\text{sec}$) |
| $S_{PGA,90\%}$ | peak ground acceleration which captures 90% of possible outcomes |
| $t_{gap}$ | thickness gap between wall panels |
| $t_s$ | total (through wall) sealant thickness in on vertical joint |
| $T$ | total tension forces provided by prestress and energy dissipator |
| $T$ | effective (second) period vibration |
| $T_1$ | axial force in tendon 1 |
| $T_2$ | axial force in tendon 2 |
| $T_a$ | time for acceleration |
| $T_d$ | period at junction of constant spectral acceleration |
| $T_v$ | time for velocity |
| $T_r$ | return period |
| $V$ | vertical shearing force on rubber spacer block |
| $V_r$ | total shear resistance in rubber spacer block and sealant |
| $V_{dis}$ | base shear contribution from energy dissipators |
| $W_e$ | effective seismic weight from roof and wall panel |
| $W_r$ | gravity load from roof |
| $W_w$ | self-weight of wall panels |
| $W_s$ | structural seismic weight |
| $W_f$ | weight of foundation in strip footing |
| $X$ | in-plane drift (E-W direction) |
| $Y$ | out-of-plane drift (N-S direction) |
| $\gamma$ | shear strain in rubber spacer block |
| $\theta$ | phase angle |
| $\theta_c$ | "critical" drift |
| $\theta_{out}$ | out-of-plane drift |
| $\dot{\theta}_1$ | velocity before impact |
| $\dot{\theta}_2$ | velocity after impact |
| $r$ | constant related to the curvature of the R-O curve |
| $\Phi$ | standard log-normal cumulative distribution function |

| | |
|---|---|
| $\beta_C$ | coefficient of variation for the capacity |
| $\beta_D$ | coefficient of variation for the seismic demand |
| $\beta_{C/D}$ | normalized composite log-normal standard |
| $\beta_U$ | lognormal dispersion parameter for modelling uncertainty |
| $\phi$ | reduction f actor that can be calibrated against the IDA results |
| $\phi_t$ | total curvature at the base of the wall |
| $\phi_e$ | elastic curvature |
| $\phi_i$ | inelastic curvature |
| $\phi_{PGA,n}$ | reduction factor that can be calibrated against the IDA results |
| $\Delta_t$ | total displacement (elastic and plastic) |
| $\Delta_e$ | elastic displacement |
| $\Delta_i$ | inelastic displacement |
| $\Delta_1$ | displacement at Point 1 |
| $\Delta_2$ | displacement at Point 2 |
| $\Delta_3$ | displacement at Point 3 |
| $\Delta_4$ | displacement at Point 4 |
| $\Delta_5$ | displacement at Point 5 |
| $\Delta_{\max}$ | maximum displacement |
| $\Delta_{out}$ | out-of-plane lateral displacement |
| $\Delta_y$ | yield displacement |
| $\Delta$ | peak response displacement |
| $\Delta_{\max}^{DBE}$ | maximum response displacement for DBE |
| $\Delta_{\max}^{MCE}$ | maximum response displacement for MCE |
| $\xi$ | percentage effective viscous damping factor |
| $\xi_{eff}$ | total effective viscous damping |
| $\xi_{eq}$ | equivalent viscous damping |

| | |
|---|---|
| $\xi_{inst}$ | intrinsic damping |
| $\xi_{i\,rock}$ | energy radiated into half-space on one impact |
| $\xi_{hyst}$ | hysteretic damping of energy dissipator |
| $\zeta_i$ | the location of the $i^{th}$ energy dissipator with respect to pivot point |
| $\delta_h$ | uplift displacement |
| $\delta_i^{uplift}$ | uplift displacement at bottom of the wall |
| $\delta E$ | dissipated/radiated energy |
| $\sum_{i=1}^{N} \zeta_i$ | fraction width |
| $\zeta_i B$ | the location of the $i^{th}$ energy dissipators with respect to pivot point |
| $\eta$ | energy absorption efficiency factor |
| $\alpha$ | post-elastic to initial stiffness ratio |
| $\mu$ | structural displacement ductility factor |
| $\lambda_o$ | displacement amplification factor |
| $\lambda_T$ | annual frequency-dependent scale factor |
| $\varepsilon_{su}$ | fuse-bars ultimate strain |
| $\varepsilon_y$ | fuse-bars yield strain |

# CHAPTER 1

# INTRODUCTION AND LITERATURE REVIEW

## 1.1 PERFORMANCE OF PRECAST INDUSTRIAL BUILDINGS DURING PAST EARTHQUAKES

In a major earthquake event, a performance objective for the industrial/warehouse facilities is to ensure life-safety and continuing business operation after strong ground shaking. The structural components of these buildings must satisfy serviceability limit and ultimate limit requirements. Widespread damage and post-earthquake operational problems which have been observed in recent earthquakes are due to inadequate detailing and poor workmanship. Massive damage to industrial facilities demonstrates that current design standards require some improvement in terms of design approach and design philosophy. A Damage Avoidance Design (DAD) philosophy is one of the approaches whereby better performance objectives can be achieved without structural damage to the constructed industrial facilities. Such a conceptual design approach was proposed by Mander and Cheng (1997) for bridge substructures in which rocking columns form the seismic resistance mechanism. Aspects of structural flexibility and prestressed unbonded tendons were also incorporated into the pier design. This research seeks to adopt this approach for industrial/warehouse facilities.

Two major earthquakes struck Taiwan and Turkey in 1999, namely the M7.6, Chi-Chi and M7.4 Kocaeli, respectively. These events had a major impact with severe economic and insured losses for both countries. The industrial area with high-tech facilities such as the Science Based Industrial Park, Hsinchu which located 110km from the epicentre had a major business interruption following this earthquake. The earthquake had an impact

on high-tech facilities that were a crucial part of the supply chain to the worldwide computer manufacturing industries. Business interruption costing between US$50 million and US$100 million per day in these facilities had repercussions for major computer companies in the US Silicon Valley and elsewhere in the world. The total economic losses during the 1999 Chi-Chi earthquake were estimated to be up to US$14 billion (5% of Taiwan's GDP) while insured losses were US$850 million. In the Kocaeli Earthquake, the economic losses were estimated as US$40 billion while insured losses were US$750 million (Johnson, 2000). Forty percent of heavy industries which were located close to the North Anatolian fault (Turkey) were badly damaged and required major retrofitting. Even though most of the industrial facilities around this region were designed according to U.S or European seismic standards, there was still a great deal of damage to the industrial buildings. The extensive damage to the industrial facilities had a substantial impact on social and economic well being within the most affected region in terms of direct and indirect losses. The direct losses included the structural and non-structural damage, whilst the indirect losses included business interruption and economic losses. The 1999 Chi-Chi earthquake and the 1999 Kocaeli earthquake affected both the Turkish and Taiwanese economies.

## 1.2 FAILURES OF TILT-UP PRECAST WALL PANELS

Tilt-up construction is the most common technique used in precast jointed wall panels and was developed in the United States of America from 1908. It has been widely implemented in the construction of residential houses, commercial/office buildings, industrial/warehouse facilities, recreation centres, gymnasiums and community halls in New Zealand since the 1950s (CCANZ, 1990). Most of the tilt-up wall panels have the

potential to carry roof loading without using any intermediate columns. If the walls are squat (generally when the height is less than about 150% of the panel width) significant transverse shear reinforcement is required to resist horizontal shears arising from seismic and wind loading.

Historically, tilt-up buildings have been amongst the most vulnerable types of structures under earthquake excitation due to lack of attention in providing adequate detailing at connections, structural integrity and poor workmanship. The first major destructive earthquake on tilt-up buildings was in 1964 when the Alaska Earthquake with M9.2 and three minutes duration of shock caused several casualties, such as the collapse of tilt-up buildings at Elmendorf Air Force Base, Anchorage, Alaska (Berg and Stratta, 1964).This was followed by the San Fernando earthquake with M6.6 which struck on February 9, 1971 for 10 seconds close to the fault line, causing severe damage to precast tilt-up buildings. Quite a number of precast wall panels and roofs of industrial facilities collapsed. Figure 1(a) shows the partial collapse of wall panels at the Vector Electronics Building, San Fernando, California, due to stability losses and connection problems. The reaction forces which came from the ground shaking caused some parts of the precast wall panels to pull away from the roofs, and subsequently led to the partial collapse of this building (Murphy, 1973).

Figure 1.1(b) shows the partial collapse of the roofs in the industrial buildings due to lack of resistance in the connectors between wall panels and rafters. The seismic forces pulling away the edges of the plywood and glulam beam resulted in partial collapse of the tilt-up building's roof. When precast wall panels moved away from the roof, the glulam beam fell from its seat, allowing a single bay of the roof to collapse. A partial

collapse of the roof panel was also due to a poor connection between the precast wall panels and the glulam beam below the roof panels (James and Neil, 1994).

Figure 1.1 (c) depicts the crack at the top corner of the precast wall panel between two openings in the industrial buildings. The out-of-plane inertia loads came from the ground shaking pushed the wall panels causing severe bowing at the mid-height of the wall and cracks between openings of the walls. The horizontal crack at the top of the opening is due to the movement of splices, and steel bracings are required to support the wall bracing before retrofitting takes place (Wyllie and Filson, 1989).

Figure 1.1(d) demonstrates the failure of shear connectors between two perpendicular wall panels due to inadequate provision in transferring seismic shear forces using the modern "dry" panel joint connectors. This type of connection is incapable of transmitting substantial shear loads between wall panels (Hamburger et al., 1988).

Figure 1.2(a) shows the failure of a construction joint between precast wall panels and the bottom of precast beams in parking garages during the 1994 Northridge earthquake in California (Iverson and Hawkins, 1994). Severe cracks and spalling of concrete were observed on the precast shear wall and beam on the second floor of the parking garage. The construction joint in the wall immediately above this level had slipped and the connection between floors slabs and wall panels failed. Parking garages with large plan areas constructed using precast hollow core slabs did not perform as well as precast wall panels where the failure of construction joints occurred between the wall-beam, slab-beam and wall-wall interfaces. Other extensive damage was also observed in three major applications of precast concrete structural components such as commercial buildings,

applications of precast concrete structural components such as commercial buildings, warehouse/industrial buildings and foundations for multi-family residential houses.

Figure 1.2(b) shows the partial collapse of three agricultural warehouses at Arifiye during the 1999 Kocaeli earthquake. These buildings were made from precast wall panels and precast beams. The partial collapse of roofs, precast walls panels and frames is due to the failure of the connections between precast components in wall-wall and wall-foundation beam, insufficient seating and anchorage lengths of roof beams on precast wall panels and the formation of plastic hinges in precast wall panels (Krinitzsky et al., 2000). Other heavy industry facilities such as petrochemical industries, automotive industries, power generation plants and transmission systems also had extensive damage which took a few months to repair. Twenty-four industrial facilities which represented various industries within this region were visited after the earthquake. Fifty percent of these industrial facilities had major structural damage and two of them had totally collapsed. Eleven of them had major non-structural damage and were non-operational for several months (Sezen and Whittaker, 2004).

The collapse of precast concrete industrial facilities under construction was also observed during the 1999 Kocaeli earthquake as shown in Figure 1.2(c) (Saatcioglu et al., 2001). The failure of the cantilever headed connection on the top of columns was due to inadequate provision for shear connectors under seismic loading. Furthermore, this building under construction collapsed because it did not have enough props and bracings to resist lateral loading which came from earthquake excitation. Moreover, the current seismic design code did not have any provisions for buildings under construction when an earthquake strikes.

Figure 1.2 (d) shows an example of the total collapse of a primary school made from precast wall panels and frames at the Kukma Primary School, Bhuj, India during a disastrous earthquake which occurred on January 26, 2001 with M7.7 (Ghosh, 2001). It was reported that nearly one third of 318 schools made from precast wall panels totally collapsed. Poor quality workmanship, inadequate connections between walls and beams, floors to beams and roof panels to columns, insufficient seating and anchorage leading to dislodgement of top precast panels to roof trusses were several factors causing the failures. The precast wall panels collapsed due to lack of structural stability when the monolithic connection between wall and foundation ruptured and there were no extruded reinforcement bars connecting the top and bottom of the walls. Other examples of total collapse and severe damage to industrial facilities during the 1999 Kocaeli earthquake (Turkey) and the 1999 Chi-Chi earthquake (Taiwan) are shown in Appendix A1.

## 1.3 RESEARCH MOTIVATION

The construction of industrial/warehouse buildings using precast hollow core wall panels is very appealing because the units can be manufactured at low cost under factory controlled conditions. From a seismic design standpoint, the biggest challenge is to construct wall units without the need for transverse reinforcement. Precast hollow core walls with a conventional fixed base and normal longitudinal prestressing strands could not withstand seismic lateral loads without any modification of their connections. By using the principles of rocking structures and damage avoidance design, the formation of plastic hinges in a conventional way can be eliminated.

Based on the above description of the failures and visual observation of the extensive damage to tilt-up precast wall panels and precast concrete buildings, it is clear that there are some gaps in knowledge that need to be explored. The gaps are to improve the connection details and develop a new construction technology which is highly earthquake resistant by utilizing new materials in the construction of industrial facilities. In addition, a new conceptual design approach for tilt-up precast wall panels must meet modern requirements for advanced seismic performance objectives. The diverse usage of precast hollow core units from the flooring system to the wall system which offers a good opportunity to redeploy such a product in the wall systems in seismic regions is a new idea. However, it is expected that builders, developers, designers and engineers may be skeptical about its applicability, due to the non-existence of transverse reinforcement in hollow core units. This research is concerned with the viability of a system that can accommodate a significant level of lateral drift without any damage to the walls. As it is customary to provide transverse (shear) reinforcement in precast wall units, most engineers may consider it to be inconceivable that precast hollow core units that are longitudinally prestressed, but have no transverse shear reinforcement, could be used as seismic resisting wall units. The challenge, therefore, is to engineer such a system that will work.

## 1.4 THE ADVANTAGES OF USING PRECAST HOLLOW CORE WALLS

Precast hollow core units are produced in a long steel pallet by an extrusion process using an “extruder” machine with zero-slump concrete. These units are cut to the required length from the long strip of hardened concrete seats on a steel bed using a diamond

blade cutter. Hollow core panels are typically either 1200mm or 2400mm wide, with a thickness that varies between 150 and 400mm. The voided cores vary depending on the shape of the mould in the extruder machine. Good quality control and quality assurance during materials testing, production, curing, storing, lifting, transportation and erection on the construction site are properly monitored. Therefore, the usage of precast hollow core units is rapidly increasing in the construction of precast buildings around the world. The beneficial uses of high strength concrete (up to 70MPa), include reducing the construction period and other cost savings. In addition, there are several advantages of using this product which are (Lee and Sooi, 2003):

(a) The preparation of precast hollow units together with the foundation beam in plants away from the construction site and delivery to the site when required will make the site environment clean and safe.

(b) Hollow core panels can easily be placed in frigid climates that do not permit winter site casting of the concrete; the construction of buildings is not affected by weather conditions.

(c) Only a small three-person erection crew is needed to install 500 $m^2$ per day without using formwork, scaffolding and temporary props.

(d) The large hollow section inside precast hollow core walls could be used for services such as plumbing, drain pipes, internal electrical services, and the thin layer between the voids and the surface can be drilled for ventilator installation, cabling, plugs and other electrical appliance purposes.

(e) By inserting an insulation material into the voids, improved R-values can be obtained compared to solid concrete walls. This also leads to improved fire resistance and sound transmission qualities.

(f) A variety of wall finishes can be adopted such as cast (plain) finish, raked finish, tiled finish, ribbed finish, and exposed aggregate finish.

Having briefly outlined the advantages of using precast hollow core wall panels, it is therefore the intent of this research to design, construct and test this product at full scale in the laboratory, so that the outcomes are applicable to the seismic environment with minimal damage to the structures. Concept development together with a proposed design procedure, construction testing and modelling of a single seismic wall using different types of energy dissipators and multi-panel walls will be presented accordingly.

## 1.5 LITERATURE REVIEW AND THE STATE-OF-THE-ART

Several major themes pertaining to precast concrete buildings will be reviewed in this section. The first theme is related to the physical behaviour of structures such as rocking structures, rocking structures and prestressed unbonded post-tensioned systems, unbonded post-tensioned tendons in precast wall panels and rocking structures by incorporating damage avoidance design (DAD) principles. The second theme is associated with seismic design procedures. This includes a direct displacement based design, equivalent viscous damping and damping reduction factor for seismic response analysis. The third theme is regarding Performance Based Seismic Engineering (PBEE) which is included in current codes of practices both at the international level and New Zealand. By and large, these themes are applicable in developing the conceptual design stage, constructing the specimens, analyzing the experimental results, analytical modeling and risk assessment of the warehouse buildings under different earthquake motions.

### 1.5.1 ROCKING STRUCTURES

Rocking structures are not a new phenomenon. An early study by Housner (1963) defined the conceptual behaviour of a rigid rocking body under ground motion excitation. This was further investigated by Meek (1978) who considered the aspects of structural flexibility coupled with rocking structures. Yim et al. (1980) found that the response of rigid blocks is very sensitive to small changes in the sizes and slenderness ratio under horizontal and vertical ground motion. Using the rocking concept of rigid body, Priestley et al. (1978) and McManus et al. (1980) examined the seismic response of bridge structures which allowed them to rock freely on foundations beams. Similar results were found in both studies which signified that the rubber pad placed under bridge structures had no effect on the rocking period. Nevertheless, the rubber pad significantly increased the rate of decay in kinetic energy. In supporting those studies, Psycharis and Jenning (1983) suggested that the rocking of slender rigid bodies experienced uplift based on the type of connection between the base of the structure and the foundation. They revealed that there is an amplitude dependent variable rocking period for structures which contributes to energy dissipation. The radiation damping due to rocking impacts can be conceived as equivalent viscous damping which will be discussed in the following theme.

Several researchers further investigated the response and rocking mechanism of a rectangular rigid body subjected to different directions and frequency of ground motion (Shenton and Jones, 1991; Shenton, 1996; Lin and Yim, 1996; Pompei et al., 1998; Lu et al., 2001; Taniguchi, 2002; and Taniguchi and Miwa, 2006). As such, Shenton and Jones (1991) and Shenton (1996) classified the response of the rigid body under horizon-

tal and vertical ground motion into five modes namely rest, slide, rock, slide-rock and free flight. The criteria in determining the initiation of a slide, a rock and a slide-rock mode of a rigid block were derived. In addition, the finite angular acceleration occurred when the block started to rock and experienced rock and slide-rock mode. In order to avoid slide-rock mode, Pompei et al., (1998) suggested that the horizontal and vertical reaction forces must be included in the criteria. However, their investigations neglected the effect of vertical ground motion which has a significant influence on responses and criteria as revealed by Taniguchi (2002). Taniguchi proved that vertical accelerations cause lift-off, slip and lift-off-slip interaction between the rigid block and the foundation. Taniguchi and Miwa (2006) further proposed a simple procedure in determining slip displacement of a freestanding rigid body using horizontal sinusoidal acceleration.

By looking at whether interface material between the rigid block and the foundation beam has a significant effect on the coefficients of restitution $(r)$, Elgawady et al. (2005) conducted the experimental work on a rocking rigid body using a reinforced concrete base and a rubber base as the interface materials. They revealed that a rubber base has a lower coefficient of restitution as compared to a reinforced concrete base. The aspect ratio of 3 and 5 of rigid blocks were used in their experimental work. Using ten rigid blocks in their later study, Elgawady et al. (2006) discovered that a reinforced concrete base has the highest value of coefficient restitution $(r)$, followed by timber, steel and rubber. Therefore, it can be concluded that rubber pads and steel channels are used as interface materials in reducing the damage of the structure. These materials were used in this research to dissipate more energy and protect the bottom part of the wall panel from damage during ground shaking.

To date, there are only a few cases of built applications of rocking structures. For example, this concept has been implemented in the construction of a chimney at Christchurch International Airport (Skinner et al.,1983) and the South Rangitikei Rail Bridge (Cormack, 1988), both in New Zealand.

### 1.5.2 ROCKING STRUCTURES AND PRESTRESSED UNBONDED TENDONS

Rocking structures often require a supplementary self-centring force to clamp them to the foundation and allow them to rock in their original position. Aslam et al. (1980) were among the first researchers to investigate the response of rocking rigid bodies using vertical prestressed wires attached to the ground. Ishizuka (1987) used partially prestressed unbonded tendons in monolithic frame joints. These applications were further explored by Priestley and Tao (1993) who used partially debonded tendons in beam-column joints to provide primary lateral resistance for self-centring in rocking beams to column connections. Subsequently, Priestley and MacRae (1996) experimentally demonstrated that the clamping force supplemented by prestressing of the tendons could resist the shear demand in beam-column connections. Further analysis on beam-column connections using the Displacement Base Design (DBD) approach was carried out by Pampanin (2000). He developed a systematic procedure for evaluating moment capacity using a monolithic beam analogy. Analytical results were validated with experimental results and good agreement between them was obtained. This design (DBD) was carried out by Toranzo et al. (2004) by looking at a one-quarter scale three-storey rocking confined masonry wall building. The flexural bending energy dissipator was used in this model and tested on a shaking table using sixty dynamics records. Results showed that the wall did not

experience any damage except small diagonal cracks in the masonry panels near the rocking toes.

Using the concept of rocking structures and post-tensioning, Laursen and Ingham (2004a) tested two-thirds full scale post-tensioned concrete masonry (PCM) cantilever walls subjected to in-plane cyclic loading. A transverse reinforcement bar was provided at 400mm spacing so that the shear resistance in the masonry could be increased. Results of this experiment demonstrated that the wall could sustain its lateral strength up to 1.0% drift and failed at 1.5%. Slight damage occurred at the toe regions resulting in gradual strength degradation and contributed to spalling of the face shells. However, such damage was minimal and easily repaired. Further investigations were carried out using five post-tensioned concrete masonry walls subjected to in-plane cyclic loading (Laursen and Ingham, 2004b). Only a single inclined crack was observed in Wall 2 and Wall 5 due to the walls containing no transverse reinforcement. Further investigation was undertaken by Voon and Ingham (2006) who looked at the parameters that influence in-plane shear strength. The parameters consisted of shear reinforcement, axial compression load, type of grouting and the wall aspect ratio was tested on ten single-storey reinforced concrete masonry walls. Significant results were found where shear reinforcement not only provided additional shear resistance, but also improved the post cracking performance of the wall.

The above findings, to some extent, indicate that a shaking table can be used to test the behaviour of a rocking post-tensioned concrete masonry wall. In relation to that, Wight et al. (2006) tested four types of these walls subjected to five selected earthquake records with variations between PGA=0.35g and PGA=0.99g on a shaking table. The results of

the experiment revealed that rocking structures with post-tensioned tendons can exhibit larger displacement capacities and maintain the self-centring characteristics without residual displacement. Based on this concept, this research seeks to investigate the seismic performance of precast hollow core walls by incorporating unbonded tendons subjected to in-plane, out-of-plane and biaxial loading on a shaking table.

### 1.5.3 UNBONDED POST-TENSIONED TENDONS IN PRECAST WALL PANELS

Precast Seismic Structural System (PRESSS) is the research collaboration between the U.S and Japan established in 1988. The main objectives were to develop an effective seismic structural system for precast buildings and to recommend seismic design provisions for building codes. This programme consisted of three phases which were to investigate the seismic performance of joints between precast shear walls, unbonded post-tensioned precast walls and the overall performance of precast buildings (Nakaki and Englekirk, 1991). A study conducted by Schultz et al. (1994) as part of a PRESSS research project sought to study six vertical joint connections in precast concrete shear walls for a six-storey precast concrete office building exposed to moderate seismic risk. The unbonded post-tensioned tendon of the precast wall for this building was further initiated by Kurama et al. (1997). Prior to experimental work carried out by Priestley et al. (1999) on the vertical joint connections in precast buildings, Schultz et al. (1998) conducted another experimental work using four vertical shear connections which were selected from a previous study. The outcome from Schultz et al. (1998) using U-shape flexural Plates (UFP) was chosen as vertical joint connections which were welded to the adjacent precast wall panels for the PRESSS project. Results from Priestley et al. (1999)

revealed that these panels experienced minor crushing of the concrete at the base of the wall at 2.7% drift with minor cracks along the vertical joints.

Kurama et al. (1999) investigated the effect of various parameters of structural walls such as the strength of unconfined concrete, spiral reinforcement, total area of post-tensioning steel, wall length, wall thickness and initial prestressing of unbonded post-tensioned tendons that influence base shear capacities of the wall panel. They demonstrated that the lateral drift of the precast building can be reduced by adding supplemental viscous damping to the structures.

It was also demonstrated that the lateral drift of precast wall panels could be reduced significantly by using external linear viscous fluid dampers (Kurama, 2000). Later on, Kurama (2001) also proposed a simplified seismic design procedure under performance based design principles using unbonded post-tensioned precast wall panels with supplemental viscous damping. Kurama et al. (2002) further investigated the effects of site seismicity, site soil characteristics, initial prestressing and eccentricity of post-tensioning steel and assumed level of viscous damping on the response of solid precast wall panels.

In the construction of precast buildings, openings for windows and doors are very important for accessibility by the occupants. Hence, the experimental work should be conducted on wall panels with openings. In conjunction with this matter, Allen and Kurama (2002a) examined the lateral behaviour of the precast wall panels with rectangular openings under vertical loads. The top and bottom of the openings are the critical regions for cracks and are required to be provided with mild steel reinforcement around these regions. Consequently, they designed and proposed a rectangular opening in the

precast wall building subjected to the combination of vertical load (post-tensioning steel and gravity load) and lateral load (earthquake), Allen and Kurama (2002b).

The works on precast wall panels using unbonded post-tensioned tendons were further investigated by many other researchers. For instance, Perez et al. (2004a) applied unbonded post-tensioned tendons in a multi-panel precast wall by using vertical shear connectors between the walls and unbonded post-tensioned steel in each wall attached to the foundation beam. The outcomes showed that the total area of post-tensioning steel, initial prestress and total shear yield force across the vertical joint were sensitive to the total base shear capacity and hysteresis loops for a two-storey precast wall system. In addition, Perez et al. (2004b) investigated the lateral seismic behaviour of three full-height vertical precast wall panels in a two-storey building and connected to each other using vertical shear connectors. Spiral reinforcement bars were embedded inside concrete on the first floor only and the post-tensioning bars were anchored at the top of the wall and tied to the foundation beam using multi-strand tendons inside the ducts which were not grouted. During the rocking motion, high compressive stresses occurred at both edges of the base wall and the spiral reinforcement bars provided at one-quarter of its total length would avoid premature crushing and spalling of the concrete. With respect to this issue, the present study investigates the gaps in the seismic performance of precast wall panels using the design approach proposed by Mander and Cheng (1997).

### 1.5.4 ROCKING STRUCTURES AND DAMAGE AVOIDANCE DESIGN

Damage Avoidance Design (DAD) was proposed by Mander and Cheng (1997) where steel-steel interfaces in their connection can reduce local damage at the toe of concrete

structures. They adopted rocking rigid body concepts on bridge piers. Results showed that the structural damage can be entirely avoided in bridge piers. They also found the longitudinal reinforcement in the bridge column must be discontinuous between the column-foundation and the column-cap beam interface to avoid the occurrence of a plastic hinge zone. The lateral resistance of the column depends on the strength of unbonded tendons and supplemental energy dissipators provided at the four corners of the pile cap sitting on top of the foundation beam. The clamping force is provided by prestressing the unbonded tendons up to 60% of yield giving a self-centring effect to earthquake induced and rocking.

Besides primary work done by Mander and Cheng (1997), other researchers such as Holden et al. (2003), Surdano (2003), Liyanage (2004) and Ajrab et al. (2004) have used and adopted their approach to design and construct precast reinforced wall panels. For example, Holden et al. (2003) compared the experimental seismic performance between monolithic conventional reinforced precast walls and a rocking prestressed wall system by incorporating unbonded carbon fibre tendons and steel fibre reinforced concrete. They designed rocking walls using damage avoidance philosophy by putting steel plate at the bottom of walls and diagonal reinforcing bars across up to one-third of the height of the walls. Using the tie-strut model approach, the lateral forces were transferred to the unbonded post-tensioning carbon fibre to the walls and finally to the foundation beam. Dramix steel fibre was added to the concrete mix to control cracking by increasing the tensile strength of the concrete. A conventionally reinforced specimen (Unit 1) showed progressive damage starting with compressive spalling of the cover concrete occurred at 2% drift and longitudinal bars buckling at 2.5%. Lastly, the outermost longitudinal bar fractured at 3% drift. The DAD rocking specimen (Unit 2) performed very well up to

6.2 % drift without any strength degradation. The initial failure occurred when the eastern energy dissipator bars fractured, followed by of all the two eastern-duct carbon fibre tendons. Based on the comparative performance, Unit 2 performed significantly better than Unit 1 under seismic loading in spite of not following any special requirements for transverse reinforcement and longitudinal steel as used in standard ductile detailing practice.

Surdano (2003) constructed two identical sized thin precast wall panels with a slenderness ratio of 60 representing a three-eighths size of a prototype warehouse building and tested them on the shaking table using four different types of earthquake excitations. This test was to determine whether the buckling failure could happen in the slender wall panels using two different percentages of longitudinal bars of $\rho_t$=1.27%, $\rho_t$=0.54% for Unit 1 and Unit 2 respectively. The longitudinal bars D6 @47mm were connected between the wall and foundation beam using corrugated ducts for Unit 1. Eight of D6 longitudinal bars with a length of 600mm were used to connect the wall and foundation beam in Unit 2. Unit 2 was designed according to the damage avoidance design philosophy by welding a steel plate at the bottom of the wall which acted as a rocking wall system. At PGA=0.2g, Unit 1 experienced great damage especially at both bottom corners of the wall and a large deformation of buckling in out-of-plane directions. Unit 2 performed better than Unit 1 with negligible buckling at PGA=0.2g and the horizontal cracks were observed at one-third height of the wall. The longitudinal bars started to rupture at PGA=0.4g and the bottom corner of the wall uplifted to 45mm. Results showed that the rocking wall performed better than monolithic walls because it was allowed to rock on the foundation beam with larger displacement without developing any plastic hinge zone. Although a large number of reinforcement bars can increase the strength of

the walls, they do not improve the performance of the slender walls under severe earthquakes.

Liyanage (2004) later constructed two identical slender walls as Surdano (2003) did, but tested them under a biaxial controlled displacement pattern on a shaking table. Specimen 1 failed due to lateral-torsional out-of-plane buckling where the wall started to buckle at 1.15% drift. Specimen 1 collapsed after unloading maximum in-plane and out-of-plane drift simultaneously. Two major failures occurred on Specimen 2. The first failure occurred when the wet joint between the wall and the foundation cracked and spalled at 1.0% drift, followed by the second failure when the extruded longitudinal bars connected to the wall and the foundation buckled at 1.5% drift in the compression zone. The outermost rebars at both ends fractured during the first cycle of 1.5% drift and three rebars fractured at 2.0% drift.

In a recent theoretical and computational study, Ajrab et al. (2004) used damage avoidance design philosophy and the concepts of rocking shear walls in frame–wall structures by incorporating external supplemental energy dissipation and prestressed tendons as an alternative design to conventional fixed-base shear walls. A sensitivity study on various tendon prestress levels, profile of vertical tendons and width of the wall were used to investigate the seismic response of six-storey buildings. The findings showed that structural performance is significantly affected by the level of prestress tendons, tendons profile and the base wall width. From this study, they proposed a design procedure for a rocking precast shear wall with supplementary energy dissipation systems under a maximum assumed earthquake (MAE) and maximum considered earthquake ground motions (MCE).

## 1.6 SEISMIC DESIGN METHODS

Traditionally, force base design has been widely used for the seismic design of structures in most of the world's seismic codes of practices. Contemporary force-based approaches implicitly use $R-\mu-T$ relations rooted in the equal displacement and equal energy principles that have evolved from Newmark and Hall (1982) and ATC-3 (1978). These design approaches cannot be used for rocking structures because they do not adequately account for radiation damping arising from the rocking mechanism.

The capacity spectrum method was initially proposed by Freeman et al. (1975) where a linearised response along with effective viscous damping could be used in the form of conventional design spectra. The Direct Displacement Based Design (DDBD) was proposed by Kowalsky et al. (1994) who use a similar equivalent damping concept. The characteristic of this approach is known by the secant stiffness $(K_{eff})$ at maximum displacement $(\Delta_{target})$ and a level of equivalent viscous damping appropriate to the hysteretic energy absorbed during inelastic response. The maximum base shear at maximum response is given by multiplying the secant stiffness and maximum displacement. Figure 1.3 shows the flow chart of the displacement based design procedure for any structures with target displacement as their main objective. The seismic isolation design for bridges along with AASHTO uses the same concept as the capacity spectrum method by utilizing the effective viscous damping.

A ductility basis along with a force based design cannot be used in designing rocking structures because it is unable to take into account the effects of radiation damping. Therefore, the intention of this research is to propose a new design procedure for rocking

structures by incorporating the intrinsic, radiation and hysteretic damping through viscous damping formulation. This is discussed further in the following subsection.

### 1.6.1 EQUIVALENT VISCOUS DAMPING

The equivalent viscous damping is one of the key parameters in determining the amount of energy dissipated and efficiency of energy dissipators during earthquake excitation. The derivation of this parameter is defined by many researchers; such as Jacobsen (1930) who derived the equivalent viscous damping by equating the energy dissipated under a nonlinear SDOF system with energy dissipated through one cycle of the sinusoidal response of a linear system. Likewise, Hudson (1965) drew this concept by equating the energy dissipated by one cycle with energy dissipated using the spring-dashpot-mass system. Similarly, Gulkan and Sozen (1974), computed the equivalent viscous damping by equating the energy input into the system with energy dissipated using an equivalent linear viscous dashpot system. This was further defined by Chopra (1995) by equating the energy dissipated in a vibration cycle of the structure with an equivalent system.

Another important theme worth mentioning is the damping reduction factor (B) which is directly related to equivalent viscous damping. This factor has been adopted in a few seismic design building codes and its effect on the spectrum displacement was further investigated by Wu and Hanson (1989), Pekcan et al. (1999), Ramirez et al. (2002), Lin and Chang (2003), and Lin and Chang (2004). For instance, Pekcan et al. (1999) proposed an alternative approach by converting energy dissipation into equivalent viscous damping based upon power consumption considerations. They also proposed and compared the relationships for the damping reduction factor and equivalent viscous damping

with the Newmark-Hall approach. Data from Newmark and Hall (1982) have been implemented in most of the seismic codes. Some of the codes that considered the damping reduction factor on the buildings based on Newmark and Hall's (1982) study are ATC-40 (1996), SEAOC (1995), SEAOC (1999), UBC (1994), UBC (1997), NEHRP (1997), NEHRP (2000) and FEMA-273 (1997). The reduction damping factors (B) for these building codes are summarized in Table 1.1. The damping factors adopted in these codes are derived based on the effects of effective viscous damping from the displacement response spectrum without considering the soil condition. Therefore, a compressive study was carried out by Lin and Chang (2003) into considering the effects of soil characteristics on the damping reduction factors (B). Results revealed that the existing codes underestimate the B factors for shorter periods less than 2.0 seconds and overestimate the B factors for the systems having longer periods than 2.0 seconds.

Further investigation carried out by Lin and Chang (2004), using a statistical study of B factors, considered the effects of site classes from 1,037 acceleration time histories. This factor was analyzed using the period of vibration, percentage of damping and site classes. Two nonlinear regression equations were proposed. The first equation derived from the displacement response spectrum corresponding to each site class is given in the following equations:

$$B_d = 1 - \frac{aT^b}{(T+1)^c} \tag{1-1}$$

in which $T =$ natural period of vibration of systems, the coefficients $a, b$ and $c$ are dependent on the site condition and damping ratio $(\xi)$. The second equation derived from the acceleration responses spectrum corresponding to different site characteristics as

$$B_a = d + eT \tag{1-2}$$

where coefficients $d$ and $e$ depend on the site condition and damping ratio. These equations were validated based on the statistical results and a good agreement between them was obtained. Hence, the extension of their studies on the damping reduction factor will be further analyzed in this research. After completing the seismic design procedure, the next step is to evaluate the performance of building structures using Performance Based Seismic Engineering (PBEE) which will be discussed in the following section.

## 1.7 PERFORMANCE BASED SEISMIC ENGINEERING: INTERNATIONAL PRACTICE

The main objectives of any seismic design are to avoid any collapse of the buildings and loss of life. Thus, performance-based seismic engineering (PBEE) was introduced in the early over the past two decades to achieve these objectives by assessing the building structures. Some of the statistical tools that can be used to evaluate the seismic performance of buildings are Incremental Dynamic Analysis (IDA) and fragility curves. Figure 1.4 illustrates the flowchart of overall performance based-engineering seismic design. This conceptual framework covers the general scope of seismic engineering issues from the selection of objectives, identification of seismic hazards, conceptual design, preliminary and final design, design verification, design review, quality assurance during construction and building maintenance after construction. The major challenge to structural engineers is to develop effective methods for designing, analyzing and verifying the design structures to meet the selected performance objective. Currently, there are some possible design approaches available in SEAOC (1999) such as equal displacement–based design, direct displacement-based design and the capacity spectrum approach.

These conceptual frameworks also have been adopted in various international building codes (ATC-40, 1995; FEMA 273, 1997 and FEMA 356, 2000) and widely used in seismic regions. For example, Table 1.2 illustrates the overall performance objectives which are contained in these codes. Referring to this table, the design earthquake consists of four ranges of probability occurrences in 50 years which are frequent (50%), occasional (20%), rare (10%) and very rare (5%). Whereas, the design performance can be classified into four categories:

(a) Fully Operational where the facility continues to operate with negligible damage.

(b) Operational where the facility continues in operation with minor disruption in nonessential services.

(c) Life Safety is substantially protected and the damage is moderate to extensive.

(d) Near collapse where life safety is at risk, the facility suffers severe damage and structural collapse is prevented.

The diagonal matrix shows the combination of design earthquakes and design performance levels for unacceptable performance for new buildings, standard occupancy buildings, emergency response facilities and safety critical facilities. Table 1.3 shows the probability of the exceedence and recurrence interval of the earthquake design levels under frequent, occasional, rare and very rare events. This probability of occurrence with a certain return period is very important in designing the seismic building structures.

In relation to this research, warehouse buildings are designed using precast hollow core walls with the probability of exceedence of 10% in 50 years (DBE) and 5% in 50 years (MCE). Furthermore, it is also important to list out the damage states in relation to performance level and earthquake design levels. The descriptions of the damage states associated with design performance levels for precast wall panels are clearly shown in

Tables 1.4, 1.5, 1.6 and 1.7. Besides HAZUS 99-SR2 (2004), another seismic building code used to determine the performance level of damage in concrete wall panels is FEMA 356 (2000) (formerly FEMA-273 (1997)). It is expected that precast hollow core walls would perform beyond life-safety at the Maximum Considered Earthquake (MCE). In order to validate that the warehouse buildings which are constructed using precast hollow core walls can survive and perform well under different earthquake excitation, Incremental Dynamic Analysis is employed.

### 1.7.1 PERFORMANCE BASED SEISMIC ENGINEERING: NEW ZEALAND

Besides the international codes, the current codes used in seismic regions in Australia and New Zealand are known as "AS/NZ 1170". This design code comprises six parts which are AS/NZS 1170.0:2002 Part 0: General Principles, AS/NZS 1170.1:2002 Part 1: Permanent, imposed and other actions, AS/NZS 1170.2:2002 Part 2: Wind Actions, AS/NZS 1170.3:2003 Part 3: Snow and Ice Actions, AS/NZS 1170.4:2002 Part 4: Structural Design Actions-Australia and NZS 1170.5:2004 Part 5: Earthquake actions – New Zealand. All definitions of the design requirements and objectives under performance-based engineering are stated in NZS 1170.5:2004 Part 5. The design requirement is mandatory and must satisfy serviceability and ultimate limit states as stated in Clause 2.1.4. Under ultimate limits states, this clause stated that for structures which are subjected to earthquake actions the following shall be provided:

(1) Avoidance of collapse of the structural system,

(2) Avoidance of collapse or loss of support to parts of the structure that represent a hazard to human life, either inside or outside of the structure, or to parts required for life safety; and

(3) Avoidance of damage to non-structural systems necessary for emergency building evacuation, that renders them inoperative.

Two different levels of earthquake deformation are defined as SLS1 and SLS2 under serviceability limit state. These levels are classified according to the deformation in building structures;

(1) At the SLS1 level, structural system members and parts of structures shall not experience deformations that result in damage that would prevent the structure from being used as originally intended without repair.

(2) At the SLS2 level for structures of importance category level 4 (IC4), all parts of the structure shall remain operational so that the structure performs the role that has resulted in it being assigned this level of importance.

Table 1.8 (AZ/NZS 1170.5) describes the consequence of failure according to the Building Importance Category in five different categories. They are IC1 (minor structures), IC2 (normal structures), IC3 (major structures affecting crowds), IC4 (post-disaster structures) and IC5 (exceptional structures). The Building Importance Category is designed according to the annual probability of exceedance for earthquakes for a working life of 50 years. The details of these categories together with an acceptable annual probability of exceedance and return period factor are tabulated in Table 1.9 (AS/NZS 1170.5).

Most modern seismic design codes have stated the objectives outlining what structural engineers are attempting to achieve. These objectives form the basis for provisions in some seismic codes such as AS/NZS 1170.4:2002. The first objective is related to serviceability limit states where in the event of an SLS1 earthquake, the structure and its parts will not require repair. To prevent unacceptable damage, deflections and residual

interstorey drifts must be within the appropriate limits. After an SLS2 earthquake, the structure can continue to be used for its function without immediate repair. The second objective is related to ultimate limit states. Structures should have a high degree of reliability in achieving the strength and ductility with the intention to provide the structure with a high level of protection for life-safety within or around the buildings. The probability of collapse, failure of parts and elements and the failure of the building evacuation system must be maintained at low level risk. For normal use of building structures, the design return period of the earthquake motion must be verified for 500 years (10% probability in an assumed 50-year life). The third objective is to make sure that the structure has sufficient capacity to sustain the maximum considered earthquake with a small margin against collapse. For normal structures, the maximum considered earthquake in most instances has a return period of 2,500 years (2% probability in 50 years). For low seismicity regions, the damped hazard spectra have been modified by superimposing the ground motion resulting from an M6.5 earthquake to 20km from any site. In high seismicity regions, such as Wellington, the damped hazard spectra are much larger than the moderate earthquake shaking estimation.

### 1.7.1 INCREMENTAL DYNAMIC ANALYSIS

An advanced probabilistic based analysis is essential to assess the damage states of the structures with respect to the incremental earthquake acceleration. One of the methods under performance-based earthquake engineering (PBEE) is known as IDA (Incremental Dynamic Analysis). This parametric method of analysis developed by Vamvatsikos and Cornell (2002) involves a structural model subjected to numerous ground motion records, scaled to multiple levels of intensity that are suitably selected to uncover the full

range of the model's behaviour (from elastic to yielding and nonlinear inelastic, and global dynamic instability). This produces a curve response to intensity level from elastic response to collapse using statistical outcomes; assigned damage limit states; performed hazard-recurrence risk relation and used risk modelling to determine the probability of occurrence for structures. The direct estimation of seismic demand and capacity of multi-degrees of freedom systems of the structures can also be simplified to a single degree of freedom approximation model (Vamvatsikos and Cornell, 2005). In this study, a single degree of freedom model is used to represent the seismic rocking precast hollow core walls subjected to static pushover analysis (SPO) and non-linear dynamic analysis will be conducted. Detailed procedures are discussed in Chapter 4.

## 1.8 STATE-OF-THE-PRACTICE: CONSTRUCTION OF PRECAST WALL PANELS IN NEW ZEALAND (HIGH SEISMIC REGION)

New Zealand's construction industry experienced a boom cycle in the 1980s and the demand for precast structural components increased rapidly. The application of precast components in moment resisting frames, non-structural claddings, flooring systems and load bearing walls also forced the manufacturers to increase their production. In order to improve the performance and productivity of precast wall panels, more research and experimental work should be conducted to suit this product to the current code of practice. New Zealand Concrete Structures Standard (NZS 3101:1995) contains numerous general provisions for reinforced and prestressed concrete structures for cast-in-situ construction, but only a few provisions which include precast concrete construction. In spite of the new trend shifting from conventional methods to precast construction, only a single design guideline was produced in the application of structural precast concrete in building (CAE, 1991). Therefore, the intention of this research is to propose an alternative mate-

rial and technology in constructing warehouse buildings using precast hollow core units as replacements for conventional monolithic fixed-base wall panels.

Precast wall panels are commonly used for the construction of warehouses, shopping complexes, residential houses, commercial buildings, community halls and gymnasiums. Most of these buildings have incorporated the precast structural walls as a primary lateral seismic resisting system. This design followed the emulation approach as stated in the New Zealand Concrete Structures Standard (NZS 3101:1995). The standard requires the slenderness ratio (height over thickness) of the wall to be limited to 30. In other words, the precast wall panel is designed with rectangular sections with thicknesses of 125 to 150mm, an unsupported height to thickness ratio less than 30 using a single layer of longitudinal and transverse reinforcement. However, some structural engineers violated this requirement by using a slenderness ratio up to 70. This slenderness ratio can cause instability to the structures under severe earthquake excitation. The experimental results carried out by Surdano (2003) showed that slender precast wall panels lose their stability at PGA=0.4g and collapse under a maximum considered earthquake with PGA=0.8g. This issue becomes a huge concern to designers, developers, builders, precast manufacturers and territorial authorities in New Zealand. Thus, the slenderness ratio and detailing connection between their interfaces become the two main design parameters for precast hollow core wall panels.

Detail connections between wall to roof, wall to column, wall to wall, wall to foundation beam and wall to floor slab are extremely important in designing and constructing the tilt-up precast building system. The connections between these structural elements must allow some movements between wall panels when exposed to internal sources (early-age

movement from the rise in concrete temperature during hydration of concrete, irreversible drying shrinkage and creep under stress) and external loading (imposed load, self-weight of the structure, wind and seismic loading).

To date, a lot of research has been conducted with regard to the slenderness ratio and types of connection between wall-foundation in New Zealand. Much of this research has focused on the performance of single wall panels under quasi-static cyclic lateral loading (McMenamin, 1999; Rahman Restrepo, 2000; Holden et al., 2003; Laursen and Ingham, 2006; Voon and Ingham, 2006), dynamic loading (Surdano, 2003; Wight et al., 2006) and biaxial loading (Liyanage, 2004). One research investigation conducted by Rahman and Restrepo (2000) used three units of precast wall panels. These complied with the current standard of confinement details located at the end toes of the walls. Figure 1.5 shows the reinforcement details, location of tapered energy dissipators and unbonded post-tensioned tendons in precast reinforced concrete wall panels. A further investigation was undertaken by Holden et al., (2003) comparing current standard of practice (NZ 3101:1995) and Damage Avoidance Design philosophy (DAD). Two identical walls with half-scale precast wall panels representing a prototype of a four-storey building were constructed and tested under reverse cyclic lateral loading. Unit 1 was designed and constructed according to the conventional method for a full ductile response. In contrast, Unit 2 was designed according to DAD using two energy dissipators located at the centre of the wall, unbonded post-tensioned tendons and some additional steel fibre in the concrete mixture. Figure 1.6 shows the reinforcement details of the wall panel and foundation beam in Unit 2.

This research is aligned with the contemporary connection detailing along with the current code of practice in New Zealand. As such, Figure 1.7 shows the modern connection design between precast wall panels and roof steel trusses for warehouses/industrial facilities in seismic regions. The function of post-installed fixing of the bolt connected to a steel cleat and purlin is to transfer shear and tension axial forces produced by the purlin reactions. The post-installed fixings are bolted to the steel angle which is attached to the purlins. Typically, this type of connection is used in the construction of single storey precast tilt-up buildings.

Figure 1.8 depicts another current example of a precast wall panel embedded into a foundation beam using grout. In this system, the precast wall panels are seated inside the recess in the foundation beam and then grouted to them using mortar. A minimum recess depth is calculated based on the basic deformed bar development length for hooked bars in tension as stated in the current standard. The transverse reinforcement bars are passed through the horizontal holes left in the wall panels. The longitudinal reinforcing bars are anchored in the wall at a distance at least equal to the development length, $(L_{DH})$. The amount of transverse reinforcement passing through the foundation beam can be calculated using the strut-and tie model as proposed by Holden et al. (2003).

Figure 1.9 shows an example of the jointed system which connects the foundation to cantilever walls through grouted ducts. The precast wall panels are positioned on top of the foundation beam. To ensure that the vertical reinforcing bars protruding from the foundation beam are located at the centre of the wall, the protruding bars must be inserted inside the centre of galvanized corrugated ducts in the walls. The grout is pumped through the gap and ensures that the flow is in one direction to avoid any entrapment of air. Before

grouting, the bottom of the wall and foundation surfaces must be roughened and cleaned to improve shear transfer. The connection relies on the force transfer from vertical reinforcement bars and lapping bars in the walls. During ground shaking, large strains are expected to occur in vertical reinforcing bars at the wall-foundation interface resulting in the yielding and buckling of bars.

There are several methods of connecting precast wall panels to the foundation beam of single to three-storey buildings in New Zealand. The first method is by inserting a steel channel into one end of the wall panel and welding steel channel, steel plate and steel shim together. Figure 1.10 shows the welded steel section is sitting on top of the foundation beam and anchoring the welded hooked bars to the bottom of longitudinal bars. This type of connection is designed for the tilt-up wall to resist in-plane and out-of plane loading within the uncracked section. In other words, this connection can resist in-plane bending, shear force and bending moments induced by the wall panels during ground motion.

Figure 1.11 shows another typical connection between tilt-up wall and foundation beam which has been practised in New Zealand's construction industry. The corrugated steel duct is embedded inside the precast walls and continuous longitudinal protruding bars are inserted from the foundation beam into the steel duct to avoid the sliding of the wall along the connection during the ground motion. The protruding reinforcing bars are tied to the reinforcement in the foundation beam. Dry packed mortar is used to level the position of the wall for waterproofing purposes. Normally, tilt-up wall panels are connected to each other by bolting both steel angle legs to the walls, welding a perforated steel plate to the transverse bars which are embedded inside precast concrete. The gap between the

precast walls is sealed using a special sealant which is weathertight and durable with a life span between 10 and 20 years. This is to accommodate some movement of temperature changes, humidity, and settlement of soil and ground motion from earthquake excitation. This method can increase the in-plane flexural strength of the tilt-up wall.

## 1.9 STATE-OF-THE-PRACTICE: CONSTRUCTION OF PRECAST WALL PANELS IN MALAYSIA: A LOW SEISMIC REGION

Malaysia is categorized as a low-seismic region due to its location of about 650km from the Sunda trench which separates the Sunda plate, the India plate and the Australia plate. Most of the reinforced concrete buildings are designed according to British Standard (BS 8101-1:1997: Part 1: Code of practice for design and construction) which does not have any provision for earthquake resistant design. Therefore, precast wall panels are designed and constructed by considering dead load and imposed load only. A simple connection is designed to connect between roof steel frame and precast hollow core wall panels. The requirement in the current code of practice states that as long as this type of connection can support the factored vertical loading it will be sufficient. Some examples of typical types of connection used in the construction of precast buildings using precast hollow core walls are illustrated and described in the following figures.

Figure 1.12 shows the connection between steel roof metal decking comprising steel trusses and bar joist and load bearing precast hollow core wall panels using anchorage bolts. The steel roof trusses are connected to wall panels using anchorage bolts and grouting them with the mortar in the void sections of the wall panels. Anchorage bolts are connected to a steel angle which is seated on top of a precast hollow core wall. Figure 1.13 shows another typical example of the connection between the precast hollow

core wall and precast double tee roof slabs. Precast roof slabs are supported by precast hollow core walls and bolted to steel angles located between precast systems. This system is well-known as the “total precast building system”. One of the steel angle legs is bolted to the precast double tee and another leg is bolted to precast hollow core walls to carry the gravity load and to transmit shear force from the roof. Precast hollow core wall panels could also be used as non-load bearing walls because of easy handling, erecting, maintenance costs and good appearance (ribbed finish, raked finish, tiled finish and exposed aggregate finish).

Figure 1.14 shows the connection detailing between non-load bearing walls and a steel frame structure. This type of connection has been practised in the construction of residential houses, industrial buildings, warehouses as well as shopping and recreation centres. Besides being used as exterior load bearing walls, these wall panels can also carry the internal loadings of the structures such as floor self-weight, internal wall partition, roof tiles and imposed load.

Figure 1.15 presents the details connection between precast hollow core slabs and an internal precast hollow core wall in double-storey houses as one of its application in the non-seismic regions. The internal precast hollow core walls are connected to each other using tie bars and grouted at the top end and bottom end of precast wall panels. A strip of bearing pads is placed underneath precast hollow core slabs to allow some movement due to the change in temperature and humidity, but does not accommodate any earthquake movements.

Figure 1.16 shows the connection detailing between the foundation beam and the precast hollow core wall panels. The longitudinal reinforcement bars from the foundation caging are protruded into the voids sections of the precast hollow core wall and grouted at the bottom portion of the units. The connection between wall and foundation beam is designed to place the wall in the correct position during construction and to resist in-plane loading and gravity load. This panel however, does not allow it to rock on the foundation beam during ground shaking. The bottom part of the precast hollow core walls is very brittle and easy to crack or spall at highly concentrated stresses when subjected to horizontal loading. All the above connections are designed mainly to carry dead imposed and wind load according to the current Malaysian standard code of practice. The partial safety factor for gravity load including the self-weight of structures $(G_k)$ is 1.4, imposed load including heavy machinery and maintenance $(Q_k)$ is 1.6 and wind load $(W_k)$ is 1.2. The worst combination of these loadings is normally used to design the structures together with their connections.

Production of precast hollow core units in concrete plants using an extruder machine consumes less time and ensures a good quality product. Figure 1.17 depicts a stack of precast hollow core units at a plant which are ready for erection. Precast hollow core walls consist of two longitudinal prestressing strands on top and three prestressing strands at the bottom of the voids sections. The compressive strength of the wall panel is 70MPa which is designed to resist in-plane lateral load using the uncracked section. These walls are joined together using a special sealant. This sealant is weatherproof and allows some movement of the wall panels due to the changes in temperature, humidity and mild exposure. Generally, these precast wall panels are connected to each other either using single sealant from inside the walls or double sealants from both sides of the

walls. Figure 1.18 shows two methods of connecting precast wall panels using silicone sealant. The specialist sealant applicator usually uses a caging crane when installing and tooling the sealant between the gaps wall in industrial buildings. Such a process is shown in Figure 1.19.

Doors and windows must be provided in all buildings for access and air ventilation. A wider opening is required for accessibility of vehicles into the warehouse/industrial buildings. The frames for such openings are commonly made from timber and steel. Figure 1.20 shows an example of openings in the construction of warehouses/industrial buildings in Malaysia. Another typical example of the single-storey industrial building using precast hollow core wall panels with the opening is shown in Figure 1.21. This industrial building was designed to resist gravity and imposed load. To date, there are no seismic design provisions in the current code of practice in Malaysia. For that reason, the intention of this research is to use precast hollow core walls in the construction of warehouse/industrial buildings and demonstrate their viability for both low and high seismic regions.

As an earthquake struck Miri and Bintulu in East Malaysia in May 2004, the importance of seismic design provisions should be given priority by federal and local authorities. Even though this earthquake was only M4.8 on the scale Richter, it caused several cracks in buildings close to the epicentre. This argument is further strengthened by the recent earthquake on the West Coast of Northern Sumatra (M9.0 scale Richter, December 26, 2004) which also caused massive destruction particularly in the northern coastal area of Malaysia. Hence, this study is to propose some recommendations on seismic provision to be included in current codes of practice of the Malaysian government. The Institute of

Engineers and Board of Engineers must enforce and implement the amendments in the current code of practice for end-user communities.

## 1.9 RESEARCH OBJECTIVES

Based on the above literature review, most of the previous studies have focused on the direct-displacement approach and unbonded post-tensioned tendons precast wall panels using spiral reinforcements and transverse reinforcement bars (Priestley et al., 1999; Kurama, 2001; Allen and Kurama, 2002a; Perez et al., 2004a). However, to date there has been only limited study of the application of rocking structures in solid reinforced concrete precast wall panels using the Damage Avoidance Design (DAD) philosophy (Holden et al., 2003; Ajrab et al., 2004). Mander and Cheng (1997) have introduced a DAD philosophy by investigating the rocking of bridge piers on their foundation. They found that by steel-armouring at the bottom of the column they could prevent all structural damage to the bridge piers. In an extension of their work, this study investigates the overall seismic behaviour of precast hollow core walls without horizontal reinforcing bars. In particular, the connection interface between wall-foundation, the most efficient energy dissipators and the combination of seismic and non-seismic walls as a rocking wall system are investigated. In researching this, the following objectives have been set:

(i) To provide an alternative way of using precast hollow core units as precast wall panels and introduce a new construction technology for warehouse/industrial buildings.

(ii) To advance a concept based on Damage Avoidance Design (DAD) by conducting experimental works to demonstrate that precast hollow core walls (PHCW) are an alternative way of constructing tilt-up buildings rather than

the highly reinforced solid precast wall system only with fixed base rigid ductile connections.

(iii) To permit larger displacement of precast hollow core panels during strong earthquake excitation and simultaneously avoiding seismically-induced damage to PHCW.

(iv) To ascertain the expected behaviour of PHCW under ground motions those well exceed the design basis earthquake.

The experimental results of this study would also further validate the Mander and Cheng (1997) conceptual framework for DAD.

## 1.10 SIGNIFICANCE OF THE STUDY

As previously mentioned, this research is to demonstrate that the precast hollow core walls could endure, without transverse reinforcement, strong ground shaking, with neither structural nor non-structural damage. The aim of this research is to contribute to a broader usage of precast hollow core walls in seismic regions. Engineers may find that these wall panels can resist seismic loads, require less intensive labour, are speedier to construct and minimize the overall cost of construction. In addition, steel-armouring at the bottom corner of the walls can protect the rocking toe from spalling and crushing of the concrete. The strength of wall panels could be improved by increasing the level of initial prestressing in unbonded post-tensioned tendons or fuse-bars. This strength can resist the earthquake shaking without causing damage to any parts of the wall panels.

The proposed rocking system also allows panels to rock back and forth without incurring any damage to the structural components due to the absence of a conventional plastic

hinge zone. Overall, the development of this new proposed design procedure for precast hollow core walls will benefit construction industries and seismic regions in general.

## 1.11 SCOPE OF THE STUDY

This thesis is organised into six chapters. Following this introductory chapter which has briefly reviewed the literature on the subject matter, Chapter 2 presents experimental results for 'seismic' precast hollow core wall panels. The two full-scale precast hollow core wall specimens were constructed in the laboratory and tested under reversed quasi-static cyclic bi-lateral loading on a shaking table.

Chapter 3 provides an experimental investigation into the seismic performance of a multi-panel precast hollow core wall system, representing part of a warehouse building. Tests were conducted on a strong floor under reversed cyclic quasi-static in-plane loading. The superassemblage multi-panel consists of two 'seismic' wall panels rocking on the steel base plate and four 'non-seismic' wall panels seated on a strip of rubber pad.

Chapter 4 proposes a design procedure for single storey warehouse buildings constructed from precast hollow core wall panels. In addition to the design example presented a quantitative assessment procedure is developed. This uses an incremental dynamic analysis (IDA) methodology to evaluate probabilistic levels of performance through global instability.

Chapter 5 compares the performance assessment in terms of the Hazard-Survival curve and fragility curve between a precast hollow core wall and a fixed-base monolithic wall.

Incremental Dynamic Analysis is performed for both types of walls using five steps as described in the chapter.

Finally, a summary of findings, overall discussion, conclusions and recommendations are presented in Chapter 6.

## REFERENCES


Ajrab, J.J., Pekcan, G., and Mander, J.B. (2004). “Rocking wall-frame structures with supplemental tendon systems." *Journal of Structural Engineering*, ASCE, 130(6), 895-903.

Allen, M.G., and Kurama,Y. (2002a). “Design of rectangular openings in precast walls under vertical loads." *PCI Journal*, 47(1), 50-65.

Allen, M.G., and Kurama,Y. (2002b). “Design of rectangular openings in precast walls under combined vertical walls and lateral loads." *PCI Journal,* 47 (2), 58-79.

Applied Technology Council. (1978). "Applied Technology Council, tentative provisions for the development of seismic regulations for buildings." *ATC-3*, National Bureau of Standards Specification Publications, 510.

Applied Technology Council. (1995). "Guidelines and commentary for the seismic rehabilitation of buildings." *ATC-40*, Redwood City, California.

Aslam, M., Goddon, W.G., and Scalise, D.T. (1980). "Earthquake rocking response of rigid bodies." *Journal of Structural Engineering*, ASCE, 106 (2), 377-392.

Berg, G.V., and Stratta, J.L. (1964). "Anchorage and the Alaska Earthquake on March 27, 1964." *American Iron and Steel Institute*, 63.

Bristish Standard. (1997). " Structural use of concrete - Part 1: Code of practice for design and construction." *BS 8110-1:1997. (1997)*, London, UK, 172.

Cement and Concrete Association of New Zealand (CCANZ). (1990). "Tilt-up construction - course manual." *Seminars Notes*, Wellington, New Zealand.

Centre for Advanced Engineering (CAE). (1991). "Guidelines for the use of structural precast concrete in buildings." *Manual Design*, Study group of New Zealand Concrete Society and New Zealand National Society for Earthquake Engineering, University of Canterbury, Christchurch, New Zealand, 174.

Chopra, A.K. (1995). *Dynamics of structures: theory and applications to earthquake engineering*. Prentice-Hall, Englewood Cliffs, N.J., U.S.A.

CIRIA. (1998), "Sealant joints in the external envelope of buildings." A guide to design, specification and construction, *Report 178*, London, UK.

Cormack, L.G. (1988). "The design and construction of the major bridges on the Mangaweka Rail Division." *Transactions*, Institutions of Professional Engineers, New Zealand, 15, I/CE, 16-23.

Elgawady, M.A., MA, Q.T., Ingham, J.M., Butterworth, J.W. (2005). " Experimental investigation of rigid body rocking." The New Zealand Concrete Industries Conference, *Proceedings of the New Zealand Concrete Industries Conference,* CD Rom, Auckland, New Zealand.

Elgawady, M.A., MA, Q.T., Butterworth, J.W., and Ingham, J.M. (2006). "The effect of interface material on dynamic behaviour of free rocking blocks." *8th U.S National Conference of Earthquake Engineering,* San Francisco, California, U.S.A.

Federal Emergency Management Agency. (1997). "NEHRP guidelines for the seismic rehabilitation of buildings." *FEMA-273,* BSSC Building Seismic Safety Council, Washington, D.C.

Federal Emergency Management Agency. (2000). "Prestandard and commentary for the seismic rehabilitation of buildings." *FEMA-356*, ASCE, American Society of Civil Engineers, Virginia, U.S.A.

Federation International du Beton (FIP). (2000). "Special design considerations for precast prestressed hollow core floors." *fib Bulletin No. 6,* Wexham Springs, Slough, England.

Freeman, S.A, Nicoletti, J.P., and Tywell, J.V. (1975). "Evaluation of existing buildings for seismic risk - A case study of Puget Sound Naval Shipyard." *Proceedings of the U.S National Conference on Earthquake Engineering*, Michigan, U.S.A, 113-127.

Ghosh, S.K. (2001). "Observations from the Bhuj Earthquake of January 16, 2001." *PCI Journal*, 46(2), 34-42.

Gulkan, P., and Sozen, M.A. (1974). "In-elastic responses of reinforced concrete structures to earthquake motions." *Proceedings of the ACI Journal*, 71(12), 605-610.

Hamburger, R.O., McCormick, D.L., Eerri, M., and Hom, S. (1988). "The Whittier Narrows, California Earthquake of October 1, 1987, performance of tilt-up buildings." *Earthquake Spectra*, 4(1), 219-254.

HAZUS 99-SR2. (2004). "Earthquake loss estimation methodology." *HAZUS Technical Report*, Federal Emergency Management Agency and National Institute of Buildings Sciences, Washington D.C, http://www.fema.gov/hazus/[accessed 5/8/03].

Holden, T.J. (2001). " A comparison of the seismic performance of precast wall construction : emulation and hybrid approaches." *Research Report 2001-04,* Department of Civil Engineering, University of Canterbury, New Zealand.

Holden, T. J., Restrepo, J., and Mander, J.B. (2003). "Seismic performance of precast reinforced and prestressed concrete walls." *Journal of Structural Engineering*, ASCE, 129(3), 286-296.

Housner, G.W. (1963). "The behaviour of inverted pendulum structures during earthquake." *Bulletin of the Seismological Society of America*, 53(2), 403-417.

Hudson, D.E. (1965). "Equivalent viscous friction for hysteretic systems with earthquake-like excitations." *3rd World Conference on Earthquake Engineering*, *New Zealand,* II-185/II-201.

IBC. (2000). " International building code 2000." *International Conference of Building Officials*, Whittier, CA.

Ishizuka, T. (1987). "Effect of bond deterioration on seismic response of reinforced and partially prestressed concrete ductile moment-resisting frames." thesis, presented to University of Washington, Seattle, WA, in partial fulfillment of the requirements for the degree of Doctor of Philosophy.

Iverson, J.K., and Hawkins, N.M. (1994). "Performance of precast/prestressing building structures during Northridge Earthquake." *PCI Journal*, 36(2), 38-55.

Jacobsen, L.S. (1930)."Steady forced vibrations as influenced by damping." *Transactions ASME*, 52(1), 169-181.

James, K.I., Neil, M.K. (1994), " Performance of precast/prestressed concrete building structures during Northridge Earthquake." *PCI Journal,* 36(2), 38-55.

Johnson, L.A. (2000)."Earthquake loss modelling applications for disaster management: lessons from the 1999 Turkey, Greece and Taiwan Earthquakes." *Proceedings of EuroConference on Global Change and Catastrophe Risk Management: Earthquake Risk in Europe*, Laxenburg, Austria.
http://www.iisa.ac.at/Research/RMS[accessed 8/9/03].

Kowalsky, M.J., Priestley, M.J.N. and MacRae, G.A. (1994). "Displacement based design of RC bridge columns." *Proceedings of the Second International Workshop*, New Zealand, 145-169.

Krinitzsky, E.L., Chowdhury, M. R., and Al-Chaar, G. (2000). "Structures and industrial facilities." *Earthquake Spectra, 1999 Kocaeli, Turkey Earthquake Reconnaissance Report*, 16, 237-279.

Kurama, Y., Sause, R., Pessiki, S., and Lu, L-W. (1997). "Seismic design and response evaluation of unbonded post-tensioned precast concrete walls." *Research Report No.EQ-97-01*, Department of Civil and Environmental Engineering Lehigh University, Bethlehem, PA, USA,184.

Kurama, Y., Dessiki, S., Sause, R., and Lu, L.-W. (1999). " Seismic behaviour and design of unbonded post-tensioned precast concrete walls." *PCI Journal*, 38(3), 72-73.

Kurama, Y. (2000). "Seismic design of unbonded post-tensioned precast walls with supplemental viscous damping." *ACI Journal,* 97(4), 648-658.

Kurama, Y. (2001). " Simplified seismic design approach for friction-damped unbonded post-tensioned precast concrete walls." *ACI Structural Journal*, 98(5), 205-716.

Kurama, Y., Sause, R., Pessiki, S., and Lu, L.W. (2002). "Seismic response evaluation of unbonded post-tensioned precast walls." *ACI Structural Journal,* Technical Paper, 99(5), 641-651.

Laursen, P.T., and Ingham, J.M. (2004a). "Structural testing large-scale post-tensioned concrete masonry walls." *Journal of Structural Engineering*, ASCE, 130(10), 1497-1505.

Laursen, P.T., and Ingham, J.M. (2004b). "Structural testing enhanced post-tensioned concrete walls." *ACI Journal Structural,* 101(6), 852-862.

Laursen, P.T., and Ingham, J.M. (2006). "Experimental in-plane shear strength investigation of reinforced concrete masonry walls." *Journal of Structural Engineering*, ASCE, 132(2), 400-408.

Lee, H.T., and Sooi, T.F., (2003), "Advantages of using precast hollow core walls in multi-storey building." Design Manual, Eastern Pretech (Malaysia) Sdn, Bhd, Beranang, Negeri Sembilan, Malaysia, 44.

Lin, Y.Y., and Chang, K.C. (2003). "Study on damping reduction factor for buildings under earthquake ground motions." *Journal of Structural Engineering*, ASCE, 129(2), 206-214.

Lin, Y.Y., and Chang, K.C. (2004). "Effects of site classes on damping reduction factors." *Journal of Structural Engineering*, ASCE, 130(11), 1667-1675.

Lin, H., and Yim, S.C.S. (1996). "Non-linear rocking motions. I: chaos under noisy periodic excitations." *Journal of Engineering Mechanics*, ASCE, 122(8), 719-727.

Liyanage, L.U. (2004). "Biaxial lateral loading behaviour of thin concrete walls." thesis, presented to University of Canterbury at Christchurch, New Zealand, in partial fulfillment of the requirement for the degree of Master of Engineering.

Lu, Y., Hao, H., Ma, G., and Zhou, Y. (2001). "Simulation of structural response under high-frequency ground excitation." *Earthquake Engineering and Structural Dynamics*, 30, 307-325.

Mander, J.B., and Cheng, C.T. (1997). "Seismic resistance of bridge piers based on Damage Avoidance Design." *Technical Report NCEER-97-0014*, Department of Civil, Structural and Environmental Engineering, State University of New York at Buffalo, New York, USA.

McManus, K.J., Priestley, M.J.N. and Carr, A.J. (1980). " The seismic response of bridge structures free to rock on their foundations." *Research Report No. 80/4*, Department of Civil Engineering, University of Canterbury, New Zealand.

McMenamin, A. (1999). "The performance of slender precast reinforced concrete cantilever walls with roof level lateral displacement restraint under simulated in-plane seismic loading," thesis, presented to University of Canterbury at Christchurch, New Zealand, in partial fulfillment of the requirements for the degree of Master of Engineering.

Meek, J.W. (1978). "Effects of foundation tipping on dynamic response." *Journal of Structural Engineering*, ASCE, 101(7), 1297-1311.

Murphy, L.M. (1973). " San Fernando, California, Earthquake of February 9, 1971 ." Volume 1: Effects on building structures, *National Oceanic and Atmospheric Administration*, U.S. Department of Commerce, Washington, D.C., USA, 841.

Nakaki, S.D., and Englekirk, R.E. (1991). "PRESSS industry seismic workshops: concept development." *PCI Journal*, 36(5), 54-61.

NEHRP. (1997). "Recommended provisions for seismic regulations for new buildings." *Federal Emergency Management Agency*, Washington, DC.

NEHRP. (2000). "Recommended provisions for seismic regulations for new buildings." *Federal Emergency Management Agency*, Washington, DC.

Newmark, N.W. and Hall, W.J. (1982). "Earthquake spectra and design." *Earthquake Engineering Research*, Buffalo, New York.

Pampanin, S.(2000). "Alternative design philosophies and seismic response of precast concrete buildings." thesis, presented to Politecnico Di Milano, Milan, Italy, in partial fulfillment of the requirements for the degree of Doctor of Philosophy.

Pekcan, G., Mander, J.B., and Chen, S.S. (1999). " Fundamental considerations for design of non-linear viscous dampers." *Earthquake Engineering and Structural Dynamics*, 28, 1405-1425.

Perez, F.J., Pessiki, S., and Sause, R.S. (2004a). "Seismic design of unbonded post-tensioned precast concrete walls with vertical joint connectors." *PCI Journal*, 49(1), 58-59.

Perez, F.J., Pessiki, S. and Sause, R.S. (2004b). "Lateral load behaviour of unbonded post-tensioned precast concrete walls with vertical joints." *PCI Journal*, 49(2), 48-63.

Pompei, A., Scalia, A., and Sumbatyan, M.A. (1998). "Dynamics of rigid block due to horizontal ground motion." *Journal of Engineering Mechanics*, ASCE, 124(7), 713-717.

Precast Technology. (1991). "Design and reference manual PT-9111, Industrialised building systems using spiroll hollow core slabs." IJM Shd Bhd, Shah Alam, Ma laysia, 66

Priestley, M.J.N., Evison, R.J., and Carr, A.J. (1978). "Seismic response of structures free to rock on their foundation." *Bulletin of the New Zealand National Society For Earthquake Engineering* , 20(3), 141-150.

Priestley, M.J.N., and Tao, J.R.T. (1993). "Seismic response of precast prestressed concrete frames with partially debonded tendons." *PCI Journal*, 38(1), 58-69.

Priestley, M.J.N., and MacRae, G.A. (1996). "Seismic testing of precast beam-to-column joint assemblage with unbonded tendons." *PCI Journal*, 41(1), 64-80.

Priestley, M.J.N., Sritharan, S., Conley, J.R., and Pampanin, S. (1999). "Preliminary results and conclusions from the PRESSS five-story precast concrete test building." *PCI Journal*, 44(6), 42-67.

Psycharis, I.N. and Jennings, P.C. (1983). "Rocking of slender rigid bodies allowed to uplift." *Earthquake Engineering and Structural Dynamics*, 11, 57-76.

Rahman, A.M., and Restrepo, J.I. (2000). "Earthquake resistant precast concrete buildings: seismic performance of cantilever walls prestressed using unbonded tendons." *Research Report 2000-05*, Department of Civil Engineering, University of Canterbury, New Zealand.

Ramirez, O.M., Constantinou, M.C., Whittaker, A.S., and Chrysostomou. (2002). "Elastic and inelastic seismic response of buildings with damping systems." *Earthquake Spectra*, 18(30), 531-547.

Restrepo, J.I., Crisadulli, F.J., and Park, P. (1996). "Earthquake resistance of structures: the design and construction of tilt-up reinforced concrete building." *Research Re port 96-11*, Department of Civil Engineering, University of Canterbury, New Zealand.

Saatcioglu, M., Mitchel, D., Tinawi, R., Gardner, N.J., Gillies, A.G., Ghobarah, A., Anderson, D.L. and Lau, D. (2001). "The August 17, 1999 Kocaeli (Turkey)

earthquake-damage to structures." *Canadian Journal of Civil Engineering*, 28(4), 715-737.

Schultz, A.E., Magana, R.A., Tadros, M.K., and Huo, X. (1994). "Experimental study of joint connections in precast concrete walls." *Proceeding, 5th U.S National Conference on Earthquake Engineering,* EERI, Chicago, IL, U.S.A., 579-589.

Schultz, A.E., Cheok, G.S. and Magana, R.A. (1998). "Performance of precast concrete shear wall." *Proceeding on 6th U.S National Conference on Earthquake Engineering,* EERI, Seattle, WA, U.S.A., 321-335.

SEAOC. (1995). "Vision 2000 - A framework for performance based design." Volumes I,II,III, *Vision 2000 Committee*, Sacramento, California.

SEAOC. (1999). "Recommended lateral force requirements and commentary." *Seismology Committee*, Structural Engineers Association of California, California.

Sezen, H., and Whittaker, A.S. (2004). "Performance of industrial facilities during the 1999, Kocaeli, Turkey earthquake." *13th World Conference on Earthquake Engineering,* Vancouver, B.C., Canada, August 1-6, Paper No. 282.

Shenton III, H.W., and Jones, N.P. (1991). "Base excitation of rigid bodies. I: formulation." *Journal of Engineering Mechanics*, ASCE, 117, 2286-2306.

Shenton III, H.W. (1996). "Criteria for initiation of slide, rock and slide-rock rigid-body modes." Journal of Engineering Mechanics, ASCE, 122(7), 690-693.

Skinner, R. I., Robinson, W.H., and McVerry, G. H. (1983). *An introduction to seismic isolation*. Wiley, New York, USA.

Standards Association of New Zealand. (1995). "Concrete structures standard, Part 1: the design of concrete structures." *NZS 3101:1995*, Wellington, New Zealand.

Standard Australia/ Standard Association of New Zealand. (2004)."Structural design actions, earthquake actions-New Zealand." *AS/NZS 1170.5:2004 Part 5*: Wellington, New Zealand.

Surdano, I. (2003). "Performance of thin precast concrete wall panels under dynamic loading." thesis, presented to University of Canterbury at Christchurch, New Zealand, in partial fulfillment of the requirements for the degree of Master of Engineering.

Taniguchi, T. (2002). "Non-linear response analyses of rectangular rigid bodies subjected to horizontal and vertical ground motion." *Earthquake Engineering and Structural Dynamics*, 31, 1481-1500.

Taniguchi, T., and Miwa, T. (2006). "A simple procedure to approximate slip displacement of freestanding rigid body subjected to earthquake motions." *Earthquake Engineering and Structural Dynamics (in press).*

Toranzo, L.A., Restrepo, J.I., Carr, A.J., and Mander, J.B. (2004). "The use of rocking walls in confined masonry structures: a performance-based approach." *13th World Conference on Earthquake Engineering*, Vancouver, B.C., Canada, August 1-6, Paper No. 599.

UBC. (1994). "Uniform building code." *International Conference of Buildings Officials,* Whittier, CA.

UBC. (1997). "Uniform Building Code 1997: Structural engineering design provisions (Uniform Building Code Vol 2: Structural Engineering Division)." *International Conference of Buildings Officials,* Whittier, CA.

Vamvatsikos, D., and Cornell, C.A. (2002). "Incremental dynamic analysis." *Earthquake Engineering and Structural Dynamics,* 31, 491-514.

Vamvatsikos, D., and Cornell, C.A. (2005). "Direct estimation of seismic demand and capacity of multidegree-of-freedom system through incremental dynamic analysis of single degree of freedom approximation." *Journal of Structural Engineering*, ASCE, 131(4), 345-355.

Wight, G.D., Ingham, J.M., and Kowalsky, M.J. (2006). "Shake table testing of rectangular post-tensioned concrete masonry walls." *ACI Structural Journal*, 103(4), 587-595.

Wu, J., and Hanson, R.D. (1989). "Study of inelastic spectra with high damping." *Journal Structural Engineering*, ASCE, 115(6), 1412-1431.

Wyllie Jr., L.A., and Filson, J.R. (1989). "Armenia Earthquake Reconnaissance Report." *Earthquake Spectra Publication,* 89-01, Special Supplement, 152.

Yim, C.S., Chopra, A.K. and Penzien, J. (1980). "Rocking response of rigid blocks to earthquake." *Earthquake Engineering and Structural Dynamics*, 8, 565-587.

Table 1.1: Modification of the damping factor, B used in the current codes (after UBC-94, UBC-97, ATC-40 and FEMA-273)

| Damping ($\xi_{eff}$) | UBC-94 (NEHRP 94) | UBC-97 (NEHRP 97) (IBC 2000) | ATC-40 (1995) | | FEMA-273 (1997) | | |
|---|---|---|---|---|---|---|---|
| | | | Short Period | Long Period | Short Period | Long Period | NEHRP (2000) |
| 2% | - | 0.80 | 0.78 | 0.81 | 0.80 | 0.80 | 0.80 |
| 5% | 1.00 | 1.00 | 1.00 | 1.00 | 1.00 | 1.00 | 1.00 |
| 10% | 1.19 | 1.20 | 1.30 | 1.20 | 1.30 | 1.20 | 1.20 |
| 20% | 1.56 | 1.49 | 1.82 | 1.53 | 1.78 | 1.49 | 1.49 |
| 30% | 1.89 | 1.69 | 2.38 | 1.79 | 2.33 | 1.69 | 1.69 |
| 40% | - | 1.88 | 3.03 | 2.08 | 2.70 | 1.89 | 2.08 |
| 50% | - | 2.00 | 3.85 | 2.33 | 3.03 | 2.00 | 2.38 |

Table 1.2: The VISION 2000 Performance Objectives (after SEAOC, 1999).

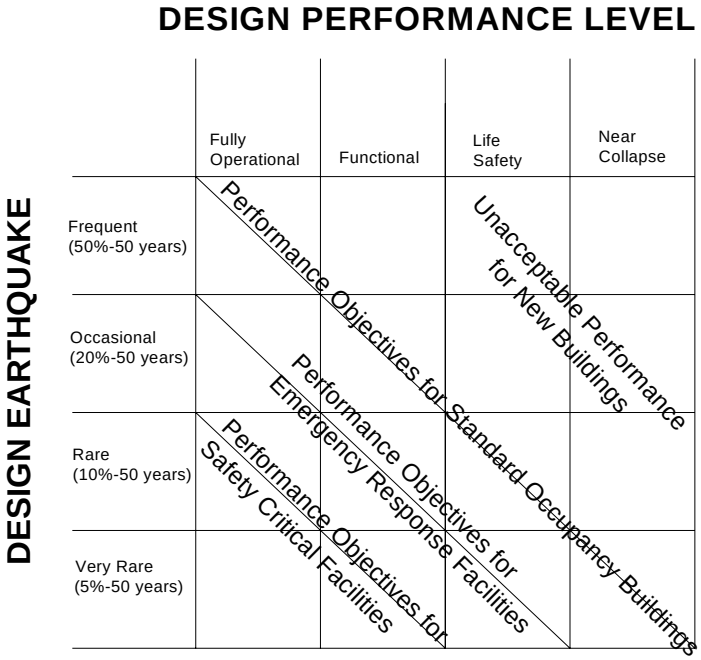


Table 1.3: Earthquake Design Levels for the study (after SEAOC, 1999)

| Event | Recurrence Interval | Probability of Exceedence |
|---|---|---|
| Frequent | 43 years | 50% in 30 years |
| Occasional | 72 years | 50% in 50 years |
| Rare | 475 years | 10% in 50 years |
| Very Rare | 970 years | 10% in 100 years |

Table 1.4: Standard Performance Level Definitions
(after ATC-40, 1995 and SEAOC,1995)

| DESIGNATION | | DESCRIPTION |
|---|---|---|
| Guidelines and Commentary (ATC,1995) | Vision 2000 (SEAOC,1995) | |
| Operational | Fully Operational | Only very minor damage has occurred. The building retains its original stiffness and strength. Non-structural components operate, and the building is available for normal use. Repairs, if required, may be instituted at the convenience of the building users. The risk of life-threatening injury during the earthquake is negligible. |
| Immediate Occupancy | Functional | Only minor structural damage has occurred. The structure retains nearly all its original stiffness and strength. Non-structural components are secured, and if utilities are available, most would function. Life-safety systems are operable. Repairs may be instituted at the convenience of the building users. The risk of life-threatening injury during the earthquake is very low. |
| Life Safety | Life Safety | Significant structural and non-structural damage has occurred. The building has lost a significant amount of its original stiffness, but retains some lateral strength and margin against collapse. Non-structural components are secure, but may not operate. The building may not be safe to occupy until repaired. The risk of life-threatening injury during the earthquake is low. |
| Collapse Prevention | Near Collapse | A limiting damage state in which substantial damage occurred. The building has lost most of its original stiffness and strength, and has little margin against collapse. Non-structural components may become dislodged and present a falling hazard. Repair is probably not practical. |

Table 1.5: Performance Levels and Permissible Structural Damage-Vertical Elements
(after SEAOC, 1999)

| Elements | Performance Level | | | |
|---|---|---|---|---|
| | Fully Operational | Operational | Life Safety | Near Collapse |
| Concrete Frame | Negligible | Minor hairline cracking (0.02"): limited yielding possible at a few locations; no crushing (strains below 0.003) | Extensive damage to beams; spalling of cover and shear cracking (<1/8") for ductile columns; minor spalling in nonductile columns; joints cracked < 1/8" width | Extensive cracking and hinge formation in ductile elements; limited cracking and/or splice failure in some nonductile columns; severe damage in short columns |
| Concrete Shear Walls | Negligible | Minor hairline cracking (0.02") of walls; coupling beams experience cracking < 1/8" width | Some boundary elements distress including limited bar buckling; some sliding at joints; damage around openings; some crushing and flexural cracking; coupling beams-extensive shear cracks; some crushing, but concrete generally remains in place | Major flexural and shear cracks and voids; sliding at joints; extensive crushing and buckling of rebar; failure around openings; severe boundary element damage; coupling beams shattered, virtually disintegrated |
| Cladding | Negligible Damage | Connections yield; some cracks or bending in cladding | Severe distortion in connections; distributed cracking, bending, crushing and spalling of cladding elements; some fracturing of cladding, falling of panels prevented | Severe damage to connections and cladding; some falling of panels |

Table 1.6: Descriptions of Damage States for Precast Walls (after HAZUS 99-SR2,2004)

| Types of structure | Damage State | Description |
|---|---|---|
| Precast Concrete Tilt-up Walls (structural) | Slight Structural Damage | Diagonal hairline cracks on concrete shear wall surfaces; larger cracks around door and window openings in walls with large proportion of openings; minor concrete spalling at few locations; minor separation of walls from the floor and roof diaphragms; hairline cracks around metal connectors between wall panels and at connections of beams to walls. |
| | Moderate Structural Damage | Most wall surfaces exhibit diagonal cracks; larger cracks in walls with door or window openings; few shear walls have exceeded their yield capacities indicated by larger diagonal cracks and concrete spalling. Cracks may appear at top of walls near panel intersections indicating "chord" yielding. Some walls may have visibly pulled away from the roof. Some welded panel connections may have been broken, indicated by spalled concrete around connections. Some spalling may be observed at the connections of beams to walls. |
| | Extensive Structural Damage | In buildings with relatively large areas of wall openings most concrete shear walls have exceeded their yield capacities and some have exceeded their ultimate capacities indicated by large, through-the-wall diagonal cracks, extensive spalling around the cracks and visibly buckled wall reinforcement. The plywood diaphragms may exhibit cracking and separation along plywood joints. Partial collapse of the roof may result from the failure of the wall-to-diaphragm anchorages sometimes with falling of wall panels. |
| | Complete Structural Damage | Structure has collapsed or is in imminent danger of collapse due to failure of the wall-to-roof anchorages, splitting of ledgers, or failure of plywood-to-ledger nailing; failure of beam connections at walls; failure of roof or floor diaphragms; failure of the wall panels. Approximately 15% of the total area of precast wall panels' buildings with complete damage is expected to have collapsed. |
| Partitions Walls (non-structural components) | Slight Non-structural Damage | A few cracks are observed at intersections of walls and ceilings and at corners of door openings. |
| | Moderate Non-structural Damage | Larger and more extensive cracks requiring repair and repainting, some partitions may require replacement of gypsum board or other finishes. |
| | Extensive Non-structural Damage | Most of the partitions are cracked and a significant portion may require replacement of finishes; some door frames in the partitions are also damaged and require re-setting. |
| | Complete Non-structural Damage | Most partition finish materials and framing have to be replaced; damaged studs repaired, and walls finished. Most door frames may also have to be repaired and replaced. |
| Exterior Wall Panels | Slight Non-structural Damage | Slight movement of the panels, requiring realignment. |
| | Moderate Non-structural Damage | The movements are more extensive; connections of panels to structural frame are damaged requiring further inspection and repairs; some windows frames may need realignment. |
| | Extensive Non-structural Damage | Most of the panels are cracked or otherwise damaged and misaligned, and most panel connections to the structural frame are damaged requiring through review and repairs; a few panels fall or are in imminent danger of falling; some window panels are broken and some pieces of glass have fallen. |
| | Complete Non-structural Damage | Most panels are severely damaged, most connections are broken or severely damaged, some panels have fallen and most are in imminent danger of falling; extensive glass breakage and falling. |

Table 1.7: Structural Performance Levels and Damage for Concrete Walls (after FEMA-273, 1997)

| Types of structures | Performance Level | Descriptions |
|---|---|---|
| Concrete Walls (structural components) | Operational | Negligible |
| | Immediate Occupancy | Minor hairline cracking of walls, < 1/16" wide. Coupling beams experience < 1/8" width. Drifts with 0.5% transient and negligible permanent. |
| | Life Safety | Some boundary element distress, including limited buckling of reinforcement. Some sliding at joints. Damage around openings. Some crushing and flexural cracking. Coupling beams: extensive shear and flexural cracks; some crushing, but concrete generally remains in place. Drift at 1.0% transient; 0.5% permanent. |
| | Collapse Prevention | Major flexural and shear cracks and voids. Sliding at joints. Extensive crushing and buckling of reinforcement. Failure around openings. Severe boundary element damage. Coupling beams shattered and virtually disintegrated. Drift at 2% transient or permanent. |
| Precast Concrete Connections (structural components) | Operational | Negligible |
| | Immediate Occupancy | Minor working at connections; cracks <1/16" width at connections. |
| | Life Safety | Local crushing and spalling at connections, but no gross failure of connections. |
| | Collapse Prevention | Some connection failures but no elements dislodged. |
| Cladding (non-structural components) | Operational | Connections yield; minor cracks (<1/16" width) or bending in cladding. |
| | Immediate Occupancy | Connections yield; minor cracks (< 1/16" width) or bending in cladding. |
| | Life Safety | Severe distortion in connections. Distributed cracking, bending, crushing, and spalling of cladding elements. Some fracturing of cladding, but panels do not fall. |
| | Collapse Prevention | Severe damage to connections and cladding. Many panels loosened. |

Table 1.8: The consequences of failure according to the Building Importance Category (after, AS/NZS 1170.5).

| Types Structures | Consequence of failure | Importance Category | Descriptions |
|---|---|---|---|
| Minor structures | Low | 1 | Low consequence for loss of human life, or small or moderate economic, social or environmental consequences. |
| Normal structures | Ordinary | 2 | Medium consequences for loss of human life, or considerable economic, social or environmental consequences. |
| Major structures | High | 3 | High consequences for loss of human life, or very great economic, social or environmental consequences. |
| Post-disaster structures | | 4 | |
| Exceptional structures | Exceptional | 5 | Circumstances where reliability must be set on a case by case basis |

Table 1.9 : Design annual probability of exceedance for earthquake 50 year design of working life (after, AS/NZS 1170.5)

| Annual probability of exceedence | Return Period Factor R | Building Importance Category | | | |
|---|---|---|---|---|---|
| | | 1<br>Low hazard structures | 2<br>Normal Buildings | 3<br>Important buildings | 4<br>Critical Post Diaster Buildings |
| 1/2500 | 1. 8 | | | | ULS |
| 1/1000 | 1. 3 | | | ULS | |
| 1/500 | 1. 0 | | ULS | | SLS2 |
| 1/100 | 0. 5 | ULS | | | |
| 1/25 | 0. 25 | | SLS1 | SLS1 | SLS1 |

(a)

(b)


(c)

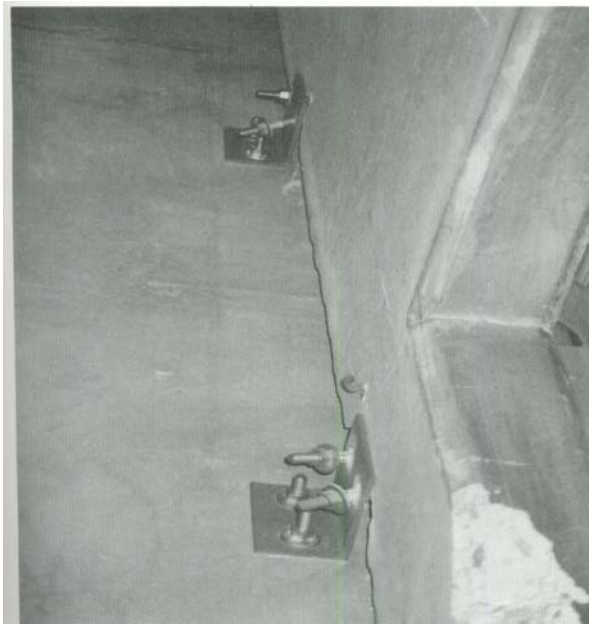

(d)

Figure 1.1: Several examples of structural damage to precast wall panels after earthquake: (a) the collapse of wall panels and roofs at Vector Electronics industrial building during San Fernando Earthquake (Murphy,1973); (b) partial collapse of roof due to connectors at wall pulling through edges of plywood panels and glulam beam (James and Neil, 1994); (c) wall panels bowed severely due to out-of-plane inertial loads and required bracing (notes: the arrow shows the crack at top of openings) (Wyllie and Filson, 1989); and (d) the shear connectors between two perpendicular precast wall panels were damage during the earthquake (Hamburger et al.,1988).

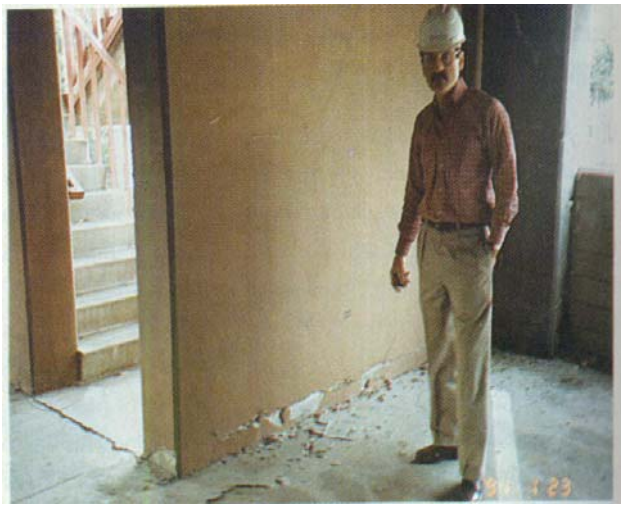

(a)

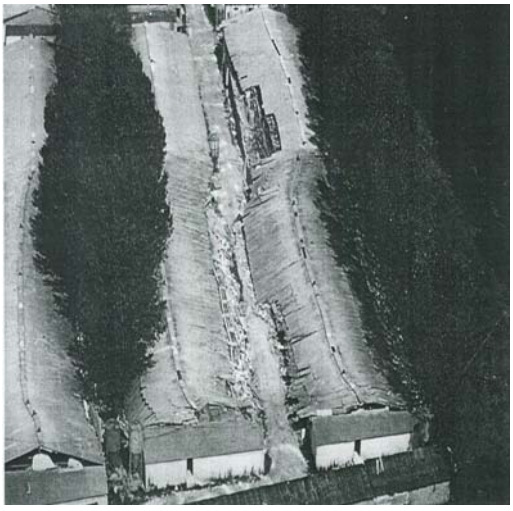

(b)

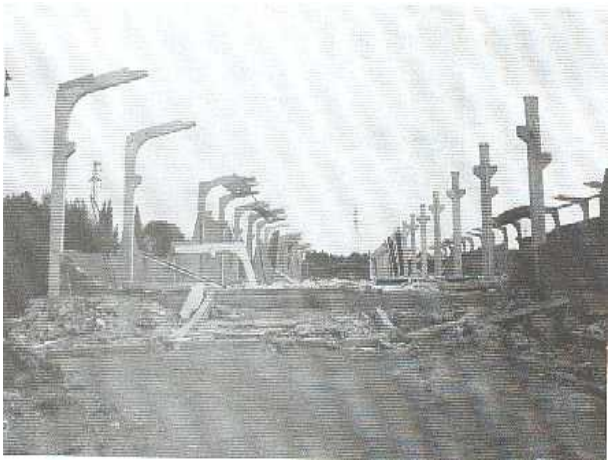

(c)

(d)

Figure 1.2: The construction failure and collapse of precast wall panels ; (a) failure of construction joint and connection precast wall panels and beam at garage parking during Northridge Earthquake, 1994 (Iverson & Hawkins, 1994); (b) partial collapse of three agriculture warehouse at Arifiye during Turkey Earthquake, 1999 (Krinitzsky et al., 2000); (c) failure of cantilever head connection on top of columns and total collapse of industrial facilities during Kocaeli Earthquake,1999 (Saatcioglu et al., 2001); and (d) connection failures between precast wall panels at Kukma Primary School during Bhuj Earthquake, 2001 (Ghosh, 2001).

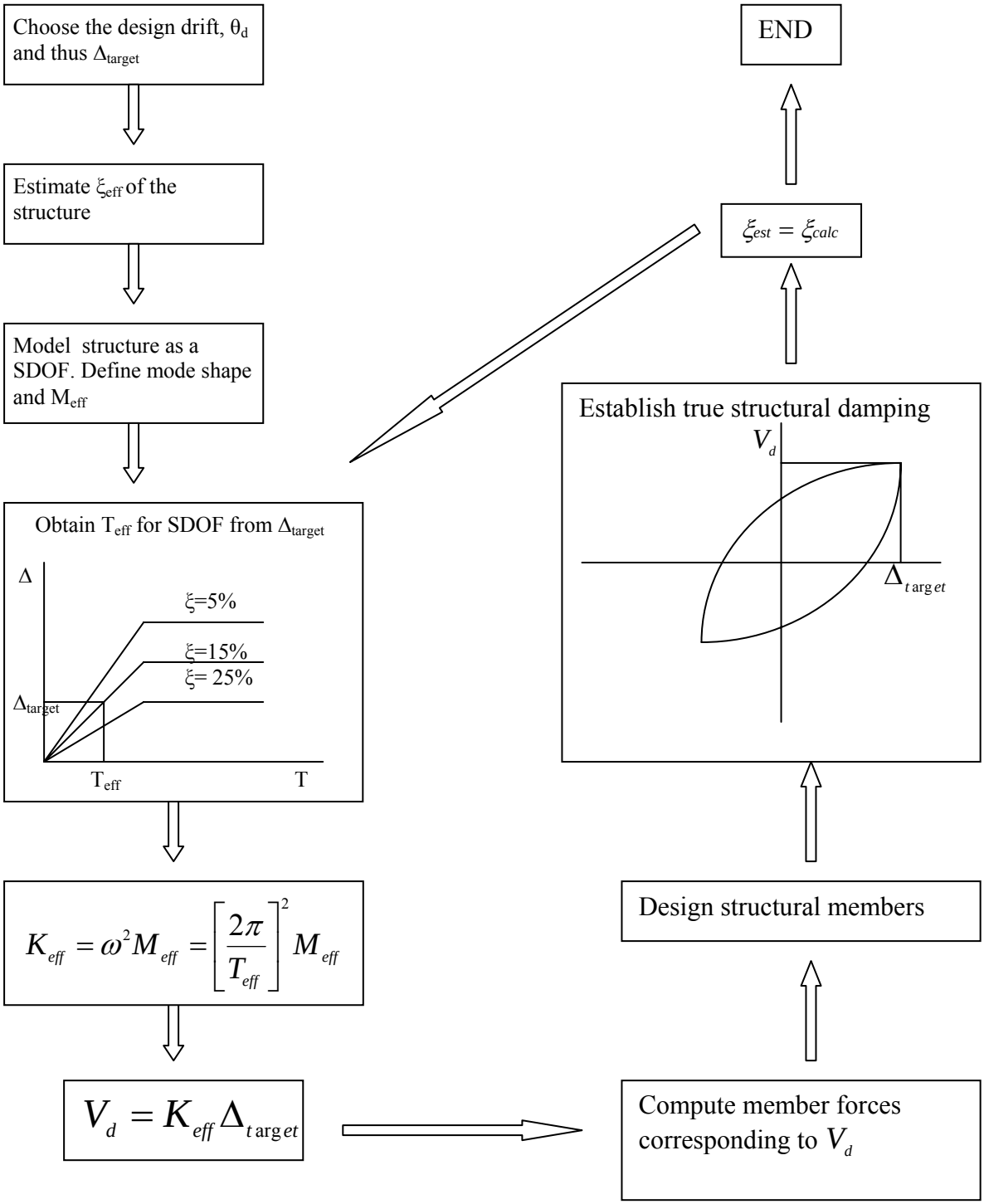


Figure 1.3: The flowchart for direct displacement based design procedure (FIP, 2000).

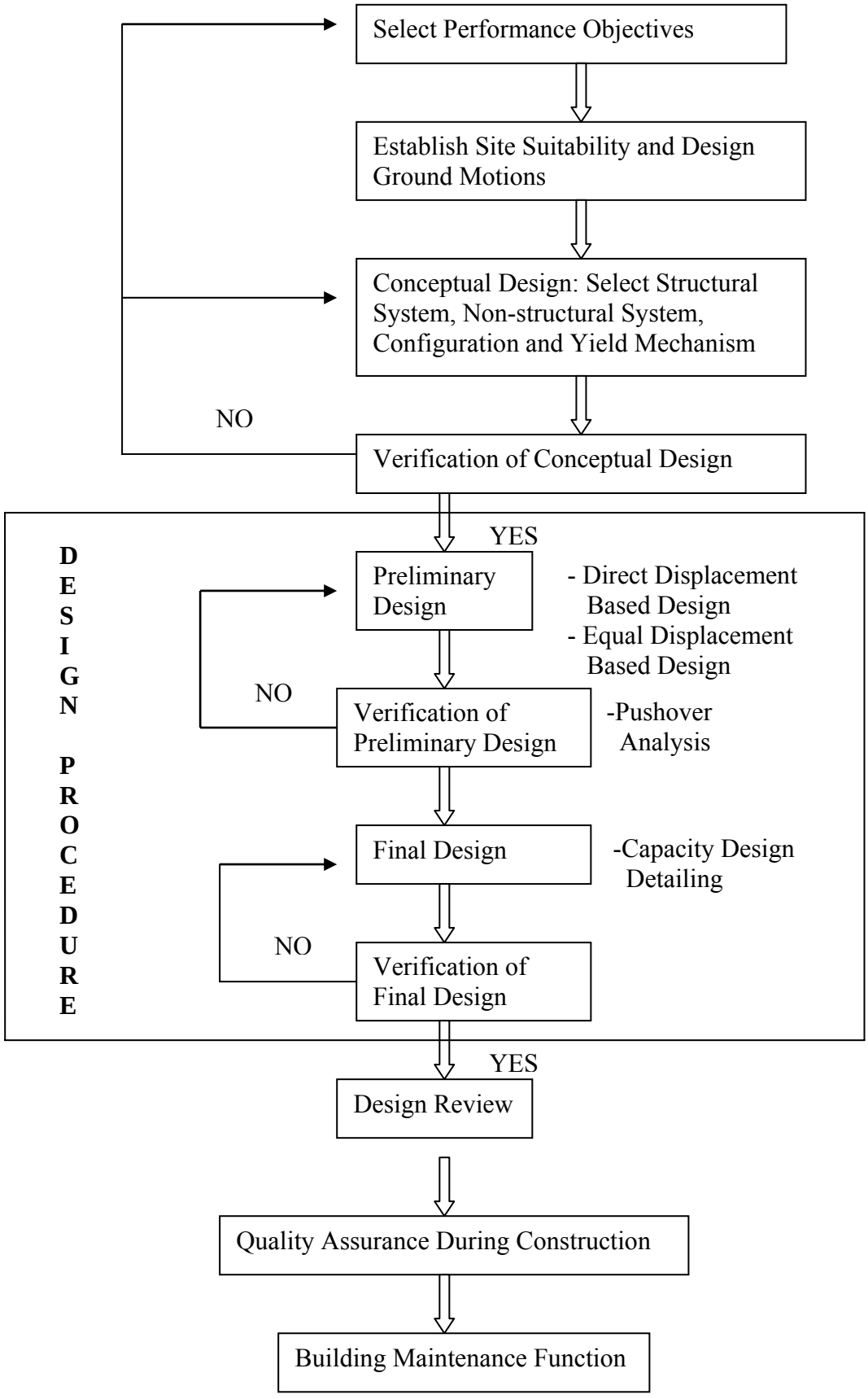


Figure 1.4: Flow chart of the performance-based seismic engineering design (after SEAOC, 1999).

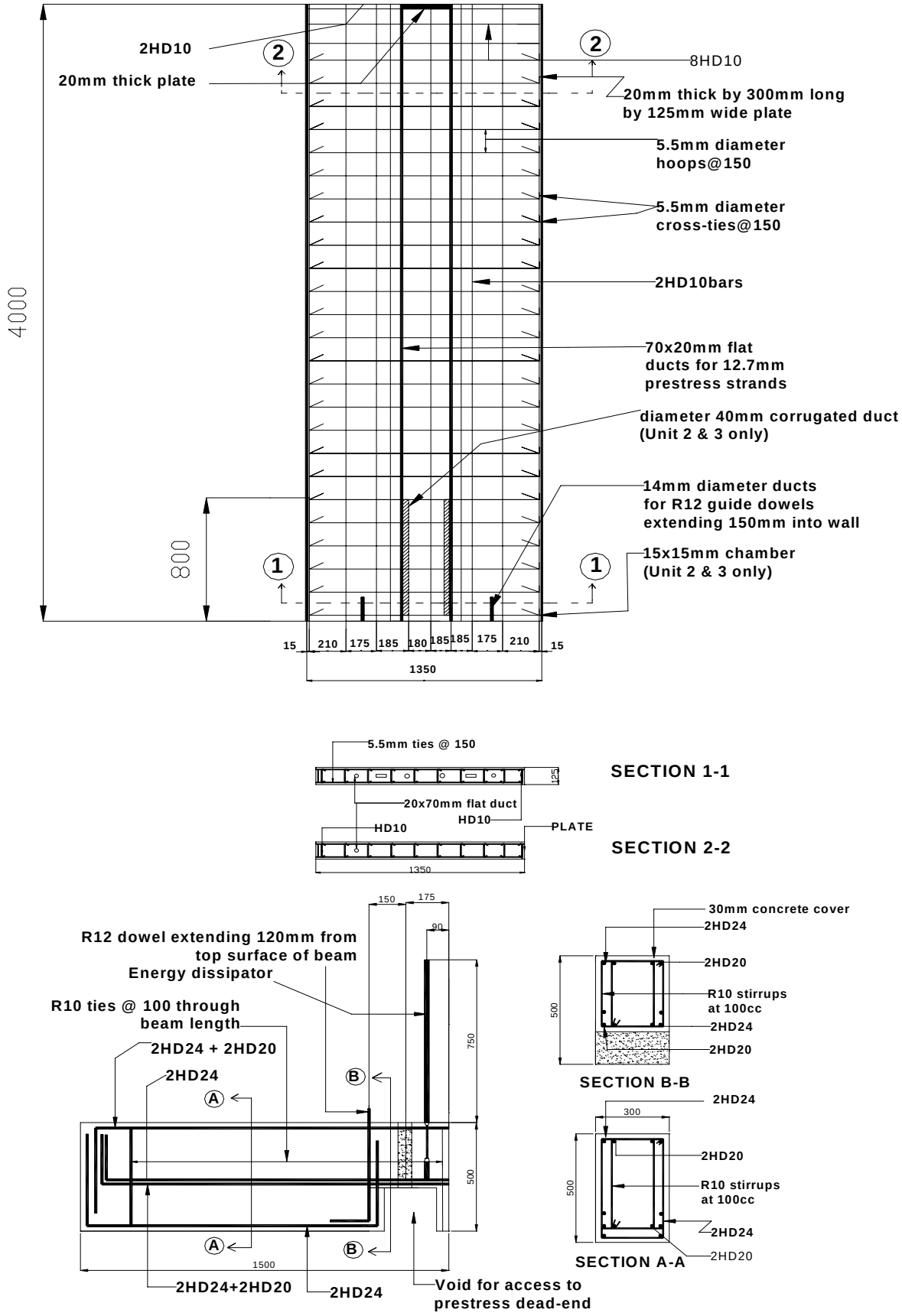


Figure 1.5: Reinforcement detail of Unit 1, Unit 2 and Unit 3 (Rahman and Restrepo, 2000).

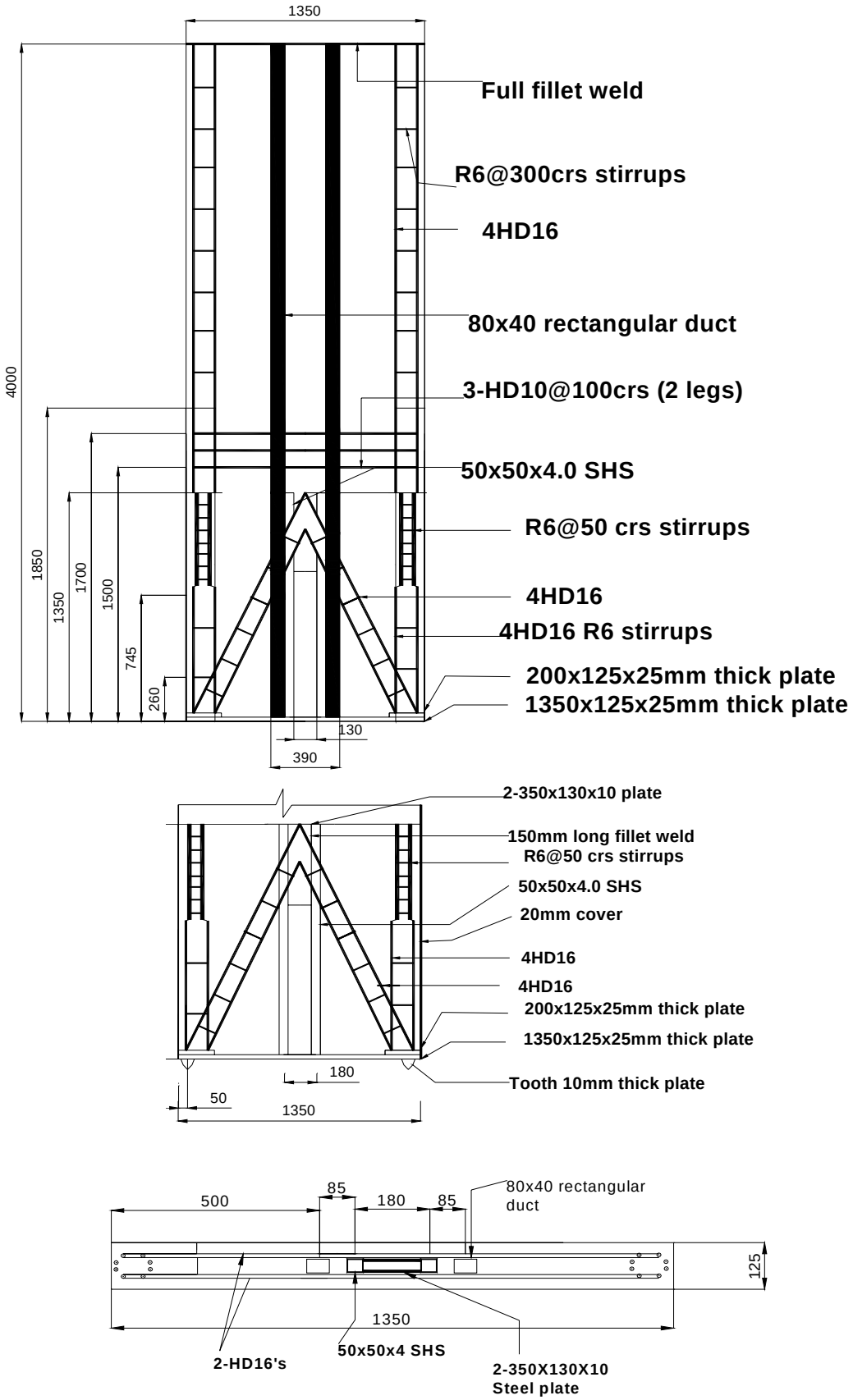


Figure 1.6: The detailing of wall panel in Unit 2 of hybrid system (Holden, 2001)

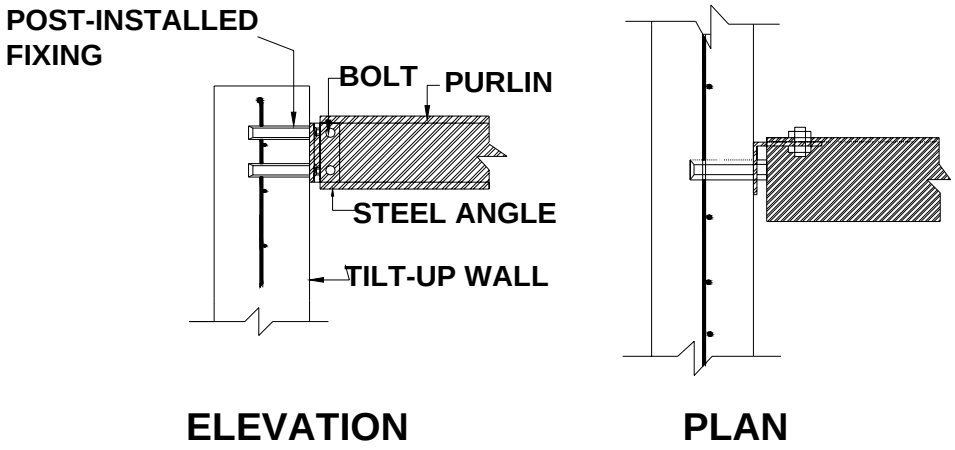


Figure 1.7: The detail connection between precast wall and roof steel trusses (Restrepo et al.,1996).

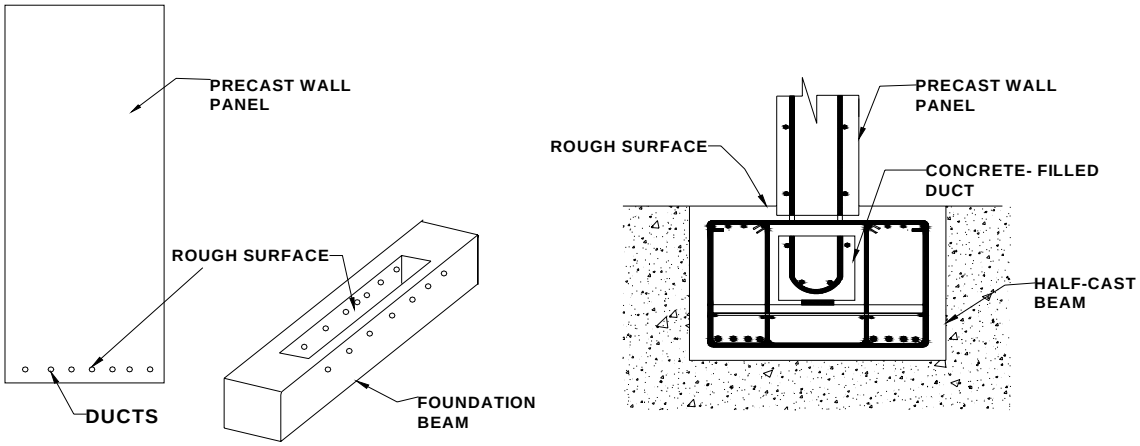


Figure 1.8: Connection detail for walls embedded in the foundation beam (Holden et al.,2003).

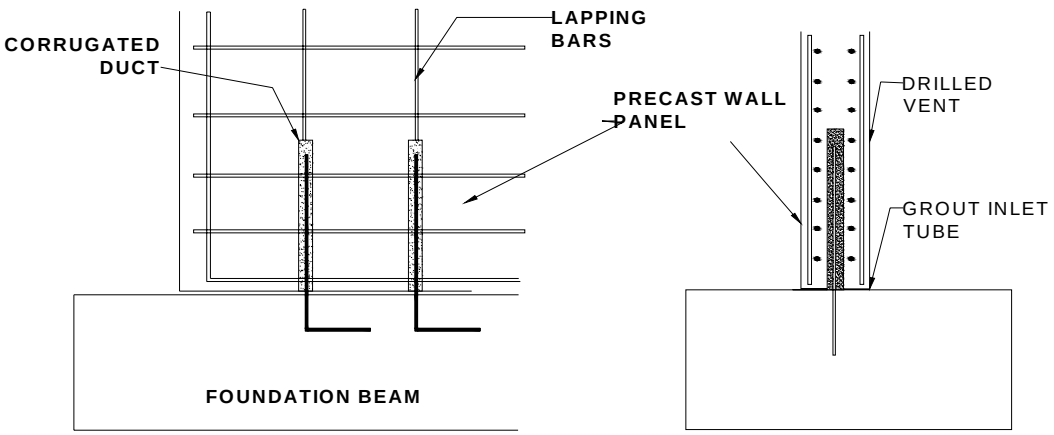


Figure 1.9: Wall-foundation beam connection through grouted ducting (Restrepo et al.,1996).

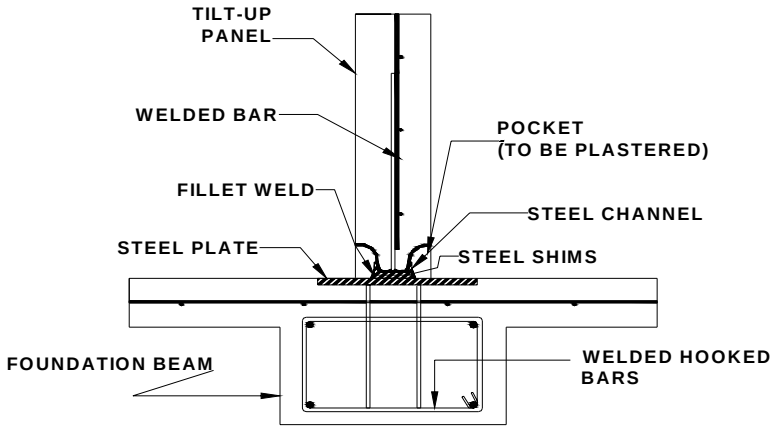


Figure 1.10: The connection between wall and foundation beam (Restrepo et al., 1996).

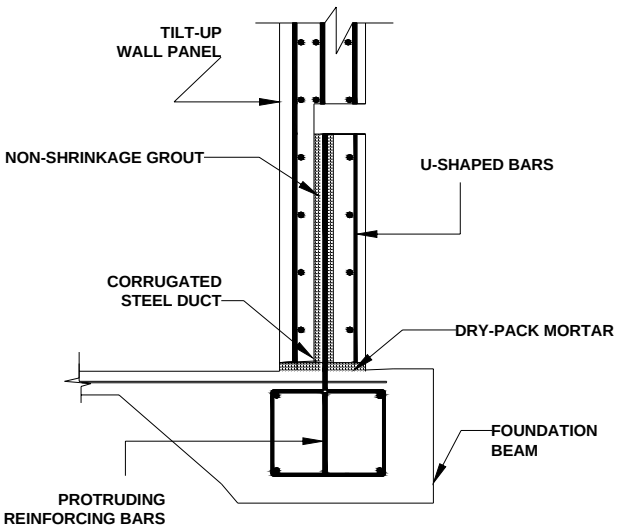


Figure 1.11: The typical connection between tilt-up wall and foundation beam (Liyanage, 2004).

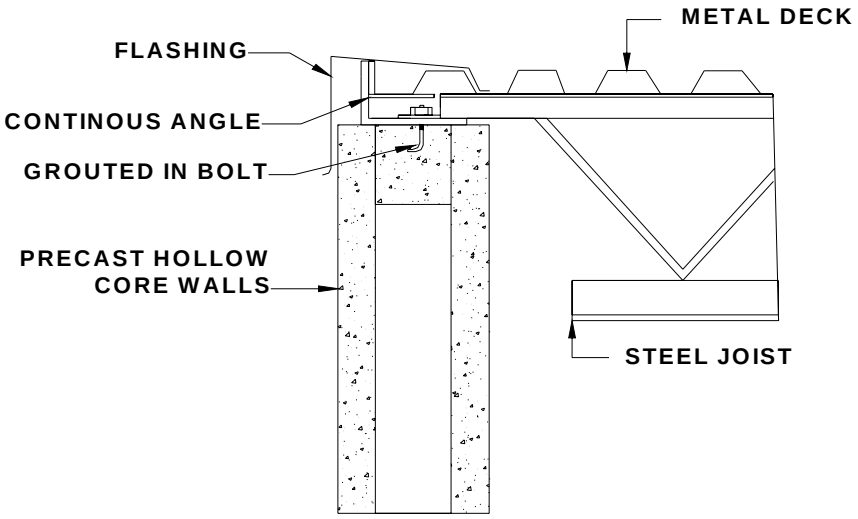


Figure 1.12: Load bearing precast hollow core wall panels supporting the steel frame (Precast Technology, 1991).

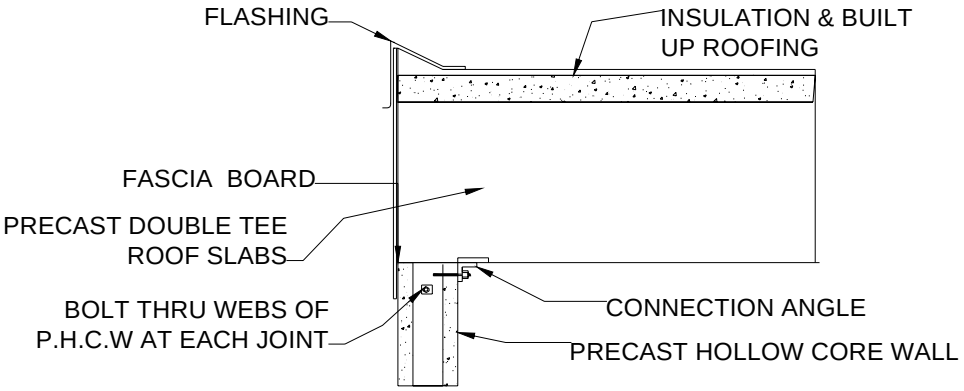


Figure 1.13: Precast roof slabs sitting on precast hollow core walls (Precast Technology, 1991).

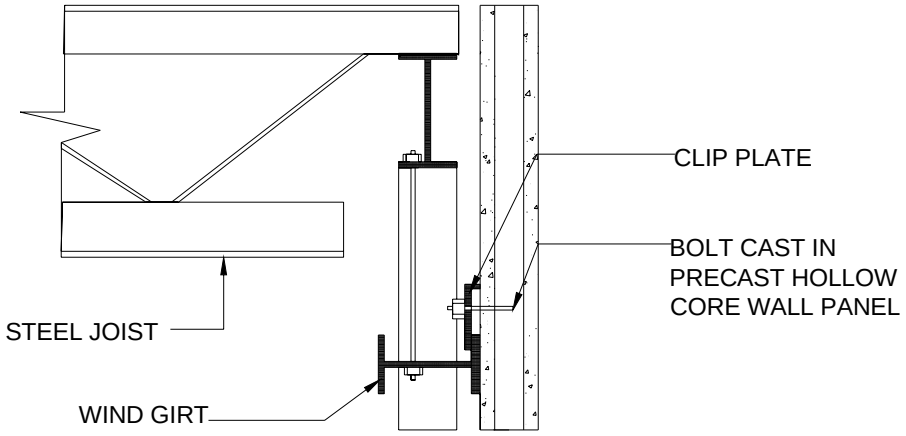


Figure 1.14: Steel frame structure sitting on non-load bearing precast hollow core wall (Precast Technology, 1991)

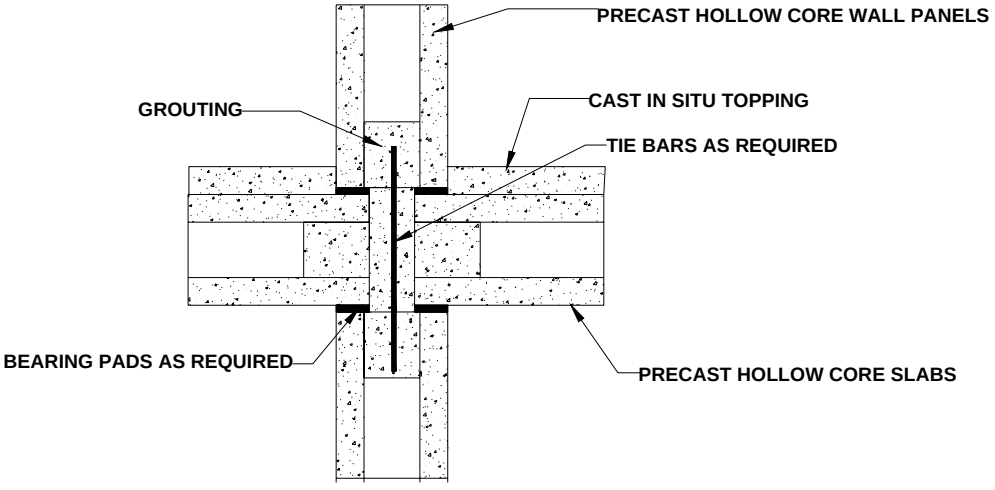


Figure 1.15: Connection between precast hollow core slabs and internal precast hollow core walls (Precast Technology, 1991).

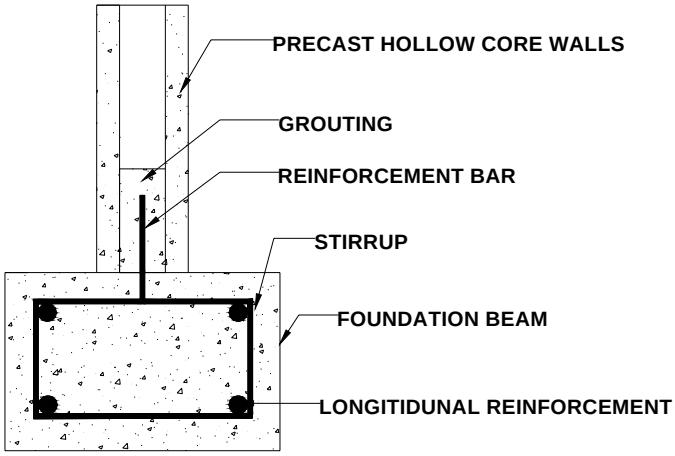


Figure 1.16: Precast hollow core wall is located at the centre of foundation (Precast Technology, 1991)

Figure 1.17: A stack of precast hollow core wall panels are ready for erection.

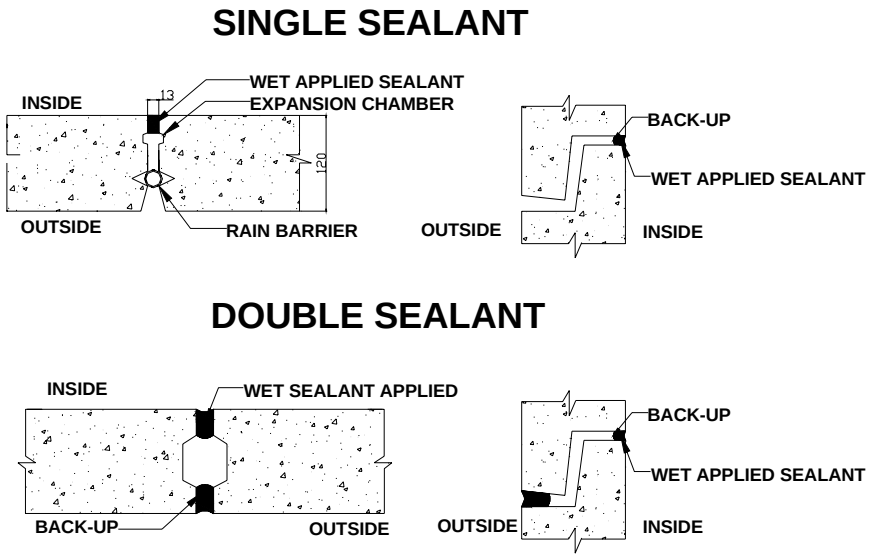


Figure 1.18: Two methods connecting precast wall panels using sealant (CIRIA, 1998)

Figure 1.19: Sealing process in connecting precast hollow core walls using a crane.

Figure 1.20: Precast hollow core wall panels with opening.


Figure 1.21: A typical industrial building using precast hollow core walls as load-bearing wall constructed in Malaysia.

# CHAPTER 2

# SEISMIC BI-LATERAL PERFORMANCE OF PRECAST CONCRETE HOLLOW CORE WALLS

## SUMMARY

Two geometrically similar precast concrete hollow core walls with their foundations are tested under reversed cyclic quasi-static in-plane, out-of-plane and bi-lateral loading. Both of the walls are designed to carry roof (gravity) loading and resist lateral loads by rocking on their foundation. A shaking table is used in slow motion to perform the bi-lateral quasi-static experiments. Wall specimens are detailed with steel-armouring at their base-to-foundation interfaces to provide a measure of damage protection. In addition to the longitudinal pretensioned prestress in the hollow core wall units, both specimens are detailed so that supplementary post-tensioned prestress along with sacrificial mechanical energy dissipators and fuse-bars can be added. Wall 1, with a fixed location of bonded fuse-bars and unbonded tendons, is tested under various biaxial load paths including "4-leaf clover" patterns. Wall 2 is tested with four different configurations of mechanical energy dissipators utilizing unbonded post-tensioned tendons and unbonded fuse-bars. Experimental results show that due to the damage avoidance details both walls perform very well under various load paths without any discernible structural damage up to 2.0% drift. Results also demonstrate that the main determinant of wall performance is the level of post-tensioned prestress applied. Prestress also affects the initial stiffness and uplift strength along with the post-uplift (rocking) performance. The location and cross-sectional area of energy dissipators and unbonded tendons can also markedly affect performance. These experimental results are used to validate rigid body kinematic design models including equivalent viscous damping resulting from the presence of the me-

chanical energy dissipators. It is concluded that for initial design equivalent viscous damping of 10 percent may be able to accommodate the effects of hysteretic behaviour.

## 2.1 INTRODUCTION

Historically, the principal criterion in designing seismic resistant buildings is to maintain life-safety of the structure even though some damage is permitted. Fintel (1995) concluded that based on 30 years of evidence, reinforced concrete buildings with shear walls performed well in earthquakes. However, on the contrary, evidence from the 1964 Alaska earthquake (Berg and Stratta, 1964), the Armenia earthquake (Wyllie and Filson, 1989), the1994 Northridge earthquake (Iverson and Hawkins, 1994), the 1999 Koceali (Turkey) earthquake (Youd et al., 2000) and the 2001 Bhuj (India) earthquake (Ghosh, 2001) show that precast concrete wall buildings did not perform very well, particularly at connections and junctions with other structural components. And although many buildings did perform sufficiently well that life-safety was preserved, substantial damage to the walls in many buildings led to loss of amenity including major business interruption.

This research investigates the viability of a Damage Avoidance Design (DAD) philosophy applied to a class of single storey wall buildings. The objective is to explore the seismic performance of a single precast hollow core wall unit under quasi-static and bi-directional lateral loading including the effects of gravity load. This research extends the DAD work of Holden et al. (2003) who demonstrated that good seismic performance of precast wall systems can be achieved by avoiding the formation of a plastic hinge at the bottom of the wall through disconnecting the wall-foundation interface and clamping the precast wall unit to the foundation using post-tensioned unbonded tendons. They further

showed that if steel armouring is used at the wall base-foundation interface, then the damage to the precast panels can be avoided.

This research examines an alternative type of precast wall by substituting conventional solid reinforced concrete precast panels with precast hollow core panels which only possess minimal longitudinal prestress and no other reinforcing bars. Thus, a second main purpose of this study is to investigate whether hollow core precast wall panels without transverse reinforcement can behave well under seismic loading conditions. This study also investigates the efficacy of different classes of internal and external mechanical energy dissipation devices along with different levels of initial prestress. Recommendations related to an optimum solution for the cross-sectional area and lengths of energy dissipators with initial prestressing of unbonded tendons are also described.

## 2.2 DESIGN CONCEPTS OF PRECAST WALL PANELS

Figure 2.1(a) presents the conceptual design of a prototype warehouse or industrial building where it is envisaged precast hollow core wall units would be used as the principal structural and cladding elements. The plan view of the conceptual prototype structure used in this study is shown in Figure 2.1(b). The "seismic walls" carry gravity and wind loads from the roof where rafters are seated on top of these structural elements. Steel portal column legs are not needed as the wall panels act as load-bearing members. Infill panels are used between the "seismic walls" which are referred to as "non-seismic walls" which are principally designed to act as cladding. These infill wall units are only required to sustain their self-weight and wind face-loads. The tributary area from roof loading is designed to be carried by the seismic wall panels. Resistance of lateral wind

and seismic forces is via a longitudinal “wind truss” system that acts through a roof diaphragm.

Figure 2.1(c) shows the front elevation of 1200mm wide wall units that are held in position by an inverted channel which acts as an edge chord of the “wind truss”. This continuous steel channel is also used to seat the rafters and anchor the vertical post-tensioned prestress and unbonded fuse-bars. This research seeks to design, construct and test a subassembly “seismic wall” under bi-lateral loading. The “seismic wall” is designed and detailed according to Damage Avoidance Design (DAD) principles as proposed by Mander and Cheng (1997) where the bottom of the wall is protected with steel-armouring.

## 2.3 THEORETICAL RESPONSES OF A SINGLE ROCKING PRECAST HOLLOW CORE WALL

This section examines wall behaviour during rocking. Displacements are amplified before and after rocking due to the wall being discontinuous with its foundation. Figure 2.2 shows the basis for determining the displacement amplification factor $(\lambda_o)$ for a rocking wall. This can be approximately assessed by adopting St Venant’s principle along with a modified distribution of curvatures in the disturbed zone at the base of the wall. Figure 2.2(a) depicts the total lateral displacement of a structural wall panel that consists of the elastic displacement that arises from two components of curvature: linear elastic curvatures; and nonlinear curvatures in the end disturbed zone. Although the moment diagram is linear, as shown in Figure 2.2 (b), it leads to an overall curvature distribution shown in Figure 2.2(c). The triangular curvature distribution represents the uncracked (gross sec-

tion) elastic curvatures, while the additional nonlinear curvature at the base of the wall is assumed to follow a cubic curve that is inversely proportional to the effective depth of the member participating in the calculation of the local second moment area. This reduced section effect is shown in Figure 2.2(d) where only a portion of the concrete above the armouring $(B_r)$ is compressed at the toe of the wall, whereas the other part (shaded black) is a non-participating "dead zone". This modified curvature effect amplifies the wall displacement and can be approximately represented using modified beam theory as follows.

The total displacement $(\Delta_t)$ is made up of a usual linear elastic part $(\Delta_e)$ plus a non-linear (inelastic) portion $(\Delta_i)$ such that $\Delta_t = \Delta_e + \Delta_i$. The displacement amplification factor $(\lambda_o)$ is defined as the ratio of total displacement divided by the usual (fixed-base) linear elastic displacement as follows

$$\lambda_o = \frac{\Delta_t}{\Delta_e} = \frac{\Delta_e + \Delta_i}{\Delta_e} = 1 + \frac{\Delta_i}{\Delta_e} \tag{2-1}$$

From this the effective section modulus can be calculated as follows:

$$EI_{eff} = \frac{EI_g}{\lambda_o} \tag{2-2}$$

Based on the curvature distribution (see Figure 2.2(c)), the component of displacement from the linear elastic curvature is given by

$$\Delta_e = \frac{1}{3}\phi_e H^2 \tag{2-3}$$

where $\phi_e$ = elastic curvature and $H$ = wall height.

When the wall is laterally loaded, the concrete at the base (toe) of the wall is not fully compressed and the effective rigidity needs to be reduced accordingly. By invoking St Venant's principle, it will be assumed herein that the partial dead zone, shown in Figure 2.2 (d), extends over one-wall width $(B)$.

The added displacement arising from amplification of the curvature at the toe of the wall can be found by assuming a cubic distribution as shown in Figure 2.2(c) as derived below

$$\Delta_i = \frac{1}{4}\phi_i B(H - B/5) \tag{2-4}$$

where $\phi_i$ = added inelastic curvature due to the concentration of forces toward the toe of the wall; and $B$ = wall width. The total curvature at the base of the wall is $\phi_t = \phi_e + \phi_i$.

Substituting equation 2-3 and 2-4 into equation 2-1, the displacement amplification factor becomes

$$\lambda_o = 1 + \frac{3}{4}\frac{\phi_i}{\phi_e}\frac{B}{H}\left(1 - \frac{B}{5H}\right) \tag{2-5}$$

The ratio $\phi_i / \phi_e$ can be found as follows. First, by assuming an average beam rigidity $EI_{re}$ in the disturbed region at the bottom of the cantilever, the relationship between effective rigidity and curvature can be expressed as

$$\frac{M/EI_{re}}{M/EI_g} = \frac{I_g}{I_{re}} = \frac{\phi_t}{\phi_e} = \frac{\phi_i + \phi_e}{\phi_e} = \frac{\phi_i}{\phi_e} + 1 \tag{2-6}$$

The ratio of the gross inertia $(I_g)$ to a reduced inertia $(I_{re})$ is given by the following equation

$$\frac{M/EI_{re}}{M/EI_g} = \frac{I_g}{I_{re}} = \frac{b_w B^3/12}{b_w B_r^3/3} = \frac{1}{4}\left(\frac{B}{B_r}\right)^3 \tag{2-7}$$

in which $M$ = maximum moment at the base of the wall, $E$ = Young's Modulus of concrete, $I_g$ = gross moment of inertia, $I_{re}$ = reduction moment of inertia, $b_w$ = wall thickness and $B_r$ = in-plane contact base width of compressed concrete (immediately above any steel armouring).

By equating equation 2-6 with equation 2-7, the curvature ratio becomes

$$\frac{\phi_i}{\phi_e} = \frac{1}{4}\left(\frac{B}{B_r}\right)^3 - 1 \tag{2-8}$$

The axial compression force $(P)$ is assumed to exert a triangular pressure distribution in the concrete at the toe of contact width $(B_r)$ which represents a certain portion of the wall's width. Thus, the axial compression force $(P)$ exerted on the wall is given by the following equation

$$P = \frac{1}{2} f_c b_w B_r = \frac{1}{2} f_c A_g \frac{B_r}{B} \tag{2-9}$$

in which $P$ = total compression force, $f_c$ = maximum concrete compressive stress and $A_g$ = gross bottom cross-section of the wall. By assuming a maximum concrete compression stress of $f_c = 0.8 f_c^{'}$ the compressed stressed length ratio may be found as

$$\frac{B}{B_r} = \frac{0.4}{P/f_c^{'} A_g} \tag{2-10}$$

By substituting equation 2-10 into equation 2-8, thus it becomes

$$\frac{\phi_i}{\phi_e} = \frac{1}{4}\left(\frac{B}{B_r}\right)^3 - 1 = \frac{0.016}{\left(P/f_c^{'} A_g\right)^3} - 1 \tag{2-11}$$

Finally, substituting equation 2-11 into equation 2-5, the displacement amplification factor becomes

$$\lambda_o = \frac{\Delta_t}{\Delta_e} = 1 + \left( \frac{0.012}{\left(P / f_c^{'} A_g\right)^3} - \frac{3}{4} \right) \left( \frac{B}{H} \right) \left( 1 - \frac{B}{5H} \right) \qquad (2\text{-}12)$$

For the wall tested herein typical values are $P = (W_r + W_w + P_p + P_d) = 1000kN$, $f_c^{'} = 40N/mm^2$, $B = 1200mm$, $b_w = 200mm$ and $H = 2800mm$, hence

$$\lambda_o = \frac{\Delta_t}{\Delta_e} = 1 + \left( \frac{0.012}{(0.104)^3} - \frac{3}{4} \right) \left( \frac{1200}{2800} \right) \left( 1 - \frac{1200}{5(2800)} \right) = 4.9$$

Thus from equation 2-2, $EI_{eff} \approx 0.2EI_g$. It should be noted that the outcome in calculating $\lambda_o$ is quite sensitive to the level of maximum axial compressive stress assumed at the toe of the wall. A maximum value of $0.8 f_c^{'}$ was assumed as subsequent experimentation did not indicate any compressive cracks. It will also be subsequently shown that the effective stiffness is in the order of 20% of $EI_g$ as indicated by the above approximate assessment.

Figure 2.3 shows six stages of the load displacement behaviour of a single wall subjected to in-plane loading. The location of the unbonded post-tensioned tendon, fuse-bar and gravity load from the roof is assumed to act at the centre of the block. The wall rocks at its pivot point (O) which is situated at the bottom corner of the wall. Each position on the curve can be represented by a simple mathematical formula in terms of their lateral loads and displacements as follows. The initial stiffness of the wall depends on the effective rigidity $(EI_{eff})$ as derived above.

- Pre-rocking: Points 0-1

Initially the wall behaves elastically with respect to lateral load and displacement. The lateral displacement can be derived using the combination of flexural deformation of an uncracked section. Thus at Point 1 the lateral resistance is provided by gravity load and the prestress force within the tendons

$$F_1 = (W_e + P_p)\frac{B}{2H} - \frac{W_e \Delta_1}{H} \quad \text{and} \quad \Delta_1 = \frac{H^3 F_1}{3E_c I_{eff}} \tag{2-13}$$

in which $F_1 =$ lateral force at Point 1, $W_e = W_r + 2/3W_w$, $W_e =$ effective seismic weight acting at the top of the wall made up from tributary weight of the roof $W_r$, and $W_w =$ weight of one wall panel, $P_p =$ prestressing of unbonded tendons, $B =$ wall width, $H =$ wall height, $\Delta_1 =$ lateral displacement at Point 1 and $EI_{eff} = EI_g / \lambda_o$.

- Elastic Rocking: Points 1-2

Between Points 1 and 2 elastic rocking of the wall is initiated. The apparent stiffness is due to the elastic straining of the unbonded prestressing tendons and fuse-bars. The lateral load and displacement at Point 2 are formulated as:

$$F_2 = \left(W_e + P_p + P_d\right)\frac{B}{2H} - \frac{W_e \Delta_2}{H} \quad \text{and} \quad \Delta_2 = \frac{F_2 - F_1}{K_p + K_{ed}} + \Delta_1 \tag{2-14}$$

in which $F_2 =$ lateral force at Point 2, $\Delta_2 =$ lateral displacement at Point 2, $P_d =$ forces in fuse-bars before yielding, $K_p = \frac{B}{2H}\left(\frac{E_{sp}\Sigma A_p}{L_p}\right) =$ stiffness of the unbonded tendons before yielding, $K_{ed} = \frac{B}{2H}\left(\frac{E_{sd}\Sigma A_f}{L_f}\right) =$ stiffness of the energy dissipators before yielding, $E_{sp} =$ Young's Modulus for unbonded tendons, $E_{sd} =$ Young's Modulus for energy dissipators, $\sum A_p =$ summation of the area for unbonded tendons, $L_p =$ length of un-

bonded tendons, $\sum A_f$ = summation of the area for fuse-bars and $L_f$ = length of fuse-bars.

- Rocking with yielded fuses and elastic tendons: Points 2-3

Although the wall is still mostly elastic, the stiffness of the wall is reduced due to yielding of the fuse-bars, while the tendons remain elastic. The fuse-bars reach the strain hardening plateau at Point 3. The equations for the lateral load and displacement are given below:

$$F_3 = \left(W_e + P_p + P_d^{'}\right)\frac{B}{2H} - \frac{W_e \Delta_3}{H} \quad \text{and} \quad \Delta_3 = \frac{F_3 - F_2}{K_{ed}^{'} + K_p} + \Delta_2 \tag{2-15}$$

in which $F_3$ = lateral force at Point 3, $\Delta_3$ = lateral displacement at Point 3, $P_d^{'} = \sum A_f f_{su}$ = ultimate force in fuse-bars, $K_{ed}^{'} = \frac{B}{2H}\left(\frac{E_s^{'} \Sigma A_f}{L_f}\right)$ where $E_s^{'} = (f_{su} - f_y)/(\varepsilon_{su}/2 - \varepsilon_y)$, $f_y$ = fuse-bars' yield strength, $f_{su}$ = fuse-bars' ultimate strength, $\varepsilon_y$ = fuse-bars' yield strain and $\varepsilon_{su}$ = fuse-bars' ultimate strain.

- Rocking with yielded tendons: Points 3-4

Both fuse bars and tendons yield and fuse-bars operate in the plastic range. P-Δ effect should be deducted from the wall stiffness owing to large lateral displacement. The static lateral equations for load and displacement are as follows:

$$F_4 = \left(W_e + P_d^{'} + P_{py}\right)\frac{B}{2H} - \frac{W_e \Delta_4}{H} \quad \text{and} \quad \Delta_4 = \frac{F_4 - F_3}{K_p} + \Delta_3 \tag{2-16}$$

in which $F_4$ = lateral force at Point 4, $\Delta_4$ = lateral displacement at Point 4 and $P_{py} = f_y \sum A_p$ = forces in unbonded tendons when they yield.

- Elastic Unloading: Points 4-5

The forces in fuse-bars and tendons are on the unloading branch 4-5. The stiffness of the wall is similar to line 2-3 but moving in the opposite direction. This continues until the dissipator forces are balanced and the equations are given below:

$$F_5 = \left(W_e + P_p\right)\frac{B}{2H} - \frac{W_e \Delta_5}{H} \quad \text{and} \quad \Delta_5 = \Delta_4 - \left(\frac{F_4 - F_5}{K_p + K_{ed}^{'}}\right) \tag{2-17}$$

$F_5 =$ lateral force at Point 5 and $\Delta_5 =$ lateral displacement at Point 5.

- Elastic Recentring: Points 5-6

From Point 5, the unloading path returns to its original position due to the self-centring effect of the unbonded tendons.

The rocking mechanism of precast hollow core walls in an out-of-plane direction can be modelled using similar rigid body kinematics but with greater significance on the P-Δ effects. The initial flexural behaviour for out-of-plane force is given by:

$$F_{out} = \frac{3E_c I_{eff}}{H^3}\Delta_{out} = \frac{3E_c I_{eff}}{H^2}\theta_{out} \tag{2-18}$$

For equilibrium of the wall, $\dfrac{(P_p + P_d + W_r)b_w}{2H} - W_r\theta_{out} = \dfrac{3E_c I_{eff}}{H^2}\theta_{out}$ (2-19)

$$\theta_{out} = \frac{(P_p + P_d + W_r)b_w H}{(2H^2 W_r + 6E_c I_{eff})} \tag{2-20}$$

where $F_{out} =$ out-of-plane lateral force; $\theta_{out} =$ out-of-plane drift; and $b_w =$ thickness of the wall in an out-of-plane direction.

## 2.4 CONSTRUCTION OF SEISMIC PRECAST WALL PANELS

Figure 2.4 presents the details of the two specimens including reinforcement bars, location types of energy dissipators and unbonded tendons. Also shown is the mix of prestress and mechanical dissipating devices investigated. Wall 1-P+A was designed with a pair of bonded fuse-bars (Type A) and Wall 2 was designed with two replaceable energy dissipators which were unbonded fuse-bars (Type B) and a mechanical energy dissipator (Type C). The dimensions of Wall 1-P+A and Wall 2 were identical with an effective height of $H = 3000mm$, width of $B = 1200mm$, thickness of $b_w = 200mm$, aspect ratio of $A_r = H / B = 2.33$ and slenderness ratio of $\lambda = H / b_w = 14$. The difference in these walls is that Wall 1-P+A used bonded fuse-bars (Type A) whilst Wall 2 used different flexibilities in terms of location, length, diameter of unbonded fuse-bars (Type B) and mechanical energy dissipators (Type C).

Figure 2.4(a) shows details of reinforcement for the foundation beam and the cross-section of each wall. The bottom of each specimen was protected against damage by grouting the base of the wall panels into a steel channel. A steel plate was embedded on top of the foundation beam and unbonded post-tensioned tendons were locked at the wall-foundation interface (refer to Figure A2.1 for the preparation of the foundation beam). This allowed the walls to rock from heel to toe, steel-on-steel, under a dynamic response. The walls were clamped to the foundation beam by bolting the nuts (RB25N) at the top of the concrete block and screwing unbonded tendons to the couplers cast within the foundation beam. By implementing this type of discontinuous connection, the formation of a conventional plastic hinge zone at the base of the wall is avoided; damage within this area is essentially eliminated in contrast to monolithic conventional precast

wall panels (Holden et al., 2003). Self-compacting concrete (SCC) with compressive strength of 70MPa was poured from the top of both walls into the six voids of the sections up to 1320mm height from the foundation beam. The selected height was grouted based on the theoretical value of the plastic hinge zone occurring in the wall panel. A 20mm diameter hole was drilled 1320mm above the base at each void of the section. The holes served as depth indicators when pouring the self-compacting concrete (SCC). Pintles were welded beneath the steel channel of both walls to act as shear keys. The intent was to stop the wall from sliding and transfer all the lateral loads to the foundation beam.

Figure 2.4(b) exhibits a special fitting for installation of mechanical energy dissipators (Type C) made from a steel block with a hole at the centre. The steel block and steel plate were clamped together using two nuts at the top and bottom of longitudinal thread bars located inside the first and sixth voids of the hollow sections. Two longitudinal reinforcing thread bars, located 30mm apart, were screwed inside nuts (RB25N) which were welded to the steel channel web to resist the longitudinal forces from both mechanical energy dissipators during uplifting of the rocking wall. Two 20mm diameter threaded rods were inserted into the steel block and wall before pouring the self-compacting concrete. The bottom part of the mechanical energy dissipators were welded to steel angles and the flanges of the steel angles were welded to a steel plate with two holes placed on the foundation beam (refer to Figure A2.2). Subsequently, 12mm threaded bars were inserted inside these holes and screwed into a steel plate on the shaking table to ensure the foundation block remained stationary.

Figure 2.4(c) shows the bonded fuse-bars (Type A) at the two-middle void sections of Wall 1-P+A. The bonded fuse-bars were cast into the foundation beam and the extruded

parts were screwed using nuts (RB25N) from the steel channel before pouring the concrete. Two thread bars (RB25) were used as unbonded tendons which were located at the second and fifth voids of the hollow section. The mass concrete block, with a self-weight of 34kN, was placed on top of Wall 1-P+A which represented the gravity load from the roof and cladding. This block was connected to Wall 1-P+A and the foundation beam using unbonded tendons with the bottom part screwed to couplers that were cast into the foundation beam. Figure A2.3 shows the construction and assembling of Wall 1 on a strong floor.

Figure 2.4(d) presents Wall 2 with a different combination of unbonded tendons and two types of energy dissipators (unbonded fuse-bars (Type B) and mechanical energy dissipators (Type C)). Unbonded fuse-bars (Type B) were joined to the thread bars (RB25) using couplers at two-thirds height and screwed to the couplers embedded inside the foundation beam. This class of energy dissipator can be replaced or re-prestressed if fuse-bars undergo significant strain well into the strain hardening region. They were designed to give similar equivalent viscous damping and moment contribution to the system employed in Wall 1-P+A. The unbonded fuse-bars and unbonded tendons were prestressed at different levels before being tested under various biaxial displacement patterns. Figure A2.4 shows the assembling and lifting of Wall 2 on to the shaking table.

## 2.5 EXPERIMENTAL AND THEORETICAL PERFORMANCE OF THE ENERGY DISSIPATORS

As shown in Figure 2.5, three different types of energy dissipators were designed, fabricated and tested under cyclic loading. To define their effectiveness an energy absorption

efficiency factor ($\eta$) with respect to elasto-perfectly-plastic (EPP) behaviour is assigned as:

$$\eta = \frac{E_h}{E_{EPP}} \tag{2-21}$$

in which $E_h$ = absorbed hysteretic energy observed during a characterisation experiment; $E_{EPP}$ = energy dissipated by a theoretical elasto-perfectly plastic system given by $E_{EPP} = 2F_y(\Delta_{\max} - \Delta_y)$ where $F_y =$ yield force of the bar, $\Delta_{\max} =$ maximum displacement and $\Delta_y =$ yield displacement. The respective observed energy absorption efficiency factors, $(\eta)$ for energy dissipators Types A, B and C are 0.75 (41 cycles), 0.38 (24 cycles) and 0.78 (25 cycles). These values are subsequently used to estimate the overall equivalent viscous damping factor $(\xi_{eq})$ for the combined wall systems. Hysteretic energy absorption $(E_h)$ by wall per cycle is given by the area of force-displacement loop. One cycle of loading is defined as one complete reversal between positive and negative drift amplitudes. Other types of energy dissipators were also tested using the Instron Machine as shown in Figure A2.5.

Figure 2.5(a) presents the stress-strain relationship, shape, cyclic behaviour and energy absorption efficiency factor for the bonded fuse-bar (Type A). This fuse-bar was machined from reinforcing thread bars (RB25) with yield strength of $f_y = 530MPa$. The overall fuse-bar length was 1200mm while the machined down 16mm diameter was over the central 260mm. When the bar unloaded on compression reversal some buckling was observed.

Figure 2.5(b) gives the overall experimental results for the Type B unbonded fuse-bars, the lengths of which were 500mm, diameter 16mm and yield strength $f_y = 530MPa$. This fuse-bar was prestressed up to 50% of its yield capacity and tested under cyclic loading. No buckling was observed during unloading because the Type B energy dissipator was designed to only behave in tension.

Figure 2.5(c) shows the results of the externally mounted Type C axial tension-compression mild steel energy dissipator device. The dissipator was laser-cut and machined from a 18mm thick mild steel plate. The axial extension under post-yield conditions took place over an 18mm x18mm cross-section and 210mm long. A major problem with this type of energy dissipator is that it can easily buckle under compression due to the slenderness of the unsupported length $(kL/r = 28)$. Nevertheless, this type of dissipator is easily removed and replaced if damaged or fractured in a severe earthquake.

## 2.6 INSTRUMENTATION, EXPERIMENTAL SET-UP AND TESTING PROCEDURE

Bi-lateral loading experiments were conducted on both specimens based on the experimental set-up shown in Figure 2.6. A shaking table was used under quasi-static sinusoidal motion to apply in-plane displacements at the base of the specimen, while simultaneously lateral out-of-plane displacements were applied via an external reaction frame to the top of the specimens as shown in Figure 2.6(a). The in-plane lateral load was applied by a 440kN servo-controlled actuator mounted at a height of 2830mm from the base plate of the shaking table. One end of the in-plane actuator was connected to a reaction

frame bolted to the shaking table while the other end was connected to the top of the walls.

The out-of-plane loading was applied by a 150kN ± 750mm stroke servo-controlled actuator. This pin-ended actuator was connected to a steel plate embedded in the centre of the longitudinal side of the top block at a height of 3330mm from the shaking table while the other end was connected to a purpose built reaction frame that in turn was connected to the laboratory strong floor.

The foundation beam was clamped to the shaking table by inserting fourteen 12mm diameter high strength threaded rods into the holes in the foundation beam and screwing them to the steel bed of the shaking table to prevent the foundation block from either uplifting or sliding.

Instrumentation for both of the wall specimens is shown in Figure 2.6(b). A total of twenty-seven potentiometers were used to measure uplift, sliding and in-plane and out-of-plane displacements. Three linear potentiometers were used to trace any uplifting, whilst the other two 30mm potentiometers recorded any sliding of the foundation beam. Five potentiometers were used to measure in-plane displacement on the wall and two of them were to detect any sliding at the top of concrete block when the lateral load was exerted on the wall. Nine rotary potentiometers were attached to the steel frame with 600mm spacing and M12; bolts were screwed to the steel tube clamped on both faces of the wall unit to measure out-of plane movement. For recording in-plane movement, six linear potentiometers were placed along one side of the wall (refer to Figure A2.6).

Six strain gauges were attached to each of the unbonded tendons in order to monitor prestress levels and to detect when yielding occurred. Additionally, four strain gauges were fixed to each of the internal and external fuse-bars for recording behaviour before and after yielding. Two strain-gauge based load cells were also placed beneath the upper tendon anchorages to measure the axial loads during cyclic loading. The experimental set-up together with the instrumentation is shown in the photograph Figure 2.6 (c).

The specimens, Walls 1-P+A and 2, were loaded separately in-plane and out-of-plane under increasing drift amplitudes to ± 2.0%. The specimens were also loaded bi-laterally, that is under concurrent in- and out-of-plane displacements. Only results of the latter are presented herein, a full set of test results is presented in Appendix A2 (refer from Figure A2.8 to Figure A2.19). Two bi-lateral loading patterns were developed and are referred to herein as "4-leaf clover" and "double 4-leaf clover" patterns. Table 2.1 shows various combinations of bi-lateral displacement controlled patterns, initial prestressing and energy dissipators of Wall 1-P+A and Wall 2.

Table 2.1: The arrangement of unbonded tendons, types of energy dissipators, levels of prestress and drift amplitudes.

| Test | Level of prestress | Drift Amplitudes |
|---|---|---|
| 1 – P + A | 64%P | ± 0.1%, ± 0.5%, ± 1.0%, ± 1.5% |
| 2 – P + O | 64%P | ± 0.1%, ± 0.5%, ± 1.0%, ± 1.5%, ± 2.0% |
| 2 – O + B | 50%B | ± 0.1%, ± 0.5%, ± 1.0%, ± 1.5%, ± 2.0% |
| 2 – P + B | 0%P + 50%B | ± 0.1%, ± 0.5%, ± 1.0%, ± 1.5% |
| 2 – P + C | 50%P | ± 0.1%, ± 0.5%, ± 1.0%, ± 1.5% |

The various combinations of tests for Wall 2, as given in Table 2.1, used a "double 4-leaf clover" pattern in displacement control. The arrangement of unbonded tendons, energy dissipators and the level of prestress along with the drift amplitudes for each test group

conducted on Walls 1 and 2 following notation are given in Column 1: P = ordinary prestress applied at the level given in Column 2; A = bonded fuse-bars (Type A) grouted in place at the base of the wall; B = tension only fuse-bars located in the top two-thirds of the wall (Type B); and C= external mechanical energy dissipators connected by through bolts to the wall, bolted and welded to the foundation bed plates (Type C).

The biaxial displacement controlled pattern used for this experimental work consisted of two Lissajous functions referred to herein as a "double 4-leaf clover" pattern. This function satisfies all the critical conditions ((i) X= maximum displacement in x-x direction and Y=0, (ii) X=0 and Y=maximum displacement in y-y direction, (iii) X=maximum displacement in x-x direction and Y=maximum displacement in y-y direction). These functions comprise cosine and sine functions and are defined in Cartesian coordinates as:

$$X = a\cos 2\theta \cos\theta \quad \text{and} \quad Y = a\cos 2\theta \sin\theta \tag{2-22}$$

$$X = a\sin 2\theta \cos\theta \quad \text{and} \quad Y = a\sin 2\theta \sin\theta \tag{2-23}$$

where $X$ = in-plane drift (E-W direction), $Y$ = out-of-plane drift (N-S direction), $\theta$ = phase angle and $a$ = drift amplitude. The in-plane load (E-W) and out-of-plane load (N-S) followed a similar pattern as a displacement function in the elastic range, except when the wall exceeded the yield drift the graph became a plateau. Figure A2.7 exhibits various combinations of Lissajous functions which were tested on Wall 1 and Wall 2.

## 2.7 EXPERIMENTAL RESULTS FOR WALL 1-P+A

Figure 2.7 presents the overall experimental and theoretical results of the seismic bi-lateral performance of Wall 1-P+A at ±1.5% drifts amplitude under the "4-leaf clover" displacement pattern. The location of unbonded tendons, 16mm diameter and 260mm

length of bonded fuse-bars (Type A), foundation beam and the top concrete block of Wall 1-P+A are presented. As expected, the specimen performed very well under various kinds of load paths without any visible damage to the wall throughout the entire experiment. The initial level of prestress applied (20% of yield) was insufficient to overcome the compression capacity of centrally located unbonded fuse-bars, so the test was repeated at a level of 64% present, the results of which are presented herein.

Figure 2.7(a) presents the experimental "4-leaf clover" displacement controlled pattern used to provide bi-lateral loading. This pattern was chosen to examine the extreme seismic behaviour when the out-of-plane loading reached maximum drift while zero drift at in-plane directions or vice-versa. Figure 2.7(b) presents the in-plane force-displacement response to the applied displacements, while Figure 2.7(c) presents the theoretical behaviour assuming rigid body kinematics. The initial stiffness of the wall depends on the full gross rigidity $(EI_g)$ shown as a dotted line under in-plane loading only. But the stiffness reduces when the wall is subjected to biaxial loading, marked as a dark line. The explanation for this disparity is that only a small portion of the wall width is under compression (outside the dead zone) due to additional out-of-plane loading effects. Based on the displacement (drift) amplification factor theory as discussed earlier, the effective rigidity $(EI_{eff})$ of the wall reduces according to the contact base width. By using equation 2-2, the ratio of effective rigidity with respect to full gross rigidity is $EI_{eff} = 0.2EI_g$. Therefore, the initial stiffness of the slope is reduced while maintaining force capacity with a bigger displacement of 25mm. Thus, this theoretical result is in good agreement with the experimental results.

Figure 2.7(d) presents the experimental and theoretical results for out-of-plane behaviour. The theoretical results show that an elastic response is expected out-of-plane, but the non-linear response is somewhat evident. It should be noted, however, that the out-of-plane forces are only some 10% of the in-plane forces; most of the energy absorbed is attributed to friction in the fittings of the experimental apparatus.

Figure 2.7(e) and (f) show a similar shape between the experimental and theoretical biaxial loading path when applying the '4-leaf clover' displacement controlled pattern. A flat plateau of the in-plane load was observed when the drift reached $\pm 1.5\%$. This is due to the fact that bonded fuse-bars yielded at 1.0% drift and then reached a maximum plateau of 1.5% drift.

## 2.8 EXPERIMENTAL RESULTS FOR WALL 2

The experimental results on Wall 2 under four combinations at different levels of prestressing of unbonded tendons and fuse-bars along with mechanical energy devices are presented herein:

### 2.8.1 WALL 2-P+O

Figure 2.8 presents the experimental and analytical results using 64% prestressing of the unbonded tendons. The location of the unbonded tendons with initial prestress level, foundation beam and top concrete block is also shown in this figure. The tests were conducted using the "double 4-leaf clover" controlled displacement pattern. This pattern satisfies all the three critical conditions of displacements for in-plane and out-of-plane dis-

placement. There is maximum in-plane displacement with zero out-of-plane displacement, maximum out-of-plane displacement with zero in-plane displacement, and maximum in both directions. An example of the displacement controlled pattern is given in Figure 2.8(a).

The experimental results of the in-plane behaviour of unbonded tendons at ± 2.0% under 64% level of prestress is presented in Figure 2.8(b). Results show that there is mostly a bi-linear elastic relationship between load and displacement. The self-centering characteristics are maintained and only a little of the energy is dissipated during the out-of-plane motion. The first tendon started to yield at 1.25% drift $(\Delta = 30mm)$. As the level of drift increased, prestress-losses increased and this was detected by strain gauges attached to the tendons. At the end of the test, the elongation of the tendons was 4mm due to plastic deformation. This result is in keeping with the theoretical in-plane behaviour as shown in Figure 2.8(c).

Figure 2.8(d) shows the comparison between theoretical and experimental results for the out-of plane behaviour of Wall 2-P+O. The graph shows a linear relationship between out-of-plane displacement and out-of-plane loading (N-S direction). The overall bi-lateral force response to the "double 4-leaf clover" displacement path is presented in Figure 2.8(e). This overall experimental result is in reasonable agreement with the theoretical results as shown in Figure 2.8(f).

### 2.8.2 WALL 2-O+B

Figure 2.9 shows the experimental results for Wall 2-O+B. A pair of unbonded 16mm diameter fuse-bars located within the central two voids of the cross section were prestressed to 50% of their yield capacity.

Figure 2.9(a) shows the applied "double 4-leaf clover" displacement path to 2.0% drift amplitudes with the respective experimental in-plane and theoretical in-plane responses to that loading in Figures 2.9(b) and 2.9(c) along with the out-of-plane response in Figure 2.9(d). The fuse-bars yielded at 1.5% drift and dissipated most of their energy at the first compared to the second cycle. The base shear capacity of fuse-bars in Wall 2-O+B is less than in Wall 2-P+O due to less cross-sectional area. The experimental and theoretical results for bi-lateral loading under the "double 4-leaf clover" using unbonded fuse-bars are shown in Figure 2.9(e) and (f), respectively. Figures 2.9(g) and (h) present photographs that show there was neither structural nor cosmetic damage to the wall at one of the 2% drift amplitude peaks.

### 2.8.3 WALL 2-P+B

Figure 2.10 presents the experimental and theoretical results of Wall 2-P+B which had a pair of unbonded tendons together with a pair of unbonded fuse-bars. The specimen was tested at four drift levels (±0.1%, ±0.5%, ±1.0% and ±1.5%) using the "double 4-leaf clover" displacement pattern as shown in Figure 2.10(a). The unbonded fuse-bars were prestressed to 50% of their yield capacity.

For the lower drift amplitude (±0.1%, ±0.5% and ±1.0%) the wall remained "mostly elastic", whereas nonlinear "flag-shape" behaviour occurred at 1.5% drift amplitudes when the main tendons yielded. For the latter, the unbonded tendons remained in the elastic region but the fuse-bars yielded and dissipated most of their energy as shown in Figure 2.10(b). Figure 2.10(c) shows the theoretical in-plane behaviour where the "flag-shape" is slightly bigger than the experimental results due to higher stiffness in unbonded tendons and unbonded fuse-bar. Under biaxial loading testing, some of the lateral loading was lost due to friction in the actuator and connections. Out-of-plane, the wall behaved in a mostly elastic fashion. However, from Figure 2.10(d) some hysteretic behaviour is evident. This is attributed to changes in the level of prestress during the concurrent in-plane behaviour, as well as some friction present in the connections of the experimental apparatus. The overall force response to the applied displacement pattern is shown in Figure 2.10(e). A slight degree of asymmetry in response is evident, and this is attributed to eccentric placement of the tendons at the top of the wall. No damage to the precast concrete unit was observed during this experiment on Wall 2-P+B. The theoretical force capacity arising from the bi-lateral push-over analysis for the "double 4-leaf clover" loading pattern is shown in Figure 2.10(f).

### 2.8.4 WALL 2-P+C

Figure 2.11 presents the overall experimental performance of Wall 2-P+C which had unbonded tendons prestressed to 50% of their yield capacity plus four external mechanical energy dissipators. The external energy dissiptors were first prefabricated, and then welded to a steel angle at the foundation and attached to the wall through bolts that were grouted in place across the centre of the first and sixth of void section (refer to Figure

2.11(g)). Wall 2-P+C was tested using the "double 4-leaf clover" pattern up to 1.5% drift as given Figure 2.11(a). The in-plane force response to the applied displacement pattern is shown in Figure 2.11(b) where a modest amount of hysteresis is evident. Results show that Wall 2-P+C maintained a self-centring capability with only a small value of residual displacement recorded during unloading. It should be noted that buckling of the mechanical energy dissipator devices caused minor residual displacement. It can be seen in Figure 2.11(c) where the theoretical result shows that during the unloading path, the wall went back to its original position without any residual displacement. Figure 2.11(d) shows experimental and theoretical results for the out-of-plane response. Figure 2.11(e) illustrates the experimental bi-lateral loading path behaviour while Figure 2.11(f) shows the theoretical bi-lateral loading path response. At +1.0% drift under in-plane loading, the threaded bars, which were holding the mechanical energy dissipators, bent and the through-bolts became loose. When the drift increased up to 1.5%, the concrete immediately surrounding the threaded through-bolts started to crush and crack lines propagated around the bolts. This slight degree of damage is evident in the photographs of Figure 2.11(g) and (h). During the 1.5% drift amplitude, the mechanical energy dissipators buckled outwards from the wall. Such behaviour was expected, as shown previously in Figure 2.5(c), where the compression forces, although present, are less effective than tensile behaviour.

## 2.9 DISCUSSION

The following discussion focuses on stiffness, strength, comparative performance and equivalent viscous damping of the walls using three types of energy dissipators. The initial stiffness of the wall under biaxial loading mainly depends on the compression forces,

the effective contact base-width and the resulting displacement (drift) amplification factor. It is evident that not all of the concrete is fully compressed as compared to an in-plane loaded fixed-end monolithic wall. Only a small portion of the concrete is under compression, the remainder forms a "dead zone". The contact base width at the bottom corner of the wall depends on the drift levels, seismic loading, energy dissipator forces and unbonded post-tensioned forces. It has been demonstrated that this simplified concept of flexibility enhancement is in keeping with the observed experimental results.

- Comparative Performance

Table 2.2 describes the advantages and disadvantages of employing three different types of energy dissipators. Energy dissipator Type A is used in Wall 1 and Wall 2 utilized energy dissipators Type B and Type C. Unbonded fuse-bars (Type B) are generally recommended because the wall "sits-up" on the base steel plate as compared to the other two types of energy dissipators which did not sit on the base plate after a strong earthquake. It is recommended that in accordance with the Damage Avoidance Design philosophy, post-tensioned tendons with 50% prestress and in-series unbonded fuse-bars are adequate for satisfactory seismic behaviour.

- Stiffness and Strength

Other parameters that influenced the stiffness, strength and base shear of these walls were also identified. These parameters were the location, cross-sectional area and initial prestressing of energy dissipators and unbonded tendons. The cross-sectional area and initial prestressing of unbonded fuse-bars and tendons affect the initial stiffness (pre-rocking), post-yield stiffness and yield drift. The location of the energy dissipator along wall-foundation interface also has significant influence on the base shear. This is further improved by using the following equations where uplift displacement at bottom of the wall, $\delta_i^{uplift}$ is given by:

$$\delta_i^{uplift} = \zeta_i B\theta \tag{2-24}$$

where $\zeta_i B$ = the location of the $i^{th}$ energy dissipators with respect to pivot point, O of the wall and $\theta$ = the level drift. Base shear contribution from all the $(N)$ energy dissipators participating is given by:

$$V_{dis} = F_{ydis} \frac{B}{H} \sum_{i=1}^{N} \zeta_i \tag{2-25}$$

in which $F_{ydis}$ = energy dissipator force depending on its cross-sectional area and yield strength , $\sum_{i=1}^{N} \zeta_i$ is the fraction width, $H$ = height of the wall and $B$ = width of the wall. The bonded fuse-bars (Wall 1-P+A) and unbonded fuse-bars (Wall 2-P+B) were placed at the same location at the centre of the third and fourth void sections whereas external energy dissipators were positioned outside the bottom corners of the wall. The outcomes showed that the base shear of Wall 2-P+C is bigger than Wall 1-P+A and Wall 2-P+B.

- Equivalent Viscous Damping

The theoretical equivalent viscous damping for a system with hysteretic behaviour is calculated using the following (Chopra, 2001):

$$\xi_{eq} = \frac{1}{4\pi} \frac{E_D}{E_{SO}} = \frac{1}{2\pi} \frac{E_D}{F_{\max} \Delta_{\max}} \tag{2-26}$$

where $E_D$ = the theoretical cyclic pushover curve area with the "flag-shape" loops and $E_{SO} = 1/2(F_{\max} \Delta_{\max})$; $F_{\max}$ = average maximum strength in forward and reverse loading directions and $\Delta_{\max}$ = average maximum displacements in both loading directions. The theoretical equivalent viscous damping using the above equation based on "flag-shape" ($\xi_{eq} = 14.4\%$) has a bigger value than experimental equivalent viscous damping ($\xi_{eq} = 13.3\%$). The experimental energy absorption efficiency factor ($\eta_{\exp} = 0.6$) has a bigger value than theoretical values under a "flag-shape" ($\eta_{th} = 0.5$).

Table 2.2: The Advantages and Disadvantages of Three Different Types of Energy Dissipators used in Wall 1-P+A, Wall 2-P+B and Wall 2-P+C

| Wall Arrange-ments | Example | Advantages | Disadvantages |
|---|---|---|---|
| Unbonded tendon plus bonded tension-compression fuse bars | Wall 1-P+A | -can dissipate energy well, especially on the first cycle | -cannot easily replace damaged or fractured fuse bars<br>-structure "sits up" on yielded fuses giving an apparent reduction in stiffness. |
| Unbonded prestress only | Wall 2-P+O | -can be restressed if some initial prestressing is lost. | -cannot be replaced easily<br>-little energy dissipation |
| Unbonded tension fuse bars | Wall 2-O+B | -can be restressed or replaced after an earthquake<br>-can be used to limit force impact foundation | -unable to dissipate energy on unloading cycles<br>-energy dissipation capacity is limited<br>-can lose re-centering ability when drifts are substantial. |
| Unbonded tendon plus unbonded fuse-bars | Wall 2-P+B | -can dissipate energy<br>-high lateral resistance<br>-can repair/replace fuse bars<br>-can be restressed after an earthquake | -unbonded tendon cannot be easily replaced |
| Unbonded tendon plus external me-chanical energy dissipators | Wall 2-P+C | -dissipates some energy<br>-mechanical energy dissipators can be easily replaced. | -structure "sits up" on yielded fuses giving an apparent reduction in stiffness.<br>-some limited damage to the wall possible |

The main reason is that the theoretical elasto-perfectly plastic area is slightly greater than the experimental elasto-perfectly plastic area. The hysteretic performance for three different types of energy dissipators is shown in Figure 2.12 (a), (b) and (c). The experimental and theoretical equivalent viscous damping for Wall 1-P+A, Wall 2-P+B and Wall 2-P+C is presented in Figure 2.12 (d), (e) and (f). These results indicate that Wall 2-P+C has better seismic performance in dissipating energy during ground shaking. Nevertheless, energy dissipator Type C caused minor cracks around the threaded-bars when more lateral forces were required to uplift Wall 2-P+C as compared to Wall 1-P+A and Wall 2-P+B.

## 2.10 CONCLUSIONS AND RECOMMENDATIONS

Based on the experimental study on single bi-laterally loaded rocking precast prestressed concrete hollow core wall units presented herein, the following conclusions are drawn:

1) The experiments have demonstrated that precast prestress concrete hollow core units can be used as a viable alternative to solid reinforced concrete walls. This is in spite of the lack of any transverse reinforcement for shear resistance. This gives a wider scope for the use of hollow core units which have customarily been used mostly for floor units in buildings.

2) The success of the rocking hollow core walls is attributed to the Damage Avoidance Design (DAD) approach that requires carefully detailed armouring at the base of the wall to enable high point load stresses to be dispersed up the wall and also into the foundation.

3) Rocking walls in themselves dissipate little energy, but this can be improved through the use of supplementary energy dissipators. Of the dissipators tested in this study each had advantages and disadvantages. It would appear that the best trade-off is to use prestressed fuse-bars only as these always keep the wall clamped firmly to the foundation when not rocking. Other dissipator types can cause the walls to "sit up" on the devices when they yield, this effectively softens the structure.

4) By providing pintles or shear keys at the bottom corners of walls, the seismic lateral base shear can be resisted by rocking without sliding. No transverse reinforcement in precast hollow core walls needs to be used. In the present study, to help improve shear resistance at the base of the wall the hollow core

voids were filled to a height equivalent to one unit width (1.2m). Future research could potentially show that this extent of infilling be relaxed.

5) This research has demonstrated the efficacy of single panel wall units. How individual walls interact with surrounding walls units will be subsequently investigated through the design, construction and testing of a multi-panel superassemblage in the following chapter.

## REFERENCES


Berg, G.V., and Stratta, J.L. (1964). "Anchorage and the Alaska Earthquake on March 27, 1964." *American Iron and Steel Institute*, 52-63.

Copra, A.L. (2001). *Dynamic of Structures: Theory and Applications to Earthquake Engineering.* Second Edition, Prentice Hall, Upper Saddle River, New Jersey, U.S.A.

Fintel, M. (1995). "Performance of buildings with shear walls in earthquakes in the last thirty years." *PCI Journal*, 40(3), 62-80.

Ghosh, S.K. (2001). "Observations from the Bhuj Earthquake of January 16, 2001." *PCI Journal*, 46(2), 34-42.

Holden, T. J., Restrepo, J., and Mander, J.B. (2003). "Seismic performance of precast reinforced and prestressed concrete walls." *Journal of Structural Engineering*, ASCE, 129(3), 286-296.

Iverson, J.K., and Hawkins, N.M.(1994). "Performance of precast/prestressing building structures during Northridge Earthquake." *PCI Journal*, 36(2), 38-55.

Mander, J.B., and Cheng, C.T. (1997). "Seismic resistance of piers based on damage avoidance design." *Technical Report NCEER-97-0014*, State University of New York at Buffalo, Department of Civil, Structural and Environmental Engineering, Buffalo, New York, U.S.A.

Wyllie Jr, L.A., and Filson, J.R. (1989). "Armenia Earthquake reconnaissance report." *Earthquake Spectra*, Special Supplement, August 1989.

Youd, T.L., Bardet, J.P., Bray, J.D. (2000). " Kocaeli, Turkey, Earthquake of August 17, 1999 reconnaissance report." *Earthquake Spectra*, Supplement A to Volume 6, December 2000.

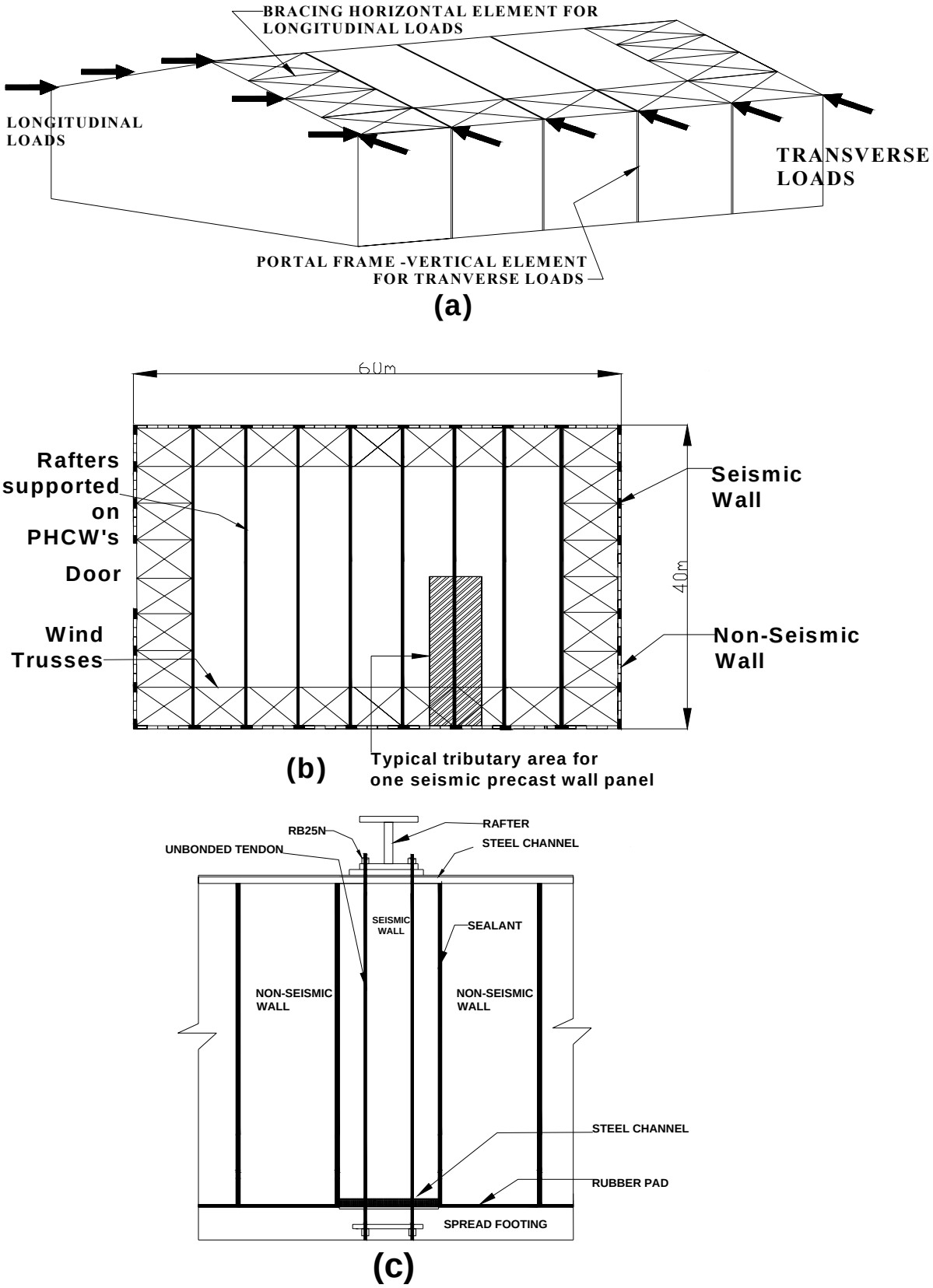


Figure 2.1: The prototype of a warehouse building; (a) 3D isometric view of the warehouse; (b) layout plan showing the schematic arrangement of seismic and non-seismic walls together with wind trusses; and (c) side elevation showing the locations of unbonded tendons inside the seismic wall screwed to the couplers inside the foundation beam.

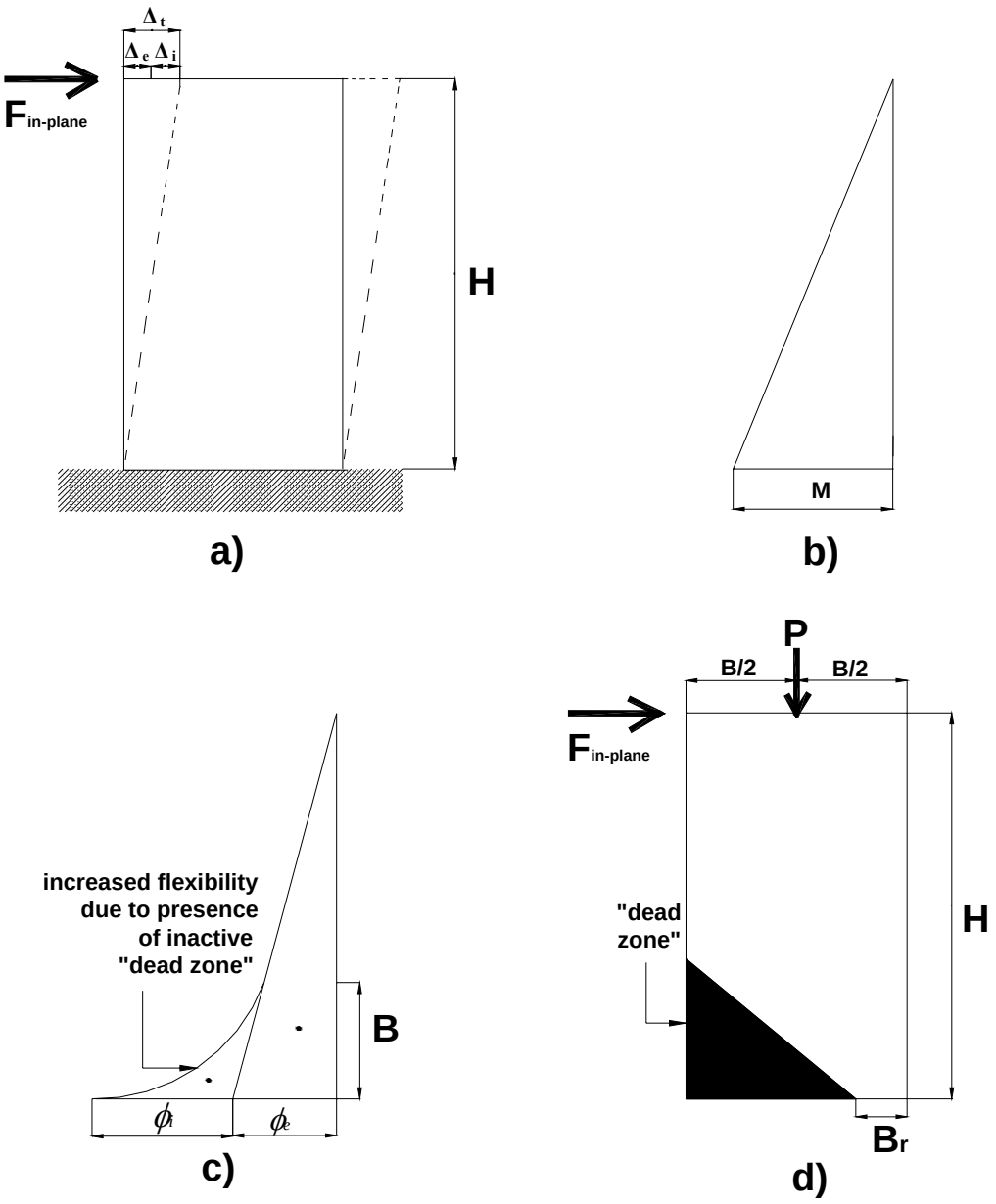


Figure 2.2: In-plane displacement amplification factor due to biaxial loading effects; (a) in-plane member of rocking wall; (b) fixed-end moment of the wall; (c) curvature distribution showing the location of centroids for the purpose of calculating wall deflection; and (d) dead load due to rocking effect of lateral loading.

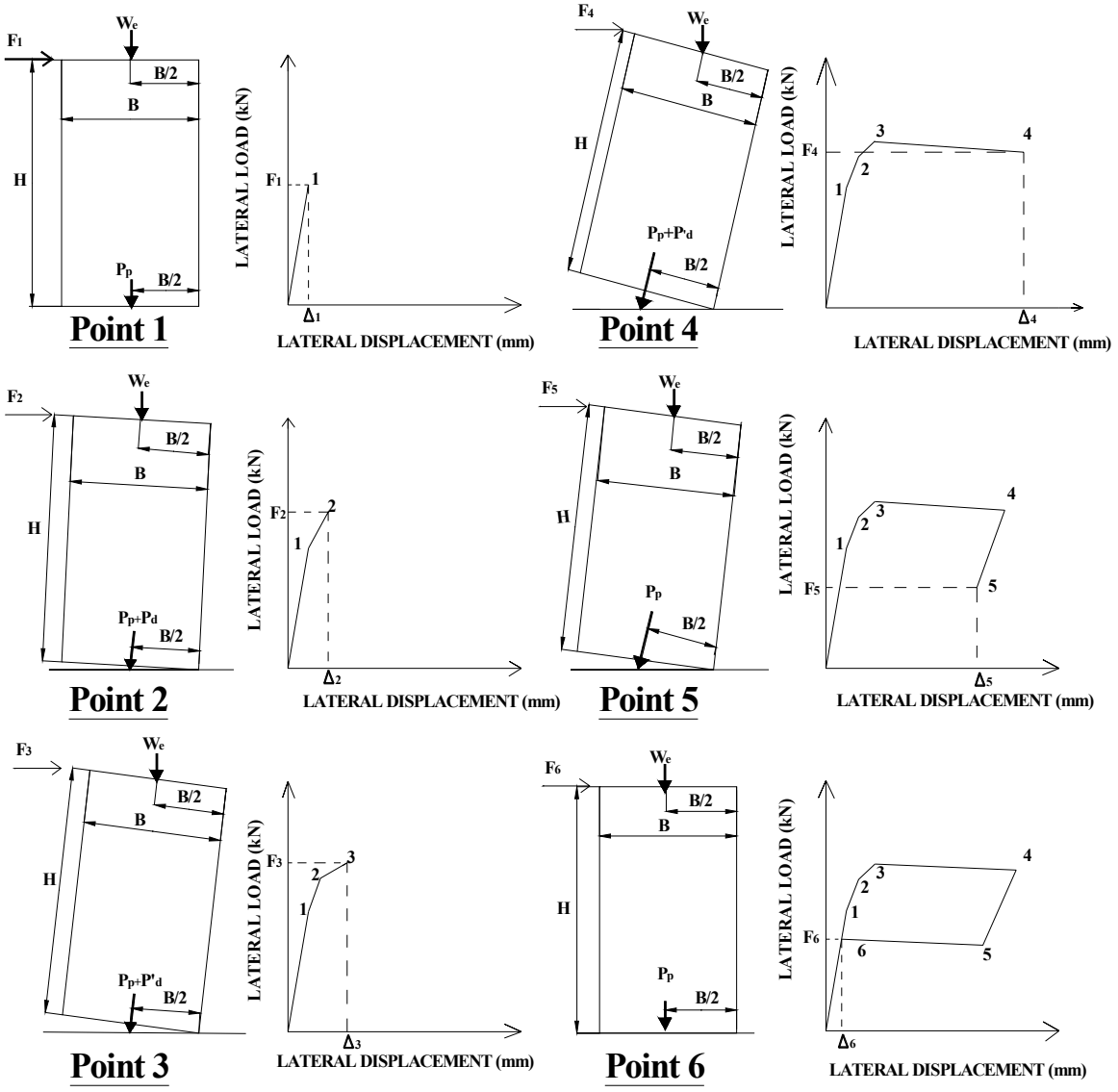


Figure 2.3: Static lateral load displacement response of the rocking precast hollow core wall.

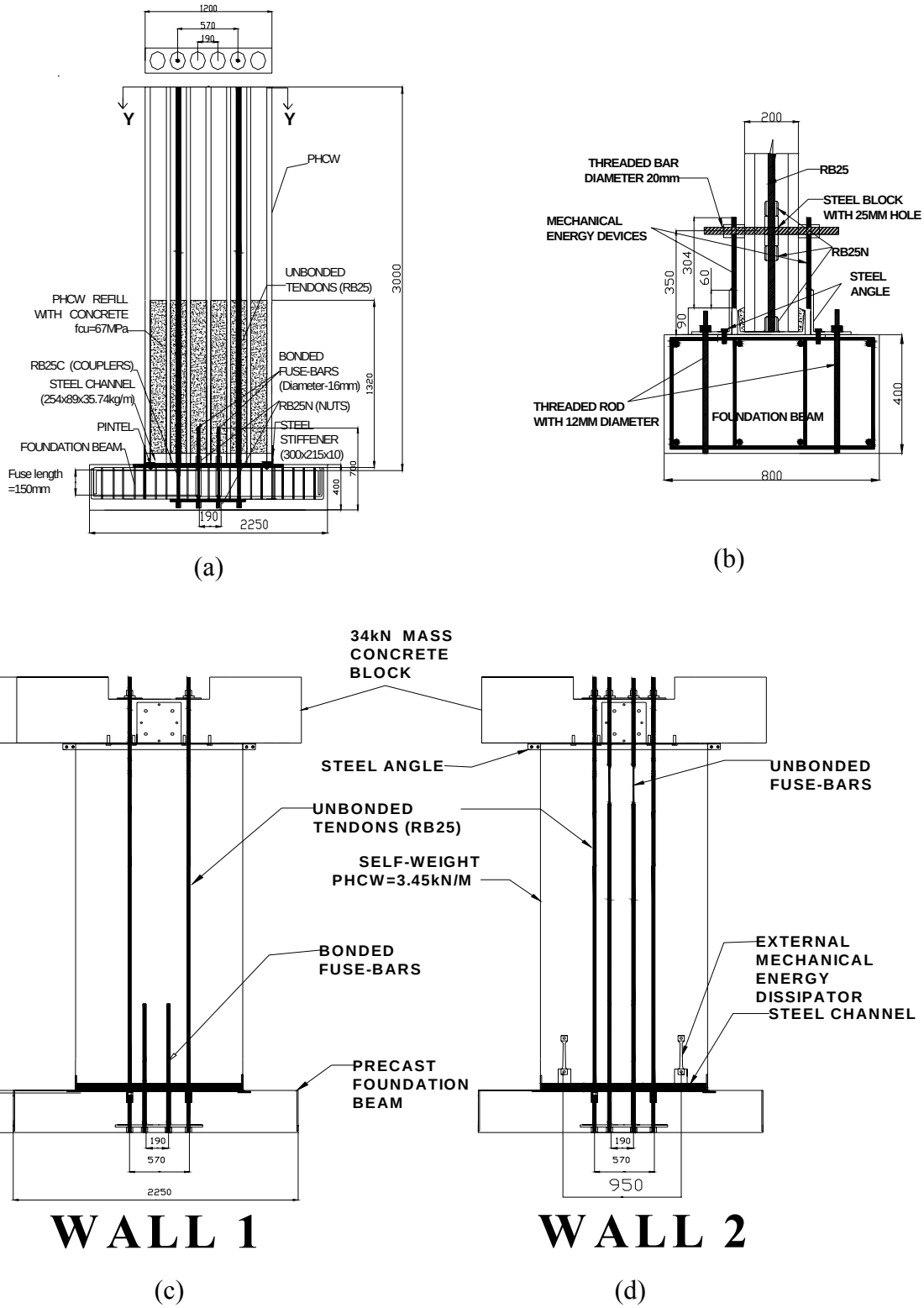


Figure 2.4: Test specimens used in the experimental investigation; (a) PHCW in-filled with concrete together with the connection interface between PHCW and foundation beam; (b) connection detailing for mechanical energy dissipators; (c) location energy dissipators inside Wall 1-P+A; and (d) combination of unbonded tendons and energy dissipators on Wall 2.

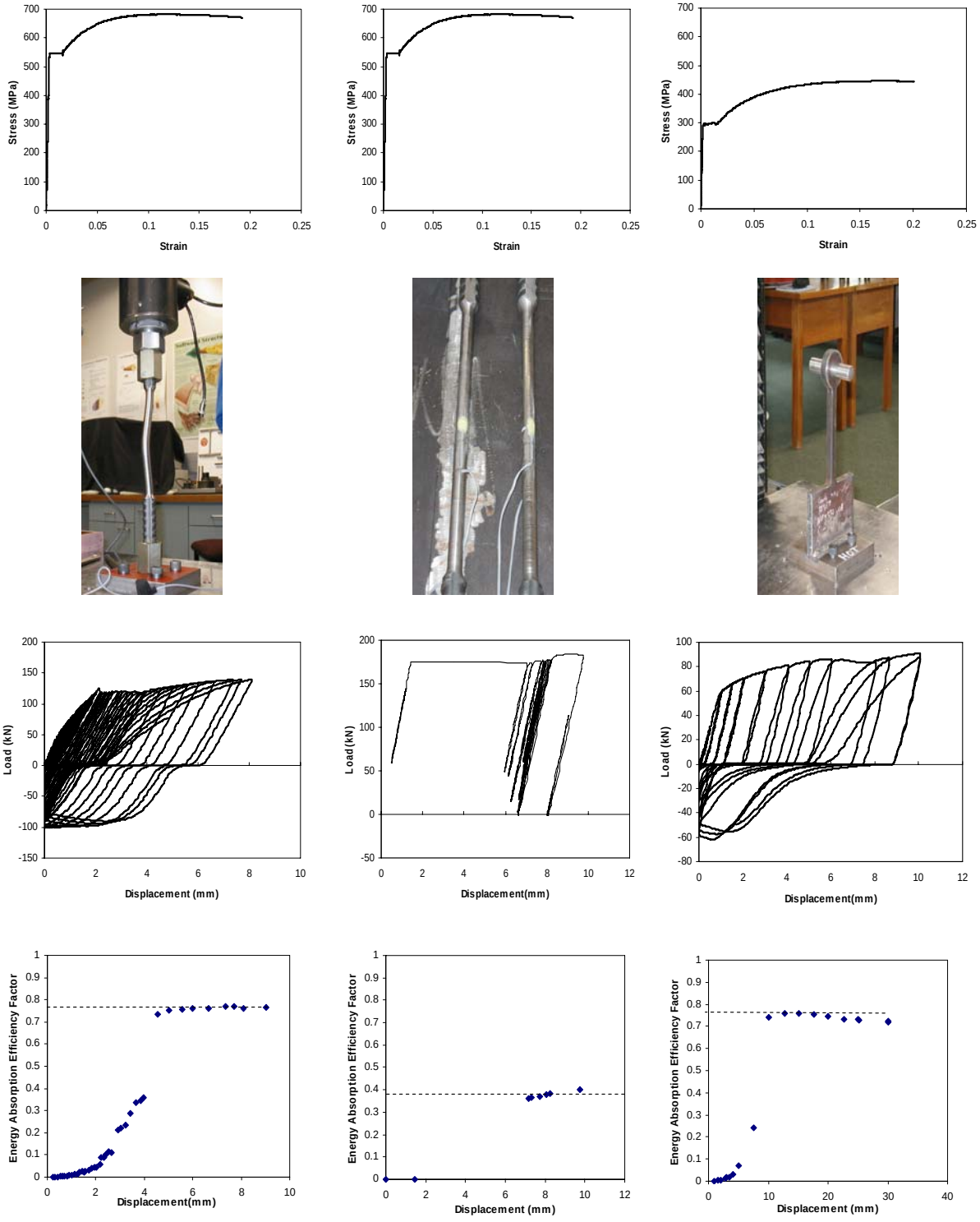


(a) (b) (c)

Figure 2.5: Three different types of energy dissipators showing their stress-strain relationship, shape, cyclic behaviour and energy absorption efficiency factor; (a) Type A (tension-compression bonded fuse-bars made from reinforcing thread bar- RB25); (b) Type B (tension-only fuse-bars); and (c) Type C (external mechanical energy dissipators acting as a sacrificial compression-tension yield elements).

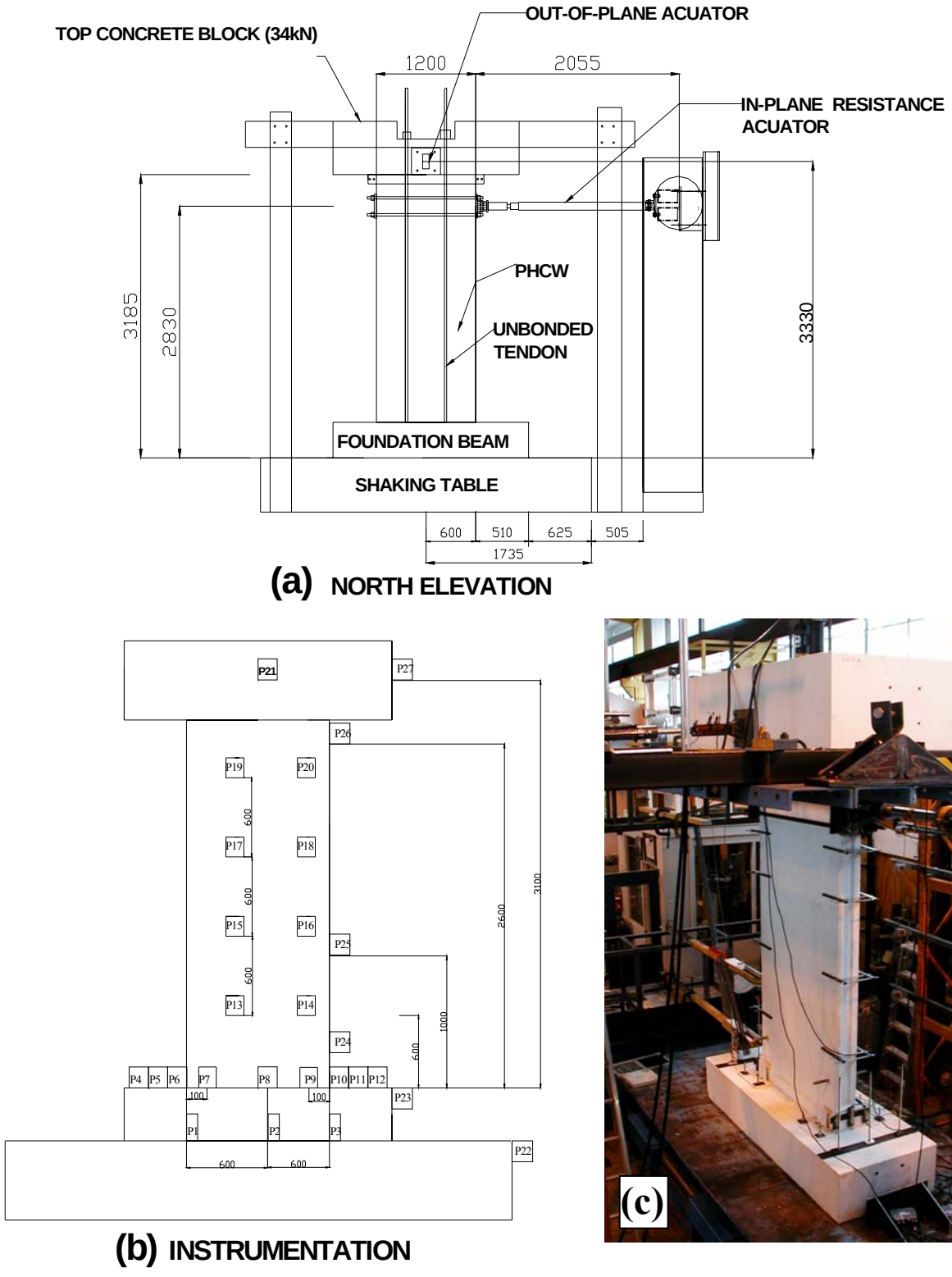


Figure 2.6: Experimental set-up and instrumentation: (a) schematic loading frame for Wall 1-P+A and Wall 2 on the shaking table; (b) instrumentation arrangement for Wall 1-P+A and Wall 2 on the shaking table; and (c) a photograph looking south-east of the wall specimen ready for testing.

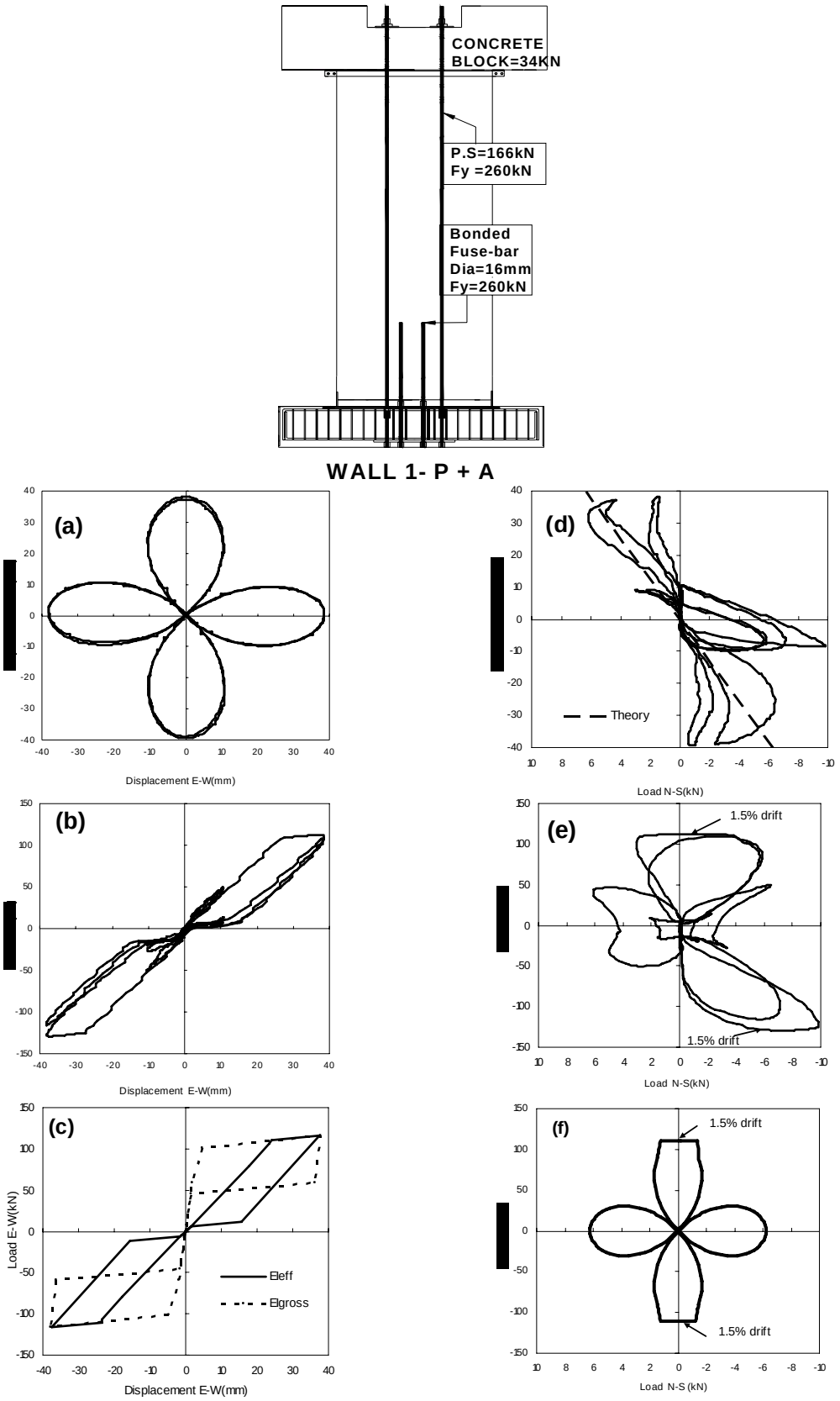


Figure 2.7: Theoretical and experimental results for Wall 1-P+A with 64% prestressing of unbonded tendons tested on the shaking table: (a) "4-leaf clover" displacement controlled pattern; (b) experimental in-plane behaviour; (c) theoretical in-plane behaviour; (d) experimental and theoretical out-of-plane behaviour; (e) experimental biaxial loading path; and (f) theoretical biaxial loading path.

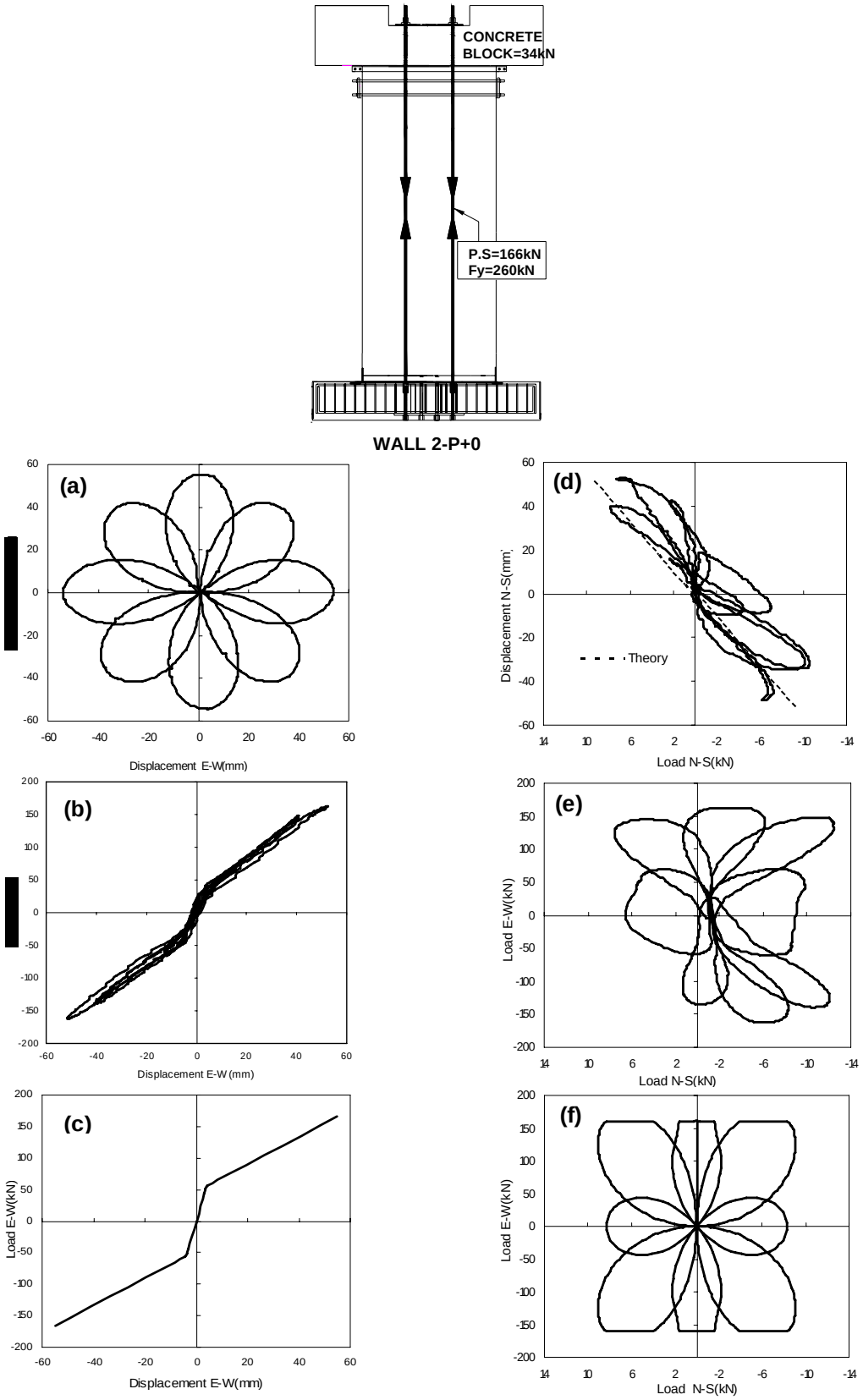


Figure 2.8: Theoretical and experimental results of Wall 2-P+O on the shaking table: Performance of the unbonded tendon only at 64% prestressing unbonded tendon; (a) "double 4-leaf clover" displacement controlled pattern; (b) experimental in-plane behaviour; (c) theoretical in-plane behaviour; (d) experimental and theoretical out-of-plane behaviour; (e) experimental bi-lateral loading; and (f) theoretical bi-lateral loading.

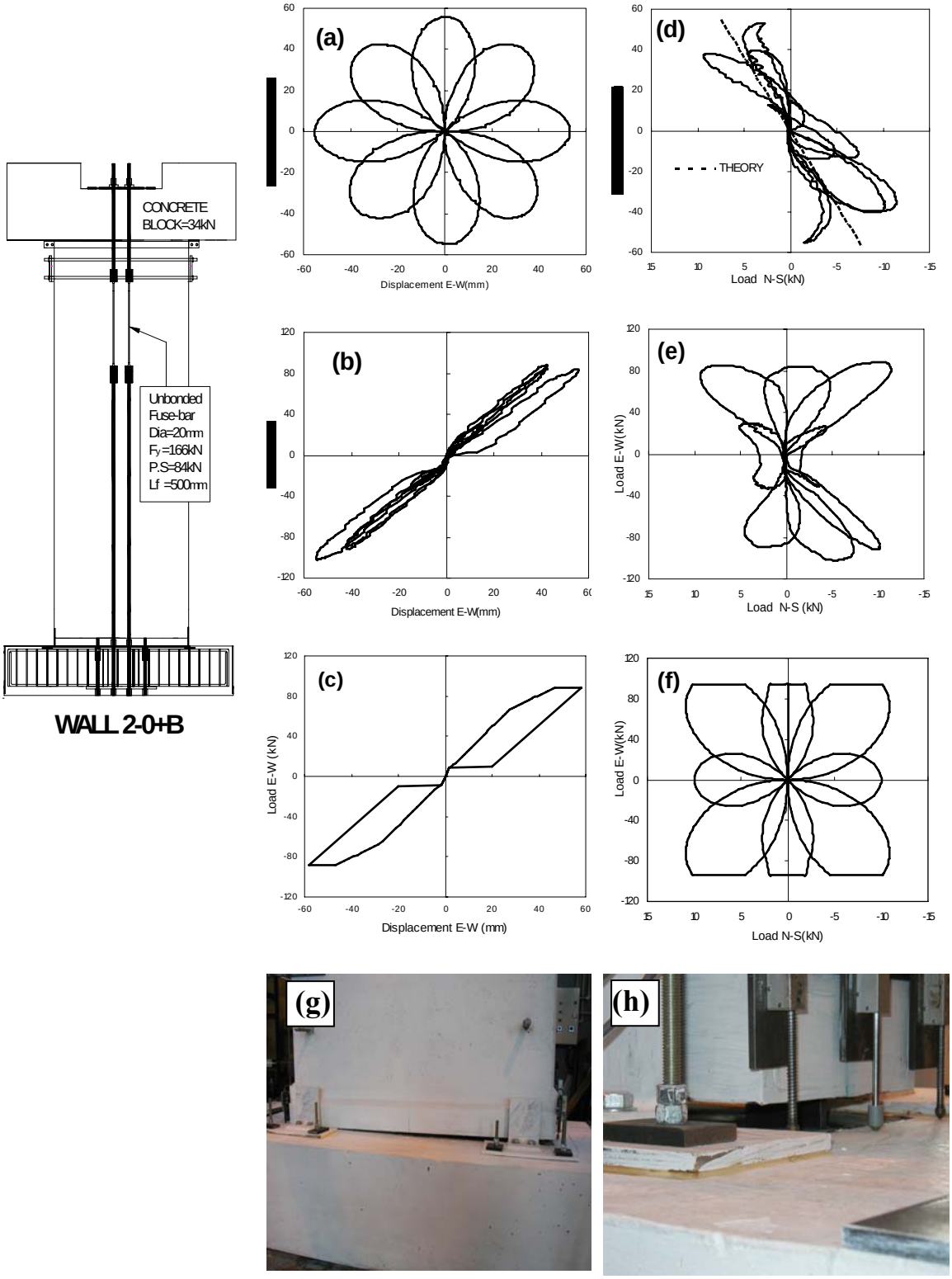


Figure 2.9: Experimental and theoretical Wall 2-0+B: Performance with fuse bars only with 50% prestressing of fuse bars; (a) "double 4-leaf clover" controlled displacement pattern; (b) experimental in-plane behaviour; (c) theoretical in-plane behaviour; (d) experimental and theoretical out-of-plane behaviour; (e) experimental bi-lateral load path; (f) theoretical bi-lateral loading path; (g) no structural damage at the bottom of the wall; and (h) the uplift of the bottom corner of the wall at the worst condition.

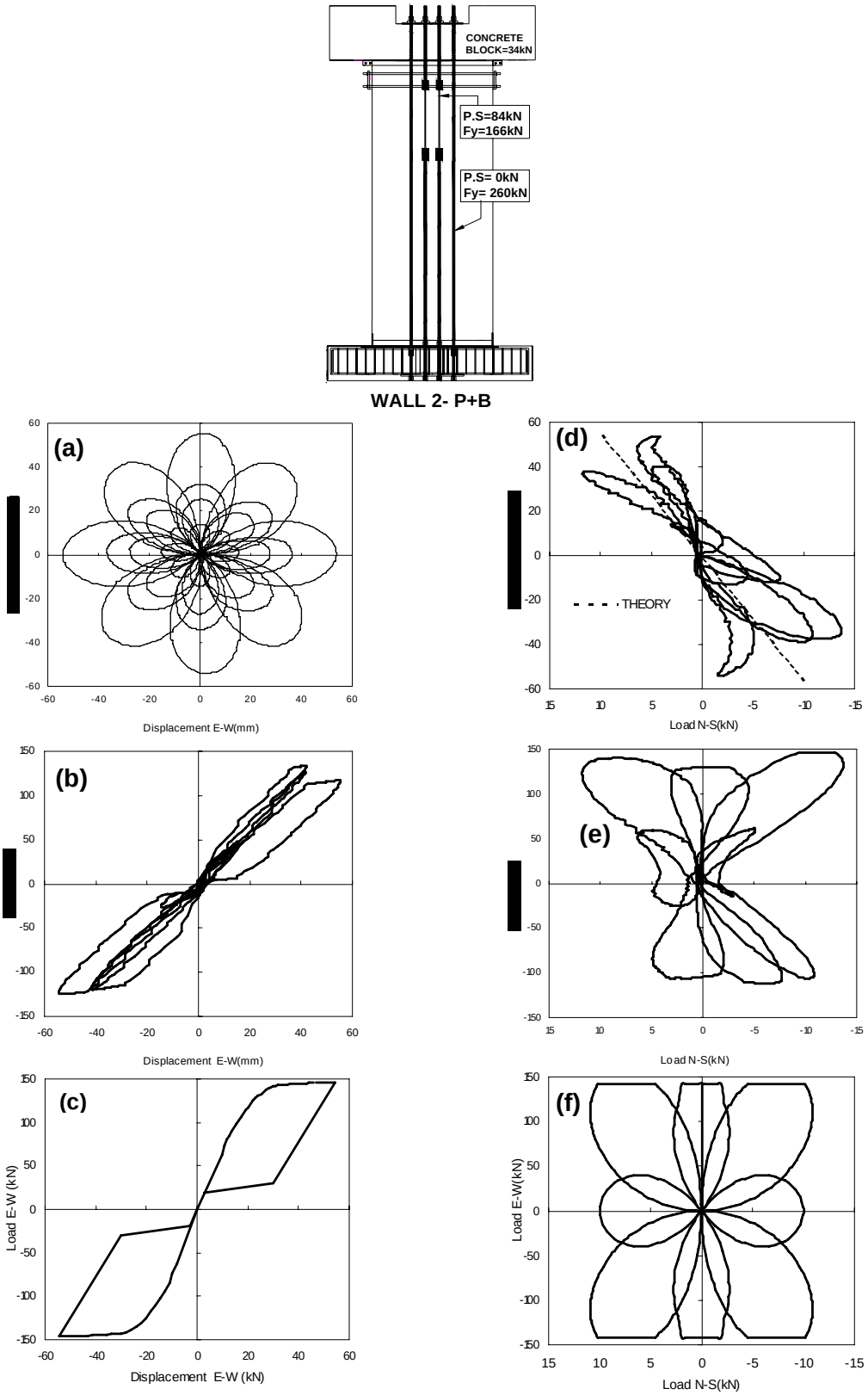


Figure 2.10: The experimental and theoretical results of Wall 2-P+B : Performance snug tight unbonded tendons and 50% prestressing unbonded fuse-bars; (a) "double 4-leaf clover" displacement controlled pattern at different levels of drift; (b) experimental in-plane behaviour; (c) theoretical in-plane behaviour; (d) experimental and theoretical out-of-plane behaviour ; (e) experimental bi-lateral loading path; and (f) theoretical loading path.

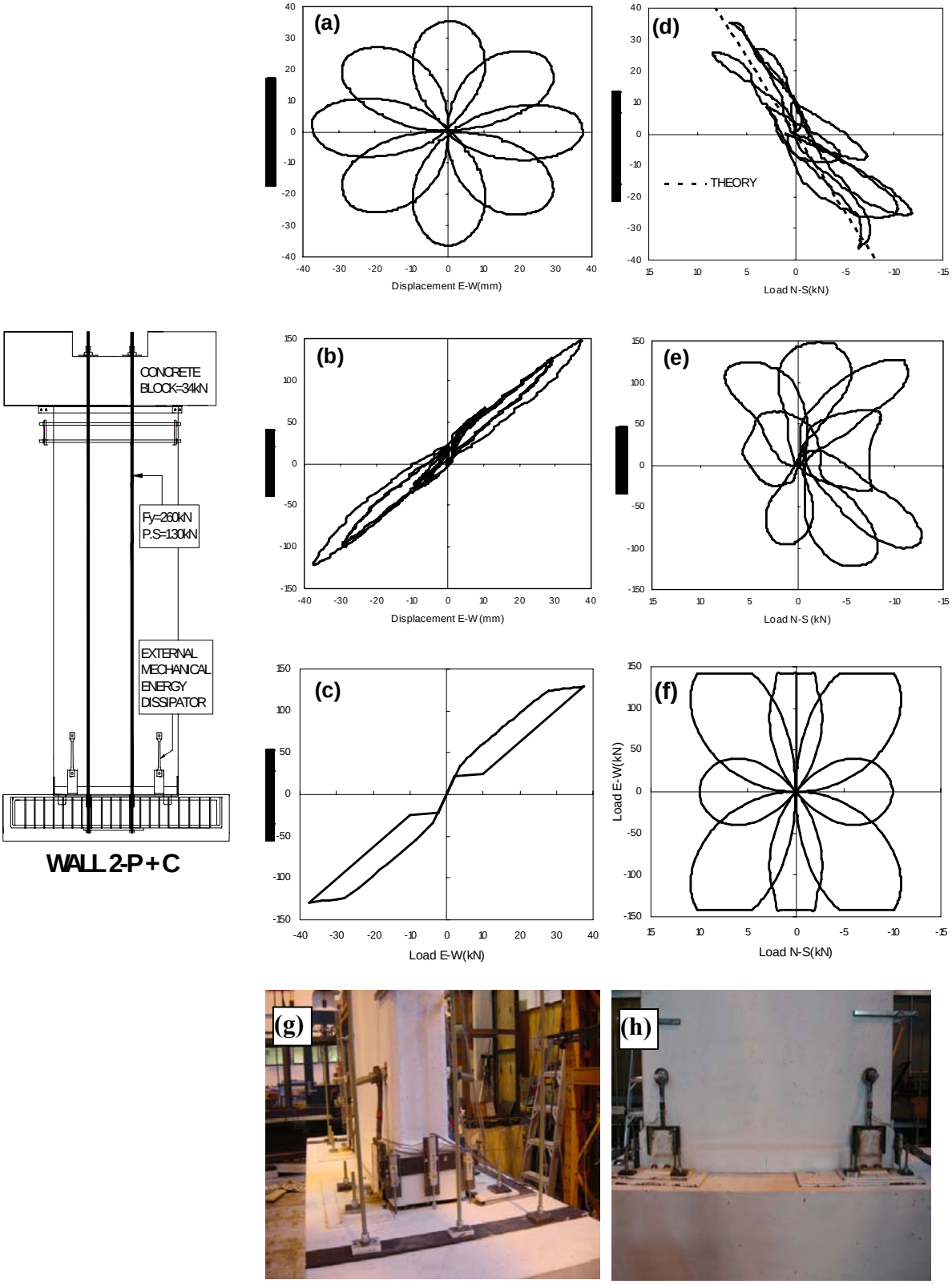


Figure 2.11: Wall 2-P+C: Performance with 50% prestressing unbonded tendons and external mechanical energy dissipators; (a) "double 4-leaf clover" displacement controlled pattern; (b) in-plane behaviour; (c) theoretical in-plane behaviour; (d) theoretical and experimental out-of-plane behaviour; (e) experimental biaxial load path; (f) theoretical biaxial load path; (g) buckling of energy dissipators; and (h) location of energy dissipators at front view.

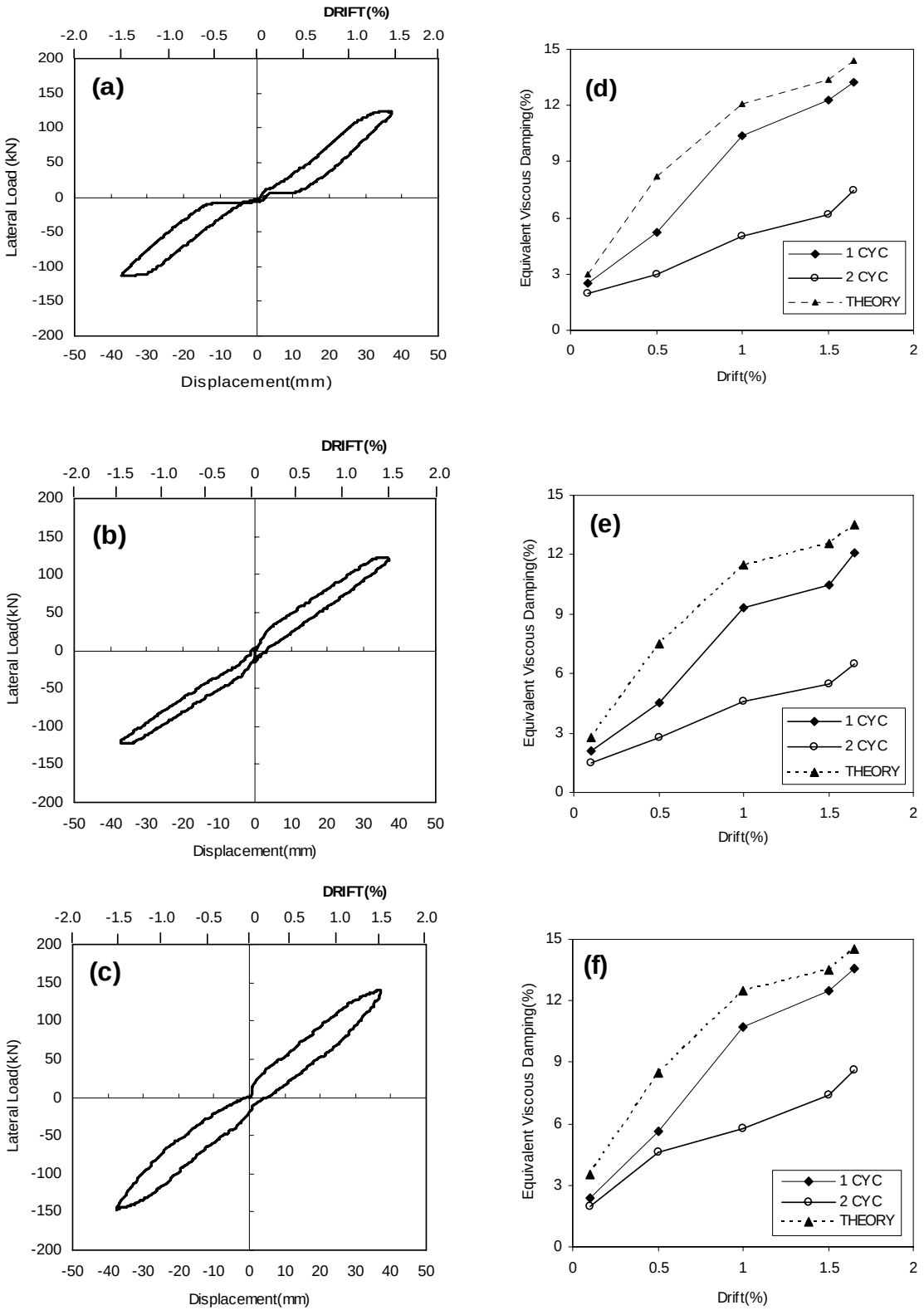


Figure 2.12: A comparative performance of single precast hollow core walls using three different types of energy dissipators at 1.5% drift; (a) a hysteresis loop of bonded fuse-bars; (b) a hysteresis loop of unbonded fuse-bars; (c) a hysteresis loop of mechanical energy dissipators; (d) equivalent viscous damping using bonded fuse-bars; (e) equivalent viscous damping using unbonded fuse-bars; and (f) equivalent viscous damping using external energy dissipators.

# CHAPTER 3

# LATERAL SEISMIC PERFORMANCE OF MULTI-PANEL PRECAST HOLLOW CORE WALLS

## SUMMARY

The seismic resistance of a superassemblage of precast hollow core wall units is investigated. The superassemblage consists of six prestressed concrete 1.2m wide hollow core units. Two of the units are tied to the foundation via unbonded vertical tendons while the other four units primarily act as “non-structural” cladding. The superassemblage represents the wall of a single storey warehouse type structure. The longitudinal unbonded prestressing tendons consist of regular thread-bars with an in-series portion of those bars possessing a reduced diameter to act as “fuses”. Prior to testing, the fuse-bars are prestressed to 50% of their yield capacity. The multi-panel wall is tested under several different conditions: in-plane quasi-static reverse cyclic loading with different sizes of fuse-bars; and with and without rubber block spacers and sealant between units. Experimental results demonstrate that smaller diameter fuses lead to superior behaviour, as foundation uplift is inhibited. No structural damage occurs up to the experimental ± 4% drift limit. Some minor non-structural distress is observed to commence with sealant failure at 3% drift but this damage, however, is inexpensive to repair. Results also show that the hysteretic energy absorption that arises from the yielding tendons as well as the interacting rubber spacers and panel sealants provides an equivalent viscous damping factor of 10% at a design drift amplitude of 2%. The overall good performance of the multi-panel wall system well satisfies the requirements of an emerging seismic Damage Avoidance Design (DAD) philosophy.

## 3.1 INTRODUCTION

The application of precast hollow core slabs without transverse reinforcement as wall panels is common in certain non-seismic regions like Malaysia. Precast hollow core walls offer several advantages compared to monolithic conventional reinforced walls: design flexibility; faster construction; improved economy; no formwork; a load-bearing ability without the need for columns; and a variety of concrete finishes. The research presented herein seeks to extend the use of precast hollow core walls so that they can be constructed in moderate to high seismic regions. It has been demonstrated in the previous chapter that single hollow core walls are capable of resisting substantial lateral loads in spite of their lack of transverse/shear reinforcement, providing the connection details are modified. But a study on a single wall panel alone is insufficient to assess the overall building performance under earthquake ground shaking. This research, therefore, utilizes an assemblage of precast hollow core wall panels to form a rocking wall system that would be representative of a prototype warehouse building. The superassemblage is tested under in-plane quasi-static reversed cyclic lateral loading. The objective of this experimental work is to investigate the relative contributions of strength and equivalent viscous damping of various components that make up a multi-panel wall system. In addition to the post-tensioned seismic wall panels, components included are rubber block spacers, sealant and bearing pads, and a steel channel cap beam that is used to tie the panels together.

The main criteria in designing multi-panel walls are the diameter of the fuse-bars and the initial level of prestress. The fuse-bar capacity must be sufficient to resist seismic and wind loads, but at the same time there should be no tensile uplift of the foundation.

As determined in the previous chapter, the most suitable initial prestress of the fuse-bar is about 50% of its yield capacity; this gives the best trade-off between energy dissipation and displacement capacity. The main reason for choosing fuse-bars as the only means of energy dissipation is because they are easy to restress or replace after a strong earthquake. Moreover, the fuse-bars operate in tension only, thus they are not prone to buckle, nor do they tend to "soften" the structure as do tension-compression bonded fuses or external mechanical energy dissipators such as those used by Holden et al. (2003).

As mentioned in Chapter Two, the absence of transverse reinforcement in precast hollow core wall units is not a major problem when using hollow core units in seismic regions. But the base of each seismic resisting wall unit needs to be "damage protected". The basic hypothesis of this research is to combine the self-centring concepts of rocking, together with Damage Avoidance Design (DAD) armouring details (Mander and Cheng,1997). The multi-panel wall system consists of seismic and non-seismic wall panels which are designed to rock on their foundations; the system can be implemented and constructed in high seismic regions. This chapter first reviews important findings from associated research, and then goes on to present a concept development for single storey warehouse type structures. An experimental study is presented next and finally the results are discussed in terms of seismic behaviour attributes.

## 3.2 FINDINGS FROM PREVIOUS RESEARCH

To date, minimal research has been conducted on multi-panel wall panels as compared to single wall panels. Much of the past research has focused on the performance of single wall panels under quasi-static cyclic lateral loading, dynamic loading and biaxial loading (McMenamin, 1999; Rahman and Restrepo, 2000; Holden et al., 2003; Surdano, 2003; Liyanage, 2004; and Voon and Ingham, 2006). A number of studies also have focused on the shear slip and opening gap which occurred in a stack of horizontal panels by incorporating unbonded post-tensioning in precast multi-storey buildings (Kurama et al.,1997; Kurama et al., 1999; Kurama, 2000; Kurama, 2001; Furutani et al., 2000; Ile and Reynoud, 2004). The PRESSS (Precast Seismic Structural Systems) research programme has carried out experimental work on a 60% scale five-storey precast building with two vertical precast wall panels joined to each other using U-shaped Flexure Plate mechanical energy dissipating connectors (Nakaki et al., 1999; Priestley et al., 1999; Conley et al., 1999; Wallace and Wada, 2000). However, these previous studies (apart from some work by Holden et al. (2003), Surdano (2003) and Liyanage (2004)) did not integrate and protect the bottom part of precast wall using the Damage Avoidance Design (DAD) approach developed by Mander and Cheng (1997) for bridges.

Stanton and Nakaki (2002) used self-centring concepts on four precast wall-panels by utilizing unbonded tendons on each wall and shear connectors between the walls. Rocking took place on a grouted bed. They proposed unbonded post-tensioning steel and gravity loads located at the centre of each wall with one initial prestressing tendon. They only considered one limit state at the onset of yielding in post-tensioning tendons.

In a recent study, Perez et al. (2004a) investigated the seismic performance of three two-storey, full-height precast concrete panels using two groups of post-tensioning steel tendons with additional limit states such as loss of initial prestress, crushing of confined concrete and fracture of the prestressing steel. They used the same vertical joint shear connectors for jointing two pieces of wall panels. Two unbonded post-tensioning steel tendons were used for each wall across the horizontal joints which were not located at the centre of the wall. Spiral reinforcement was employed to confine each bottom corner of the wall to sustain large compressive strains during the closing and opening gap of the wall. Following that study, Perez et al. (2004b) developed a fiber-based analytical model for three panel walls under monotonic pseudo static lateral loads. They recommended that the lateral load behaviour of this wall can be controlled by adjusting the total area of post-tensioning steel tendons, the initial prestressing and total shear yield force of vertical joint connectors. Despite the usefulness of this model in seismic design, it has not been validated with experimental work.

## 3.3 PROTOTYPE DESIGN OF MULTI-PANEL WALLS

Following from Chapter 2, the new design approach employed in this study seeks to demonstrate that no transverse or spiral reinforcement is required for a seismic resistant multi-panel precast concrete hollow core wall system. This is achieved through permitting individual panel units to be free to rock on the foundation. The multi-panel wall system is divided into “seismic” and “non-seismic” panels–the former carrying the gravity (inertia) loads, while the latter eventually becomes non-structural cladding. This research will seek to determine whether only a limited number of the wall panels

(say 15 to 20 percent) are sufficient to be prestressed to provide seismic resistance. By dividing the wall into seismic and non-seismic panels it is important to understand the interaction between the two, and what the weathertightness (sealant) needs should be under both normal (service) and extreme (seismic loading) conditions.

Based on the foregoing criteria, a prototype structural system has been conceived. Figure 3.1 shows a warehouse type industrial building that consists of a series of multi-panel precast concrete hollow core walls. Figure 3.1(a) shows longitudinal and transverse lateral seismic (or wind) loading acting on the single-storey structure. A roof truss diaphragm system is used to transfer these loads to an edge member that is shown as a steel channel in Figure 3.1(b). The channel is attached at each rafter location via post-tensioned prestressing tendons which in turn are anchored into the foundation. Thus the “seismic walls” are clamped to the foundation under normal service loads. Under high lateral loading the walls are free to rock, but they are also restrained by the elastically elongating tendons which permit re-centring at the termination of seismic shaking. Under uplift during earthquake excitation, seismic energy can be dissipated by using in-line fuses that restrict the amount of force that can be transmitted to the foundation.

Between these “seismic wall” panels, non-seismic panels are placed and seated on a continuous rubber bearing pad. In order to permit large in-plane movement between these “non-seismic” panels it is necessary to provide a “seismic gap” and detail the vertical joints between individual panels with care. Figure 3.1(c) shows the design joint width for the installations of sealant and rubber block spacers between the walls’ gaps. For an upper target design drift the shear strain on the rubber spacer blocks is given by

$$\gamma = \frac{\delta_h}{t_{gap}} = \theta \frac{B}{t_{gap}} \tag{3-1}$$

in which $t_{gap} =$ the horizontal gap between two wall panels, $\delta_h =$ uplift of bottom wall panel; $\theta =$ wall drift angle and $B =$ wall width. The vertical shearing force on one rubber block is given by the following equation:

$$V = GA\gamma = GA\theta \frac{B}{t_{gap}} \tag{3-2}$$

where $G =$ shear modulus of rubber pad; and $A =$ cross-sectional area of rubber pad.

Thus, the overturning moment of resistance provided by one panel surrounded by four rubber blocks is

$$M_{rpad} = 4V \frac{B}{2} = \frac{n}{2} GA\theta \frac{B^2}{t_{gap}} \tag{3-3}$$

For the silicone sealant that exists between two wall panels, the resistance provided by one vertical joint is defined as

$$M_{rsealant} = VB = \frac{GAB^2\theta}{t_{gap}} = \frac{GHt_sB^2\theta}{t_{gap}} \tag{3-4}$$

where $H =$ wall height; and $t_s =$ total (through wall) sealant thickness in one vertical joint.

The lateral load necessary to mobilize all the rubber blocks in the multi-panel wall superassemblage is

$$F_{pad} = \frac{n}{2} \frac{M_r}{H} = \frac{n}{2} GA\theta \frac{B^2}{Ht_{gap}} \tag{3-5}$$

Similarly for the sealant

$$F_{sealant} = n_j G \frac{t_s B^2}{t_{gap}} \theta \tag{3-6}$$

where $n_j$ = number of vertical joints containing the sealant. The force exerted on the rubber pad is calculated using equation 3-5 and force in silicone sealant can be calculated using equation 3-6.

Example 3.1 : Force exerted on rubber pad

Shear modulus of rubber pad, $G = 810kPa$ (manufacturer's catalogue)
Area of one rubber pad, $A = 4450mm^2$
Gap between rubber pad, $t_{gap}$ =40mm
Wall height, $H = 2800mm$
At 2% drift , $\theta = 0.02$
The number of rubber pad surrounding multi-panel wall, $n = 20$

The lateral force exerts on rubber pad is calculated using equation 3-5 as follows:

$$F_{pad} = \frac{20}{2} \times 810 \times 4450 \times 0.02 \times \frac{1200^2}{40 \times 2800 \times 1000} = 9.26kN$$

Example 3.2 : Force exerted on silicone sealant

Shear Modulus of silicone sealant, G = 12kPa (manufacturer's catalogue)
Area of silicone sealant attached to wall panel, A = 2800mmx20mm=56000mm$^2$
Gap between rubber pad, $t_{gap}$ = 40mm
Wall height, $H = 2800mm$
At 2% drift , $\theta = 0.02$

The lateral force exerts on silicone sealant is calculated using equation 3-6 as

$$F_{sealant} = 5 \times 12 \times 56000 \times 0.02 \times \frac{1200^2}{40 \times 2800 \times 1000} = 0.86kN$$

From the above it is evident that at 2% drift there is a contribution of some 10kN to the overall wall resistance that results from panel-to-panel interaction.

## 3.4 RESISTANCE MECHANISMS IN A MULTI-PANEL WALL SYSTEM

There are four principal components of forces that contribute to the overall resistance of a multi-panel wall system, as shown in Figure 3.2. These are given by

$$F_H = F_{SW} + F_{NS} + F_V + F_{CH} \tag{3-7}$$

where $F_H =$ total lateral force applied at the eaves level, $F_{SW} =$ resistance provided by the post-tensioned seismic wall including the effects of fuses and mechanical energy dissipators (if any); $F_{NS} =$ resistance arising from the self-weight of the non-seismic walls; $F_V =$ shear resistance contribution arising from the sealant compound between the walls; and $F_{CH} =$ contribution of the plastic mechanism of the steel channel.

Figure 3.2(a) shows the principal resistance mechanism arising from the post-tensioned walls. By taking moments about the toe of the rocking wall unit

$$F_{SW} = \frac{B}{2H}\left(W_r + W_W + T_1 + T_2\right) + \frac{e_p}{H}\left(T_1 - T_2\right) \tag{3-8}$$

in which $B =$ panel width; $H =$ wall height; $W_r =$ reaction load from the rafter; $W_W =$ self-weight of the wall panels; $T_1$ and $T_2 =$ respective forces in the first and second tendons; $e_p =$ the eccentricity between the unbonded post-tensioned tendons.

Figure 3.2(b) shows the resistance of one non-seismic wall panel as a result of its self-weight

$$F_{NS} = \frac{B}{2H} W_W \tag{3-9}$$

The lateral resistance provided by imposing shear deformations along each vertical wall joint as shown in Figure 3.2(c) can be found from

$$F_v = \frac{B}{H} V_r \tag{3-10}$$

where $V_r$ = total shear resistance provided by rubber spacing blocks plus the sealing compound.

Figure 3.2(d) shows the seismic walls connected by the steel channel along with Figure 3.2(e) which depicts the deformed plastic mechanism that leads to plastic hinges in the channel. Using virtual work principles it can be shown that the resistance contributed by the mechanism is

$$F_{CH} = \frac{2M_p}{H}\left(1 + \frac{1}{n_{ns}}\right) \tag{3-11}$$

where $n_{ns}$ = the number of standard non-seismic walls placed in between the seismic walls; and $M_p$ = the plastic capacity of the reduced channel section.

Substituting equations 3-8 to 3-11 into equation 3-7 and normalizing with respect to the total seismic weight $(W_T)$ gives the base shear capacity.

$$C_c = \frac{F_H}{W_T} = \frac{B}{2H}\left(\frac{W_r + W_W + T_1 + T_2}{W_T}\right) + \frac{e_p}{H}\left(\frac{T_1 - T_2}{W_T}\right) + n_{ns}\frac{B}{H}\frac{W_W}{W_T}$$

$$+ \frac{B}{H}\frac{V_r}{W_T}(n_s + 1) + \frac{2M_p}{HW_T}\left(1 + \frac{1}{n_{ns}}\right) \tag{3-12}$$

where the total seismic weight is given by $W_T = W_r + (n_{ns} + 1)W_W$, $n_s$ = the number of seismic walls and $e_p$ = the distance between the tendon and the centre of the wall.

## 3.5 DESIGN AND CONSTRUCTION OF THE MULTI-PANEL WALL SUPERASSEMBLAGE

Figure 3.3 shows the reinforcement details and the experimental setup of the super-assemblage. Wall 1 and Wall 2 together with their own foundation from the previous tests were re-used with four new hollow core units as the non-seismic infill wall panels. Initially, 20mm diameter, 500mm long fuse-bars were used in series with the 25mm thread bar tendons. They were inserted into the second and fifth void sections of the seismic walls and screwed into couplers located at two-thirds height of the walls, as shown in Figure 3.3(a). An infill spread footing foundation beam (4730x350x400mm) was constructed between the original seismic foundation beams (that were located beneath the seismic panels) and connected contiguously to the seismic foundation beam (refer to Figure A3.1). The entire foundation beam was anchored to the laboratory strong floor to inhibit sliding, but note that no uplift or hold down restraint was provided. This was to ensure the foundation beam was a true representation of a spread footing. Beneath the non-seismic wall panels a 4730x350x20mm rubber pad (IRHD55) was placed to seat those panels.

A 9000mm long 254x79x28.9kg/m steel channel cap beam was placed on top of the seismic walls to tie them together. The channel spanned across, but did not touch, the non-seismic wall panels. The channel was prestressed to the seismic walls to ensure it acted as a tie beam. A V-shape cut to the channel flanges was applied to allow the lateral load to transmit to the next seismic wall only through the steel web (refer to Figure A3.2). The purpose of this cut was to minimize flexural bending of the channel. Mass concrete blocks, 34kN each, were placed on top of the seismic walls to represent the gravity load reaction from the roof/rafter system. The bottom concrete blocks were

bolted to the top of the steel channel using 20mm bolts with six steel plates welded on each flange of the steel channel (refer to Figure A3.3). The main reason for bolting each concrete block to the steel channel was to ensure proper transfer of lateral load from the hydraulic actuator to the first and second seismic walls.

Two different sizes of rubber blocks were used, 100x50x40mm which were placed into the inner wall gap and 100x50x25mm which were inserted into the outer wall gaps (refer to Figure A3.4). A photograph of the overall front elevation view of multi-panel precast hollow core wall system together with the foundation beam is shown in Figure 3.3(b). The seismic wall and seismic foundation beam are painted white, while the grey units are non-seismic infill wall panels.

## 3.6 EXPERIMENTAL SETUP, INSTRUMENTATION AND TESTING PROCEDURES

Figure 3.4 depicts the experimental set-up and instruments of the multi-panel walls as tested on the laboratory strong floor. Figure 3.4(a) shows the schematic arrangement of seismic wall, non-seismic wall, location of in-series unbonded fuse-bars, steel channel cap beam, foundation block and in-plane actuator attached to reaction frame. Lateral load was provided by a 1000kN actuator with force being measured by an in-series load cell. The experiments were conducted in “drift” control where drift was defined as the angle difference between upper and lower displacement transducers mounted on the wall panel adjacent to the hydraulic actuator (P4). A quasi-static cyclic reversed lateral force regime was applied at the center of the mass which was located at 3400mm height from the strong floor.

Figure 3.4(b) shows the instrumentation used during the experiments. Twenty seven linear potentiometers that were used to monitor uplift and sliding of the wall units, the foundation beam, top concrete blocks and rocking toe of each wall were employed. Six rotary potentiometers were attached on both sides of the seismic walls to trace any rotation of the seismic wall panels and sliding of the top mass concrete blocks. Six inclinometers were used to measure the inclination angles of each panel during the rocking process. They were positioned at the mid-width of each wall and at a 2450mm height above the foundation beam. “Demec” points (demountable mechanical strain gauges) were placed on a 250mm grid on Walls 1 and 2 to infer concrete strains at different levels of drift and determine the stress contour distribution under the reverse seismic loading. Demec points were also used to measure gap movement between wall units (refer to Figure A3.5). Strain gauges were affixed to each of the unbonded fuse-bars and calibrated to measure prestress levels and force changes under uplift of the panel units during lateral loading. Prior to testing, the fuse-bars were prestressed individually up to 50% of their yield capacity.

The super-assemblage was tested under completely reversed cyclic lateral load in three phases as follows:

Phase 1: Rubber blocks spacers between the gap with 20mm diameter and 500mm length of fuse-bars were tested at ± 0.1%, ± 0.5% and ±1.0% for two cycles at each level drift. The positive semi-cycles drift was imposed by loading the double-actuator ramp from west to east and conversely, the negative semi-cycles drift from an east to west direction. Any uplift of the foundation block was recorded by two linear potentiometers located at both ends of the seismic foundation block.

Phase 2: To mitigate the potential for foundation uplift, a smaller 13mm diameter unbonded fuse-bar was used. The new fuses were also strain gauged and the superassemblage was re-tested under two cycles at each drift amplitude of ± 0.1%, ± 0.5%, ±1.0%, ±1.5% and ± 2.0%.

Phase 3: A silicone sealant was installed on both faces on the walls. After a two week curing period the specimen (with 13mm diameter fuse-bars, sealant and rubber blocks) was tested under two reversed cycles at drift amplitude of ± 0.1%, ± 0.5%, ±1.0%, ±2.0%, ± 3.0% and ± 4.0%.

Based on the foregoing criteria a joint width of 40mm between wall panels was adopted along with 100x50x40mm rubber block spacers. A proprietary silicone sealant (Silaflex MS) was then applied to fill the remaining gaps between wall panels (refer to Figure A3.6). It should also be noted that besides these structural requirements, the gaps must also fulfill the usual non-structural requirements such as durability, sound insulation, fire resistance, thermal insulation, watertightness, appearance and accessibility for inspection, maintenance and replacement.

## 3.7 EXPERIMENTAL RESULTS AND OBSERVATIONS

The overall and individual seismic performance of multi-panel walls on each phase as described above is presented in this section. The experimental results are classified according to their overall hysteretic performance, visual observation deformation of rubber block, sealant and damage on sealant. An important comparison is the potential for uplifting of the foundation block when using the 20mm and 13mm fuse-bars. The seismic performance of Phase 3 which represented the final construction state of a multi-

panel precast hollow core wall system at 2.0% and 4.0% drift is also presented in this section.

### 3.7.1 HYSTERETIC PERFORMANCE OF PHASES 1, 2 AND 3

Figure 3.5 shows the overall hysteretic performance of the multi-panel precast hollow core walls system under Phases 1, 2 and 3. The initial run was conducted at ± 0.1% drift to ensure that all instruments recorded the correct magnitudes and directions of the lateral, uplift and rotation movements. Figure 3.5(a) shows the overall performance of multi-panel walls system at ± 0.1%, ± 0.5% and ± 1.0% drift tested under Phase 1 using 20mm diameter fuse-bars and rubber block spacers. The yield base shear of multi-panel walls is 90kN with yield drift of 1.0% (refer to Figure A3.7, Figure A3.8 and Table A3.1). As the level of drift increased, more energy was dissipated by engaging the base rubber pad and rubber blocks spacers. Under Phase 1, the superassemblage was only tested up to 1.0% drift because of a 7mm recorded uplift of the foundation block. The uplift caused some cracks within the foundation.

Figure 3.5(b) depicts the overall seismic performance of multi-panel walls under Phase 2 at ± 2.0% drift with 13mm fuse-bars and rubber block spacers between the walls. The analytical results of base shear capacity show acceptable agreement with the experimental results. The overall system produced a reasonably good behaviour with self-centring provided by the unbonded fuse-bars and cap beam on top of the walls. The detail of experimental results for Phase 2 is shown in Figure A3.9.

Figure 3.5(c) shows the overall performance of multi-panel walls under Phase 3 using 13mm fuse-bars, rubber block and sealant tested up to ± 4.0% drift. Similar experimental results were obtained as predicted analytically. The base shear at 2.0% drift was 94kN and under Phase 3 is slightly higher than 83kN under Phase 2. The multi-panel precast hollow core wall system with sealant (Phase 3) dissipated more energy than Phase 2 (without sealant) as indicated by the increased area enclosed by the hysteretic loops. Full details of the experimental results for Phase 3 are shown in Figure A3.10, Figure A3.11 and Table A3.2.

### 3.7.2 VISUAL OBSERVATIONS AND DAMAGE

Several photographs taken during the course of the experimental study are presented in Figure 3.6. The in-plane lateral movements of the multi-panel superassemblage at + 2.0% and – 4% drift are shown in Figure 3.6(a) and (b), respectively. The steel channel effectively transferred the lateral force from the first to the second seismic wall. However, owing to the compressibility of the rubber block spacers, all non-seismic walls had smaller displacements than the drifts imposed on the seismic walls.

Figure 3.6(c) shows how the shear strain distribution of the rubber block spacer varied linearly between Wall 5 and Wall 6. A similar, almost linear, shear strain distribution is evident in the silicone sealant between the panels as shown in Figure 3.6(d). Based on the overall visual observation, the super-assemblies of multi-panel walls performed very well up to almost 3.0% drift. Although no structural damage was observed in any of the superassemblage specimens, some minor non-structural damage was evident in the silicone sealant which became torn following the 3% drift amplitude (refer to Figure

A3.12 and Figure A3.13). No structural damage occurred to the rocking toe of both seismic walls as expected throughout the entire experiments.

Figure 3.6(e) shows a local tensile bond failure at the sealant of Wall 5 and Wall 6 at -3.0% drift. This failure occurred when the cohesive strength of the sealant was greater than the cohesive strength on the edges of the walls. This is also attributed to imperfect preparation of the concrete surfaces. Owing to the presence of concrete debris attached to the sealant, tearing away from that surface commenced early. Figure 3.6(f) illustrates the second example of failure known as folding failure. This failure arose when the silicone sealant experienced an excessive movement in compression resulting in permanent set leading to folding of the sealant. Figure 3.6(g) shows a general adhesion failure at + 4.0% drift. This failure occurred when the sealant generally lost its adhesive bond with the concrete panel surface. This became more pronounced when the sealant peeled off from the walls and displaced it from its original position (refer to Figure A3.14).

Similar to the conclusions drawn by Holden et al.(2003), this experiment showed that multi-panel precast hollow core walls are able to perform better than conventional cast-in-situ reinforced walls because of the non-existence of a conventional plastic hinge zone (PHZ) at the wall-foundation interfaces. In addition, a self-centering rocking connection between wall and foundation block produced a pinching on hysteresis loops during unloading and allows them to rock backwards and forwards on their bases. The rubber pad, rubber block spacers and silicone sealant together provide a means to cushion and absorb seismic energy during rocking excursions. These materials are therefore recommended as suitable for future construction of industrial type buildings such as warehouses.

### 3.7.3 FOUNDATION UPLIFT

Figure 3.7 shows the uplift of the foundation block that occurred during the Phase 1 experiment as measured by potentiometers labeled as P31 and P5 (see Figure 3.4(b) for location). It is evident from these results that if the fuse-bars are permitted to transmit large forces, then foundation uplift, rather than wall rocking, will occur. To inhibit foundation uplift from occurring, the foundation block should either be made heavier or tension piles provided. Both solutions may be unduly expensive. Therefore, an alternative (counter-intuitive) solution is to provide a smaller prestress force through using smaller diameter fuses. Thus in Phases 2 and 3 of the experiments 13mm diameter fuses were chosen to replace the 20mm diameter fuses used initially in Phase 1.

Figure 3.7 also shows the comparison of uplifting two bottom corners of a foundation block under Phase 1 and Phase 2 with same length of 500mm fuse-bars and rubber block spacers between infill walls. Potentiometers labelled as P31 and P5 were located on the left and right hand side far end bottom corner of the foundation block. This graph shows that there is no uplift of the foundation block when using the 13mm fuse-bars with 50% initial prestress. With the bottom corners of foundation block being uplifted by 7mm, the bearing pressures beneath the remaining contact area increased. Although this was not a problem in the laboratory, in prototype field conditions resisting these increased bearing pressures could be unduly expensive.

### 3.7.4 INFILL WALL DISPLACEMENTS

While Walls 1 and 6 showed similar displacement performance to the overall behaviour under Phase 1 as shown in Figure 3.8(a), the non-seismic panels, Walls 2 to 5 displaced somewhat less as shown in Figure 3.8(b) to (e), respectively.

Figure 3.9 presents the comparative displacement results of the performance of each of the individual wall units in the superassemblage during Phase 3 of the experiment. Visual observation of rocking multi-panel walls is shown in Figure A3.15. The thin and thick lines represent the performance when the overall specimen was cycled through the 2% and 4% drift amplitudes, respectively. It will be noted that the seismic wall units (Walls 1 and 6) were both forced to experience the full displacement imposed, whilst the non-seismic wall units (Walls 2-5) experienced a decreasing amount of the imposed displacement as this was transmitted through the series of compressible rubber spacer blocks. Thus, at the 4% drift amplitude between Walls 5 and 6 there was a drift deficiency of 2.2%. This translates into a 65mm widening of the gap between Walls 5 and 6. This tearing displacement contributed to the deterioration of the sealant between the units.

## 3.8 EQUIVALENT VISCOUS DAMPING

Each graph shows the experiment results of points plotted for equivalent viscous damping for the energy absorbed over the previous full cycle of lateral loading at that drift amplitude. Experimental results are plotted for the first and second cycles. For the

second cycle the equivalent viscous damping is approximately 60% of the first cycle. The reduced energy absorption results from tendon yielding that occurred in the previous (first) cycle and leads to hysteresis loops with a smaller enclosed area on the subsequent (second) cycle.

Figure 3.10 also shows the theoretical equivalent viscous damping ($\xi_{eq}$) where the analytical hysteresis model is used for one equi-amplitude cycle. In the realistically constructed condition (Phase 3) where the panel-to-panel sealant was present, the theoretical prediction is some 10% in excess of the experimental observation. Notwithstanding this outcome, it appears that the equivalent viscous damping is reasonably constant for drifts in excess of 2%. Thus a value of, say, 12% of equivalent viscous damping could be used for seismic design purposes.

## 3.9 CONCLUSIONS AND RECOMMENDATIONS

Based on the experimental findings presented herein the following conclusions are drawn:

1. The experimental work on a superassemblage of multi-panel precast concrete hollow core wall units has demonstrated that the seismic and non-seismic wall units can be implemented in the construction of single storey warehouses. Under large drifts (>3%) damage is limited to the sealants. Such damage is inexpensive to repair.
2. By steel-armouring seismic wall units at the wall-foundation interface, and seating the non-seismic walls on rubber bearing pads a damage avoidance performance can be achieved. These damage avoidance design (DAD) details

accommodate higher displacement and contact pressures at the rocking toe during uplift of precast hollow core walls. The thickness of the rubber pad and rocking steel plate can be designed based on the maximum base shear imposed on their rocking base to dissipate energy during ground shaking. Shear keys or pintles can be welded beneath the steel seating channel to inhibit sliding.

3. There were no cracks observed either on seismic walls or non-seismic walls up to 4.0% drift.
4. The rubber seating pad, silicone sealant and rubber block spacer are good materials to accommodate differential displacements between units and to absorb some energy. Such materials provide an economical alternative to using vertical shear connectors.
5. It recommended that each seismic wall panel be located at the centre of a single precast foundation beam unit. Each foundation beam unit should be discontinuous with neighbouring units in order to reduce soil bearing pressure which could prevent the uplifting of the foundation beam during severe shock. Joints between foundation units should be detailed to transmit some shear force, but no moment.

## REFERENCES


Conley, J., Priestley, M.J.N., and Sritharan, S. (1999). "Wall direction modeling of the five-story PRESSS precast test building." *Report SSRP 99/19*, University of California, San Diego, CA, USA.

Furutani, M., Imai, H., and Matsumoto, T. (2000). "Shear strength evaluation method for multi-story precast concrete structural walls." *12th World Conference on Earthquake Engineering*, 12WCEE 2000, Auckland, New Zealand, Paper No. 1797.

Holden, T.J., Restrepo, J., and Mander, J.B. (2003). "Seismic performance of precast reinforced and prestressed concrete walls." *Journal of Structural Engineering,* ASCE, 129(3), 286-296.

Ile, N., and Reynoud, J.M. (2004). "Seismic behaviour of R/C walls subjected to multi-directional seismic loading." *13th World Conference on Earthquake Engineering,* Vancouver, B.C., Canada, Paper No.3243.

Kurama, Y., Dessiki, S., Sause, R., Pessiki,S., Lu, L.W., and Sheikh., M.El. (1997). "Seismic design and response evaluation of unbonded post-tensioned precast concrete walls." *Research Report No. EQ-97-01*, Departmental of Civil and Environmental Engineering Lehigh University, Bethlehem, PA, USA, 184.

Kurama, Y., Dessiki, S., Sause, R., and Lu, L.W. (1999). "Seismic behaviour and design of unbonded post-tensioned precast concrete walls." *PCI Journal*, 38(3), 72-73.

Kurama, Y. (2000). "Seismic design of unbonded post-tensioned precast concrete walls with supplemental viscous damping." *ACI Structural Journal*, 7(4), 72-73.

Kurama, Y. (2001). "Simplified seismic design approach for friction-damped unbonded post-tensioned precast concrete walls." *ACI Structural Journal*, 8(5), 705-715.

Liyanage, L.U. (2004). "Biaxial lateral loading behaviour of thin concrete walls," thesis, presented to University of Canterbury at Christchurch, New Zealand, in partial fulfillment of the requirements for the degree of Master of Engineering.

Mander, J. B., and Cheng, C.-T. (1997). "Seismic resistance of bridge piers based on damage avoidance design." *Technical Report NCEER-97-0014*, NCEER, Departmental of Civil and Environmental Engineering, State University of New York at Buffalo, Buffalo, USA.

McMenamin, A. (1999). "The performance of slender precast reinforced concrete cantilever walls with roof level lateral displacement restraint under simulated in-plane seismic loading," thesis, presented to University of Canterbury at Christchurch, New Zealand, in partial fulfillment of the requirements for the degree of Master of Engineering.

Nakaki, S.D., Stanton, J.F., and Sritharan, S. (1999). "An overview of the PRESSS five-story precast test building." *PCI Journal*, 44(2), 26-39.

Perez, F., Pessiki, S., and Sause, R. (2004a). "Seismic design of unbonded post-tensioned precast concrete walls with vertical joint connectors." *PCI Journal*, 49(1), 58-79.

Perez, F., Pessiki, S., and Sause, R. (2004b). "Lateral load behavior of unbonded post-tensioned precast concrete walls with vertical joints." *PCI Journal*, 49(2), 48-63.

Priestley, M.J.N., Sritharan, S., Conley, J.R., and Pampanin, S. (1999). "Preliminary results and conclusions from the PRESSS five-story precast concrete test building." *PCI Journal*, 44(6), 42-67.

Rahman, A.M., and Restrepo, J.I. (2000). "Earthquake resistant precast concrete buildings: seismic performance of cantilever walls prestressing using unbonded tendons." *Research Report 2000-05*, Department of Civil Engineering, University of Canterbury, New Zealand.

Stanton, J.F., and Nakaki, S.D. (2002). "Design guidelines for precast concrete structural systems." *PRESSS Report No. 01/03-09*, Department of Civil Engineering, University of Washington Seattle, Washington, USA.

Surdano, I. (2003). "Performance on thin precast concrete wall panels under dynamic loading," thesis, presented to University of Canterbury at Christchurch, New Zealand, in partial fulfillment of the requirements for the degree of Master of Engineering.

Voon, K.C., and Ingham, J.M. (2006). "Experimental in-plane shear strength investigation of reinforced concrete masonry walls." *Journal of Structural Engineering*, ASCE, 132(3), 400-408.

Wallace, J.W., Wada, A. (2000). "Hybrid wall systems: US-Japan Research." *12th World Conference on Earthquake Engineering*, 12WCEE, Auckland, New Zealand, Paper No.2619.

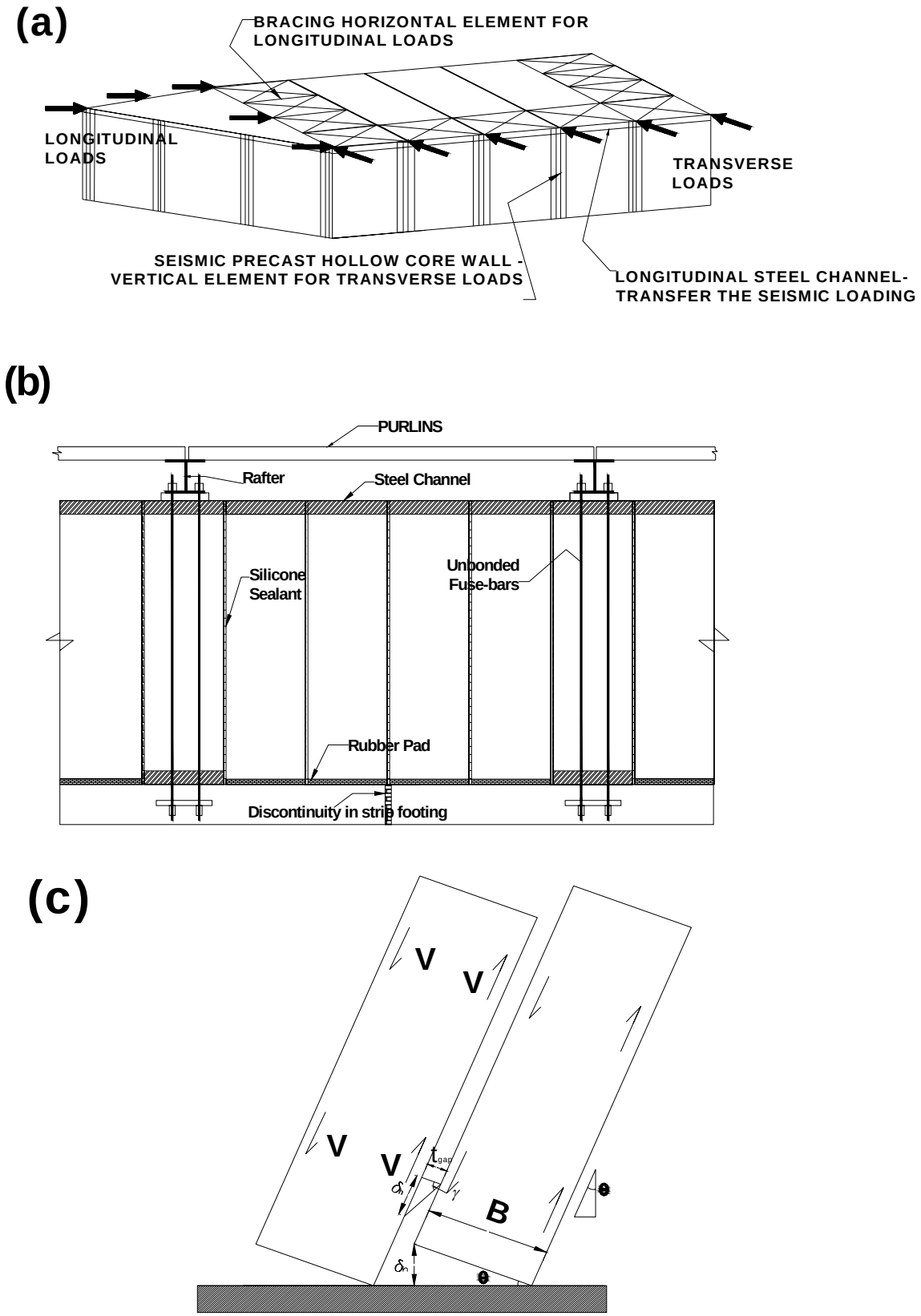


Figure 3.1: The superassemblage multi-panel wall is represented as part of a prototype warehouse; (a) the isometric warehouse showing the directions of loading and schematic arrangement of seismic walls; (b) side elevation of a multi-panel wall consisting of seismic and non-seismic wall; and (c) the design joint width between the gap of the walls.

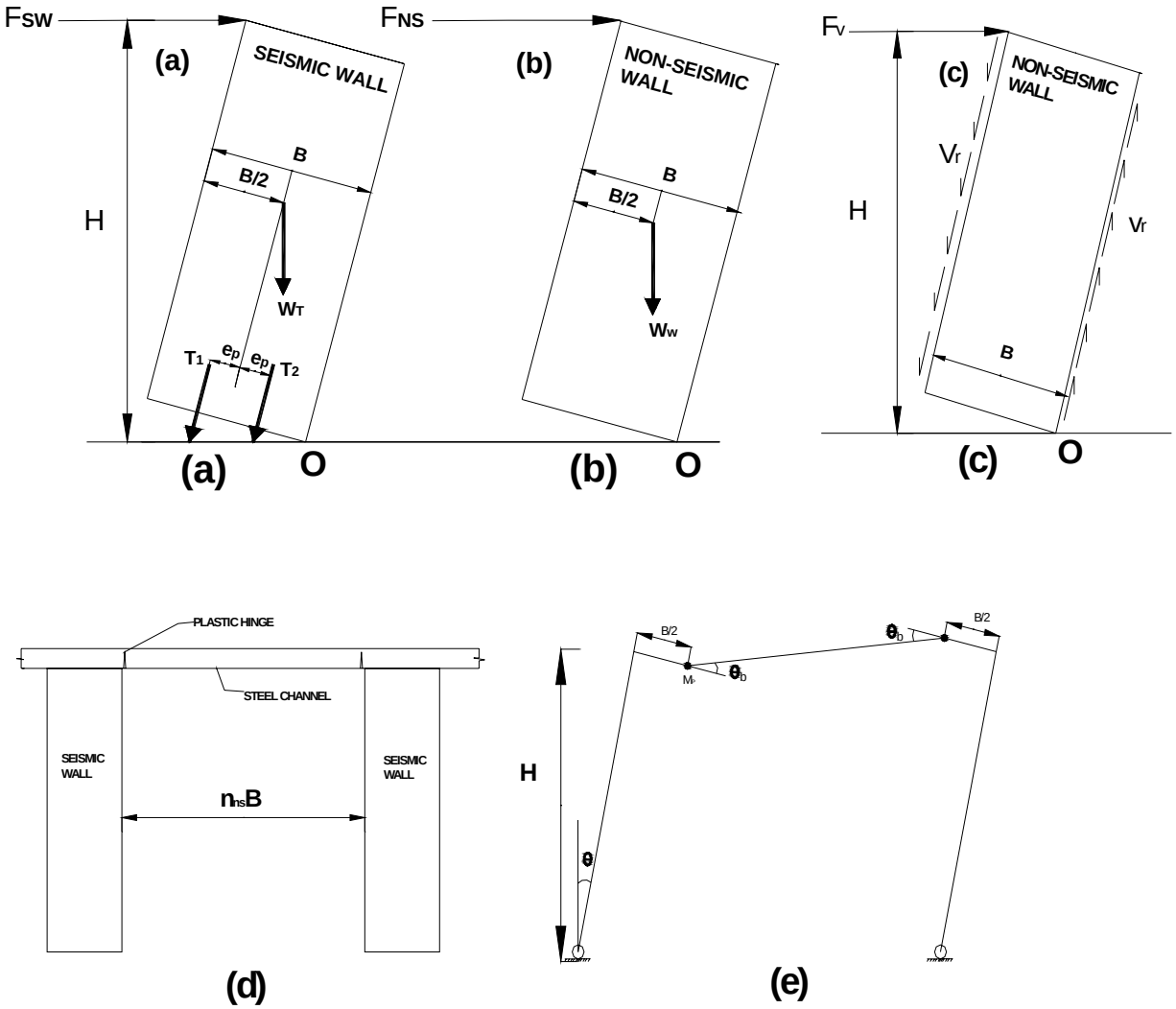


Figure 3.2: Resistance mechanism of a multi-panel wall system; (a) lateral resistance due to post-tensioned tendons and self-weight of seismic walls; (b) lateral resistance coming from the self-weight of a non-seismic wall; (c) shear resistance from silicone sealant; (d) plastic hinge occurred at the V-cut shape of the steel channel close to the seismic wall; and (e) the plastic mechanism on the steel channel cap beam.

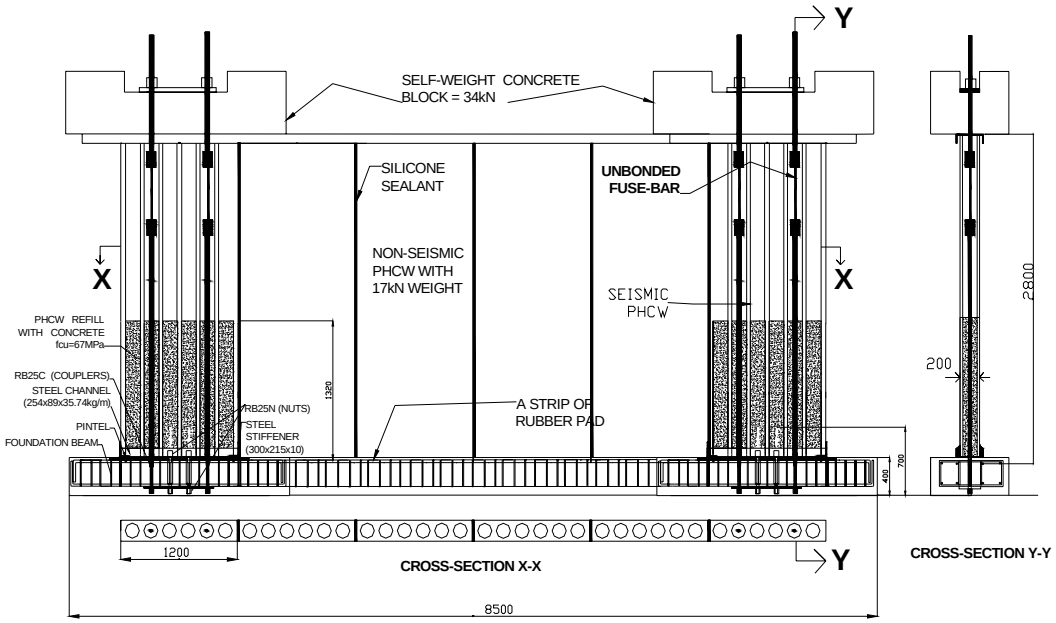


**(a)**

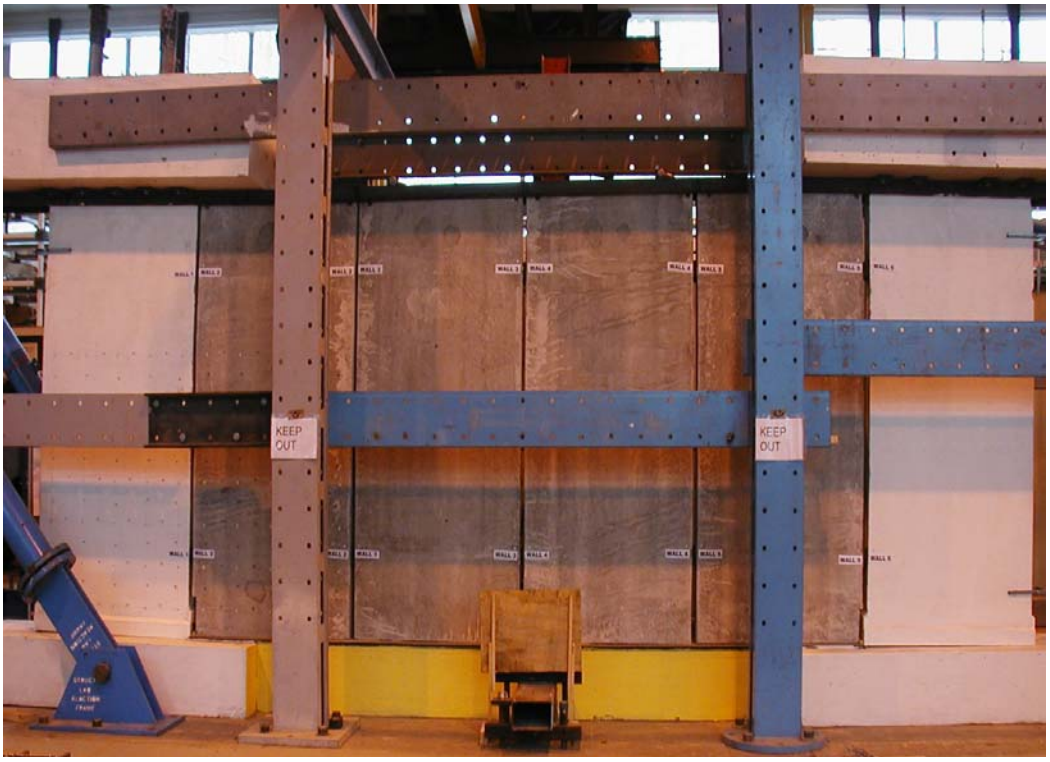


**(b)**

Figure 3.3: Construction and reinforcement detail of multi-panel precast hollow core walls; (a) details of reinforcement and front elevation of the schematic arrangement seismic wall and non-seismic wall; and (b) multi-panel super-assemblage representing part of the PHCW system in a warehouse building.

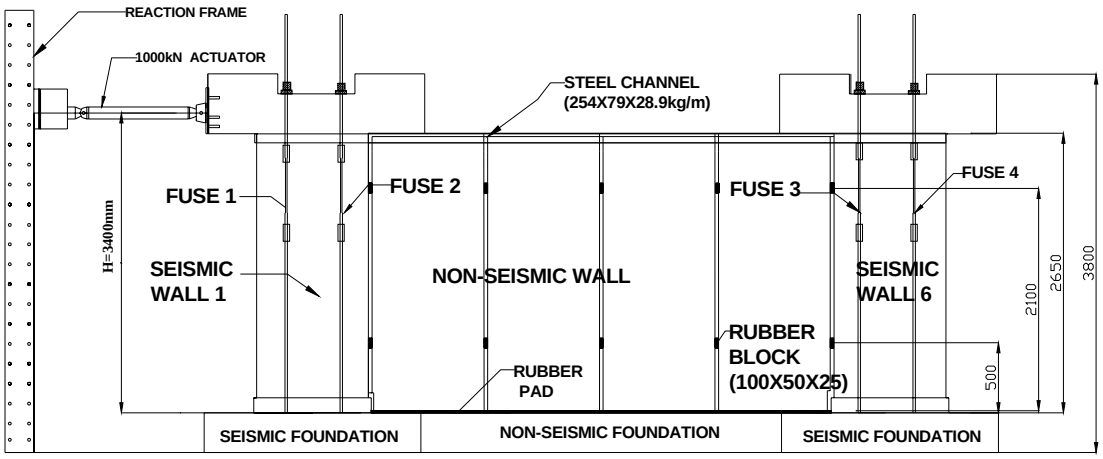


**(a)**

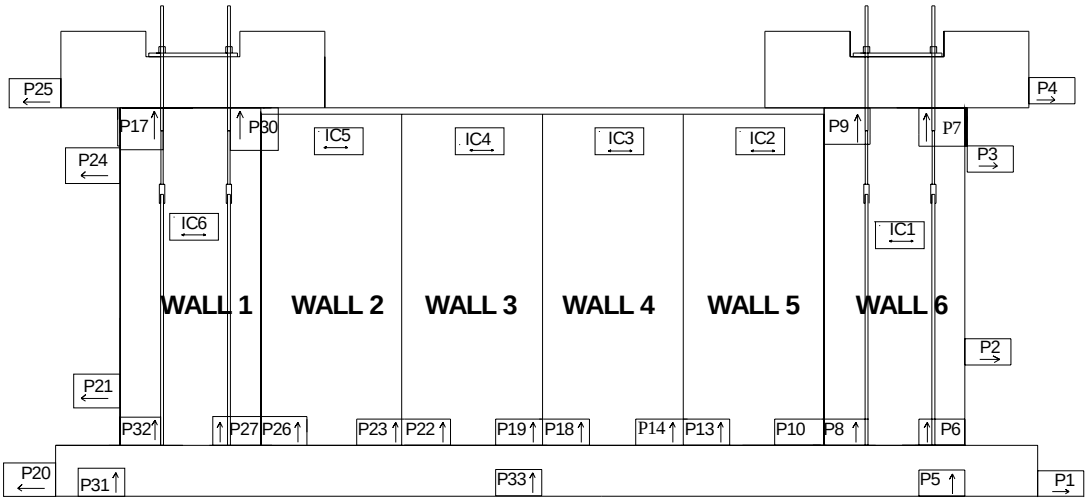


**(b)**

Figure 3.4: The experimental set-up of a multi-panel superassemblage of precast hollow core wall units; (a) the loading frame including the arrangement of seismic, non-seismic walls and fuse-bars for a multi-panel wall system; and (b) the schematic arrangement of potentiometers with their direction of measurements.

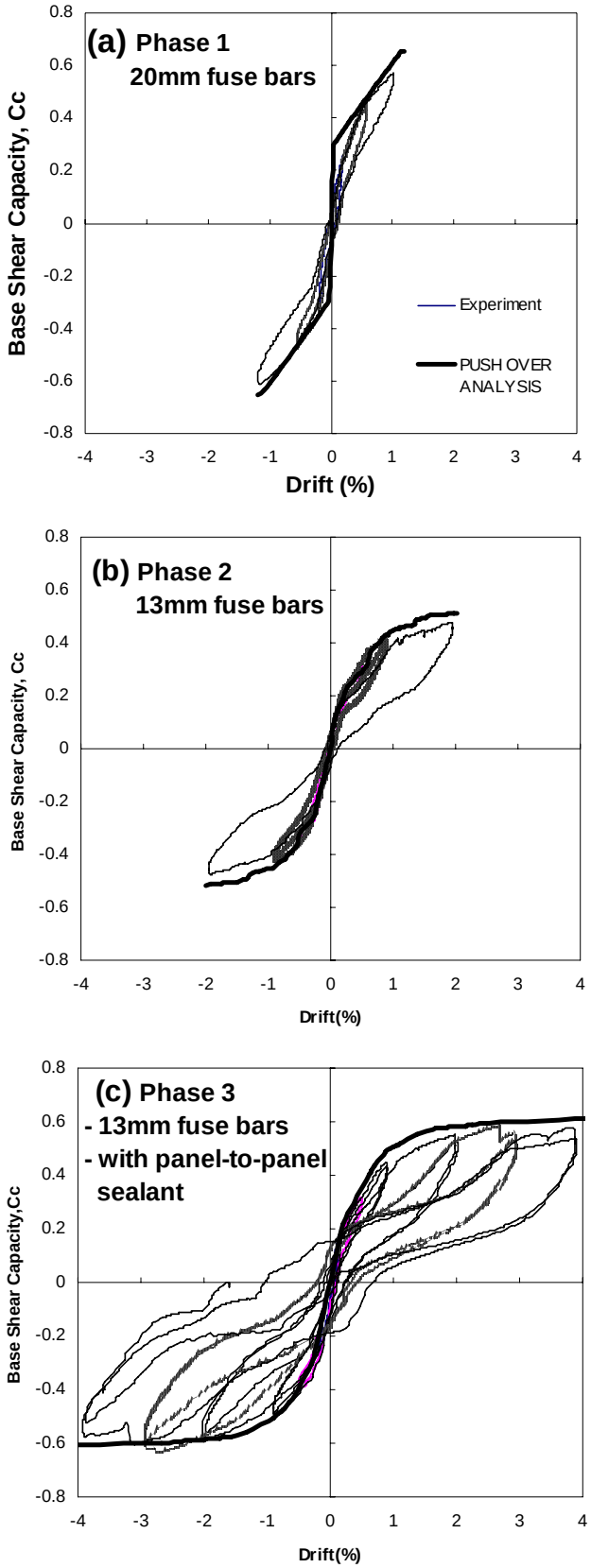


Figure 3.5: The overall hysteretic performance of Phases 1, 2 and 3: (a) experimental result for Phase 1 up to 1.0% drift; (b) experimental result for Phase 2 up to 2.0% drift; and (c) experimental result for Phase 3 up to 4.0% drift.

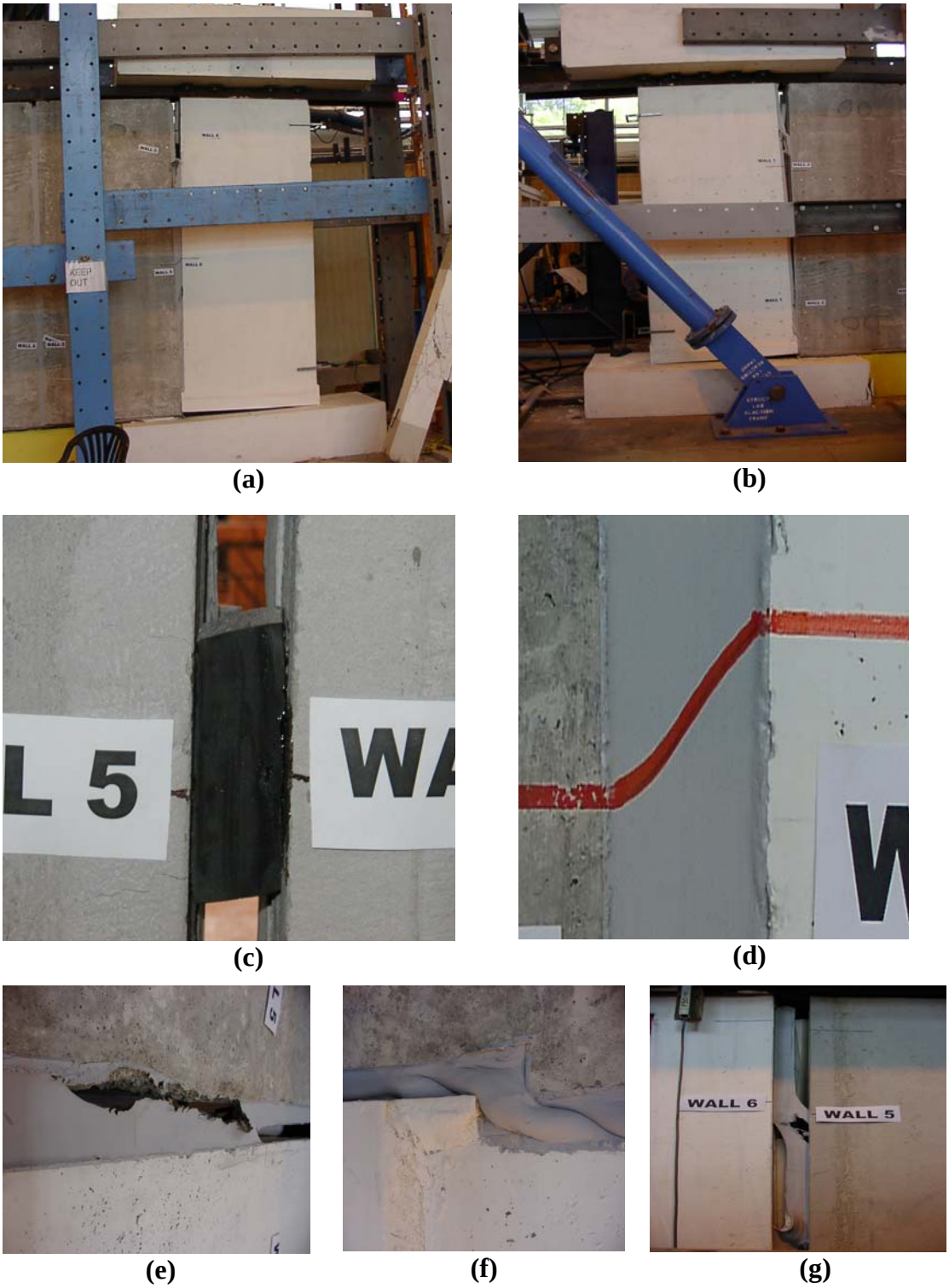


**(a)** **(b)**

**(c)** **(d)**

**(e)** **(f)** **(g)**

Figure 3.6: Visual Observation and damage; (a) the walls rocking at +2.0% drift at E-W direction; and (b) the seismic wall rocking at -4.0% drift at W-E direction; (c) deformation of the rubber block at 2.0% drift; (d) deformation of rubber block and sealant between the gap; (e) tensile bond failure when the sealant was under tension; (f) folding failure when the sealant was under excessive compression; and (g) adhesion failure when the sealant was under excessive tension.

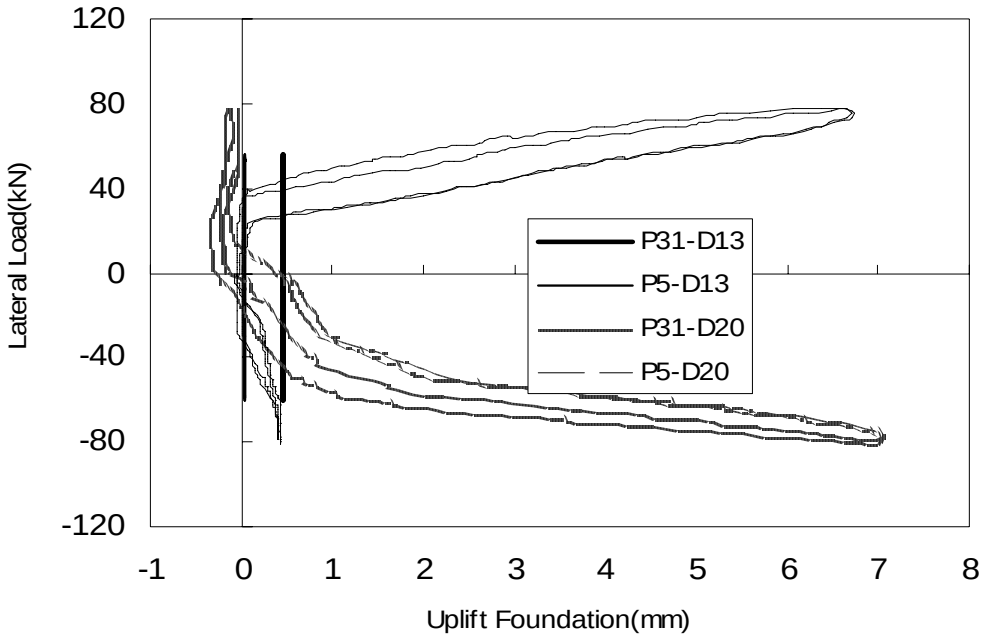


Figure 3.7: A comparison of uplift foundation block between a 20mm fuse-bar and 13mm fuse-bar in the superassemblage of a precast hollow core wall system.

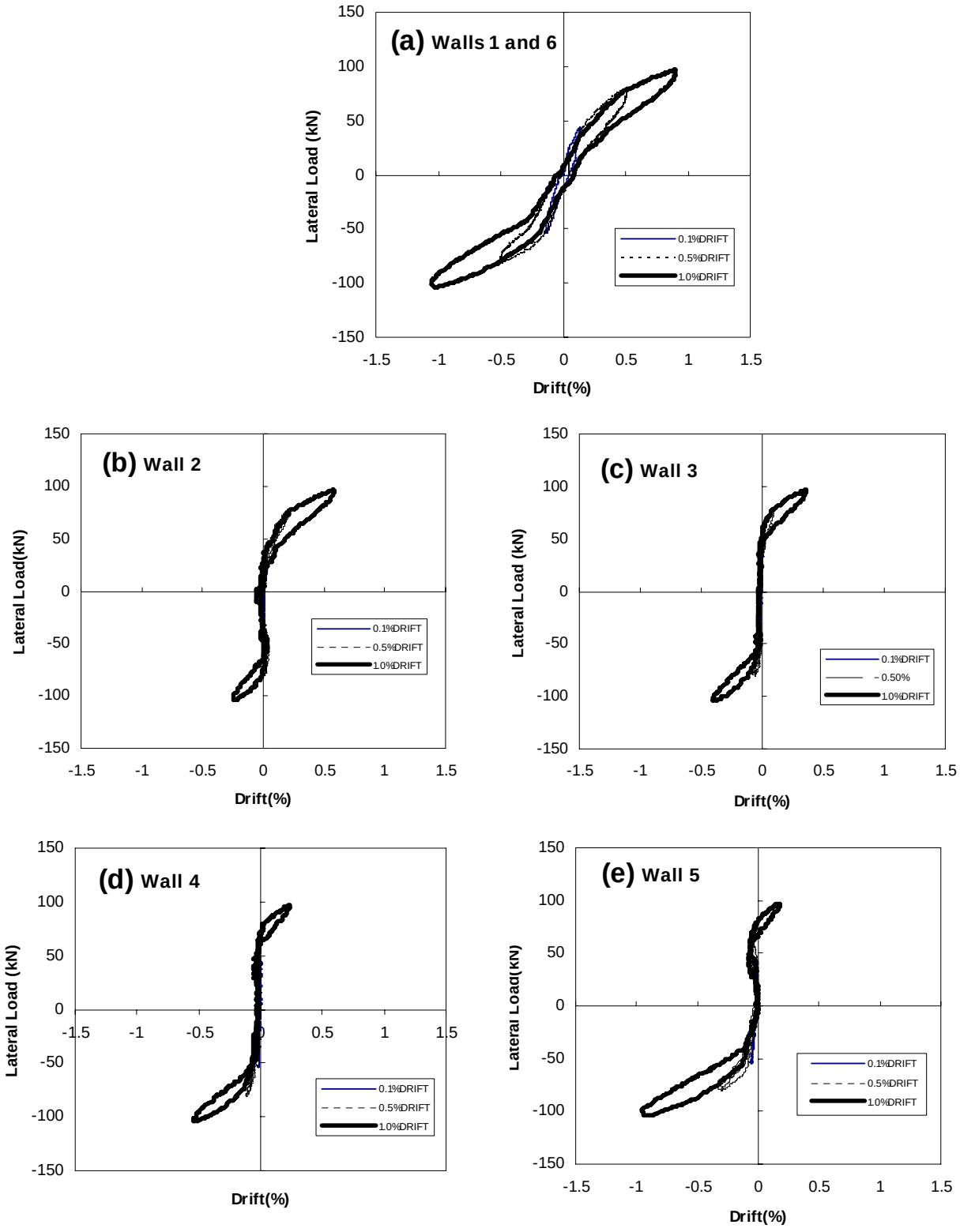


Figure 3.8: Phase 1-Experimental results of the multi-panel precast hollow core wall superassemblage where 20mm diameter fuse-bars and rubber block spacers were used. Results are presented for up to 1.0% drift amplitude showing; (a) the overall superassemblage behaviour similar to seismic Wall 1 and seismic Wall 6;
(b) non-seismic Wall 2; (c) non-seismic Wall 3; (d) non-seismic Wall 4; and (e) non-seismic Wall 5.

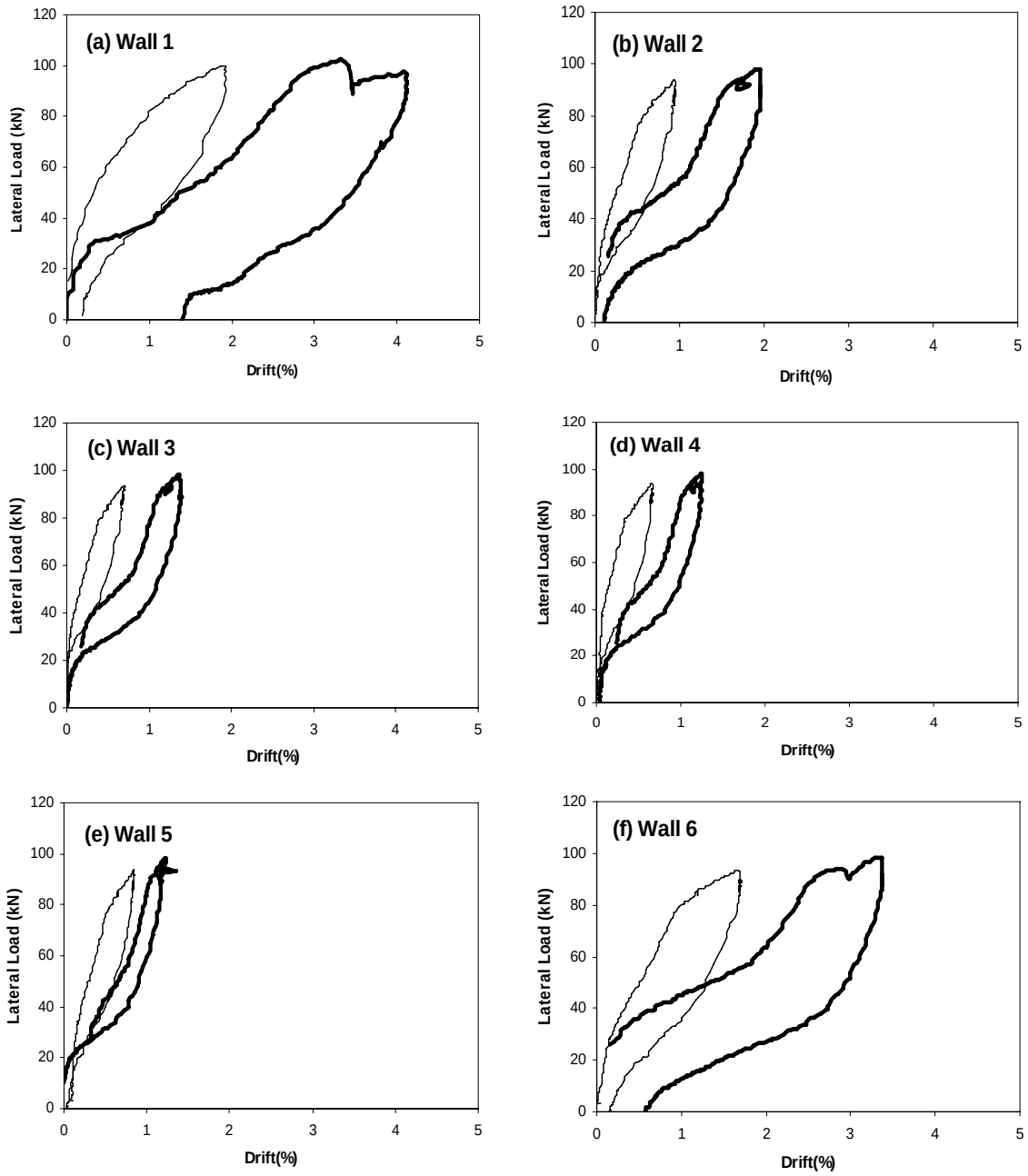


Figure 3.9: Phase 3 – the individual half-cycle performance of the wall units at 2.0% and 4.0% drift. Walls 1 and 6 are the outer seismic walls in the assemblage, while Walls 2 to 5 are the interior "non-seismic" or cladding wall units.

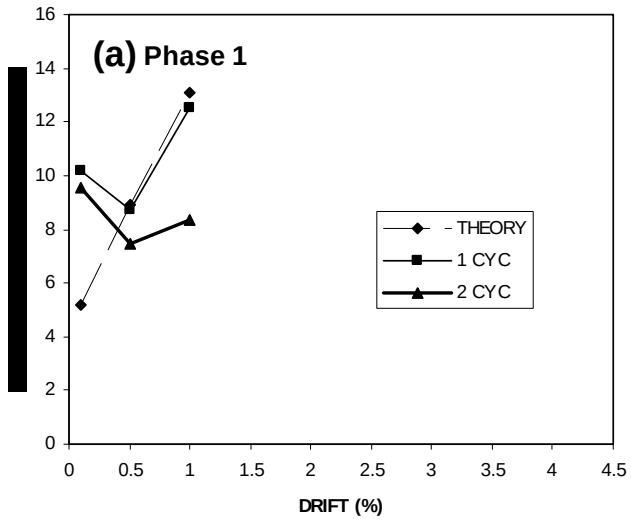


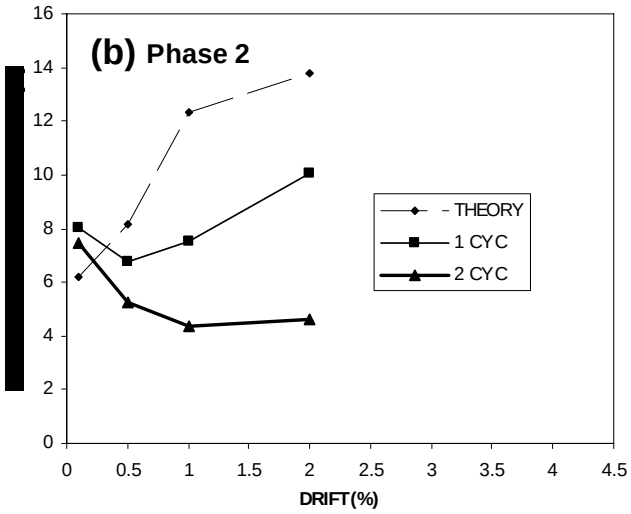


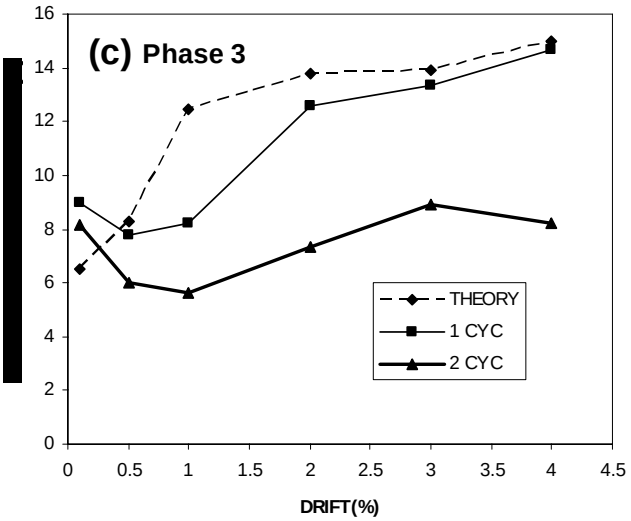


Figure 3.10: Equivalent viscous damping represents overall multi-wall panels; (a) Phase 1 using 20mm fuse-bars and rubber block spacers; (b) Phase 2 using 13mm fuse-bars with rubber block spacers; and (c) Phase 3 using13mm diameter fuse-bars, rubber block spacers and sealant.

# CHAPTER 4

# DAMAGE AVOIDANCE DESIGN OF WAREHOUSES USING THE PRECAST HOLLOW CORE WALLS SYSTEM

## SUMMARY

This chapter addresses the need for new a seismic design philosophy that has the performance traits of conventional ductile concrete monolithic wall systems, but without the potential for permanent damage. Innovative design procedures along with construction methods are proposed that avoid earthquake induced damage by using an entirely precast wall system. Damage Avoidance Design (DAD) principles are incorporated by using rocking walls with armoured steel seating. This design procedure involves seven steps which include: assessment of seismic hazard (demand); setting design target displacements (capacity); estimation of effective damping; calculation of the base shear capacity in the form of a lateral pushover curve; designing unbonded tendons and/or fuse-bars; re-evaluation of effective damping; and an assessment of seismic resistance adequacy via a demand vs capacity evaluation of the structure. A key step of this procedure is the evaluation of total effective damping which includes intrinsic, hysteretic and radiation damping arising from rocking of the wall panels. Damping reduction factors for short, medium and long periods for the seismic design demand spectrum are also considered. An illustrative design example of a warehouse building using the precast hollow core wall system is given. The walls consist of a mix of seismic wall panels and non-seismic infill cladding panels. The seismic wall panels are used to seat the rafters. Lateral loads are transmitted via diaphragm action through a roof

truss. Results are also presented for a nonlinear time-history analysis under various ground motions.

## 4.1 INTRODUCTION

Following several recent earthquakes it has become evident that present ductile design and detailing procedures are inadequate in preventing severe damage or collapse of tilt-up precast buildings that comprise industrial facilities, high-tech computer industries and parking garages. These earthquakes include the 1999 Kocaeli (Turkey) Earthquake (Sezen and Whittaker, 2004), the 1999 Chi-Chi (Taiwan) Earthquake (Johnson, 2000) and the 1994 Northridge Earthquake (Iverson and Hawkins, 1994). The conventional method of constructing wall panels using a seismic resistant ductile design philosophy failed to protect these buildings by not ensuring a measure of post-earthquake serviceability. These complete and partial failures had a significant impact on the social and economic infrastructure of the countries affected by these moderately high seismic events. The problem is related to the seismic design approach presently used which generally leads to construction of monolithic connections where plastic hinge zones (PHZ) are produced at wall-foundation interfaces. This can lead to permanent irreparable earthquake induced damage to structures. Seismic damage may also be exacerbated through out-of-plane seismic loading leading to instability of the structure due to P-$\Delta$ effects arising from the gravity load of the roof. To overcome performance deficiencies that result from ductile (conventional) seismic design it is evident that it is desirable to change to alternative design concepts that are capable of maintaining the post-earthquake serviceability of structures.

Seismic isolation is one approach where post-earthquake damage is minimised and a higher level of performance can be specified. However, seismic isolation is inappropriate for certain structural configurations including large warehouse type structures. Another promising design approach is to use rocking structures mechanism. When coupled with a "Damage Avoidance Design" philosophy, similar to that proposed by Mander and Cheng (1997) for bridges, damage-free performance can be attained by utilizing steel-armouring details at critical rocking connections. Longitudinal wall (or column) reinforcement is terminated at the foundation beam interface and the walls (or columns) are free to rock. Rocking structures, however, have only found limited application. There are two such notable structures of this type of construction in New Zealand: (i) the South Rangitikei Rail Bridge (Cormack,1988); and (ii) a chimney at Christchurch International Airport (Skinner et al.,1993).

The purpose of this chapter is to expand existing design procedures for rocking structures, and to make them applicable to the seismic design of multi-panel precast hollow core walls that are free to rock on their foundations. Following the development of design procedures, a design example and detail of a typical warehouse building will be demonstrated.

## 4.2 FINDINGS FROM PREVIOUS RESEARCH

A significant amount of research has been conducted on rocking structures under earthquake motion (Housner, 1963; Meek,1975; Aslam**,**1980; Psycharis and Jenning, 1983; Toranzo et al., 2004). Housner (1963) first investigated the basic concept of rocking rigid bodies by looking at energy dissipation and radiation under an earthquake

induced rocking response motion. Meek (1975) established the aspects of structural flexibility coupled with rocking structures, while Aslam et al.(1980) considered the influence of initial prestress with some resistance to a structure by anchoring the rigid block to the ground through prestress. Yim et al.(1980) further investigated the seismic response of rigid blocks under earthquakes and found that the performance of rigid blocks was very sensitive to small change in sizes, slenderness ratio and ground motion. Moreover, Psycharis and Jennings (1983) showed that if there is a partial separation between the base block and the foundation beam during strong shaking, instability of the rocking blocks is possible. They modelled the uplift of the block using a two-spring foundation and Winkler foundation which did not permit any slip in the horizontal direction.

Priestley et al.(1996) described the behaviour and design of rocking bridge piers by developing a response spectra design approach. However, some elements of rocking structures such as axial prestressing and supplemental damping were not incorporated in their design approach.

Toranzo et al.(2004) investigated and designed a prototype one-quarter scale three-storey rocking confined masonry wall building via a direct displacement base design approach. This model used flexural bending energy dissipators without the presence of unbonded post-tensioned tendons and was tested on a shaking table under sixty dynamics tests. The result showed that the masonry wall did not experience any damage except a minor longitudinal crack in the slab close to masonry wall panel. Therefore, the eliminated elements in this model will be used as basis for designing precast hollow core walls by

incorporating unbonded post-tensioned tendons, fuse-bars, sealant and rubber pad in this study.

Various researchers have combined the use of a Damage Avoidance Design philosophy together with rocking structures. This commenced with Mander and Cheng (1997) for bridges, and was continued by Holden et al.(2003) and Ajrab et al.(2004) for wall buildings. Holden et al.(2003) compared the seismic performance of precast partially prestressed walls with conventional monolithic walls under quasi-static reversed cyclic loading. The outcome showed that precast wall panels behaved very well without any visible damage at 3% drift whilst residual cracks up to 2mm wide were observed upon unloading at 1.0% drift on the monolithic wall. Ajrab et al.(2004) also investigated rocking walls within a multi-storey wall-frame structure coupled with a supplemental tendon based damping system. This study showed that a structure with rocking walls can provide superior performance compared with conventional fixed-based counterparts.

One of the keys to successful design of rocking structural systems is how to handle all the sources of damping-particularly radiation damping due to rocking. To date, this has not been incorporated into multi-member nonlinear time history analysis programs. Therefore, single degree of freedom idealisations need to be conceived and the radiation damping incorporated as equivalent viscous damping. There are different definitions of equivalent viscous damping given by many researchers (Jacobsen, 1930; Hudson, 1965; Gulkan and Sozen, 1974; Pekcan et al., 1999). Jacobsen (1930), for instance, derived this concept by equating the energy dissipated by the nonlinear SDOF system to the energy dissipated by one cycle of sinusoidal response of a linear system. Hudson (1965) draws upon this concept by equating the energy dissipated by one cycle with energy dissipated

using a spring-dashpot-mass system. Gulkan and Sozen (1974) computed the equivalent viscous damping by equating the energy input into the system with energy dissipated using an equivalent linear viscous dashpot system. This was further defined by Chopra (1995) by equating the energy dissipated in a vibration cycle of the structure with an equivalent viscous system. Pekcan et al. (1999) considered the energy absorption efficiency factor into the equivalent viscous damping along with how supplemental energy dissipation systems can be used. After considering all these definitions, the latter will be incorporated into this study as this is considered to be the most comprehensive way to determine the total effective damping for the structural system.

## 4.3 BASIC DESIGN OF ROCKING PRECAST HOLLOW CORE WALLS IN WAREHOUSE BUILDINGS

Figure 4.1 shows a proposed prototype warehouse building constructed using precast hollow core walls. The multi-panel walls consist of seismic and non-seismic wall panels. The former carry gravity loads from the rafters and also resist longitudinal horizontal forces, while the latter essentially act as cladding elements resisting face loads from wind. Figure 4.1(a) shows the horizontal bracing elements that form a roof diaphragm to transmit inertia loads (or wind induced forces) to the seismic wall units. Figure 4.1(b) shows the plan view of a warehouse with its seismic and non-seismic walls, wind trusses and rafter with portal frame. The number of non-seismic walls depends on the spacing of the rafters which in turn are seated on the seismic walls. The number of non-seismic wall units is equal to the spacing between rafters divided by the standard width of precast hollow core units. The portal frames or roof trusses are bolted to a steel channel web using unbonded post-tensioned tendons located in the

centre of the void sections of seismic walls and act as load bearing units without the need for providing external portal columns.

Figure 4.1(c) shows the cross-section X-X of the portal frame together with seismic wall panels. The detail, Connection A, shows the connection between the top of the walls and edges of the portal frames. Connection B depicts the joint detail between the foundation beam and the bottom of the walls. The precast foundation beam is located at the same level of the ground and the seismic walls that are attached to the foundation beam using couplers embedded within that beam.

Figure 4.2 shows the overall idealised force vs deformation behaviour of seismic precast hollow core units using unbonded tendons and energy dissipators. The concepts of rocking structures, unbonded post-tensioned tendons and Damage Avoidance Design are adopted in this research. The rocking seismic precast hollow core wall can be modelled as a SDOF system where the combined behaviour of unbonded tendons and gravity load behave as Bi-Linear Elastic elements as shown in Figure 4.2(a). Radiation damping, $(\xi_{rock})$ results from wall rocking. Also, during uplift yielding of the unbonded tendons and/or supplemental mechanical energy dissipators can occur. This leads to additional energy dissipation as depicted in the hysteresis loops of Figure 4.2(b). This energy can be converted into equivalent viscous damping, $(\xi_{hyst})$. The overall force-displacement response of the rocking wall system is shown in Figure 4.2(c). Radiation damping and hysteretic damping will be discussed in more detail in Section 4.7. The following topic is on the development of capacity spectrum design methodology.

## 4.4 CAPACITY SPECTRUM DESIGN METHODOLOGY

The capacity-demand spectrum has become popular for non-linear and design of single-degree-of-freedom (SDOF) systems in seismic prone regions where a realistic evaluation of the earthquake hazard is analysed in assessing the structural response. The seismic demand spectrum of the hazard exposure is predicted based on statistical analysis of past earthquake records.

The evaluation of the seismic demand spectrum on various effective damping levels depends on the portion of the spectrum that governs duration of the structural response. For contemporary design, the damping reduction factors are categorized into short and long period structures. The seismic demand spectrum respectively is given in equations 4-1 to 4-3 for the constant spectral acceleration, constant spectral velocity and constant spectral displacement, as follows:

$$C_d = \frac{F_a S_s}{B_a} \tag{4-1}$$

$$C_d = \frac{F_v S_1}{T B_v} \tag{4-2}$$

$$C_d = \frac{F_v S_1 T_d}{T^2 B_d} \tag{4-3}$$

whereby $F_a$ and $F_v$ are adjustments on spectral acceleration for short and long periods at different soil classes; $S_s$ and $S_1$ are spectral acceleration at short periods and the one-second period; $B_a, B_v$ and $B_d$ are factors based on effective viscous damping for the constant spectral acceleration, velocity and displacements regions of the spectra,

respectively; $T =$ the effective (secant) period of vibration; and $T_d$ = period at the junction of the constant spectral acceleration and displacement portions of the spectra. The above seismic demand equations are plotted in Figure 4.3(a) for the standard 5% damping case, and also for levels of higher viscous damping.

The secant (equivalent elastic) period of vibration for a structure can be found as follows:

$$T = 2\pi\sqrt{\frac{W}{gK}} = 2\pi\sqrt{\frac{W}{g}\frac{\Delta}{C_c W}} = 2\pi\sqrt{\frac{\Delta}{C_c g}} \tag{4-4}$$

in which $C_c =$ base shear capacity $= F_y / W$ where $F_y =$ base shear force and $W =$ seismic weight; $\Delta =$ peak response displacement; and $g =$ gravitational acceleration.

By setting the spectral displacement equal to the nonlinear structural response displacement $(S_d = \Delta)$, substituting equation 4-4 into equation 4 and setting the base shear capacity to the demand $(C_c = C_d)$, the one-second spectral acceleration $(F_v S_1)$ for a given demand can be found for seismic design and assessment purposes. The three spectral portions, shown in Figure 4.3(a) and (d), are associated with constant spectral acceleration (line 1), constant spectral velocity (line 2) and constant spectral displacement (line 3). The periods at the commencement of these portions are given by $T_a$, $T_v$ and $T_d$, respectively. Thus the entire damped capacity-spectrum can thus be taken as the greater of:

$$F_v S_1 = T_v B_a C_c \tag{4-5}$$

$$F_v S_1 = 2\pi\sqrt{\frac{C_c \Delta}{g}} B_v \tag{4-6}$$

$$F_v S_1 = \frac{4\pi^2 B_d \Delta}{g T_d} \tag{4-7}$$

where $S_1$ = one-second period spectral acceleration; $F_v$ = soil type factor for constant velocity portion of the spectra; and $B_a$, $B_v$, $B_d$ are reduction damping factors for constant acceleration, velocity and displacement. In the absence of spectral specific details $T_a$, $T_v$ and $T_d$ may be taken as 0.15, 0.4 and 3.0 seconds for normal (firms) soils. The above assessment equations can be rearranged for a direct displacement-based design format and taken as the lesser of

$$C_c = \frac{F_v S_1}{T_v B_a} = \frac{F_a S_s}{B_a} \tag{4-8}$$

$$C_c = \frac{0.25g}{\pi^2 \Delta}\left(\frac{F_v S_1}{B_v}\right)^2 \tag{4-9}$$

$$\Delta = \frac{0.25g}{\pi^2}\left(\frac{F_v S_1}{B_d}\right) T_d \tag{4-10}$$

In order to design a rocking wall system to resist a design basis earthquake (DBE) and also survive a maximum considered earthquake (MCE), the dependable base shear capacity of the structure must be greater than the spectral demand for that particular event as follows:

$$\Phi\,(F_v S_1)_c > (F_v S_1)_d \tag{4-11}$$

where $\Phi$ = global under capacity factor that relates overall uncertainty and randomness. As discussed in Chapter Five, this has been calibrated to ensure 90 percent non-exceedence probability of survival such that $\Phi = 0.6$.

## 4.5 DAMPING REDUCTION FACTORS

The damping reduction factors used above ( $B_a$ , $B_v$ and $B_d$ ) are independent of the soil types, wherever the structure may be located. This formulation is consistent with the recent research findings of Lin and Chang (2004) who pointed out that although the damping reduction factor is affected by both the site soil characteristics and the natural period of the structure, it is the latter rather than the former that is important. As the work by Lin and Chang (2004) appears to be the most comprehensive on the subject it is adopted and adapted herein as the basis of the modelling response reduction for linearised elastic SDOF systems. More recently Lin et al.(2005) evaluated and compared work with four other models which include Newmark and Hall (1982), Ashour (1987), Wu and Hanson (1989) and Ramirez et al.(2002). The statistical results showed that the Lin and Chang (2004) model provides the best estimation of maximum elastic displacement for all levels of viscous damping and all values of the vibration period as compared with those models. Even though the maximum elastic displacements are very difficult to predict within a short vibration period, their mean ratio results are within an acceptable range. Moreover, other models have some limitations such as the level of viscous damping only up to 20%, large mean ratio errors and overestimation of the maximum elastic displacements.

Figure 4.3 shows the spectrum demand capacity design adopted in this study based on damping reduction factors proposed by Lin and Chang (2004). Figure 4.3(b) shows the soil and period-dependent reduction factors for damping. Note that the values of $B$ are different from those used in the design equations 4-1, 4-2 and 4-3, in fact, they are inverse values. For analytical convenience, the results of Lin and Chang (2004) have

been parameterised differently from the manner in which they modelled their results. The approach adopted herein follows:

Three reduction factors, $B_a$, $B_v$ and $B_d$ for short, medium and long periods, respectively are used for design spectrum purposes. The first and last of these, $B_a$ and $B_d$, are the period-independent plateaux values for the respective constant acceleration and constant displacement portions of the response spectra given by:

$$B_a = \sqrt{\frac{2+\xi}{7}} \tag{4-12}$$

and $$B_d = \sqrt{\frac{8+\xi}{13}} \tag{4-13}$$

where $\xi$ = percent effective viscous damping factor.

In between these plateaux over the constant spectral velocity portion of the spectrum, linear interpolation based on either period or spectral displacement may be adopted:

$$B_v = \frac{B_d(S_{dv} - S_{da}) - B_a(S_{dv} - S_{dd})}{S_{dd} - S_{da}} \tag{4-14}$$

where $S_{dv}$ = spectral displacement within the medium period, $S_{da}$ = spectral displacement at the short period and $S_{dd}$ = spectral displacement at the long period as shown in Figure 4.3(c).

Figure 4.3(e) presents the overall design capacity-spectrum at effective viscous damping levels of 5%, 10%, 20%, 30% and 50% by incorporating Lin and Chang's model (2004).

These curves are plotted based on three reduction damping factors as discussed in this section. Generally, the values of the reduction damping factor (B) decrease when effective viscous damping increases which leads to the reduction of capacity-spectrum demand. Thus, these curves become smaller as the values of effective viscous damping increase. Moreover, these capacity-spectrum demand curves are designed based on the most recent application of a reduction damping factor by considering site soil characteristics and the natural vibration period of the structures. Furthermore, Lin and Chang's (2004) model using a total number of 216 earthquake records on firm sites in California has been validated and compared by Lin et al. (2005) with four other well-known models.

## 4.6 SEISMIC RESISTANCE OF ROCKING PHCW

Based on the foregoing design strategy it is now necessary to derive some basic equations that relate wall seismic resistance along with spread footing interaction to the base shear capacity of a rocking precast hollow core wall system. Figure 4.4 shows all the forces acting on multi-panel walls and their interaction with their supporting spread footings. In order to prevent uplift of the spread footing, it is necessary to limit the lateral load base shear capacity of the walls. This can be achieved by optimizing the size of fuse-bars and prestressing tendons. This is considered necessary, otherwise tension piles may need to be provided beneath the footing or the soil be permitted to fail. Maximum soil pressures can be minimised by locating each seismic wall panel at the centre of each spread footing unit. The total length of spread footing depends on the number of wall panels placed on top of the foundation block.

The lateral resistance of the seismic wall system is provided by the combination of roof loading and the self-weight of each wall panel. The unbonded post-tensioned tendons and/or fuse-bars also add to the lateral resistance. Figure 4.4(a) shows the seismic resistance of multi-panel walls due to all the forces acting from the roof to the spread footing. By taking moments, the lateral load capacity of a multi-panel wall *system* is given by:

$$F = \frac{B}{2H}(W_r + nW_w + T) \tag{4-15}$$

where $B =$ panel width; $H =$ panel height; $W_r =$ weight of roof reaction from rafter; $W_w =$ weight of one wall panel; $n =$ the number of wall panels; and $T =$ total vertical tension tie-down forces provided by prestress and mechanical energy dissipators, if any. Note that the lateral resistance provided by panel-to-panel sealant is relatively small as compared to the weight of wall panels and tension forces which come from fuse-bars (refer to section 3.3 in Chapter Three).

Simplification of the base shear capacity of the wall using equation 4-15 is as follows:

$$C_c = \frac{F}{W_r + nW_w} = \frac{F}{W_s} = \frac{B}{2H}\left(1 + \frac{T}{W_s}\right) \tag{4-16}$$

where $W_s = W_r + nW_w =$ structural seismic weight. By taking moments at the discontinuity point of the strip footing (refer to Figure 4.4(b)), the maximum eccentricity on the foundation reaction is derived as:

$$FH = (W_s + W_f)e \tag{4-17}$$

in which $W_f$ = weight of the foundation strip footing and $e$ = soil reaction force eccentricity beneath the foundation beam. The ratio of the eccentricity $(e)$ over total length of strip footing $(L_s)$ can be defined as:

$$\frac{e}{L_s} = \frac{e}{nB} = \frac{FH}{nB(W_s + W_f)} \tag{4-18}$$

Substituting equation (4-15) into equation (4-18):

$$\frac{e}{L_s} = \frac{e}{nB} = \frac{B}{2H} W_s \left[1 + \frac{T}{W_s}\right] \frac{H}{nB(W_s + W_f)} \tag{4-19}$$

$$\frac{e}{B} = \frac{1}{2}\left[\frac{1 + T/W_s}{1 + W_f/W_s}\right] \tag{4-20}$$

Ideally, for no tension uplift $e < L_s/6$, where

$$\frac{e}{B} < \frac{L_s}{6B} = \frac{nB}{6B} = \frac{n}{6} \tag{4-21}$$

This is the well-known Kern-point limit.

By relating the base shear capacity of the system with eccentricity underneath the foundation block where equation 4-20 is equal to equation 4-21, the eccentricity ratio becomes

$$\frac{e}{B} = \frac{1 + T/W_s}{1 + W_f/W_s} < \frac{n}{3} \tag{4-22}$$

The tension force limit for prestress and/or mechanical energy dissipators, if any, is given by:

$$T < \frac{n}{3}\left(W_s + W_f\right) - W_s \tag{4-23}$$

Also, before any prestress of unbonded post-tensioned tendons can be applied, the right hand side of equation 4-23 must be positive where

$$n > \frac{3}{1 + W_f / W_s} \tag{4-24}$$

For a light foundation where $W_f \to 0$, in order to prevent the uplifting of the light foundation beam the number of wall panels should be greater than 3 ($n > 3$). Also, for example, if the foundation beam is designed to carry six panels plus the roof loading, the ratio of tension force over seismic weight of the system is derived as:

$$\frac{T}{W_s} < \frac{6}{3}\left(1 + \frac{W_f}{W_s}\right) - 1 = 1 + \frac{2W_f}{W_s} \tag{4-25}$$

By substituting equation 4-25 into equation 4-16, the design base shear capacity becomes:

$$C_c = \frac{B}{H}\left(1 + \frac{W_f}{W_s}\right) \tag{4-26}$$

Figure 4.4(c) shows the interaction between multi-panel walls and spread footings during ground shaking. The steel channel on top of the walls is used to transmit lateral forces from one seismic wall to the next seismic wall through its web. If the lateral displacement is large, a plastic hinge mechanism will occur at the V-cut location on its flange. During earthquake excitation, the seismic and roof loads are transferred to the spread footing and the shear key/pintles underneath the seismic walls will prevent the walls from sliding. The non-seismic walls transmit the gravity load through the rubber pad placed between the wall and foundation beam.

With regard to seismic resistance of the rocking wall system, four different conditions of base shear capacity at different level of prestressing are considered. These are: (i) walls

without tendons, (ii) walls with snug tight, (iii) walls with 50% prestressing, and (iv) walls with 100% prestressing. The derivations of equations for these conditions are as follows:

No tendons:

The base shear capacity of a wall without unbonded tendons is given by the following equation:

$$C_c = \frac{F}{W} = \left( \frac{B}{2H} - \frac{\Delta}{H} \right) = \frac{B}{2H} - \theta \tag{4-27}$$

where $B =$ the width of wall; $H =$ height of wall; $\Delta =$ the lateral displacement of wall; and $\theta = \Delta / H =$ wall drift (angle in radians).

Snug Tight (0% Prestressing):

The base shear capacity of a wall with snug tight or 0% prestressing is given by;

$$C_c = \frac{B}{2H} \left( 1 + \frac{A_f E_s / W}{\frac{L_f}{B} + \frac{L}{B}\frac{A_f}{A_p}} \theta \right) - \theta \tag{4-28}$$

where $A_f =$ cross-sectional area of fuse-bars, $A_p =$ main prestress area of unbonded tendons, $E_s =$ Young Modulus of prestressing steel, $L_f =$ fuse-bars length, $L =$ main prestress length of unbonded tendons and $\theta =$ drift of the wall.

0% to 100% Prestressing:

The base shear capacity for a wall with initial prestressing between 0% and 100% is given by:

$$C_c = \frac{B}{2H}\left(1 + \frac{P_o}{W} + \frac{A_f E_s / W}{\frac{L_f}{B} + \frac{L}{B}\frac{A_f}{A_p}}\theta\right) - \theta \qquad (4\text{-}29)$$

where $P_o$ = the initial prestressing of unbonded tendons; $W$ = self weight of the walls and roof loading; and $P_o + A_f E_s < P_y$ where $P_y$ = the yield strength of unbonded post-tensioned tendons.

100% Prestressing:

The base shear capacity of a wall with 100% prestressing of tendons is given by the following equation:

$$C_c = \frac{F_y}{W} = \frac{B}{2H}\left(1 + \frac{P_y}{W}\right) - \theta \qquad (4\text{-}30)$$

Figure 4.5 presents graphs for base shear capacity without tendons, snug-tight, 50% and 100% level of prestressing tendons based on the equation derived above. For the example shown (where $H = 8m, B = 1.2m, P_y = 260kN, W = 150kN$), the unbonded tendons greatly increase the level of overturning drift from 6.2% with no prestress to 14.7% with initial post-tensioned prestressing tendons. The base shear capacity of the wall in pre-yield range remains the same regardless of the level of prestress.

## 4.7 TOTAL EFFECTIVE DAMPING IN ROCKING STRUCTURES

### 4.7.1 THE CONCEPT OF EFFECTIVE VISCOUS DAMPING

In a rocking wall system that may also possess supplemental energy dissipators, the total effective viscous damping, $\xi_{eff}$, arises from three components as follows:

$$\xi_{eff} = \xi_{inst} + \xi_{rock} + \xi_{hyst} \tag{4-31}$$

where $\xi_{inst}$ = the intrinsic damping of the structural system, $\xi_{rock}$ = the energy radiated into the half-space on each impact; and $\xi_{hyst}$ = the hysteretic damping from the energy dissipator devices and/or tendon's.

The intrinsic damping of the structure $(\xi_{inst})$ principally depends on the material type and the degree of interaction with non-structural elements, such as cladding. Steel and prestressed concrete, reinforced concrete and timber are common materials used in the construction of buildings and houses and these typically have intrinsic damping values in the order of 2%, 5% and 8%, respectively.

### 4.7.2 RADIATION DAMPING IN ROCKING STRUCTURES, $\xi_{rock}$

An energy approach is adopted in this study to assess radiation damping under rocking structures. Under this approach, radiation damping can be found by changing the kinetic energy to potential energy at each half-cycle of seismic loading. Referring to research by Mander and Cheng (1997) on rocking bridge piers, the equivalent viscous damping factor for one impact per half-cycle of the rocking system is given by:

$$\xi_{rock} = \frac{\delta E}{\pi F \Delta} = \frac{\delta E}{\pi W C_c \Delta} \tag{4-32}$$

where $F$ = uplift force, $\Delta$ = displacement amplitude, $W$ = total weight of structures, $C_c$ = base shear capacity and $\delta E$ = dissipated/radiated energy which is given by:

$$\delta E = (1-r)E_P = (1-r)\frac{WB\Delta}{2H} = \frac{1}{2}(1-r)WB\theta \tag{4-33}$$

in which $r$ = the kinetic energy ratio after and before impact, $B$ = the width of wall and $E_P$ = potential energy. Thus,

$$\xi_{rock} = \frac{(1-r)}{\pi C_c}\frac{B}{2H} \tag{4-34}$$

where $r$ = kinetic energy reduction ratio (after/before) impact defined by Housner (1963) as:

$$r = \frac{\frac{1}{2}I_o\dot{\theta}_2^2}{\frac{1}{2}I_o\dot{\theta}_1^2} = \left(\frac{\dot{\theta}_2}{\dot{\theta}_1}\right)^2 \tag{4-35}$$

in which $I_o$ = moment of inertia for a rigid block, $\dot{\theta}_1$ = velocity before impact and $\dot{\theta}_2$ = velocity after impact. Housner (1963) applied the principle of conservation angular momentum to a rocking block to give

$$r = \left(1 - \frac{MR^2}{I_o}(1-\cos 2\alpha)\right)^2 \tag{4-36}$$

where $M$ = mass of rigid body, $R$ = distance from the pivot point to the centre of gravity and $\alpha$ = the angle between the height of the wall to the centre of gravity.

For a slender wall, equation (4-36) can be expanded and simplified as

$$r = 1 - \frac{2mR^2\alpha^2}{I_o} = 1 - \frac{2mb^2}{I_o} \tag{4-37}$$

The moment of inertia of a rigid block is given as $I_o = \left(H^2 + B^2\right)m_w / 3$ and the moment inertia of a concrete block at the top of the wall is defined as $I_t = m_r(H^2 + B^2/4)$. By equating $I_o = I_t$, then the effective mass of the rigid block with respect to the top block and wall can be derived as:

$$m_{eff} = m_r + \frac{4m_w}{3}\left(\frac{H^2 + B^2}{4H^2 + B^2}\right) \tag{4-38}$$

in which $m_{eff}$ = effective mass, $m_r$ = mass of the top block, and $m_w$ = mass of the wall. Therefore, by substituting equation 4-38 into equation 4-37, the equation becomes:

$$r = \left(1 - \frac{2m_{eff}B^2/4}{m_{eff}(H^2 + B^2/4)}\right) \cong \left(1 - \frac{m_{eff}B^2}{m_{eff}(H^2 + B^2/4)}\right) \tag{4-39}$$

And in the form which is needed to substitute into equation 4-34:

$$1 - r = \frac{B^2}{H^2 + B^2/4} = \frac{1}{H^2/B^2 + 1/4} \tag{4-40}$$

After making this substitution, the equivalent radiation damping of a rocking structure becomes:

$$\xi_{rock} = \frac{B}{2H\pi C_c\left[\frac{H^2}{B^2} + \frac{1}{4}\right]} \tag{4-41}$$

The radiation damping of rocking structures at yield can be found by substituting equation 4-30 into equation 4-41 to become:

$$\xi_{rock} = \frac{1}{\pi\left[\frac{H^2}{B^2} + \frac{1}{4}\right]\left[\frac{P_y}{W} + 1\right]} \tag{4-42}$$

in which $P_y$ = yield strength of unbonded tendons.

### 4.7.3 HYSTERETIC ENERGY DISSIPATION, $\xi_{hyst}$

Beyond the yield point of the structure the apparent damping of the structure increases as inelastic deformation takes place due to hysteretic energy absorption associated with structural displacement ductility of the system. According to Pekcan et al. (1999), the equivalent viscous damping of the system should accommodate the shape of the actual hysteresis loop given in following equation:

$$\xi_{hyst} = \frac{2\eta}{\pi}\left(\frac{1}{1-\alpha(\mu-1)} - \frac{1}{\mu}\right) \tag{4-43}$$

where $\eta$ = the energy absorption efficiency factor as the ratio of the area enclosed by the actual hysteresis loop to the area assumed by the plastic-bilinear hysteresis loop; $\alpha$ = the post-elastic to initial stiffness ratio; and $\mu$ = the structural displacement ductility factor.

Figure 4.6 shows the total effective viscous damping made up from the above three components. In the graphical example the tendons are prestressed to 50% of yield. The radiation damping largely depends on the aspect ratio of the rocking wall (H/B).

## 4.8 DESIGN PROCEDURE FOR PRECAST HOLLOW CORE WALLS

The design procedure for rocking PHCW by incorporating unbonded tendons and fuse-bars together with the theoretical background is proposed. This procedure involves seven steps as described below and summarised in Figure 4.7.

### STEP 1: Determine Seismic Demand of DBE and MCE based on the Hazard Exposure

Two desired levels of ground motions are identified, namely, basic design earthquake (DBE- 10% probability in 50 years) and maximum considered earthquake (MCE- 2% probability in 50 years). For example, the values for DBE and MCE in Wellington (New Zealand) are 0.4g and 0.8g, respectively. Damping reduction factors as mentioned above with different level of effective viscous damping are considered in spectrum seismic demand.

### STEP 2: Determine the maximum response displacement, $\Delta_{\max}^{DBE}$ and $\Delta_{\max}^{MCE}$

For the DAD philosophy, the performance objective for DBE is that the structure remains elastic during ground shaking with target design drift, $(\theta < 2\%)$. Under MCE, the structure is allowed to yield, especially supplemental energy dissipators, but no structural damage should exist in the wall $(\theta \leq 4.0\%)$. The target design drift is calculated based on performance criteria and target design displacement at effective heights of structures as defined below:

$$\Delta_{\max}^{DBE} = \theta_{\max}^{DBE} H_{eff} \quad \text{and} \quad \Delta_{\max}^{MCE} = \theta_{\max}^{MCE} H_{eff} \tag{4-44}$$

**STEP 3: Estimate total effective damping of the system ($\xi_{eff}$)**

Total effective damping of the structure can be estimated based on equation 4-31, from which values for the damping factors $B_a$, $B_v$ and $B_d$ are estimated.

**STEP 4: Calculate the required base shear capacity of the structures, $C_c^{DBE}$ and $C_c^{MCE}$**

The required base shear capacity of the structure can be calculated from modified equations 4-8 and 4-9 as follows:

$$C_c = \frac{0.25g}{\pi^2 \Delta}\left(\frac{F_v S_1}{\phi B_v}\right)^2 \le \frac{F_v S_1}{\phi T_v B_a} \tag{4-45}$$

where $\Delta \le \frac{0.25g}{\pi^2}\left(\frac{F_v S_1}{\phi B_d}\right) T_d$

**STEP 5: Design energy dissipator and unbonded tendons**

Once the required base shear capacity of the structure is known, calculate the required cross-sectional area of unbonded fuse-bars and unbonded tendons using equation 4-29.

**STEP 6: Evaluation of hysteresis damping and total effective damping of the system**

The radiation damping ($\xi_{rock}$) and hysteretic damping of the energy dissipator ($\xi_{hyst}$) of the wall system can be calculated using equations 4-42 and 4-43, respectively. Calculate total effective damping by summing the intrinsic, radiation and hysteretic damping of the system. These values should be checked with the estimates in Step 3, and adjustments to the solutions in Steps 4 and 5 made accordingly.

**STEP 7: Assessment of Seismic Capacity**

The seismic capacity of the precast hollow core wall system can be assessed by checking that the base shear capacity of the system is bigger than the base shear demand. If the design does not conform to equation 4-11 through the evaluation of equations 4-5 to 4-7, then Steps 4 to 6 are repeated until they converge and the design is considered acceptable.

## 4.9 DESIGN AND SEISMIC EVALUATION OF A WAREHOUSE BUILDING

A typical single storey warehouse building is designed to be constructed for New Zealand's seismic hazard region in Wellington. The layout plan of the warehouse building is shown in Figure 4.1(b) with 60m long and 40m wide. The dimensions of the hollow core units are 8mx1.2mx0.2m. Three longitudinal prestressing strands of 13.5mm and two strands of 11.5mm in diameter are located at the bottom and top cross-section area of the wall, respectively. The warehouse is situated on intermediate (Type B) soil according to the customary soil classification. The following assumptions are made for the design purposes: (i) Self-weight of the roof is 1.5kPa; (ii) The soil type factor, $S = 1.0$; (iii) Compressive strength of concrete, $f_c^{'} = 50MPa$; (iv) Unbonded post-tensioned tendon, $f_y = 530MPa$, $f_{su} = 680MPa$ and $E_s = 200GPa$ and (v) For DBE $F_v S_1 = 0.4g$; and MCE $F_v S_1 = 0.8g$. Calculations for the design are given in Appendix A4.

Figure 4.8 shows the overall details design and connections for the warehouse/industrial building and its classification as a Type II structure (refer to Appendix A4 for detail

drawing). Figure 4.8(a) presents the longitudinal arrangement of the multi-panel wall connected to the foundation beam. The seismic wall shows the gravity load from the roof while the non-seismic panel acts as cladding. Figure 4.8(b) shows the steel portal frame as connected to the seismic wall which is acting as a load-bearing wall. No external columns are provided because the wall panels are designed to resist seismic, wind and gravity load. Figure 4.8(c) and (d) presents the rocking base placed on top of the foundation beam and pintles welded to the rocking toe. This rocking base is to accommodate high contact point forces at the rocking toe and allow the rocking mechanism between steel-steel interfaces.

Figure 4.9 presents the connections and joints detailing between the wall-to-wall and wall-to-foundation interfaces. Figure 4.9(a) shows the joint features between seismic walls and non-seismic wall interfaces. Silicone sealants are used on both sides of the walls with the appropriate properties for ground motion and weather tightness. Figure 4.9(b) provides connection details at seismic wall-foundation (steel-steel) and non-seismic wall-foundation (rubber-concrete) interfaces. Figure 4.9(c) presents the overall dimensions of materials used between their interfaces for the multi-panel wall system. The rubber pad is used as a suitable material for absorbing some energy and coping with the inevitable displacement disparities, whereas the steel-plate is used because of its ability to spread the high impact point forces during the rocking vibration of the structure.

The final step in the design is an evaluation of the adequacy of the structure under seismic loading in accordance with equation 4-11. This evaluation has been plotted graphically in Figure 4.10. For the DBE and MCE demand drifts/displacements of 1.9%

and 4% are found. These drifts are less than the available drift capacities of 3% and 15% which respectively represent the onset of damage and toppling collapse. This design is therefore considered to be validated. Moreover, a dynamic nonlinear time-history analysis should be carried out for the warehouse building using the precast hollow core wall system. Ideally, a comprehensive IDA (Inelastic Dynamic Analysis) should be conducted as recommended by Vamvatsikos and Cornell (2002). Full details of this approach will be provided in the next chapter. However, in the meantime, results for two examples of earthquakes under DBE and MCE which fall near to the 90$^{th}$ percentile are presented in Figure 4.11.

## 4.10 CONCLUSIONS AND RECOMMENDATIONS

The concept development of rocking wall panel structures along with the proposed design procedures for the construction of warehouse buildings is presented. Based on this study, the following conclusions are drawn:

1. The end-user community now is becoming more demanding, requiring minimal and preferably no seismic damage. By using a Damage Avoidance Design (DAD) philosophy along with the proposed design procedure, the repairable damage to industrial buildings will be minimized (re-prestressing tendons and/or replacing fuse-bars) and irreparable damage to the structures can be avoided with a high degree of confidence.
2. The kinetic energy dissipated from the rocking mechanism is quite low. It is therefore insufficient for a rocking wall building to rely on radiation damping that occurs on each impact. Therefore, a strong rocking toe and base plate to protect

concrete from cracking and spalling are essential along with supplemental damping in the form of yielding tendons.

3. In order to avoid any damage to the wall and strip footing, these structural elements should be discontinuous and require steel-steel or concrete-rubber protection against rocking motion impact. During earthquake excitation, the rocking toe experiences high point stresses between foundation-wall interfaces. By providing a steel-steel rocking interface, the rocking wall behaves in a bilinear elastic fashion and keeps the self-centring characteristics; therefore, no residual displacement or permanent damage is expected to occur.
4. The design process proceeds without the need to determine the fundamental period. This is useful, as for rocking structures the period is constantly changing during rocking excitation. Once designed and detailed, the adequacy of the design can be validated against a set of seismic demand-drift capacity curves (Figure 4.10).

## REFERENCES


Ajrab, J. J., Pekcan, G. M., and Mander, J.B. (2004). "Rocking wall-frame structures with supplemental tendon systems." *ACI Structural Journal*, 130(6), 895-903.

Ashour, S.A. (1987). "Elastic seismic response of buildings with supplemental damping." thesis, presented to University of Michigan at Michigan, U.S.A, in partial fulfillment of the requirements for the degree of Doctor of Philosophy.

Aslam, M., Goddon, W.G., and Scalise, D.T. (1980). "Earthquake rocking response of rigid bodies." *Journal of Structural Engineering*, ASCE, 106(2), 377-392.

Chopra, A.K. (1995). *Dynamic of structures: theory and applications to earthquake engineering.* Second Edition, Prentice Hall, Upper Saddle River, New Jersey, USA.

Cormack, L.G. (1988). "The design and construction of the major bridges on the Mangaweka rail division." *Transactions*, Institutions of Professional Engineers, New Zealand, I/CE, 15, 16-23.

Gulkan, P., and Sozen, M. (1974). "Inelastic response of reinforced concrete structures to earthquake motion." *ACI Structural Journal*, 71, 604-610.

Holden, T. J., Restrepo, J., and Mander, J.B. (2003). "Seismic performance of precast reinforced and prestressed concrete walls." *Journal of Structural Engineering*, ASCE, 129(3), 286-296.

Housner, G.W. (1963). "The behaviour of inverted pendulum structures during earthquake." *Bulletin of the Seismological Society of America*, 53(2), 403-417.

Hudson, D.E. (1965). "Equivalent viscous friction for hysteretic systems with earthquake-like excitations." *3rd World Conference on Earthquake Engineering, New Zealand*, Paper No. II-185/II-201.

Iverson, J.K., and Hawkins, N.M. (1994). "Performance of precast/prestressing building structures during Northridge Earthquake." *PCI Journal*, 36(2), 38-55.

Jacobsen, L.S. (1930). "Steady forced vibrations as influenced by damping." *Transactions ASME*, 52(1), 169-181.

Johnson, L.A. (2000). "Earthquake loss modelling applications for disaster management: lessons from the 1999 Turkey, Greece and Taiwan Earthquakes." *Proceedings of EuroConference on Global Change and Catastrophe Risk Management: Earthquake Risk in Europe* held on July 6-9, 2000, Paper No. 4, http://www.iiasa.ac.at/Research/RMP/july 2000/[accessed 3/4/04].

Lin,Y.Y., and Chang, K.C. (2004). "Effects of site classes on damping reduction factors", *Journal of Structural Engineering,* ASCE, 133(9), 1667-1675.

Lin, Y.Y., Miranda, E., and Chang, K.C. (2005). "Evaluation of damping reduction factors for estimating elastic response of structures with high damping." *Earthquake Engineering and Structural Dynamics*, 34, 1427-1443.

Mander, J.B., and Cheng, C.-T. (1997). "Seismic resistance of bridge piers based on Damage Avoidance Design." *Technical Report NCEER-97-0014*, Department of Civil, Structural and Environmental Engineering, State University of New York at Buffalo, New York, USA.

Meek, J.W. (1975). "Effects of foundation tipping on dynamic response." *Journal Structural Division*, ASCE, 101(7), 1297-1311.

Newmark, N.M., and Hall, W.J. (1982). "Earthquake spectra and design." *EERI Monograph Series,* Earthquake Engineering Research Institute, Oakland, CA.

Pekcan, G., Mander, J.B., and Chen, S. (1999). "Fundamental considerations for the design of non-linear viscous dampers." *Earthquake Engineering and Structural Dynamics*, 28, 1405-1425.

Priestley, M.J.N, Seible, F. and Calvi, G.M. (1996). *Seismic design and retrofit of bridges.* John Wiley & Sons, New York, USA.

Psycharis, I.N. and Jennings, P.C. (1983). "Rocking of slender rigid bodies allowed to uplift." *Earthquake Engineering and Structural Dynamics*, 11, 57-76.

Ramirez, O.M., Constantinou, M.C., Whittaker, A.S., Kircher, C.A., and Chrysostomou, C.Z. (2002). "Elastic and inelastic seismic response of buildings with damping systems." *Earthquake Spectra*, 18(3), 531-547.

Sezen, H., and Whittaker, A.S. (2004). "Performance of industrial facilities during the 1999, Kocaeli, Turkey Earthquake." *13th World Conference on Earthquake Engineering*, Vancouver, B.C., Canada, Paper No. 282.

Skinner, R.I., Robinson, W.H., and McVerry, G.H. (1993). *An introduction to seismic isolation*, John Wiley & Sons, New York, USA.

Toranzo, L.A., Restrepo, J.I., Carr, A.J., and Mander, J.B. (2004). "The use of rocking walls in confined masonry structures: a performance-based approach." *13th World Conference on Earthquake Engineering*, Vancouver, B.C., Canada, Paper No. 599.

Vamvatsikos, D., and Cornell, C.A. (2002). "Incremental dynamic analysis", *Earthquake Engineering and Structural Dynamics*, 31, 491-514.

Wu, J.P., and Hanson, R.D. (1989)."Inelastic response spectra with high damping." *Journal of Structural Division,* ASCE, 115(6), 1412-1431.

Yim, C.S., Chopra, A.K. and Penzien, J. (1980). "Rocking response of rigid blocks to earthquake." *Earthquake Engineering and Structural Dynamics*, 8, 565-587.

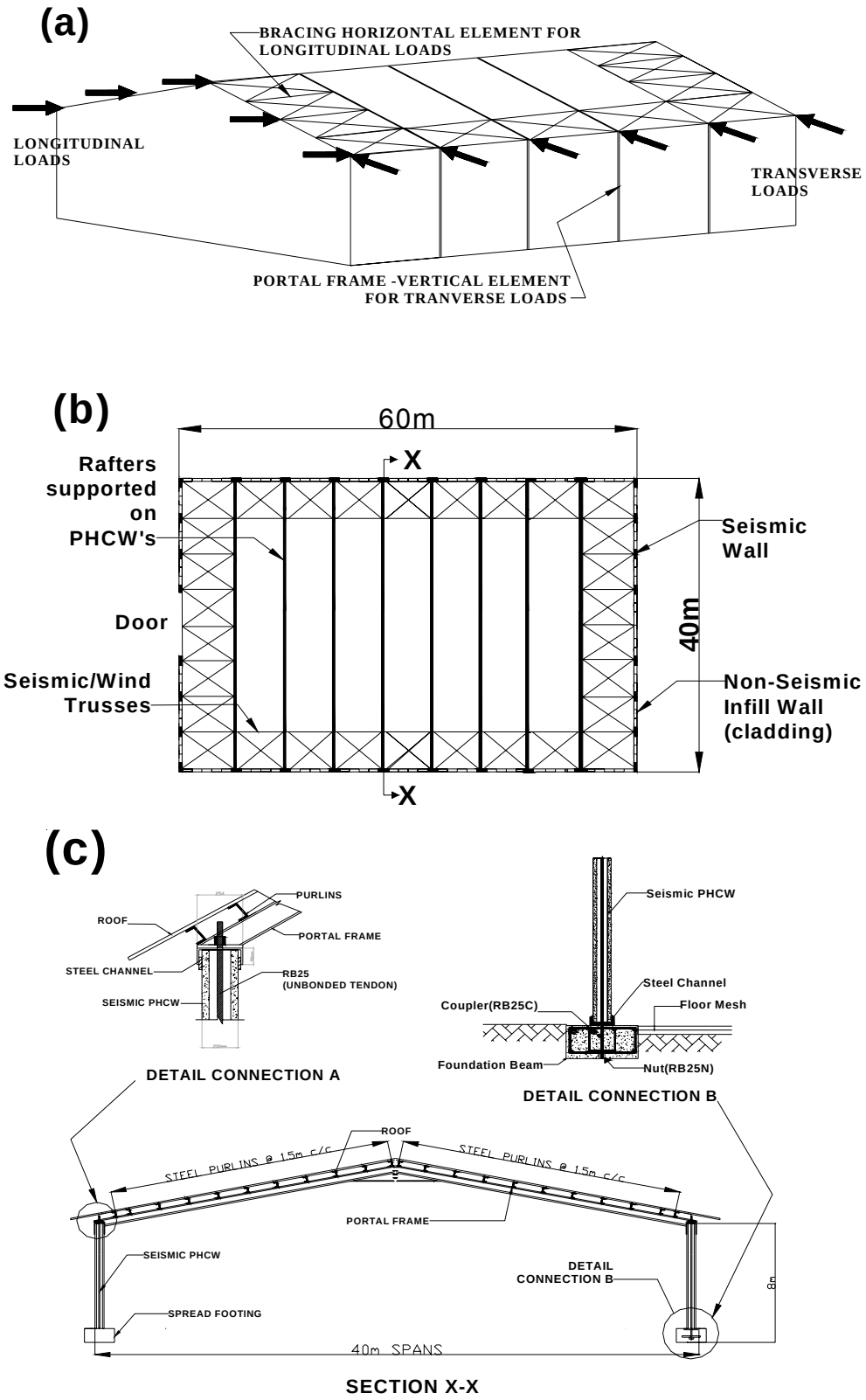


Figure 4.1: Concept overview of a warehouse building; (a) distribution of transverse and longitudinal loading arising from either wind or earthquake effects; (b) plan view of the warehouse showing lines of portal frames seated on PHCW; and (c) steel portal frame setting on PHCW together with detailing connection at the top and bottom of the wall.

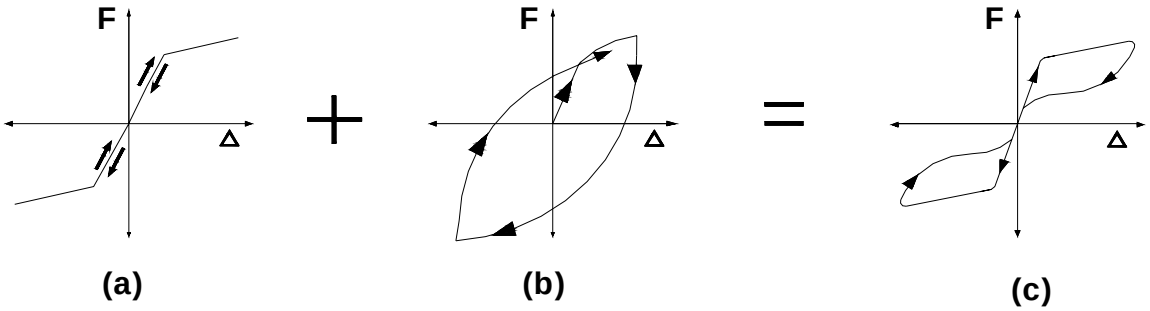


Figure 4.2: The mechanics of a rocking wall; (a) Bi-Linear Elastic behaviour due to self-weight and unbonded tendons; (b) behaviour of energy dissipators; and (c) hysteresis of flag-shape.

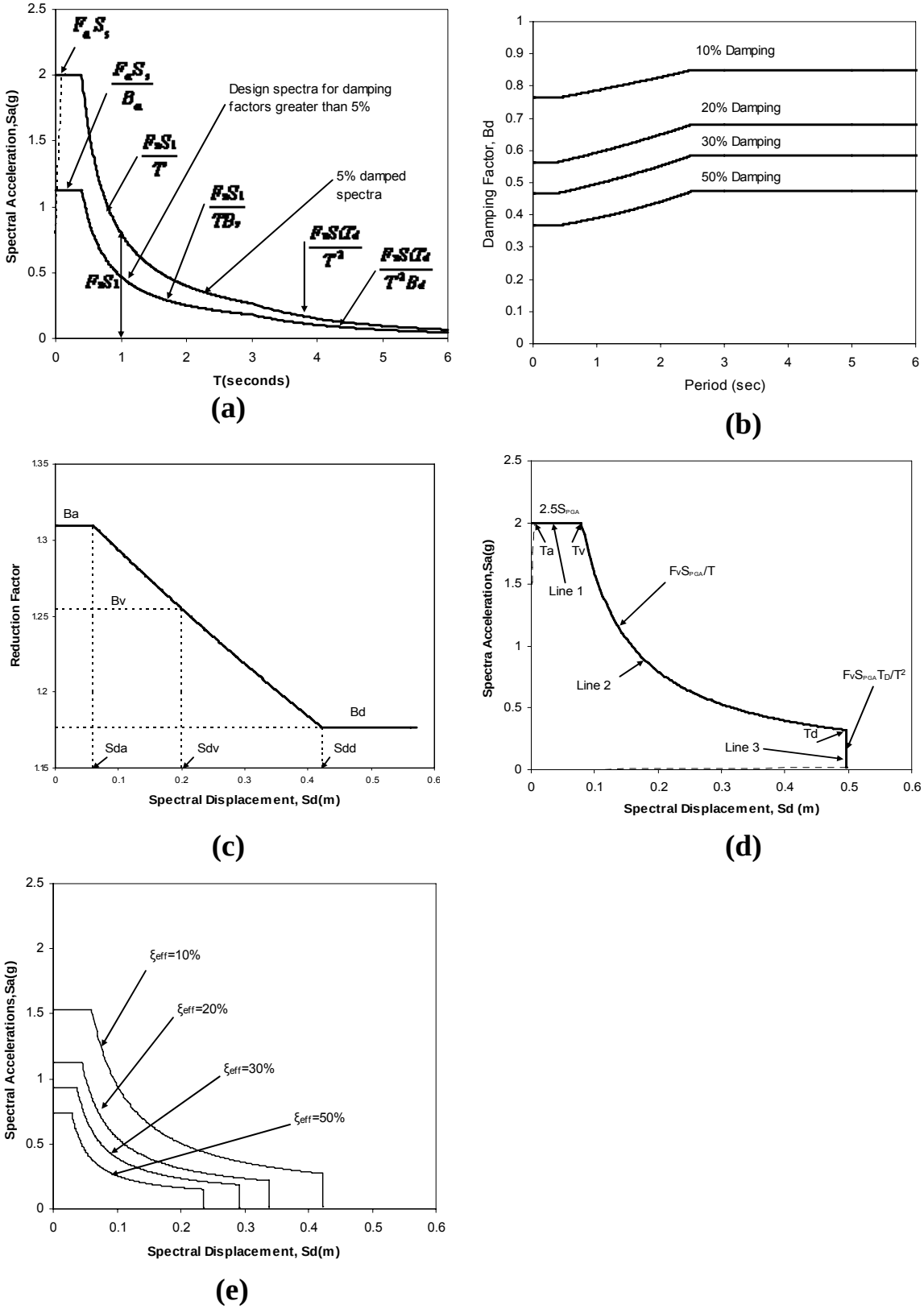


Figure 4.3: Design spectra for structures with variable effective viscous damping: (a) basic design response spectra; (b) period-dependent reduction damping reduction factor; (c) linear interpolation of $B_v$ located between $B_a$ and $B_d$; (d) spectra design with constant acceleration (line 1), constant velocity (line 2) and constant displacement (line 3); and (e) the overall spectra design at 5%, 10%, 20%, 30% and 50% effective damping.

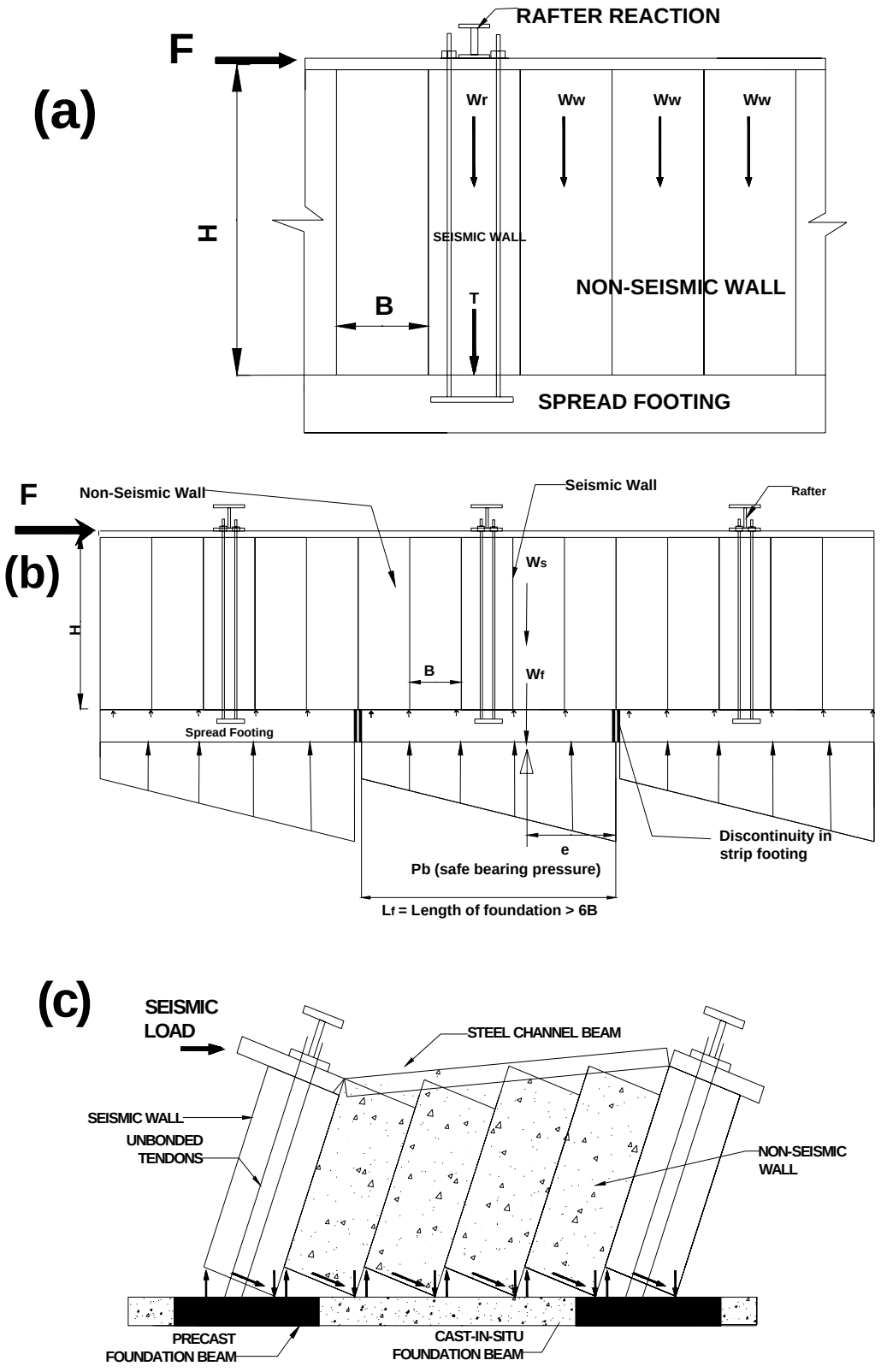


Figure 4.4: The forces and interaction of multi-panels acting on spread footing; (a) seismic resistance in the multi-panel wall system; (b) distribution of soil bearing pressure underneath spread footing; and (c) interaction between multi-panel walls and spread footing during ground shaking.

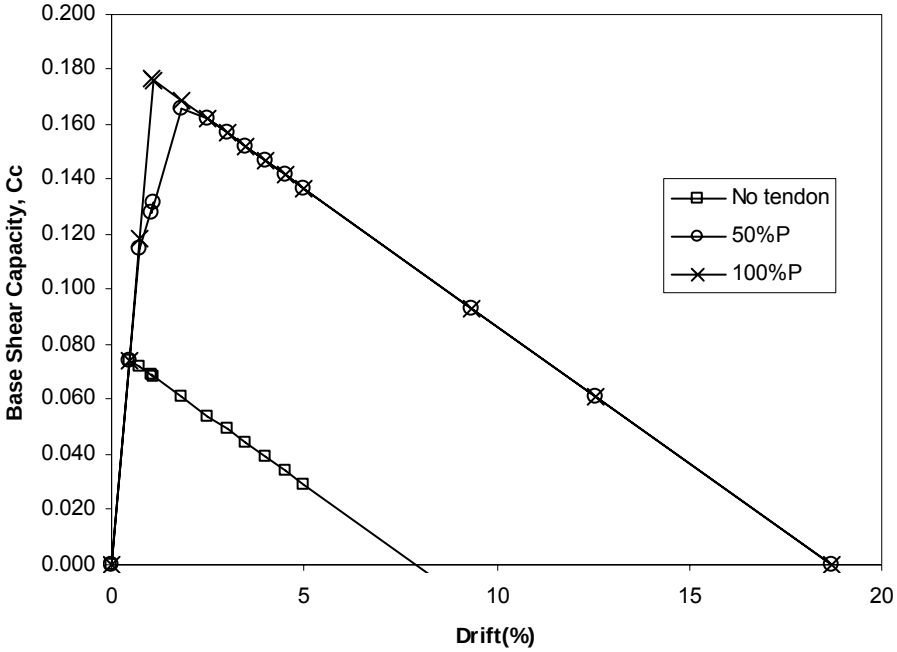


Figure 4.5: Theoretical base shear capacity of the rocking wall without tendons, 50% and 100% prestressing of unbonded tendons.

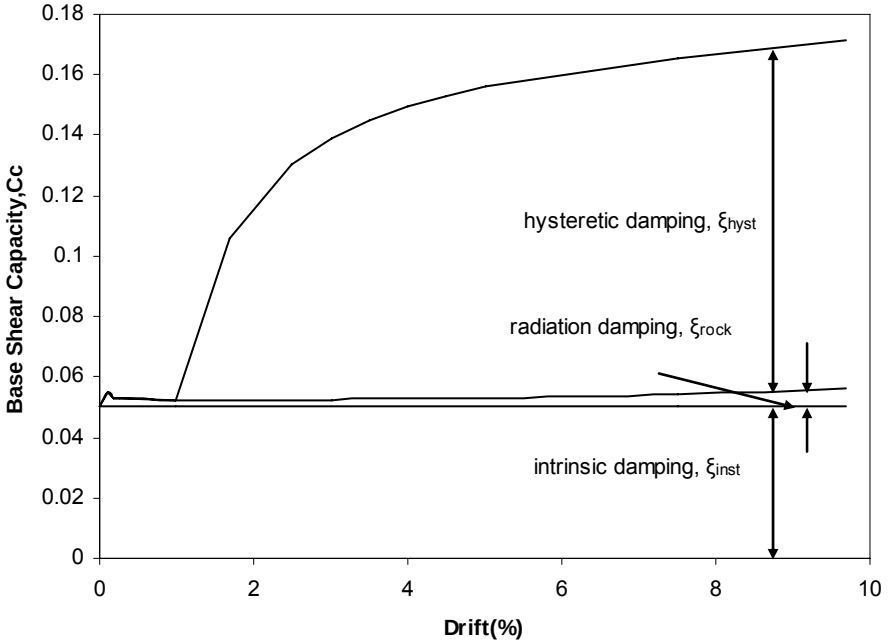


Figure 4.6: Total effective damping of the system of the rocking wall including intrinsic, radiation and hysteretic damping with 50% prestressing of unbonded tendons.

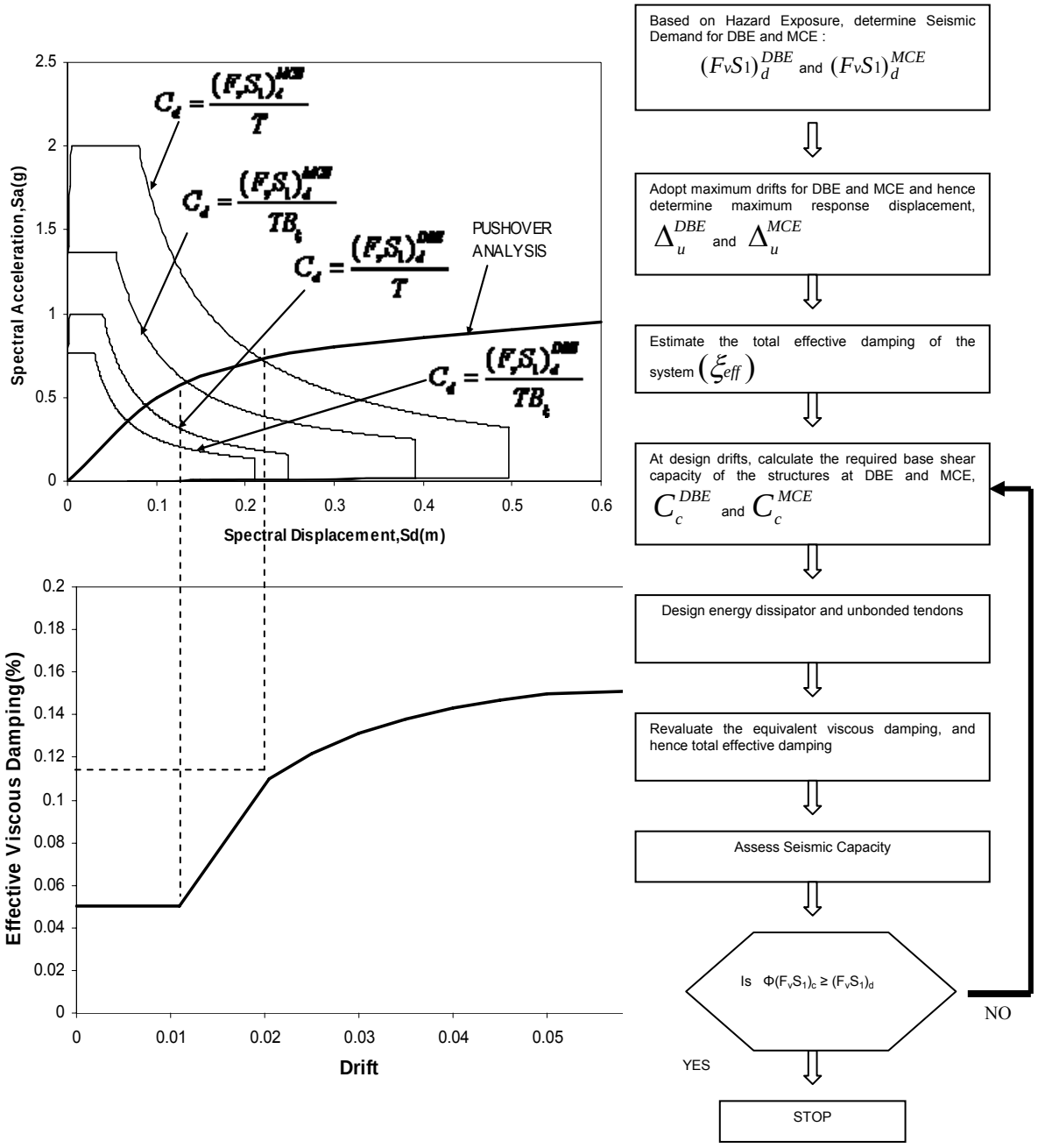


Figure 4.7: The flow chart of the proposed design procedure for rocking precast hollow core walls by adopting Damage Avoidance Design (DAD) philosophy.

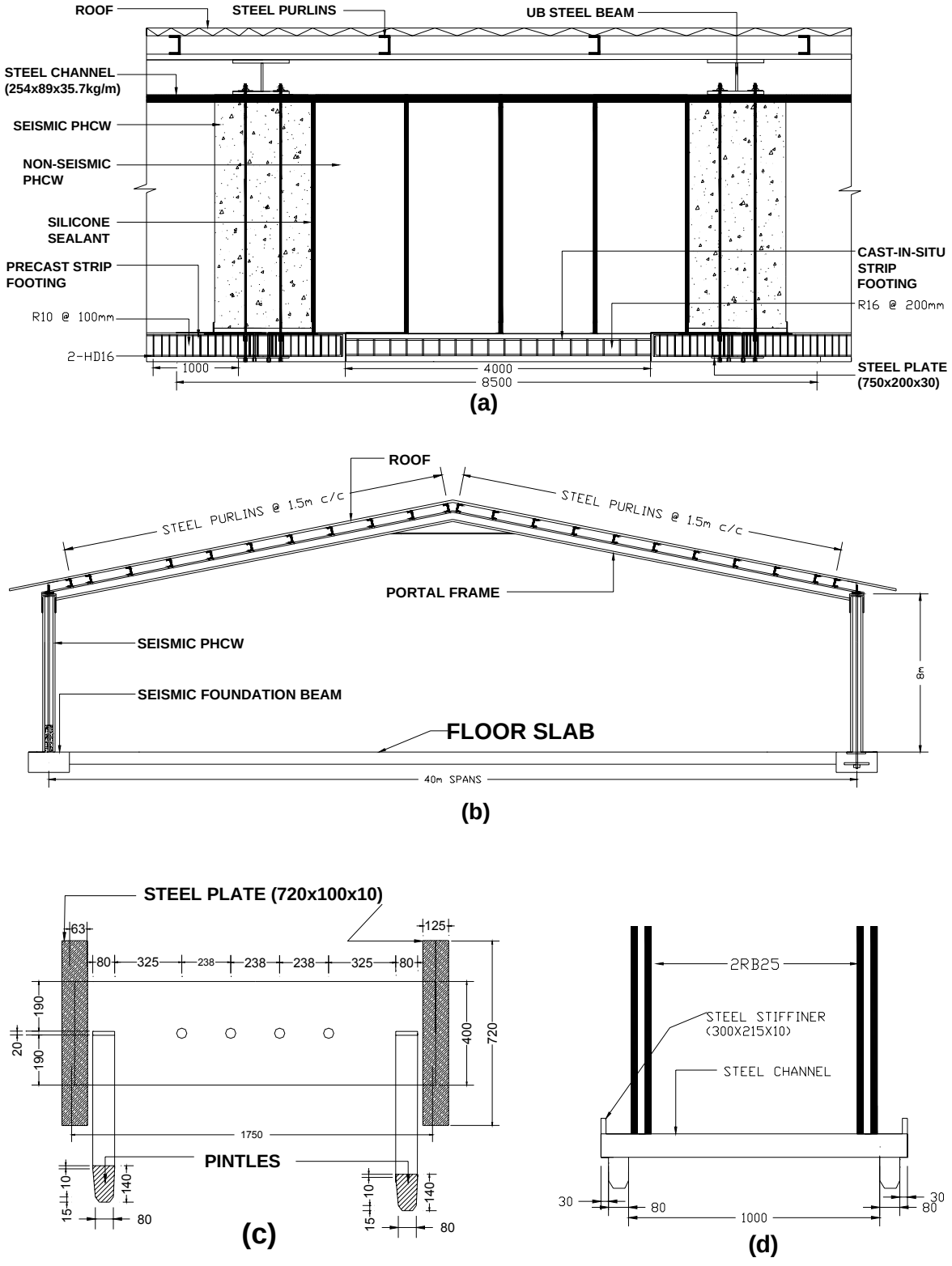


Figure 4.8: The components details used in the construction of the warehouse building; (a) arrangement of the multi-wall panel system together with the foundation beam; (b) steel portal frame sitting on the seismic wall; (c) rocking base plate and pintles; and (d) reidbars and pintles are welded to the steel channel acting as rocking toes.

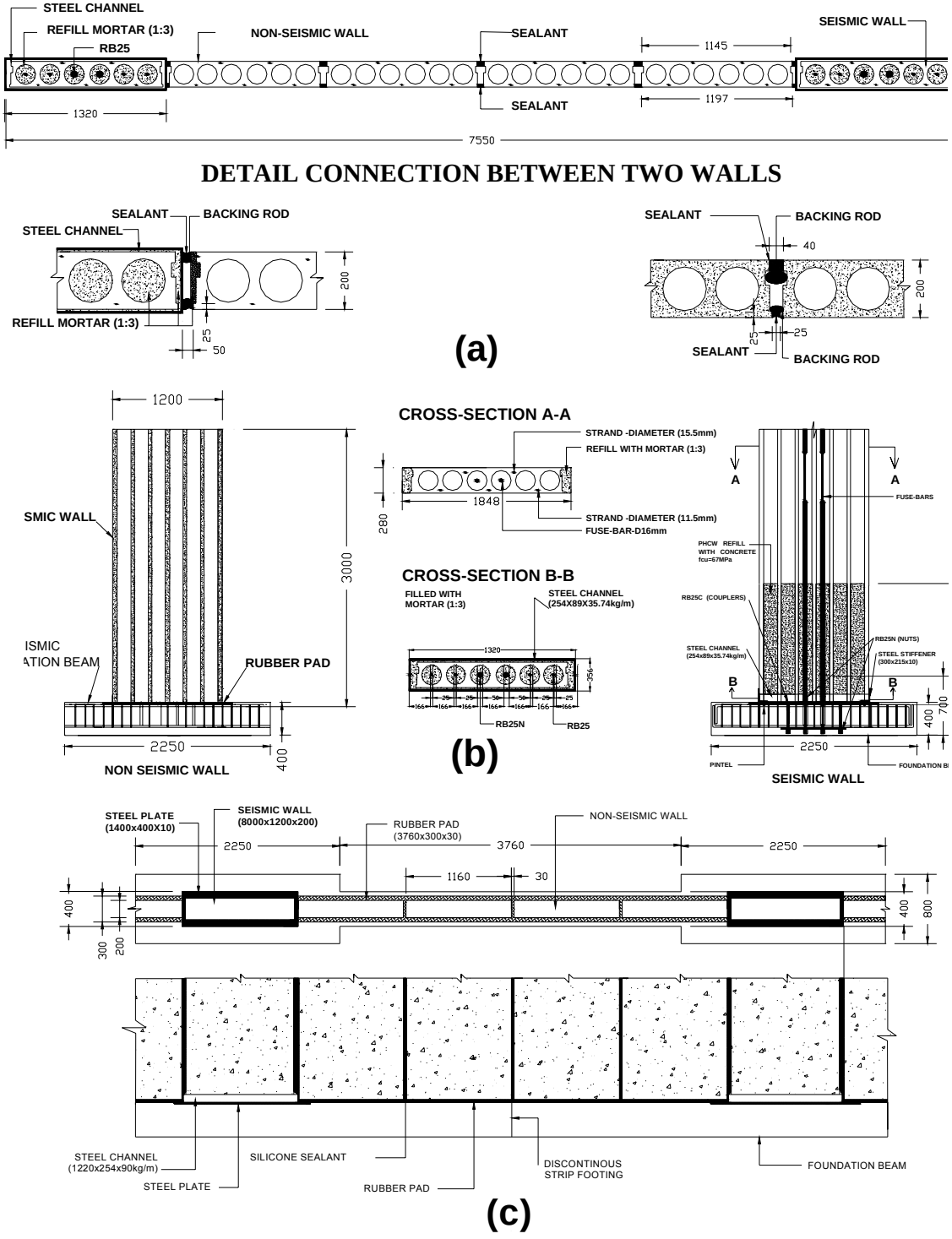


Figure 4.9: Connection details in the warehouse building; (a) connection details between walls to walls; (b) connection between wall and foundation; and (c) overall interfaces between wall and foundation of the multi-panel walls system.

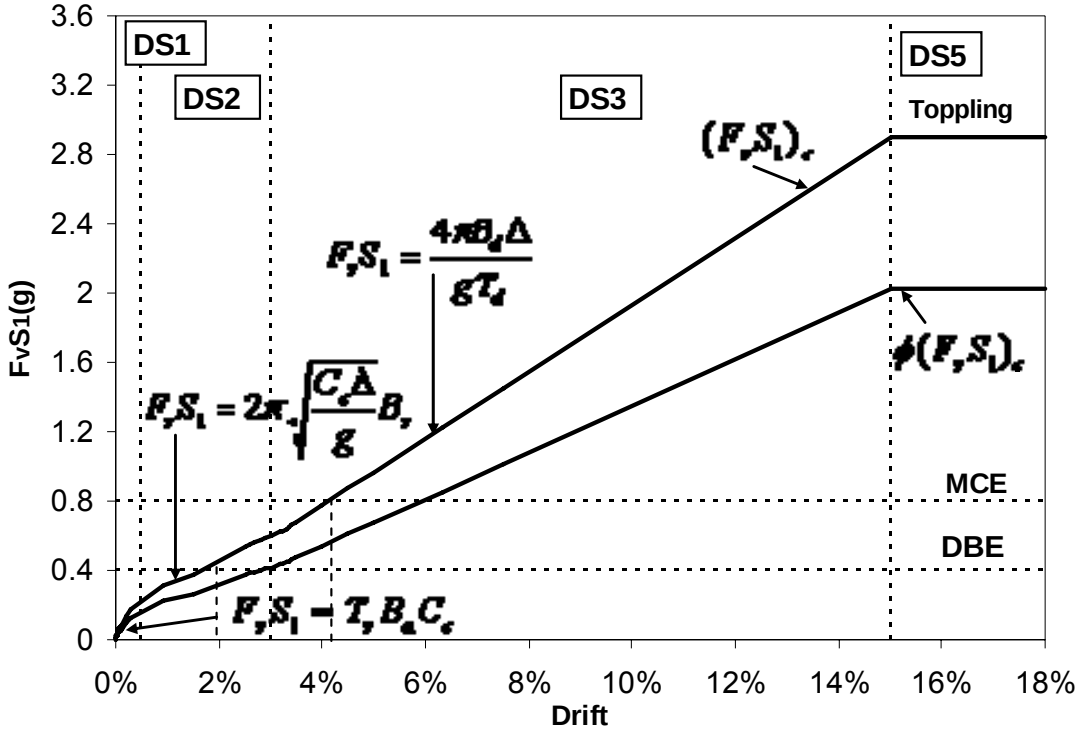


Figure 4.10: Relationship between static pushover analysis and damage states of the warehouse building using the precast hollow core wall system under MCE and DBE.

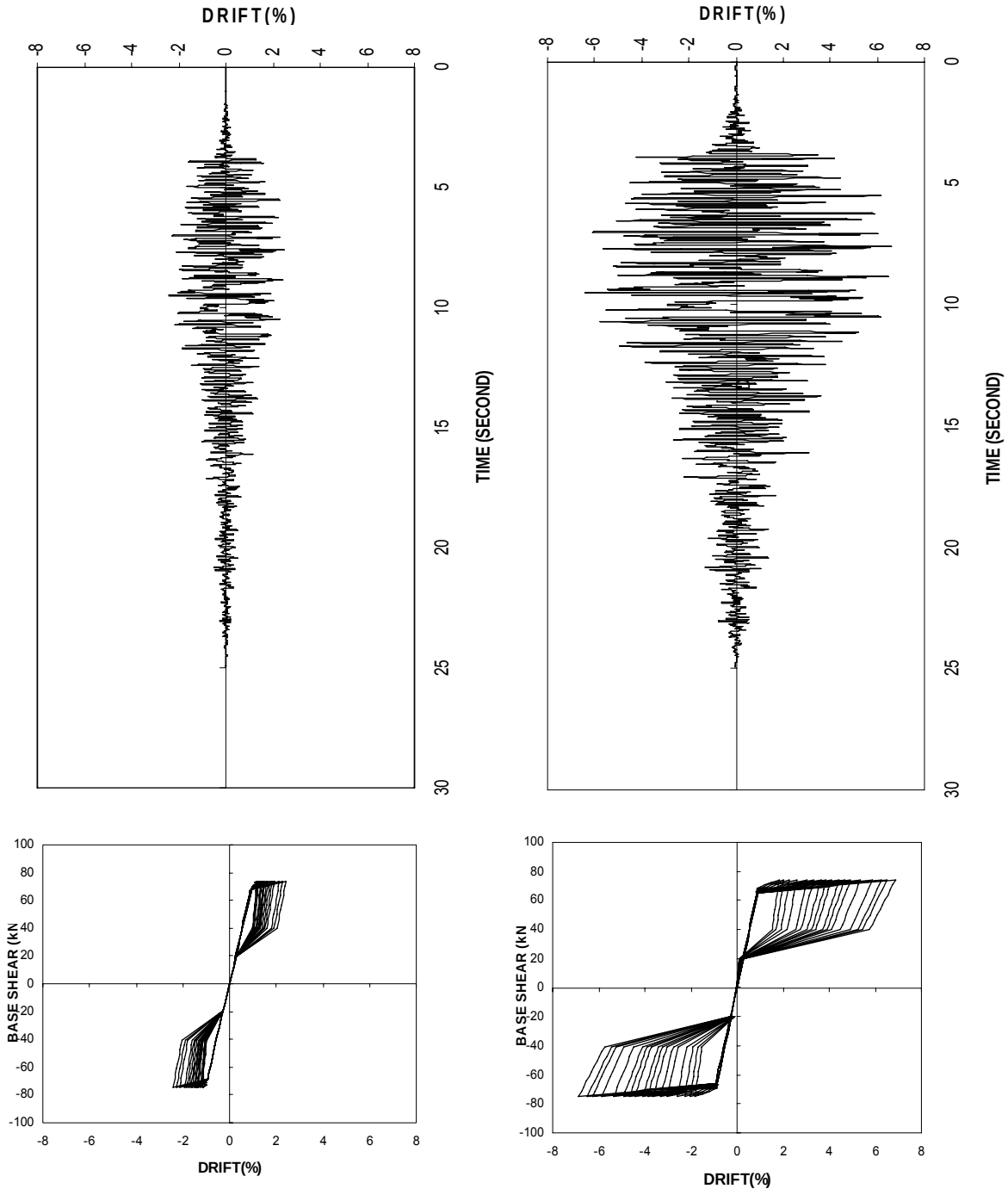


Figure 4.11: A set of results consisting of time history analysis and lateral load behaviour of a precast hollow core wall for an earthquake falling near the 90$^{th}$ percentile; (a) DBE at the 90$^{th}$ percentile; and (b) MCE at the 90$^{th}$ percentile.

# CHAPTER 5

# A COMPARATIVE SEISMIC PERFORMANCE ASSESSMENT OF PRECAST HOLLOW CORE AND CONVENTIONAL PRECAST WALLS

## SUMMARY

A comparative seismic performance assessment is made of two contrasting construction systems for warehouse buildings. The two contrasting systems have different wall types. The first is a rocking precast hollow core wall system designed in accordance with damage avoidance design (DAD) principles, while the second system has conventional fixed-base walls. Incremental Dynamic Analysis (IDA) is used as the basis for the comparative seismic performance assessment. The initial step is to model each wall type using nonlinear dynamic analysis subjected to 20 selected earthquake records. Wall performance is analysed from low to high ground motions until collapse. Responses in terms of wall displacements (drifts) are statistically examined and IDA curves are parameterized into various percentile bands. Once damage limit states are assigned and coupled with hazard-recurrence risk relations the results are integrated to indicate probable losses. A vulnerability assessment reveals that precast hollow core walls using the DAD philosophy perform considerably better than the conventional fixed-based precast wall panels designed for ductile performance.

## 5.1 INTRODUCTION

This chapter presents a comparative seismic performance analysis of two contrasting forms of construction for single storey precast concrete warehouse buildings. The purpose of this comparative analysis is to validate the hypothesis that warehouse buildings constructed with precast hollow core walls can perform better than their counterparts with conventional ductile design capacity under earthquake excitation. This chapter first examines findings from previous research related to analysis methods in a Performance Based Earthquake Engineering context (PBEE). It then goes on to outline the steps in a quantitative vulnerability assessment that employs Incremental Dynamic Analysis (IDA). A comparative study is then presented of the warehouse buildings constructed with precast panels that are either designed or detailed in accordance with (i) damage avoidance or (ii) ductility.

IDA was developed by Cornell and his research group at Stanford University. It is a new and promising computational method that can be used to examine the seismic performance through global instability and potentially collapse of structures under earthquake ground shaking. IDA is a computational procedure that involves a structural model being subjected to several ground motion records, scaled to multiple levels of intensity, to produce response curves of a prescribed intensity versus an engineering demand parameter such as displacement (or drift) until collapse occurs. Responses are related to damage measures. The IDA approach is adopted here to analyse the seismic performance and damage potential of the proposed warehouse building with precast hollow core walls. Comparative analyses are

made with buildings designed and constructed with conventional ductile detailing using fixed-based precast wall panels.

## 5.2 FINDINGS FROM PREVIOUS RESEARCH

The initial works pertaining to the effects of connection fractures on steel moment-resisting frames using nonlinear dynamic analysis were conducted by Cornell and Luco (1999). They further investigated the seismic drift response of these structures models under 20 earthquake records and divided them into three categories namely mild, moderate and rogue ground motions (Luco and Cornell, 2000). They proposed that the inelastic displacement demand of these ground motions are similar to the capacity curve imposed on linear structures under moderate period. The effect of connection fractures on steel structures under rogue and mild ground motions is not significant on the story drift response.

By looking closely at two structures which relate the drift demand and spectral acceleration of ground motion, Cornell et al. (2002) suggested that for a given spectral acceleration $(S_a)$, it is possible to predict a median drift demand $(\hat{D})$ by using the following equation:

$$\hat{D} = a(S_a)^b \tag{5-1}$$

in which $a =$ the coefficient determined by non-linear time history analyses and $b =$ an exponent. The coefficient $a$ can be estimated by the simple conventional method or using nonlinear time history analyses. Previous researchers demonstrated that $b = 1$ is sufficient for steel moment-resisting frame structures (Luco and Cornell, 2000).

Further assessment of the ductile connections of 26 moment-steel buildings which were designed according to the current seismic code (FEMA-273, 1997) using Incremental Dynamic Analysis was performed by Lee and Foutch (2002). These buildings were designed corresponding to the 2/50 hazard (2% probability of being exceeded in 50 years) and 50/50 hazard (50% probability of being exceeded in 50 years). Their results showed that the confidence levels of Collapse Prevention (CP) on these buildings ranged from 80% to 90% under the 2/50 hazard level. For Immediate Occupancy (IO), the confidence level varied between 94% and 99% under the 50/50 hazard level. Based on this evidence, Lee and Foutch (2002) recommended that the confidence level for post-Northridge moment-resisting frame buildings at CP and IO performance level is 90% coupled with 2/50 and 50/50 hazard levels, respectively. Thus, it can be concluded that the post-Northridge buildings have a high level of confidence interval for CP and IO performance objectives under PBEE requirements.

Vamvatsikos and Cornell (2002) analyzed and assessed the performance of 3, 5, 9 and 20 storey steel moment-resisting frame buildings using Incremental Dynamic Analysis (IDA). Their findings showed that a loose correlation can be made between the Static Pushover Analysis (SPO) curve and IDA curve for buildings under Damage Measure (DM). Based on these curves, it was shown that they exhibited similar ranges of Damage Measure (DM) values on the same axis. By converting SPO base shear capacity coordinate into Intensity Measure (IM), a comparison can be made between the SPO and IDA. Subsequently, Damage Measures (DM) were compared by plotting median (50%-fractile) IDA and SPO on

spectral acceleration and drift coordinates. Their results can be easily interpreted using emerging Performance Based Earthquake Engineering (PBEE) frameworks.

Recently, a 3-D version of IDA investigation was carried out by Vamvatsikos and Cornell (2004) who studied the influence of elastic spectral shape on the limit-state capacities of a 9-storey moment-resisting frame building. They performed IDA procedures using 30 earthquake records representing an earthquake scenario with a relatively large magnitude of 6.5-6.9 with moderate distances, recorded on firm soil and no signs of directivity. Therein, 5%-damped acceleration spectra of these records were plotted and better dispersion of the period was obtained. By taking the differences in the individual spectral shapes, the variability of IDA curves was reduced and subsequently improved the overall value of IM. Although a single spectral value (first-mode) could be measured accurately using structures deformation from the elastic to the nonlinear plastic region, it is not applicable for higher mode failures. Hence, the spectral shape becomes noteworthy for higher modes when IDA surfaces are mapped with direct visualization of the spectral shape on the capacities of limit-state. Vamvatsikos and Cornell (2005) also showed that this aim can be achieved by developing efficient scalar and vector intensity measures (IM) by incorporating elastic spectral information with the selected earthquake record suite.

Vamvatsikos and Cornell (2005) showed that for simplicity, the seismic demand and capacity of the MDOF model for complex structures can be converted to SDOF approximation using Incremental Dynamic Analysis. The estimation is performed by comparing MDOF of Static Pushover to Incremental Dynamic Analysis (SPO2IDA) with

fractiles of 16%, 50% and 84% of the IDA-SDOF curves. Their results show a similarity in these fractiles bands between MDOF and SDOF for 5, 9 and 20-story buildings. Thus, they recommended that it would be sufficient for structural engineers to analyze global behaviour with an SDOF model rather than a complex MDOF structure model.

In spite of the comparative experimental study of Holden et al. (2003), there has been no comparative assessment made on rocking precast hollow core walls and fixed-end monolithic wall panels across a wide range of seismic intensities. This research conducts such a comparative assessment using the IDA approach in a probabilistic framework. Thus, precast hollow core walls and fixed-base monolithic wall panels are modelled as a single degree of freedom (SDOF) and analyzed under the IDA approach using selected earthquake records. Further steps involved in IDA procedure and their hazard assessment are presented in what follows.

## 5.3 THEORY AND STEPS INVOLVED IN INCREMENTAL DYNAMIC ANALYSIS

### 5.3.1 STEP 1: SELECT GROUND MOTION RECORDS AND HAZARD-RECURRENCE RISK RELATION

Vamvatsikos and Cornell (2004) selected 20 earthquake records to analyse mid-rise buildings when they developed IDA curves. This selection of earthquake records was in-keeping with previous studies which stated that the same 10 to 20 earthquake records are sufficient for providing an estimation of seismic demand (Shome and Cornell, 1999). Thus

the same 20 earthquake records used by Vamvatsikos and Cornell (2004) are adopted herein. The details of these earthquake records are tabulated in Table 5.1. These earthquakes have magnitudes in the 6.5 to 6.9 range with moderate epi-central distances mostly ranging between 16 and 32km recorded on firm soil and no bearing signs of directivity.

Figure 5.1(a) shows each response spectra for 20 earthquake records scaled to the same Intensity Measure (IM) of PGA=1.0g. The solid heavy line shows the median response spectra curve. Figure 5.1(a) also presents a plot of the lognormal standard deviation, referred to as the dispersion factor $\beta_D$, across the spectrum. As the value of $\beta_D$ is consistent for periods up to 1.6 seconds, it is thus considered appropriate to use PGA as the IM. Another reason for this is because the New Zealand building code uses PGA as the IM that governs the seismic design of structures (A/NZS 1170.5, 2004).

An annual frequency-dependent scale factor $(\lambda_T)$ such that $S_{PGA}^{T=Tr} = \lambda_T S_{PGA}^{T=475\,yrs}$ is essential for scaling the spectra magnitudes (the IM) to the reference return periods of 475 years (or annual probabilities). Return period factor values can be derived by drawing a representative line through the hazard curves (response spectrum acceleration as a function of return period) normalized by the 475-year values for structures as illustrated in Figure 5.1(b). The relationship is given by the following equation:

$$S_{PGA}^{T=Tr} = \lambda_T S_{PGA}^{T=475} = S_{PGA}^{T=475}\left(\frac{T_r}{475}\right)^q = \frac{S_{PGA}^{T=475}}{(475\,p_a)^q} \tag{5-2}$$

where $S_{PGA}^{(T=Tr)} =$ PGA relevant to its return period; $S_{PGA}^{(T=475)} =$ PGA at a return period of 475 years (10 percent probability in 50 years); $T_r =$ return period, $p_a = (1/T_r) =$ annual

frequency; and $q =$ an exponent based on local seismic hazard-recurrence relations. For the design code of New Zealand, there is a multiplier of 1.8 between the DBE and the MCE, this gives for A/NZS 1170.5 (2004) $q = 0.333$.

### 5.3.2 STEP 2: PERFORM INCREMENTAL DYNAMIC ANALYSIS

IDA can be performed once the model and ground motions records are selected. To begin the analysis, the selected earthquake records are required to be scaled from a low IM to several higher IM levels with reasonable step-increments. For each increment of IM, a nonlinear dynamic time history analysis is performed. Analyses are continued until structural collapse is indicated by excessively large displacements at a high IM.

The maximum displacement response for each level of earthquake is converted to drift (%) by dividing it by the effective height of the wall. Locating the maximum drift observed in an analysis gives one point in the PGA vs. drift domain. Figure 5.1(c) shows an IDA curve for an individual earthquake by connecting the points obtained from all the analyses with different IMs.

It is also important to analyze the variability of outcomes response from a given IM. Figure 5.1(c) also shows a typical lognormal distribution of drift (displacement) outcomes with respect to dispersion factor $(\beta_D)$, plotted on the right side of Figure 5.1(c).

### 5.3.3 STEP 3: MODEL THE IDA CURVES AND STATISTICAL OUTCOMES

To interpolate between various calculated IMs, Vamvatsikos and Cornell (2004) used spline interpolations to model the IDA curve. Such an approach is cumbersome for subsequent analysis such as risk assessments and uncertainty modelling. As an alternative, the Ramberg-Osgood equation (Ramberg and Osgood, 1943) was adopted in this study as the most suitable means to empirically parameterise IDA curves. The R-O relation can be written in the following two forms:

$$\frac{\theta}{\theta_c} = \frac{S_a}{S_c} + \left(\frac{S_a}{S_c}\right)^r = \frac{S_a}{K\theta_c}\left(1 + \left|\frac{S_a}{S_c}\right|^{r-1}\right) \tag{5-3}$$

where $\theta = \text{drift}$ ; $\theta_c = S_c / K$ is a "critical" drift; $K = \text{slope of IDA curve in the initial}$ proportional range; $S_c =$ "critical" earthquake acceleration that occurs at the onset of large drifts that subsequently lead to collapse; $S_a = \text{earthquake acceleration; and } r = \text{constant}$ related to the curvature of the R-O curve where a high value of $r$ approximates a bilinear relationship.

The three significant control parameters $(S_c, r, \theta_c)$ in Equation (5-3) are estimated using nonlinear least squares analysis for each individual earthquake ground motion IDA data set. Figure 5.1(d) portrays the fit between the IDA data points and fitted R-O curve for one specific case. As the value of spectral acceleration grows larger than the "critical" value $(S_a > S_c)$, then the structure becomes globally unstable $(\theta > 2\theta_c)$.

Even though the values for each of the control parameters for each of the IDA curves are different, they can be assessed collectively using statistical analysis tools. Based on previous studies, such as Cornell et al. (2002) and Giovenale et al. (2004), it has been shown that this control parameter has a lognormal distribution about its median. Furthermore, by determining median values of each parameter the $50^{th}$ percentile IDA response can be represented as an individual R-O median curve. Similarly by examining variability of individual IDA distributions, the control parameters that denote the curves of other bounds of interest such as $10^{th}$ and $90^{th}$ percentiles can be found. The fitted IDA curves for 20 selected earthquakes along with three solid-marked curves for the $10^{th}$, $50^{th}$ and $90^{th}$ percentile response demand are shown in Figure 5.1(e).

### 5.3.4 STEP 4 : ASSIGN DAMAGE LIMIT STATES AND DERIVE FRAGILITY FUNCTIONS

After the three curves which represent the $10^{th}$, $50^{th}$ and $90^{th}$ percentile curves have been produced, it is possible to determine the expected drift for an earthquake with a certain level of intensity. Emerging international best practice for seismic design is leaning to the adoption of a dual level intensity approach, that is: (i) a DBE represented by a 10% in 50 years ground shaking; and (ii) a MCE represented a 2% in 50 years earthquake.

In order to be able to do the calculations needed for a PBEE assessment, it is essential to define several damage limit-states on the IDA curves developed. From previous research such as that of Lee and Foutch (2002) and Vamvatsikos and Cornell (2004) chose Immediate Occupancy (IO) and Collapse Prevention (CP) limit-states for their IDA curves

based on a steel moment-resisting frame building criteria. In this research, the definitions of damage limit states were extended by adopting the Mander and Basoz (1999) definitions of damage limit states for bridges, as listed in Table 5.2, with the result of assigning damage states to IDA fractile curves as illustrated in Figure 5.1(e).

The first and last damage states can be easily defined: $DS = 1$ is used to define the limit behaviour when rocking precast hollow core walls begin to rock under Damage Avoidance Design Philosophy (DAD) and $DS = 5$ is the "collapse" limit state where toppling or global instability occurs as defined when $\theta > 2\theta_c$.

It should also noted that because the structural system is conceived in terms of DAD, $DS = 4$ (irreparable damage) does not exist. Other damages states ( $DS = 2$ and 3) are more subjective in their definition. It is recommended that the boundary separating $DS = 2$ and $DS = 3$ be defined at the level of drift where the warehouse would be deemed to require repairs to take place such as retightening prestressing tendons, replacing mechanical energy dissipators (if present), and replacing peeled off sealant. Based on the experimental observation, this damage occurs when $\theta > 3\%$ (refer to Figure A5.1 and Table A3.1). $DS = 2$ is slight damage that can be tolerated without the need for repairs. This could mean some slight yielding of the prestress, or minor signs of distress to the sealants.

The damage limit states for a fixed-end monolithic reinforced concrete wall is defined in terms of drift limits based on experimental results carried out by Holden et al. (2003). Five damage limit-states are identified in this study. The first damage state (DS=1) is defined as

the yielding of the elastic limit when some minor cracks occurred at both sides of the wall as the drift level reached $\theta = 0.5\%$. As the wall experienced residual horizontal cracks, minor spalling of concrete at the bottom corner and moderate damage in slot-wall joints, slight damage is classified as $DS = 2$ at level drift of $\theta = 1.0\%$. The repairable damage state (moderate damage) is defined as $DS = 3$ when the level drift becomes $\theta = 2.0\%$. At this damage state, the wall has bigger cracks, buckling longitudinal reinforcement bars, extensive spalling of concrete at the bottom corner and along the joints. At $\theta = 2.5\%$, the outermost longitudinal reinforcement bar starts to fracture and the wall begins to become unstable showing heavy and irreparable structure damage (refer to Figure A5.2 and Table A5.2). This damage can be classified as $DS = 4$. The wall starts to lose its strength (strength degradation) and become globally unstable and subjected to larger cyclic loading. Once all the longitudinal reinforcement bars are buckled and fractured with severe damage to concrete, it can be classified as $DS = 5$ when $\theta_{\max}$ exceeding 4% drift.

Fragility curves are expressed as a lognormal cumulative probability density function known as a "fragility curve". The cumulative probability function is give by the following equation:

$$F(S_a) = \Phi\left[\frac{1}{\beta_{C/D}} \ln\left(\frac{S_a}{A_i}\right)\right] \tag{5-4}$$

where $\Phi =$ standard log-normal cumulative distribution function; $S_a =$ the spectral amplitude (for a period of $T = 1\text{sec}$); $A_i =$ the median spectral acceleration necessary to cause the $i^{th}$ damage state to occur and $\beta_{C/D} =$ normalized composite log-normal standard.

### 5.3.5 STEP 5: UNCERTAINTY, RISK AND RESILIENCE

The developed model of IDA curves in Step 3 can be modified elegantly by incorporating the hazard intensity curves. It can be done by substituting hazard curves as defined in equation (5-2) into equation (5-3) as the drift the function of annual probability:

$$\frac{\theta}{\theta_c} = \frac{S_a^{(T=475)}}{K\theta_c (475p_a)^q}\left(1+\left|\frac{S_a^{(T=475)}}{S_c (475p_a)^q}\right|^{r-1}\right) = \frac{S_a^{(T=475)}}{S_c (475p_a)^q} + \left(\frac{S_a^{(T=475)}}{S_c (475p_a)^q}\right)^r \quad (5\text{-}5)$$

where $S_c$, $\theta_c$ and $r$ are probability of occurrence dependent parameters.

In the foregoing analysis it must be emphasized that the resulting variability in response results entirely from the randomness of the input motion that is the seismic demand. This is because the computational modeling is conducted using crisp input data. However, the structural resistance both in terms of strength and displacement capacity is also inherently variable. Moreover, the computational modeling, although it may be sophisticated, is not exact; there is a measure of uncertainty that exists between the predicted and observed response.

To encompass the randomness of seismic demand along with the inherent randomness of the structural capacity and the uncertainty due to inexactness of the computational modeling it is necessary to use an integrated approach as suggested by Kennedy et al. (1980). The composite value of the lognormal distribution can be expressed as:

$$\beta_{C/D} = \sqrt{\beta_C^2 + \beta_D^2 + \beta_U^2} \quad (5\text{-}6)$$

in which $\beta_C$ = the coefficient of variation for the capacity which arises as a result of the randomness of the material properties that affect strength, and in the case of precast wall panels this is due to the randomness in the yield strength and assumed to be $\beta_C = 0.2$ in this study; and $\beta_D$ = the coefficient of variation for the seismic demand which arises from record-to-record randomness in the earthquake ground motion suite and assumed to be $\beta_D = 0.38$ in this study; and $\beta_U$ = lognormal dispersion parameter for modelling uncertainty which is assumed to be $\beta_U = 0.25$ in this study. The hazard recurrence curves including the uncertainty from the computational modelling can be seen as the dotted line with $\beta_{C/D} = 0.5$ in Figure 5.1(f) for the 90$^{th}$ percentile and $\beta_C = 0.2$ as a solid line. For detailed assessment, non-exceedence probabilities can also be plotted with the 50$^{th}$ and 10$^{th}$ percentile curves as shown in Figure 5.1(f). Figure 5.2 presents the final outcome of the risk assessment in the form of a so-called Hazard-Survival curve. These can be found by transforming the fragility curves via the hazard-recurrence relationship (equations 5-2 and 5-4). These new curves give the probability of surviving a given damage state for a given annual frequency of earthquake.

## 5.4 COMPARATIVE STUDY OF DIFFERENT FORMS OF PRECAST WALL PANEL CONSTRUCTION

Results of a comparative study of two types of precast wall panels for warehouse buildings, designed according to the proposed DAD as described in Chapter Four and fixed-based conventional precast wall panel in accordance with the New Zealand Standard Code of Practice for the Design Concrete Structures (NZS 3101: Part 1, 1995) are presented herein.

Both of these walls were designed using similar dimensions of 8m high, 1.2m wide and 200mm thick. They were designed to resist the same amount of seismic in-plane loading and carry a roof gravity load of 34kN. The elevation view for these two prototypes precast wall panels and their design parameters are given in Figure 5.3.

## 5.5 IDA PROCEDURES AND HAZARD-RECURRENCE RISK ASSESSMENT

Dynamic time history inelastic analyses were carried out for the 20 selected earthquake records on two prototypes of precast wall panels using a nonlinear structural analysis program RUAMOKO (Carr, 2004). Prior to Incremental Dynamic Analysis (IDA) procedures, pushover analyses were conducted to enable a single-degree of freedom (SDOF) model for each type of wall panel to be established. The precast hollow core wall panel was modelled as a "flag-shape" rule and a modified Takeda rule was adopted to model the performance of fixed-end conventional wall panels (Carr, 2004). Figure 5.4(a) presents the data obtained from the IDA computational investigations which are plotted along with their respective dispersions on the left hand side of the graphs for two different types of wall panels. Table 5.3 shows the 20 selected earthquakes used in IDA, along with the parameters obtained to fit the set of IDA results to the R-O relationship given in equation 5-3. Fitted IDA curves for the $10^{th}$, $50^{th}$ and $90^{th}$ percentile bands for each wall are shown in Figure 5.4 (b) along with five damage state bands as described above and listed in Table 5.1.

Figure 5.4(c) presents seismic risk as a series of probabilistic curves that relate hazard and consequences. From this quantitative risk analysis it is evident that both walls can survive a

DBE with some non-exceedence probability of 90%. For a rarer event such as a MCE, it is evident that the non-exceedence probability in their good seismic performance is substantially reduced. There is a 90% chance that precast hollow core walls will survive with repairable damage ($DS = 3$) chance implying a 10% chance of collapse. Moreover, a fixed-end wall has 80% chance that the wall has severe damage before collapse. There is roughly a 70% chance that irreparable damage ($DS = 4$) will occur in moderate earthquakes.

Figure 5.5(a) presents Hazard-Survival curves for each damage state listed in Table 5.2. This graph is plotted with annual frequency on x-axis and survival probability on y-axis. Note that for the case of the precast hollow core panels used in the construction of warehouse buildings, heavy damage ($DS = 4$) is not expected of the damage-free design criteria. This is due to the non-existence of a plastic hinge zone (PHZ) in this type of wall. For this construction type there is some 95% chance of surviving a MCE with repairable damage (restressing tendons and re-caulking the joints), whereas for the conventional construction the non-exceedence probability is reduced to 77%. Under DBE, the warehouse building which is constructed using precast hollow core walls has a 73% chance of surviving with only minor damage to the non-structural components, whereas with conventional precast wall panels there is a reduction to 55% survival probability with some repairable damage to structural components. Note that the precast hollow core wall does not suffer any structural damage because it has the characteristics of a rigid-body and rocking structure mechanism.

Figure 5.5(b) shows another simpler method of hazard assessment using standard fragility curves. Both graphs representing two prototype walls are plotted with PGA (g) on x-axis,

cumulative density function and confidence interval on both of the y-axis. The top corner of these graphs is assigned for lower damage states and a bottom corner is allocated for collapse limit (global instability) which is in contrast with Hazard-Survival curves. These figures show that the precast hollow core wall has a 90% chance of survival while the conventional wall has 72% survival with repairable damage $(DS = 2)$ under MCE. From these fragility curves, one can be quite confident of the survival of the precast hollow core slab without collapse for a DBE. Eventually a conventional wall has 25% chance in suffering slight damage under DBE. Under MCE – that is PGA=0.8g with a 2% probability in 50 years – the precast hollow core wall has a 98% survival probability against total collapse and the conventional wall system has a 90% chance of survival of irreparable damage and requires total demolishing. It is also observed that standard fragility curves portray similar damage states as Hazard-Survival curves.

The foregoing analysis uses the probabilistic principles of engineering to asses the seismic risk to a warehouse building constructed using rocking precast hollow core walls and fixed-end walls. The final outcome of that analysis however, tends to be effectively free from engineering jargon. This outcome can be further translated into linguistic statements that may be more useful for non-engineers to understand. The comparison statements between rocking precast hollow core walls and fixed-based conventional precast wall panels are presented in Figure 5.5(c). It can be concluded that warehouse buildings which are constructed using precast hollow core wall panels along with Damage Avoidance Design (DAD) philosophy do not suffer any structural damage at two design earthquake level (MCE

and DBE). However, the fixed-based conventional wall suffers repairable damage under DBE and irreparable damage under MCE.

The performance assessment of both walls using Incremental Dynamic Analysis implies that decision variables (for example, mean annual frequency of collapse, expected loss, survival probability) are computed and compared with specified performance targets (for example, MCE and DBE). A good design concept such as DAD can achieve performance targets and objectives as outlined by PBEE. Therefore, it is recommended that warehouse/industrial buildings which will be constructed in seismic prone regions such as Pakistan, Sumatra and New Zealand should use the rocking precast hollow core wall rather than the conventional fixed-based precast wall system. The experimental results and theoretical analysis demonstrate that the precast hollow core walls along with a damage-free design criterion and details (DAD) have a very high chance of surviving the most severe earthquake shaking unscathed.

## 5.6 RAPID-IDA AND ITS RESULTS

One useful finding is to show how one can transform a Rapid Pushover curve to approximate an equivalent median IDA curve. To achieve this, it is necessary to transform base shear coordinates into Intensity Measures (IM) corresponding to each Damage Measure (DM). In this study, base shear capacity which was obtained from rapid pushover was converted to the one-second spectral acceleration ordinate $(F_v S_1)$ using the greater of the following equations:

$$F_v S_1 = T_v B_a C_c \tag{5-7}$$

$$F_v S_1 = 2\pi \sqrt{\frac{C_c \Delta}{g}} B_v \tag{5-8}$$

$$F_v S_1 = \frac{4\pi^2 B_d \Delta}{g T_d} \tag{5-9}$$

in which $C_c =$ displacement amplitude dependent base shear capacity of the structure; $\Delta =$ maximum lateral displacement; $g =$ gravitational accelerations; $S_1 =$ one-second period spectral acceleration; $F_v =$ soil type factor for constant velocity portion of the spectra; and $B_a, B_v, B_d$ are reduction damping factors for constant acceleration, velocity and displacement. In the absence of spectral specific details $T_a, T_v$ and $T_d$ may be taken as 0.15, 0.4 and 3.0 seconds. The heavy dotted-line on Figure 5.6 shows the median Rapid-IDA curve derive from equations (5-7), (5-8) and (5-9). When the displacement exceeds the maximum pushover displacement the IM is held constant in Equation 5-9; that is the whole structure, modeled as the SDOF system, becomes "dynamically unstable" and is expected to topple.

It is of interest at this stage to compare the results of the inelastic time history analyses (IDA) and their statistical outcomes in terms of the 10, 50 and 90 percentile bands with the expected value (median) calculated from the Rapid-IDA procedure. Initially, the Rapid-IDA curve (heavy dashed line) is compared with the computed 50$^{th}$ percentile IDA curves (solid line) as plotted in Figure 5.6. These curves show that the initial region of the two curves agrees well up to 6% drift. The two curves plateau at different earthquake Intensity

Measures – that is the PGA for toppling is 1.2g and 1.4g for the Rapid-IDA and the computationally derived IDA curves, respectively. This difference is attributed to the cut-off displacement limit used in the analysis.

Secondly, the computationally derived 90$^{th}$ percentile IDA corresponds to a dependent Rapid-IDA curve given by $\phi IM$, where the median IDA curve is multiplied by an under capacity reduction factor $\phi$ in the customary fashion as follows:

$$S_{PGA,90\%} = \phi_{PGA,n} \tag{5-10}$$

where $S_{PGA,90\%}$ = a peak ground acceleration earthquake for a given drift which captures 90 percent of the possible outcomes; and $\phi_{PGA,n}$ = reduction factor that can be calibrated against the IDA results. Based on the results of this study it appears that a value of $\phi = 0.6$ is satisfactory and shown as a light dotted line in Figure 5.6. This curve follows a slightly lower value than 90$^{th}$ percentile IDA curves but within the acceptable bound limit. Thus it can be concluded that the structural engineer need not perform a formal full computation and a Rapid-IDA based on a dependable pushover curve should suffice.

## 5.7 CONCLUSIONS

The following conclusions are drawn based on the quantitative seismic risk assessment using Incremental Dynamic Analysis (IDA) for rocking precast hollow core walls and fixed-end conventional walls:

1. In order to assess the seismic performance of precast hollow core walls and to compare this performance to fixed-end conventional walls it is desirable to conduct IDA from a low to a higher level of ground shaking which finally leads to the collapse of structures.
2. A seismic risk analysis (SRA) is developed along with the combination of site-dependent hazard-recurrence relations and coupled with damage indices and survival probabilities under an IDA procedure. Through this method, the risk analysis jointly handles probabilities and consequences. It is demonstrated that precast hollow core walls can perform better with higher survival rates than the conventional fixed-based precast wall system. A precast hollow core wall has a 74% chance of survival rate of repairable damage as compared to 54% for a conventional fixed-based wall under DBE. However, if a larger earthquake occurs (MCE), the survival rate under repairable damage for precast hollow core walls is 50% and reduced to 30% for conventional fixed-based precast wall panels.
3. The computational IDA technique has been extended to Rapid-IDA methodology, which produces a median IM vs drift response. The reduction capacity factor $(\phi)$ that relates to global uncertainty of seismic performance is approximately 0.6. This value can be used to estimate the $90^{th}$ percentile of the structures without performing Incremental Dynamic Analysis (IDA).

## REFERENCES


Carr, A.J. (2004). *RUAUMOKO: Inelastic dynamic analysis program.* Department of Civil Engineering, University of Canterbury, New Zealand.

Cornell, C.A., and Luco, N. (1999). "The effects of connection fractures on steel moment resisting frame seismic demands and safety: A report on SAC Phase II Task 5.,4.6." *Rep.No. SAC-BD/99-03*, SAC Joint Venture, Sacramento, California.

Cornell, C.A., Jalayer, F., Hamburger, R.O., and Foutch, D.A.(2002). "Probabilistic basis for 2000 SAC Federal Emergency Management Agency steel moment frame guidelines." *Journal of Structural Engineering*, ASCE, 128(4), 526-531.

Federal Emengency Management Agency. (1997). "NEHRP guidelines for the seismic rehabilitation of buildings." *FEMA-273,* BSSC Building Seismic Safety Council, Washington, D.C.

Holden, T. J., Restrepo, J., and Mander, J.B. (2003). "Seismic performance of precast reinforced and prestressed concrete walls." *Journal of Structural Engineering,* ASCE, 129(3), 286-296.

HAZUS 99-SR2. (2004)."Earthquake loss estimation methodology." *HAZUS Technical Report*, Federal Emergency Management Agency and National Institute of Buildings Sciences, Washington D.C., http://www.fema.gov/hazus/[accessed 2/2/03]

Giovenale, P., Cornell, C.A., and Esteva, L. (2004). "Comparing the adequacy of alternative ground motion intensity measures for the estimation of structural responses", *Earthquake Engineering and Structural Dynamics*, 33(5), 951-979.

Kennedy, R.P., Cornell, C.A., Campbell, R.D., Kaplan, S., and Perla, H.F. (1980). "Probabilistic seismic safety study of an existing nuclear power plant." *Nuclear Engineering and Design*, 59, 315-338.

Lee, K., and Foutch, D.A. (2002). " Performance evaluation of new steel frame buildings for seismic loads." *Earthquake Engineering and Structural Dynamics,* 31(4), 653-670.

Luco, N., and Cornell, C.A. (2000). "Effects of connection fractures on SMRF seismic drift demands." *Journal of Structural Engineering*, ASCE, 126(1), 127-136.

Mander, J.B., and Basoz, N. (1999). "Seismic fragility curve theory highway bridges in transportation lifeline loss estimation, in optimizing post-earthquake lifeline system reliability." *TCLEE Monograph No. 16*, Eds Elliot and McDonough, 31-40.

Ramberg, W., and Osgood, W.R. (1943). "Description of stress-strain curves by three parameters." *Technical Note 902*, National Advisory Committee for Aeronautics.

Standard Australia/ Standard Association of New Zealand. (2004)."Structural design actions, earthquake actions-New Zealand." *AS/NZS 1170.5:2004 Part 5*: Wellington, New Zealand.

Standard Association of New Zealand. (1995). "New Zealand Standard code of practice for concrete structures standard: The design of concrete structures." *NZS 3101:Part 1: 1995,* Wellington, New Zealand.

Shome, N., and Cornell, C.A. (1999)." Probabilistic seismic demand analysis of nonlinear structures." *Report No.5*, RMS-35, RMS Program, Stanford University, Stanford. USA., http://pitch.stanford.edu/rmsweb/Thesis/NileshShome.pdf [accessed 3/4/04].

Vamvatsikos, D., and Cornell, C.A. (2002). "Incremental dynamic analysis." *Earthquake Engineering and Structural Dynamics,* 31, 491-514.

Vamvatsikos, D., and Cornell, C.A. (2004). "Applied incremental dynamic analysis." *Earthquake Spectra*, 20(2), 324-335.

Vamvatsikos, D., and Cornell, C.A. (2005). "Direct estimation of seismic demand and capacity of multidegree-of-freedom system through incremental dynamic analysis of single degree of freedom approximation." *Journal of Structural Engineering*, ASCE, 131(4), 122-134.

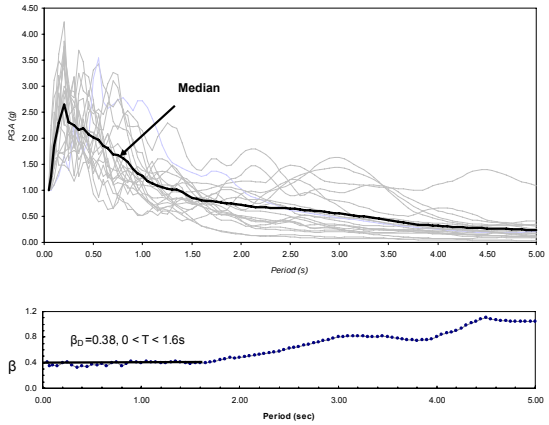


*(a) Step 1a: Ground motions records scaled to a common IM of PGA=1.0g*

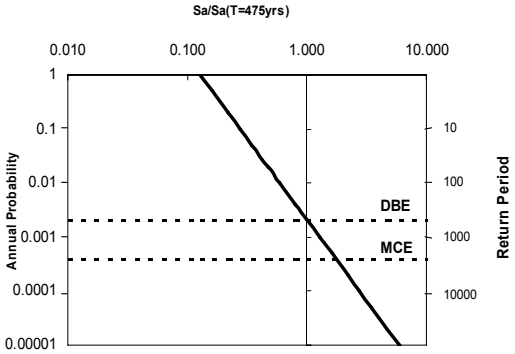


*(b) Step 1b: Hazard-Recurrence Relation*

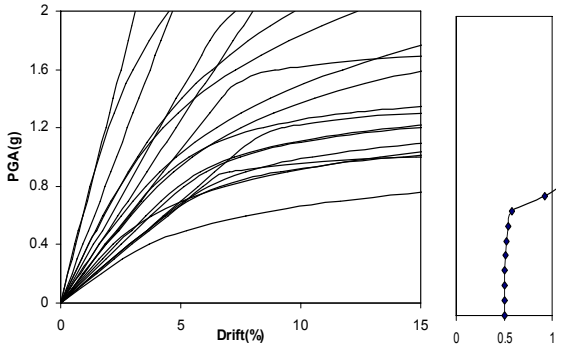


(c) Step 2: Conduct IDA

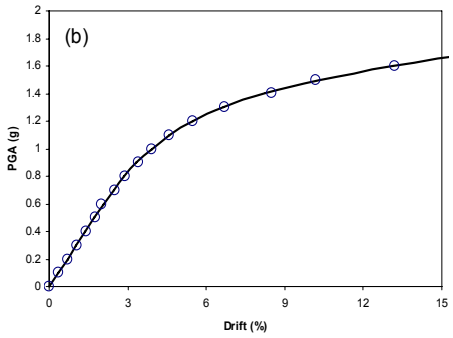


*(d) Step 3: Model IDA results with the R-O relationship.*

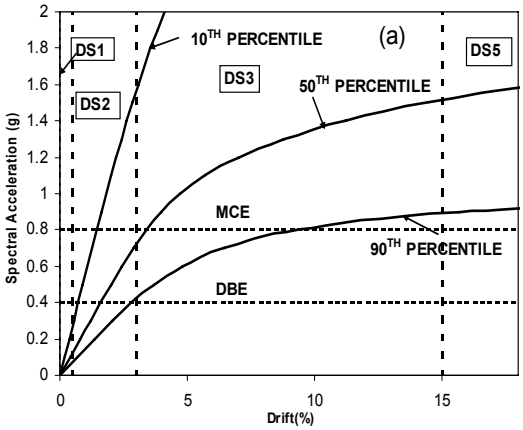


*(e) Step 4: Assign Damages States*

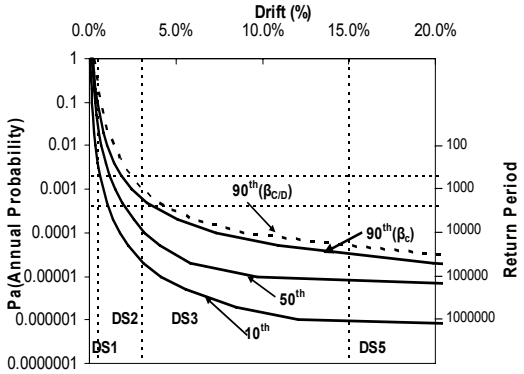


*(f) Step 5: Risk modelling accounting for uncertainty*

Figure 5.1: Step in conducting an IDA-Based Seismic Risk Assessment

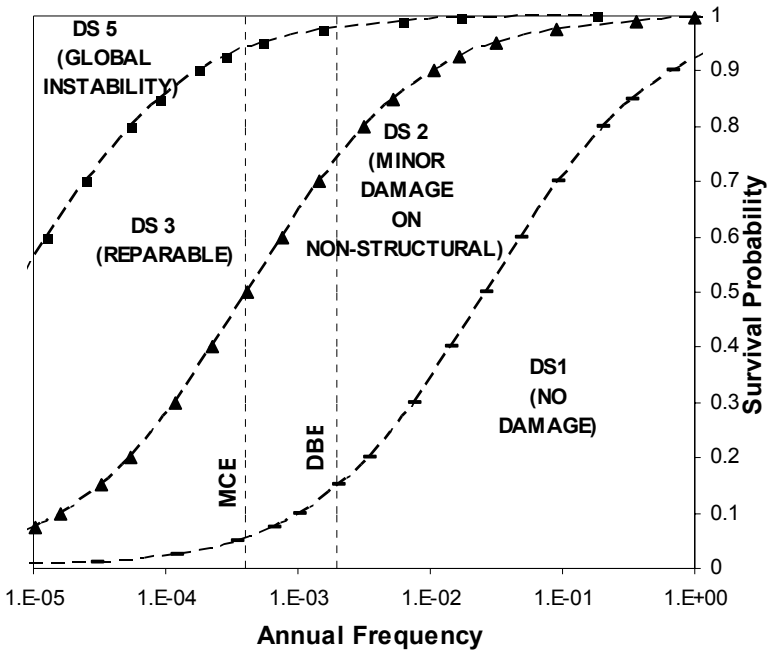


Figure 5.2: The Hazard-Survival curve shows the survival probability (for a given state of damage) with respect to the hazard exposure. Note that DBE and MCE represent 10% and 2% probability in 50 years, respectively.

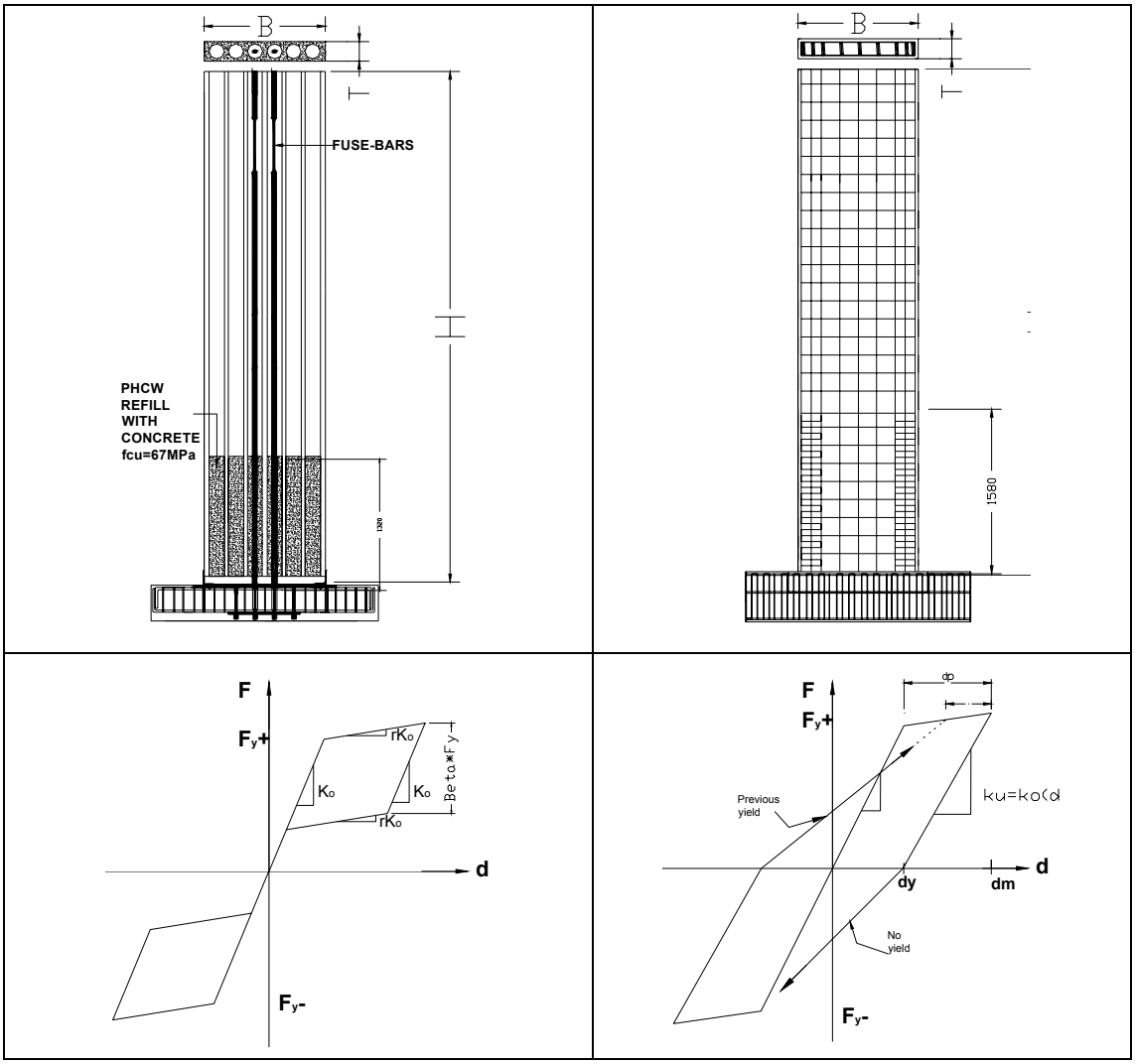


| Parameter | Precast Hollow Core Wall | Fixed-end conventional Wall |
|---|---|---|
| Height (mm) | 8000 | 8000 |
| Width (mm) | 1200 | 1200 |
| Thickness (mm) | 200 | 200 |
| Plastic Hinge Zone (PHZ) | - | 1580 |
| $P/A_g f'_c$ | 0.00567 | 0.00363 |
| Cross-sectional area ($mm^2$) | 120 000 | 312 000 |
| Bar | 5 strands (D-11mm) | 12HD10 |
| Spiral | - | 15-R6@180crs |
| $\rho_t$ (bar area/cross area) | 0.39% | 0.5% |
| $\rho_s$(spiral volume/confined concrete volume) | - | 0.96% |

Figure 5.3: Prototype precast wall panels and modeling outlines.

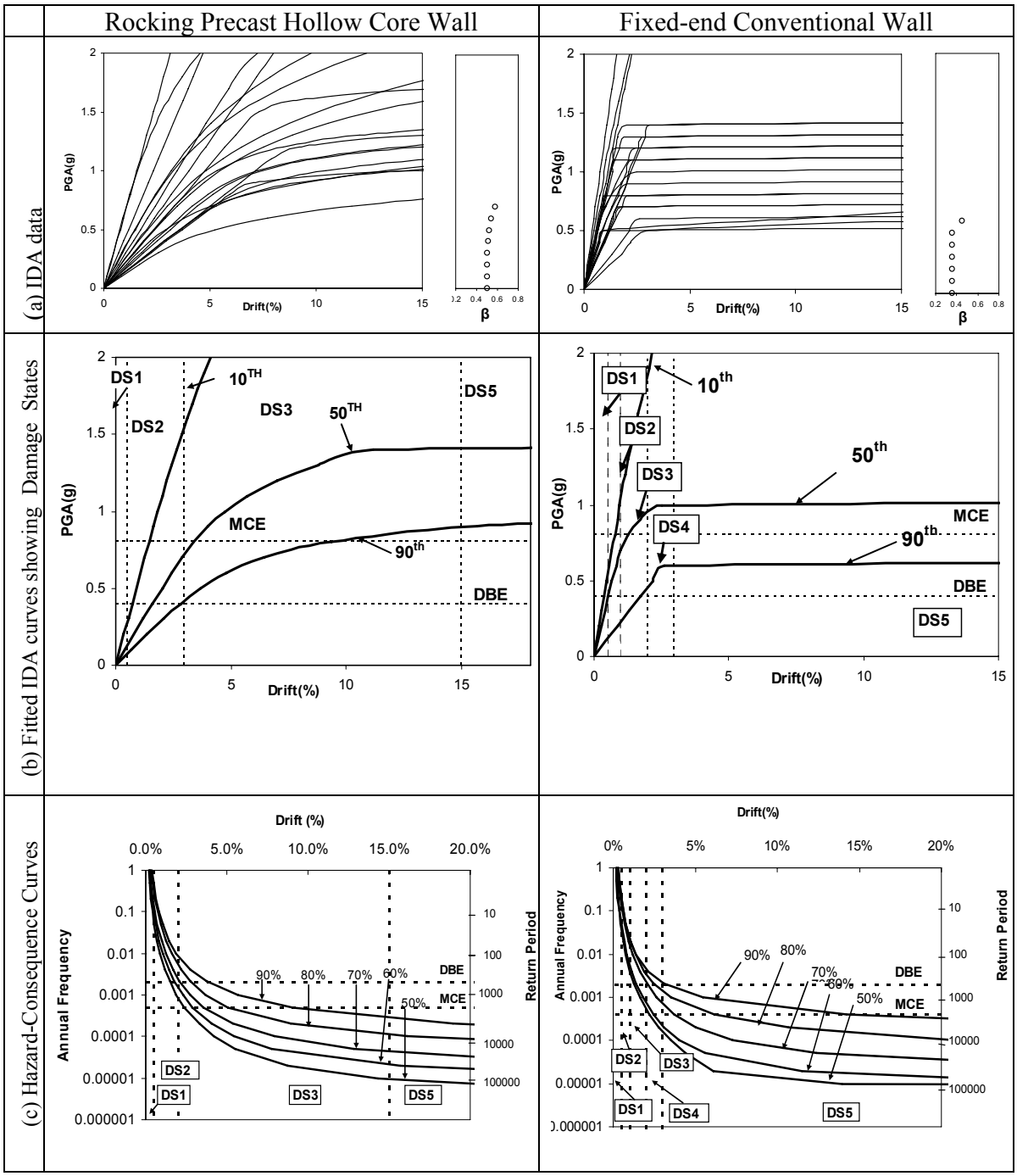


Figure 5.4: Performing IDA procedures fitted IDA curves with damage states and Hazard-Consequence curve for rocking precast hollow core wall and fixed-end conventional wall system.

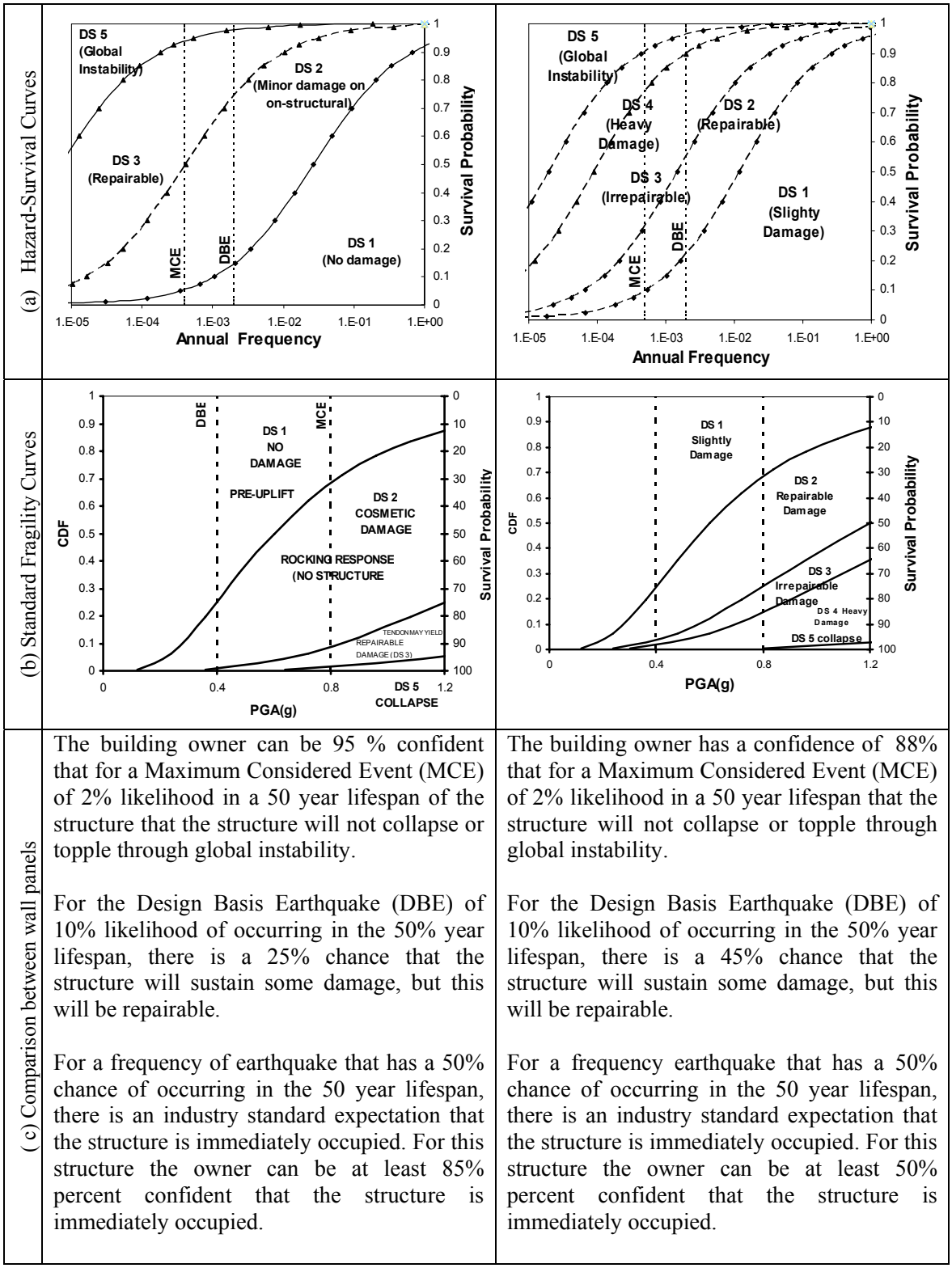


| (c) Comparison between wall panels | | |
|---|---|---|
| | The building owner can be 95 % confident that for a Maximum Considered Event (MCE) of 2% likelihood in a 50 year lifespan of the structure that the structure will not collapse or topple through global instability.<br><br>For the Design Basis Earthquake (DBE) of 10% likelihood of occurring in the 50% year lifespan, there is a 25% chance that the structure will sustain some damage, but this will be repairable.<br><br>For a frequency of earthquake that has a 50% chance of occurring in the 50 year lifespan, there is an industry standard expectation that the structure is immediately occupied. For this structure the owner can be at least 85% percent confident that the structure is immediately occupied. | The building owner has a confidence of 88% that for a Maximum Considered Event (MCE) of 2% likelihood in a 50 year lifespan that the structure will not collapse or topple through global instability.<br><br>For the Design Basis Earthquake (DBE) of 10% likelihood of occurring in the 50% year lifespan, there is a 45% chance that the structure will sustain some damage, but this will be repairable.<br><br>For a frequency earthquake that has a 50% chance of occurring in the 50 year lifespan, there is an industry standard expectation that the structure is immediately occupied. For this structure the owner can be at least 50% percent confident that the structure is immediately occupied. |

Figure 5.5: Comparison in term of Hazard-Survival curves and fragility curves for precast hollow core wall and the fixed-end conventional monolithic wall system.

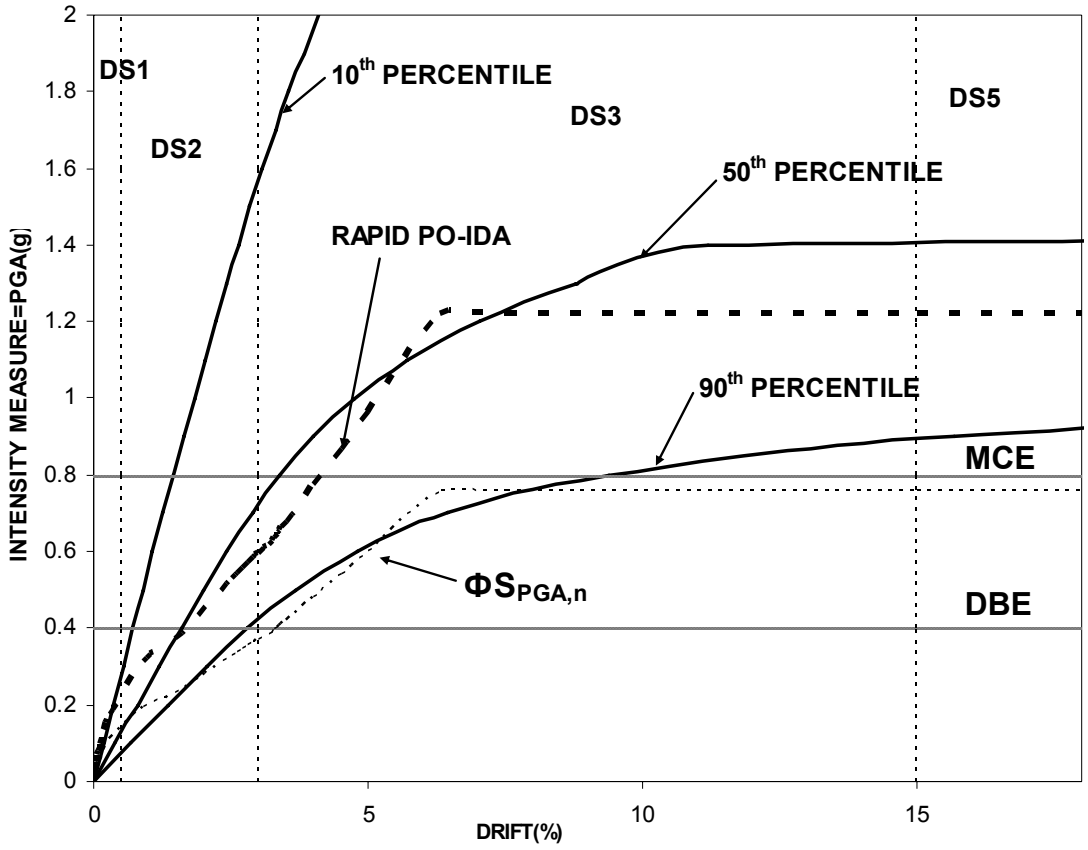


Figure 5.6: Comparison of IDA curves. The computationally derived IDA 50$^{th}$ percentile curve (central solid line) is compared with the expected value (median) curved derived via Rapid-IDA (dashed line). Also compared is the 90$^{th}$ percentile computationally derived IDA curve (lower solid line) with the Rapid-IDA curve reduced by $\phi$ (dotted line) where $\phi = 0.6$.

Table 5.1: Selection of 20 strong earthquake motions.

| Label | Event | Year | Station | Φ[*1] | M[*2] | R[*3] (km) | PGA (g) |
|---|---|---|---|---|---|---|---|
| A | Loma Prieta | 1989 | Agnews State Hospital | 90 | 6.9 | 28.2 | 0.159 |
| B | Imperial Valley | 1979 | Plaster City | 135 | 6.5 | 31.7 | 0.057 |
| C | Loma Prieta | 1989 | Hollister Diff. Array | 255 | 6.9 | 25.8 | 0.279 |
| D | Loma Prieta | 1989 | Anderson Dam | 270 | 6.9 | 21.4 | 0.244 |
| E | Loma Prieta | 1989 | Coyote Lake Dam | 285 | 6.5 | 22.3 | 0.179 |
| F | Imperial Valley | 1979 | Cucapah | 85 | 6.9 | 23.6 | 0.309 |
| G | Loma Prieta | 1989 | Sunnyvale Colton Ave | 270 | 6.6 | 28.8 | 0.207 |
| H | Imperial Valley | 1979 | El Centro Array #13 | 140 | 6.5 | 21.9 | 0.117 |
| J | Imperial Valley | 1979 | Westmoreland Fire Sta | 90 | 6.5 | 15.1 | 0.074 |
| K | Loma Prieta | 1989 | Hollister South & Pine | 0 | 6.9 | 28.8 | 0.371 |
| M | Loma Prieta | 1989 | Sunnyvale Colton Ave | 360 | 6.9 | 28.8 | 0.209 |
| N | Superstition Hills | 1987 | Wildlife Liquefaction Array | 90 | 6.7 | 24.4 | 0.180 |
| P | Imperial Valley | 1979 | Chihuahua | 282 | 6.5 | 28.7 | 0.254 |
| Q | Imperial Valley | 1979 | El Centro Array #13 | 230 | 6.5 | 21.9 | 0.139 |
| R | Imperial Valley | 1979 | Westmoreland Fire Sta. | 180 | 6.5 | 15.1 | 0.110 |
| S | Loma Prieta | 1989 | WAHO | 0 | 6.9 | 16.9 | 0.370 |
| T | Superstition Hills | 1987 | Wildlife Liquefaction Array | 360 | 6.7 | 24.4 | 0.200 |
| U | Imperial Valley | 1979 | Plaster City | 45 | 6.5 | 31.7 | 0.042 |
| V | Loma Prieta | 1989 | Hollister Diff. Array | 165 | 6.9 | 25.8 | 0.269 |
| W | Loma Prieta | 1989 | WAHO | 90 | 6.9 | 16.9 | 0.638 |

[1]Component, [2]Moment Magnitudes, [3]Closest Distances to Fault Rupture, and Source: PEER Strong Motion Database, http://peer.berkeley.edu/smcat/

Table 5.2: HAZUS damage states and the probability of occurrences.

| Damage State | HAZUS* Damage | Physical State | Operational Condition | Earthquake | Return Period(yrs) | Annual Probability |
|---|---|---|---|---|---|---|
| 1 | None | Pre-yield | Fully Operational | 100% in 50yrs | 63 | 0.016 |
| 2 | Slight | Tolerable | Immediate Occupancy | 50% in 50yrs | 150 | 0.007 |
| 3 | Moderate | Repairable | Life Safety | 10% in 50yrs | 475 | 0.002 |
| 4 | Heavy | Irreparable | Collapse Prevention | 2% in 50yrs | 2450 | 0.0004 |
| 5 | Complete | Global Instability | Collapse | | | |

*Refer to HAZUS99-SR2 (2004)

Table 5.3: R-O modelling and the parameter identification

| | Precast hollow core wall | | | Fixed-end monolithic reinforced concrete wall | | |
|---|---|---|---|---|---|---|
| No | $S_c(g)$ | $r$ | $\theta_c(\%)$ | $S_c(g)$ | $r$ | $\theta_c(\%)$ |
| A | 1.7 | 30 | 8.1 | 2.0 | 6 | 3.7 |
| B | 2.6 | 25 | 6.0 | 3.6 | 12 | 4.1 |
| C | 2.7 | 30 | 10.8 | 2.3 | 20 | 2.9 |
| D | 1.9 | 4 | 5.4 | 3.1 | 10 | 6.9 |
| E | 1.3 | 28 | 9.4 | 3.2 | 2.2 | 5.2 |
| F | 1.7 | 4 | 6.8 | 2.0 | 16 | 2.5 |
| G | 1.1 | 9 | 7.8 | 2.1 | 3.2 | 4.9 |
| H | 1.5 | 4.2 | 6.5 | 1.8 | 4.5 | 2.1 |
| J | 1.1 | 28 | 7.4 | 1.7 | 6 | 3.9 |
| K | 2.3 | 4 | 6.8 | 5.1 | 40 | 6.7 |
| M | 1.1 | 5 | 9.2 | 2.1 | 3 | 4.9 |
| N | 1.2 | 9 | 7.1 | 1.1 | 23 | 4.8 |
| P | 2.5 | 28 | 4.0 | 3.8 | 30 | 5.1 |
| Q | 0.8 | 12 | 4.7 | 1.0 | 8.5 | 1.3 |
| R | 1.2 | 10 | 7.5 | 1.1 | 10 | 6.5 |
| S | 2.5 | 4 | 3.7 | 1.2 | 22 | 2.2 |
| T | 2.3 | 28 | 7.7 | 0.9 | 2 | 0.8 |
| U | 0.9 | 5 | 4.7 | 1.2 | 3.5 | 1.8 |
| V | 1.0 | 9 | 7.1 | 1.5 | 30 | 3.3 |
| W | 1.6 | 5 | 7.6 | 6.9 | 1.9 | 5.8 |
| $10^{th}$ % | 4.8 | 4 | 8.5 | 5.1 | 40 | 6.7 |
| $50^{th}$ % | 1.2 | 6 | 6.9 | 3.0 | 20 | 3.8 |
| $90^{th}$ % | 0.7 | 12 | 4.8 | 1.1 | 23 | 4.8 |
| $\beta$ | 0.78 | 0.91 | 0.64 | 0.56 | 0.98 | 0.58 |

# CHAPTER 6

# SUMMARY, CONCLUSIONS AND RECOMMENDATIONS

## 6.1 SUMMARY

This thesis has consisted of five main chapters. Chapter 1 presented a state-of-the-art and practice summary of the field of precast wall systems in a seismic environment. It was pointed out that in spite of the historical success of ductile design for the preservation of life-safety, clients (society) and their engineers are now demanding a higher level of performance. For this reason this thesis has sought to investigate the application of Damage Avoidance Design (DAD) principles for single storey precast wall panels in warehouse type structures.

In Chapter 2, two geometrically similar precast concrete hollow core walls constructed with their foundations were tested under reversed cyclic quasi-static in-plane, out-of-plane and bi-lateral loading together with the results which were presented and discussed. Both of the walls were designed to carry roof (gravity) loading and resisted lateral loads by rocking on their foundation. A shaking table was used in slow motion to perform the bi-lateral quasi-static experiments. Wall specimens were detailed with steel-armouring at their base-to-foundation interfaces to provide a measure of damage protection. In addition to the longitudinal pretensioned prestress in the hollow core wall units, both specimens were detailed so that supplementary post-tensioned prestress along with sacrificial mechanical energy dissipators and fuse-bars could be added. Wall 1, with a fixed location of bonded fuse-bars and unbonded tendons, was tested under various biaxial loads paths including “4-leaf clover” patterns. Wall 2 was tested with four

different configurations of mechanical energy dissipators utilizing unbonded post-tensioned tendons and unbonded fuse-bars. Experimental results showed that due to the damage avoidance details both walls performed very well under various load paths without any discernible structural damage up to 2.0% drift. Results also demonstrated that the main determinant of wall performance was the level of post-tensioned prestress applied. Prestress also affected the initial stiffness and uplift strength along with the post-uplift (rocking) performance. The location and cross-sectional area of energy dissipators and unbonded tendons can also markedly affect performance. These experimental results were used to validate rigid body kinematic design models, including equivalent viscous damping resulting from the presence of the mechanical energy dissipators. It was concluded that for initial design, equivalent viscous damping of 10% is an appropriate value to accommodate the effects of hysteretic behaviour.

In Chapter 3, the seismic performance of a superassemblage of precast hollow core wall units tested under reverse quasi-static cyclic loading was presented. The superassemblage consisted of six prestressed concrete 1.2m wide hollow core units. Two of the units were tied to the foundation via unbonded vertical tendons while the other four units primarily acted as “non-structural” cladding. The superassemblage represented the wall of a single storey warehouse type structure. The longitudinal unbonded prestressing tendons consisted of regular thread-bars with the in-series portion of those bars possessing a reduced diameter to act as “fuses”. Prior to testing, the fuses were prestressed to 50% of their yield capacity. The multi-panel wall was tested under several different conditions: in-plane quasi-static reverse cyclic loading with different sizes of fuse-bars; and with and without rubber block spacers and sealant between units. Experimental results demonstrated that smaller diameter fuses led to

superior behaviour, as foundation uplift was inhibited. No structural damage occurred up to the experimental ± 4% drift limit. Some minor non-structural distress was observed to commence with sealant failure at +3% drift. This damage, however, is inexpensive to repair. Results also showed that the hysteretic energy absorption that arises from the yielding tendons as well as the interacting rubber spacers and panel sealants provided an equivalent viscous damping factor of 10% at design drift amplitude of 2%. The overall good performance of the multi-panel wall system well satisfied the requirements of an emerging seismic Damage Avoidance Design (DAD) philosophy.

In Chapter 4, the need for a new seismic design philosophy that has the performance traits of conventional ductile concrete monolithic wall systems but without permanent damage potential was addressed. Innovative design procedures along with construction methods were proposed that avoid earthquake induced damage by using an entirely precast wall system. Damage Avoidance Design (DAD) principles were incorporated by using rocking walls with armoured steel seating. This design procedure involved seven steps which included: assessment of seismic hazard (demand); setting design target displacements (capacity); estimation of effective damping; calculation of the base shear capacity in the form of a lateral pushover curve; designing unbonded tendons and/or fuse-bars; re-evaluation of effective damping; and assessment of seismic resistance adequacy via a demand vs capacity evaluation of the structure. A key step of this procedure was the evaluation of total effective damping which included intrinsic, hysteretic and radiation damping arising from rocking of the wall panels. Damping reduction factors for short, medium and long periods for the seismic demand spectrum were also considered. An illustrative design example of a warehouse building using the

precast hollow core wall system was given. The walls consisted of a mix of seismic wall panels and non-seismic infill cladding panels. The seismic wall panels were used to seat the rafters. Lateral loads were transmitted via diaphragm action through a roof truss. Results were also presented for nonlinear time-history analysis under various ground motions.

In Chapter 5, a seismic performance comparison was made for the construction of a warehouse using (a) a rocking precast hollow core wall or (b) fixed-base monolithic conventional walls. Incremental Dynamic Analysis (IDA) was used as a basis for a Performance-Based Earthquake Engineering (PBEE) assessment. The initial step was to model each wall type wall using nonlinear dynamic analysis subjected to 20 selected earthquakes. Wall performance was analysed from low to high ground motions until collapse. Responses in terms of wall displacements (drifts) were examined statistically and IDA curves were parameterized into various percentile bands. Once damage limit states were assigned and coupled with hazard-recurrence risk relations the results were integrated to indicate probable losses. This vulnerability assessment revealed that precast hollow core walls using DAD philosophy performed considerably better than fixed-based conventional wall panels designed for ductile performance.

In this final chapter, the summarization for each chapter of five main chapters is presented. The conclusions, design recommendations and future research are presented in what follows:

## 6.2 CONCLUSIONS

1. The end-user community now is becoming more demanding, requiring minimal and preferably no seismic damage. By using Damage Avoidance Design (DAD) philosophy along with the proposed design procedure, the repairable damage to industrial buildings will be minimized (mostly limited to the re-prestressing of fuse-bars) and irreparable damage to the structures can be avoided.
2. The experiments have demonstrated that precast prestressed concrete hollow core units can be used as a viable alternative to solid reinforced concrete walls. This is in spite of the lack of any transverse reinforcement for shear resistance. This also gives a wider scope for the use of hollow core units which customarily have been used mostly for floor units in buildings.
3. The success of the rocking hollow core walls is attributed to the Damage Avoidance Design (DAD) approach that required carefully detailed steel-armouring at the base of the wall to enable the high stresses from the point load reaction at the wall toe to be dispersed up the wall and also into the foundation.
4. Rocking walls, in themselves, dissipated little energy. But this can be improved through the use of supplemental energy dissipators. Of the dissipators tested in this study each had advantages and disadvantages. It would appear that the best trade-off is to use prestressed fuse-bars only as these always keep the wall clamped firmly to the foundation when not rocking. Other dissipator types may cause the walls to “sit up” on the devices when they yield and this effectively softens the structure.
5. By providing pintles or shear keys at the bottom corners of walls, the seismic lateral base shear can be resisted by rocking without sliding. No transverse

reinforcement in the precast hollow core wall panels needs to be used. In the present study to help improve shear resistance at the base of the wall the hollow core panel voids were filled to a height equivalent to one unit width (1.2m). Future research could potentially show that this extent of infilling be relaxed.

6. The experimental work on a superassemblage of multi-panel walls has demonstrated that both the seismic walls and non-seismic walls did not suffer any structural damage. This combined panel system could easily be implemented in the construction of single storey warehouses.
7. Experimental results showed that the seismic and non-seismic walls performed very well using the Damage Avoidance Design approach. By steel-armouring the wall-foundation interface of the seismic walls, and using concrete-rubber for non-seismic walls, higher displacements and contact pressures can be accommodated at the rocking toe during uplift of precast hollow core walls. The thickness of the rubber pad and rocking steel plate can be designed based on the maximum base shear imposed on the rocking base to dissipate energy during ground shaking. Shear keys or pintles can be welded underneath a steel channel to resist seismic base shear as there is no transverse reinforcement in hollow core units. Design parameters such as aspect ratio, cross-sectional area of energy dissipators and unbonded tendons, initial prestressing levels and magnitudes of pretressing in unbonded tendons have a significant influence on the base shear, shear friction and flexural capacities of precast hollow core walls.
8. The seismic panels dissipated more energy than the non-seismic panels as they were designed to carry roof loading and lateral loading. There were no cracks observed either on seismic walls or non-seismic walls up to ± 4.0% drift.

9. The rubber pad, silicone sealant and rubber block spacer are good materials to absorb energy and more economical to use in the construction industry rather than vertical shear connectors. It was demonstrated that silicone sealant and rubber block system behaved well under earthquake excitations. The rubber blocks in this system are protected against humidity and temperature changes while silicone sealant was exposed to mild or extreme conditions. Thus, the silicone sealant can be replaced easily and economically after exceeding its design life span.
10. The design process proceeded without the need to determine the fundamental period. This is useful, as for rocking structures the period constantly changes. Once designed and detailed, the adequacy of the design can be checked against rapid IDA curves. In order to assess the seismic performance of precast hollow core walls and to compare performance with fixed-end conventional walls it is desirable to conduct IDA from a low to a higher level of ground shaking which finally leads to the collapse of structures.
11. The computational IDA technique has been extended to Rapid-IDA methodology, which produces a median IM vs drift response. The reduction capacity factor ($\phi$) that is related to the global uncertainty of seismic performance was approximately 0.6. This value can be used to estimate the $90^{th}$ percentile of the structures without performing Incremental Dynamic Analysis (IDA).

## 6.3 DESIGN AND DETAILING RECOMMENDATIONS

1. For the installation of sealant, both edges for precast hollow core wall panels should be straight and the bottom corners of the wall must be perfectly square.

This provides an equal gap between wall panels and can accommodate similar lateral movement due to earthquake excitations, thermal expansion and contraction, weathertightness and changes in humidity.

2. For positioning a steel channel cap beam and steel bracing on top of the walls, it is recommended that top corners and top portions of multi-panels walls be aligned with each other. This is also easier for inserting a steel pack between the steel channel cap beam and precast wall panels.
3. It is recommended that pintles or a shear key be welded to the rocking steel channel (seismic wall) as it can transfer axial and shear forces from roof (gravity) loading and lateral seismic loading. It also can prevent the wall from sliding.
4. To improve on-site scheduling (speedier construction) and maintain the quality of walls and workmanship, the seismic wall and its foundation could be precast and fabricated in an enclosed factory environment before transporting to the site for erecting and assembling.
5. It is also recommended that the seismic wall be allocated at the centre of the precast seismic foundation beam. The foundation beams should be discontinuous with each other in order to reduce soil bearing pressure which could prevent the uplifting of the foundation beam during severe shock. The self-weight of non-seismic walls at the top of the foundation beam also contributes to a uniformly distributed load and would stop uplifting of the foundation beam.

## 6.4 FUTURE POSSIBLE RESEARCH

1. Since precast hollow core wall panels have relatively good thermal conductivity because of the existence of the voided section, this attribute should be exploited.

Thus, different [more thermally efficient] voided shapes could be explored, along with various types of insulation. Structure attributes, along with energy consumption for heating or cooling could be optimized. A prototype building could be constructed using precast hollow core units and exposed under extreme weather. Different types of insulation are filled in the void sections and further investigation on the level of efficiency in transferring heat/radiation can be studied.

2. All the wall specimens in this research were tested without openings. A similar experimental set-up consisting of multi-wall panels as described in Chapter Three with openings [preferably in the infill panels] should be investigated. An example of a door opening is shown in Figure 1.20. The bottom part of the precast hollow core wall is seated on the door frame and grouted on both sides of the wall. An identical size, instrumentation, testing procedure and loading schedule could be tested in the laboratory with an opening as shown in Figure 3.3. Flexural and shear failure are expected to occur particularly at the top corner of the opening under in-plane lateral cyclic loading. A comparative performance between wall panels with an opening and without an opening can be made in terms of their strength, lateral resistance, equivalent viscous damping, stability and others. With these comparisons, the construction of buildings using precast hollow core units can be extended to the construction of residential homes, apartments and condominiums, commercial buildings, recreation centres and hotels. The potential for extending the form of construction from single storey warehouse buildings to multi-storey systems is also worthy of investigation. Another particular challenge would be to investigate the seismic performance of connections between walls and floors in high-rise buildings.

3. A superassemblage of structural components representing a critical portion in high rise buildings should be tested in the laboratory under seismic and gravity loading for future research. The structures' components may consist of columns, precast beams, precast hollow core slabs and precast hollow core walls with openings. It is also suggested that beam-column connection, supporting beam-floor slab connection and wall-foundation connection are designed according to the Damage Avoidance Design philosophy as it has been proven to be a damage-free design. Special detailing on these connections and substantial analysis of their seismic behaviour should be undertaken before conducting the experimental work. The global structural damage in high rise buildings can be predicted using statistical tools such as Incremental Dynamic Analysis (IDA) and compared with experimental work. Therefore, damage-free buildings can be constructed using the Damage Avoidance Design philosophy in the future which parallels the needs of end user communities.
4. It is recommended that a passive control devices system such as semi-active dampers be installed in the two-middle void sections of precast hollow core walls for better energy dissipation as compared to the bar-fuses. A similar experimental work can be carried out as described in Chapters Two and Three with the replacement of a couple of bar-fuses with semi-active dampers. Experimental results can be compared between them in terms of seismic performance, stiffness, strength, equivalent viscous damping, and their merits. The advantage of this type of damper system is that it does not require any input energy to control the overall structural system, only a small amount of electrical energy is used for feedback control of valves.

Moreover, this instrument can be installed in high rise buildings in Malaysia such as Kuala Lumpur City Center (KLCC), located about 540km from the Sumatran-fault line, which is considered to be the most active tectonic plate in this part of the world at present.

# APPENDIX A1

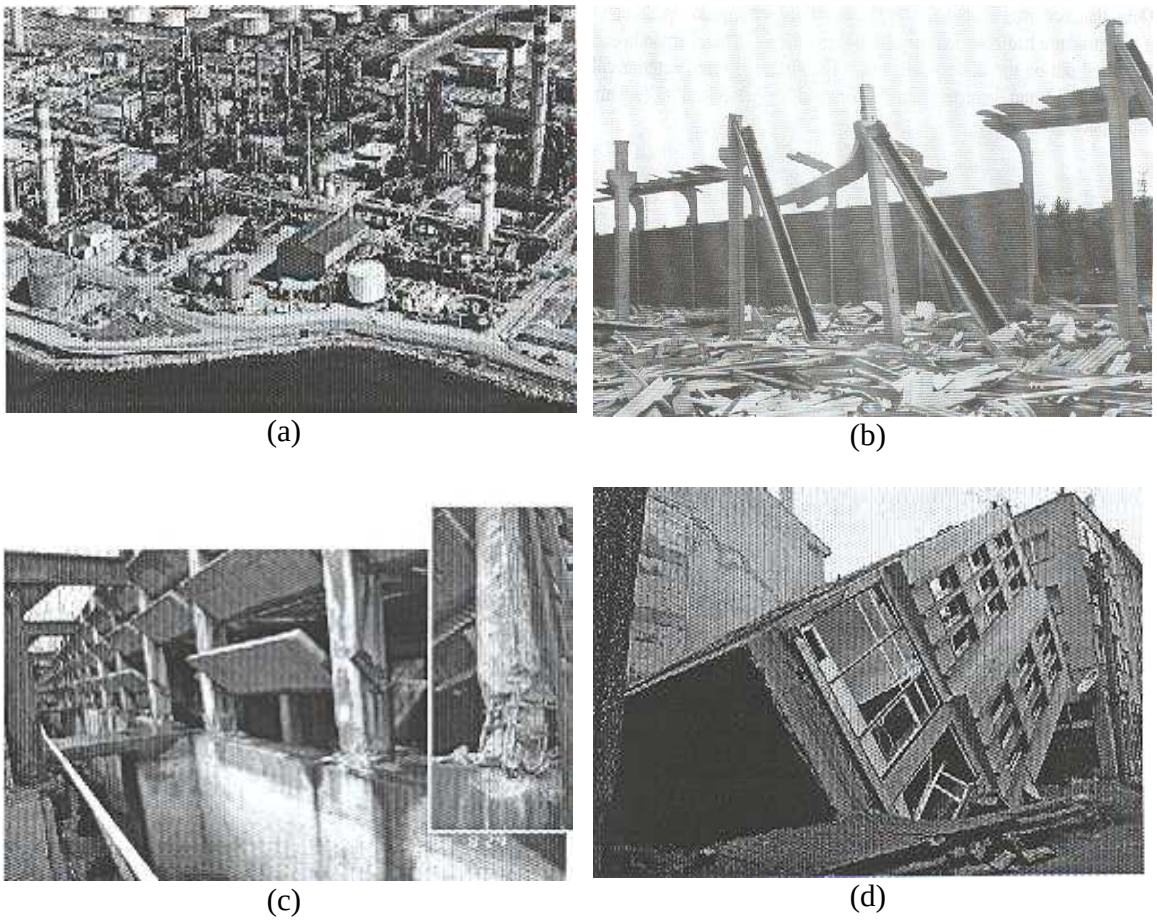

(a) (b)

(c) (d)

Figure A1.1: Damage to industrial facilities during the 1999 Kocaeli earthquake; (a) severe damage to the petrochemical industry in Tupras, Turkey; (b) failure of cantilever head connection on industrial buildings under construction; (c) damage to non-ductile precast columns at Petkim petrochemical facility; Turkey; and (d) total collapse of office buildings due to soil-bearing capacity failure at foundation beam (Johnson, 2000).

(a)

(b)

(c)

(d)

Figure A1.2: Structural failure of precast building during the 1999 Chi-Chi earthquake and the Pakistan earthquake; (a) collapsed of condominium complex made from precast concrete wall panels; (b) collapse of precast panels in double-storey residential house; (c) totally collapse of apartment at Kashmir, India; and (d) buckling of longitudinal reinforcement and spalling of concrete at external columns in precast building (Johnson, 2000).

# APPENDIX A2

(a)

(b)

(c)

(d)

(e)

(f)

Figure A2.1: Preparation of foundation beam for Wall 1 and Wall 2; (a) plan view of Wall 1's foundation caging; (b) plan view of Wall 2's foundation caging; (c) bottom section of base plate; (d) steel channel placed on top of base plate; (e) steel channel together with Type A energy dissipator; and (f) pouring concrete up to the level of base plate.

(a)

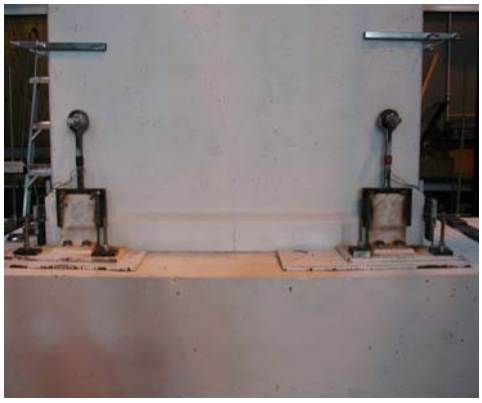

(b)

Figure A2.2: Installation of mechanical energy dissipator (Type 3) on Wall 2; (a) Type 3 is bolted to the wall; and (b) Mechanical energy dissipators are welded to steel angle attached to foundation beam.

(a)

(b)

(c)

(d)

(e)

(f)

Figure A2.3: Construction of Wall 1; (a) lifting wall panel using special connection which is hook to the crane; (b) place wall panel on top of wooden block before inserted into steel channel; (c) pouring self-compacting concrete into the void sections of the wall; (d) drilled 20mm diameter holes at 1320mm height of the wall; (e) concrete block is placed on top of wall; and (f) Wall 1 is ready for instrumentation and testing on strong floor.

(a)

(b)

(c)

(d)

(e)

(f)

Figure A2.4: Construction of Wall 2; (a) one tooth-shaped plate welded at bottom of steel channel acting as shear key; (b) two tooth-shaped welded on steel channel to protect the wall from sliding; (c) putting concrete block on top of Wall 2; (d) lifting wall panel together with foundation beam using special connection; (e) place wall on shaking table; and (f) Wall 2 is ready for instrumentation and testing on shaking table.

(a)

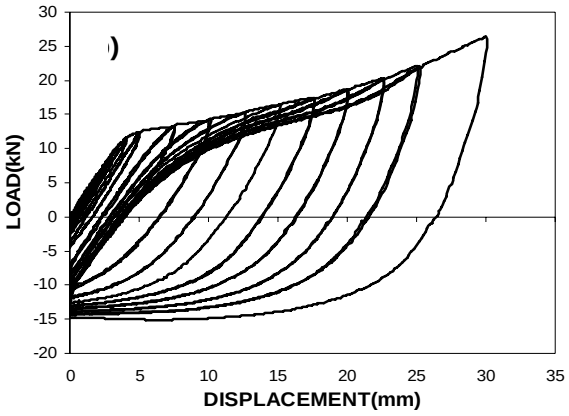


(b)

(c)

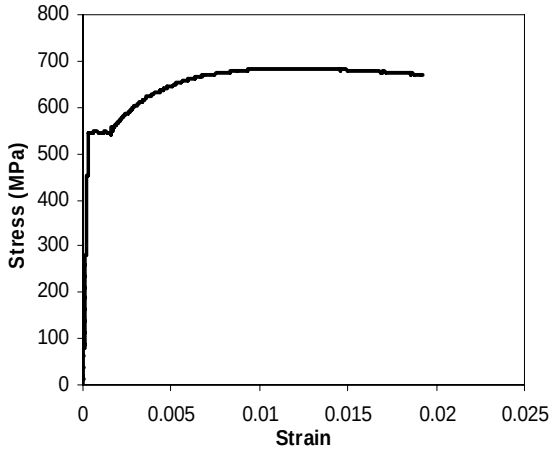


(d)

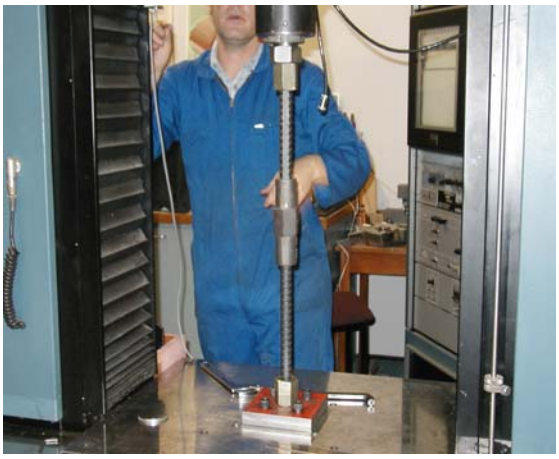

(e)

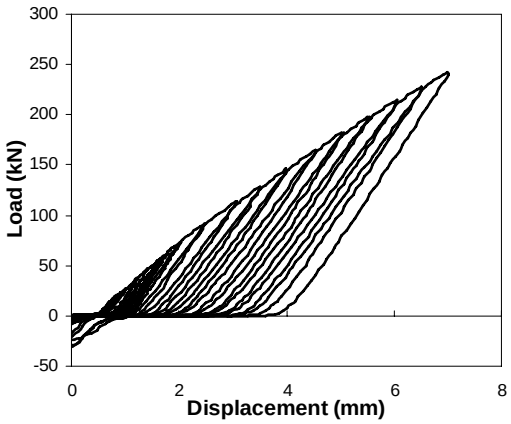


(f)

Figure A2.5: Cyclic behaviour of flexural-bending energy dissipator and reidbar; (a) flexural-bending energy dissipator tested on Instron Machine; (b) load vs displacement graph for flexural-bending energy dissipator; (c) tensile test for Reidbar (RB25); (d) stress-strain curve; (e) reidbar with coupler tested on Instron Machine; and (f) load vs displacement for reidbar with coupler.

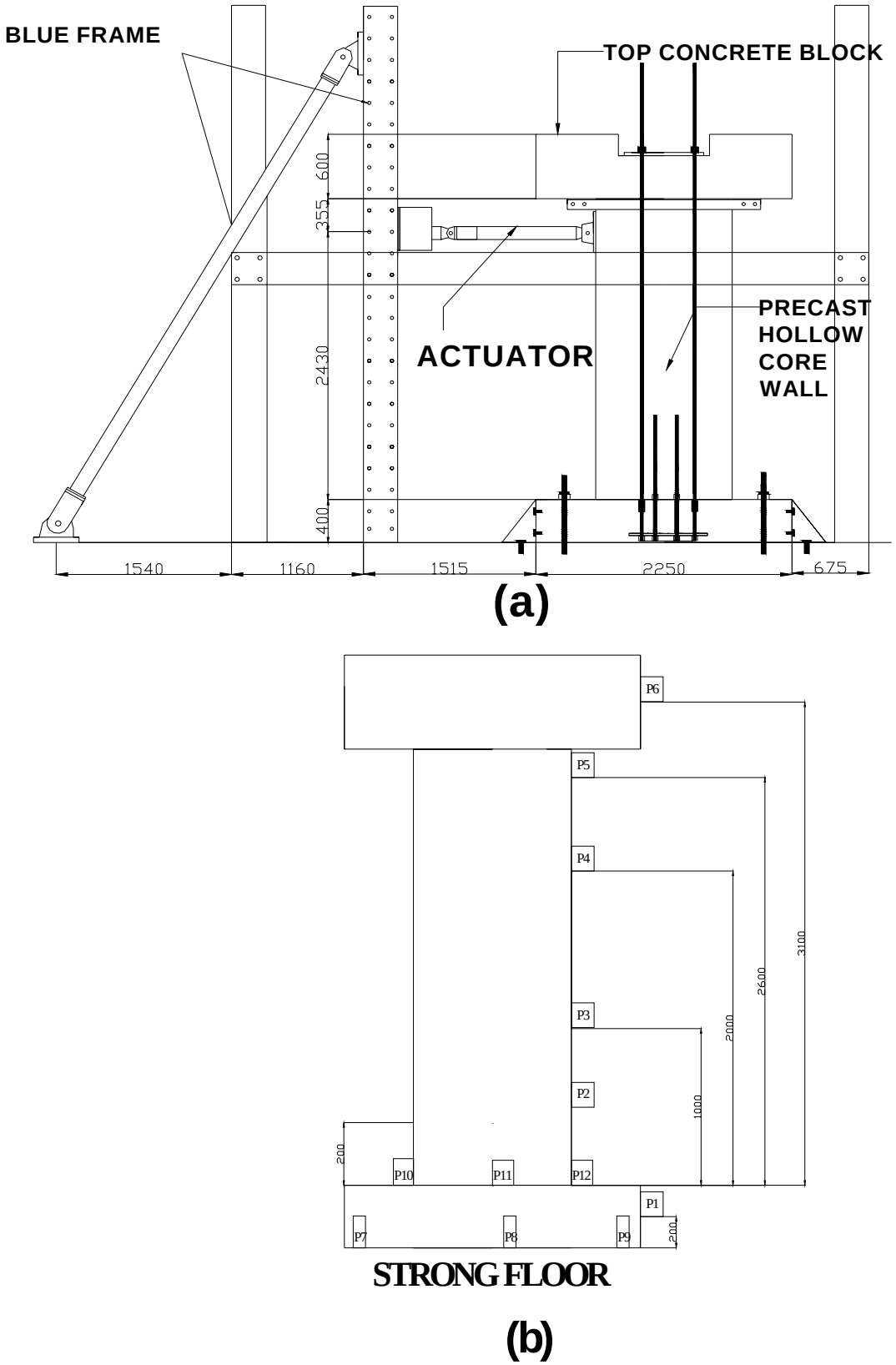


Figure A2.6: Loading frame and instrumentation of Wall 1 on strong floor; (a) the schematic arrangement of loading frame together with wall panel; and (b) the arrangement of linear potentiometers to measure in-plane lateral displacement.

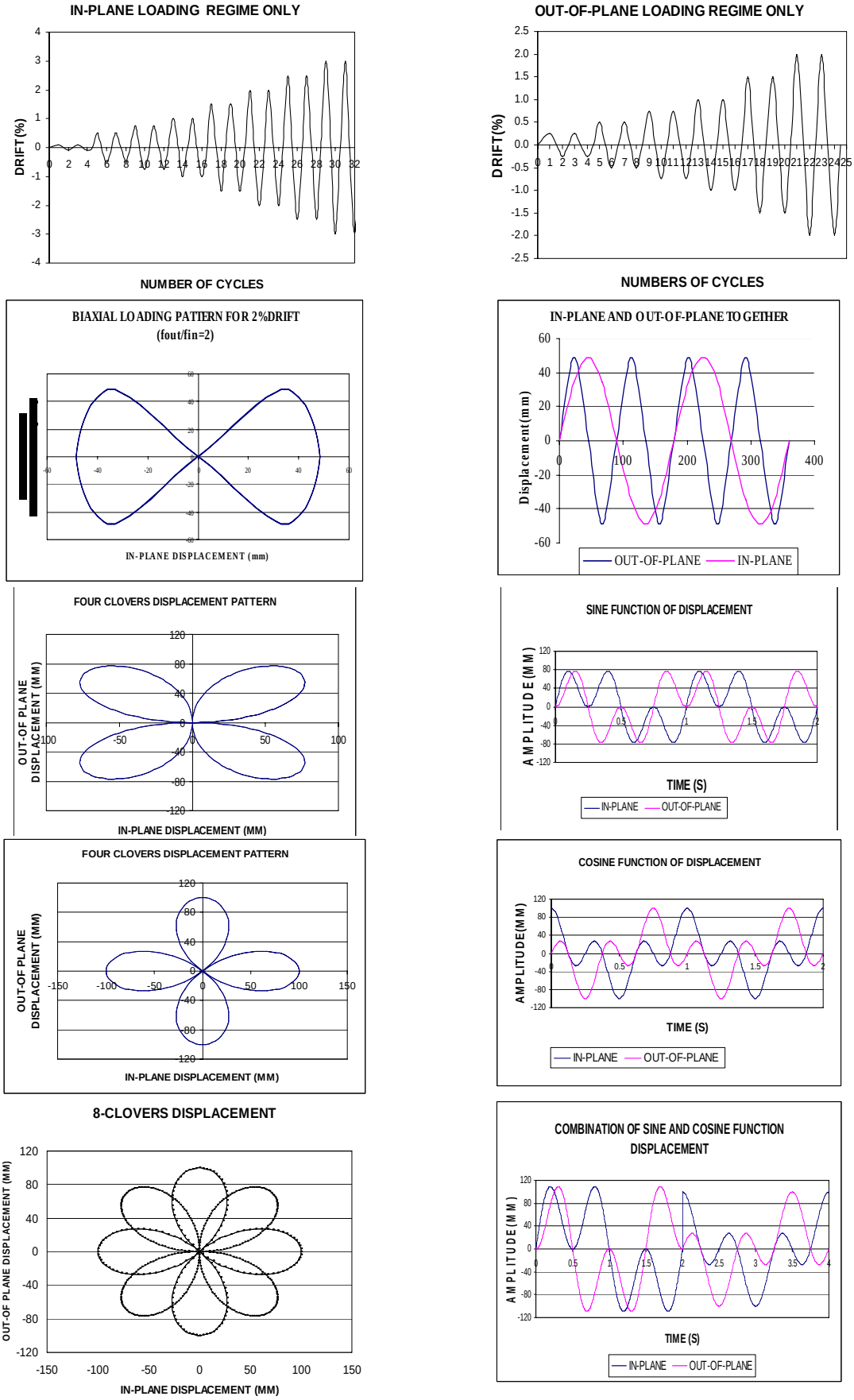


Figure A2.7: Displacement controlled patterns tested on Wall 1 and Wall 2.

(a)

(b)

(c)

(d)

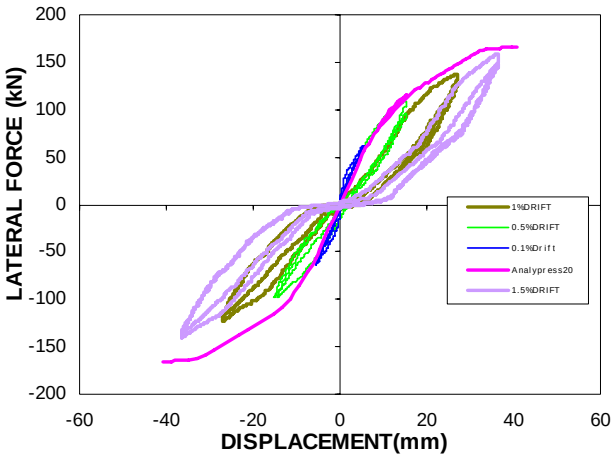


(e)

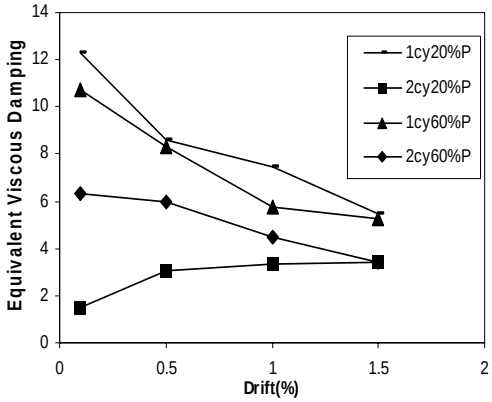


(f)

Figure A2.8: Visual observation and experimental results of Wall 1-P+A tested on strong floor; (a) uplift the bottom corner of wall at +1.0% drift on the first cycle; (b) uplift of wall at second cycle; (c) uplift of wall at ±1.5% drift at first cycle; (d) uplift of wall at +2.0% at second cycle when unbonded tendons were prestressing up to 20%; (e) in-plane vs displacement behaviour; and (f) the equivalent viscous damping when unbonded post-tensioned tendons prestressing at 20% and 60%.

(a)

(b)

(c)

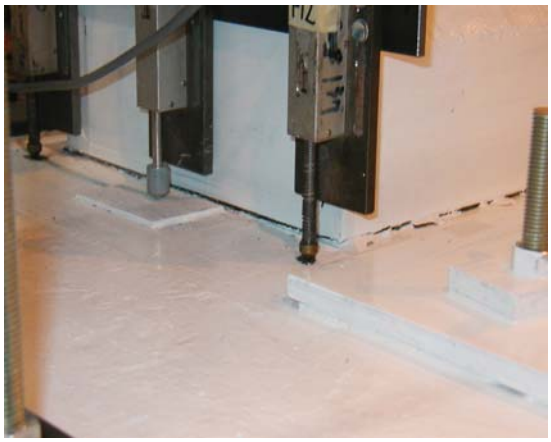

(d)

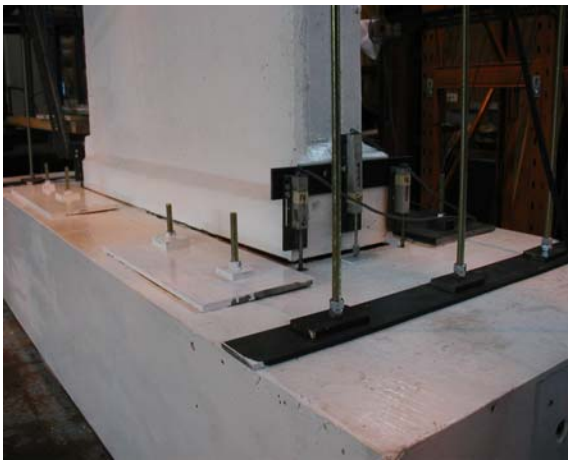

(e)


(f)

Figure A2.9: Visual observation of Wall 1-P+A tested on shaking table; (a) opening gap at bottom left of wall at +1.5% drift; (b) uplift at bottom right of wall at -1.5% drift; (c) uplift bottom corner at +0.25% drift; (d) uplift bottom corner of wall at +0.5% drift; (e) overall view of rocking wall at +1.5% drift; and (f) uplift of rocking toe at +2.0% drift.

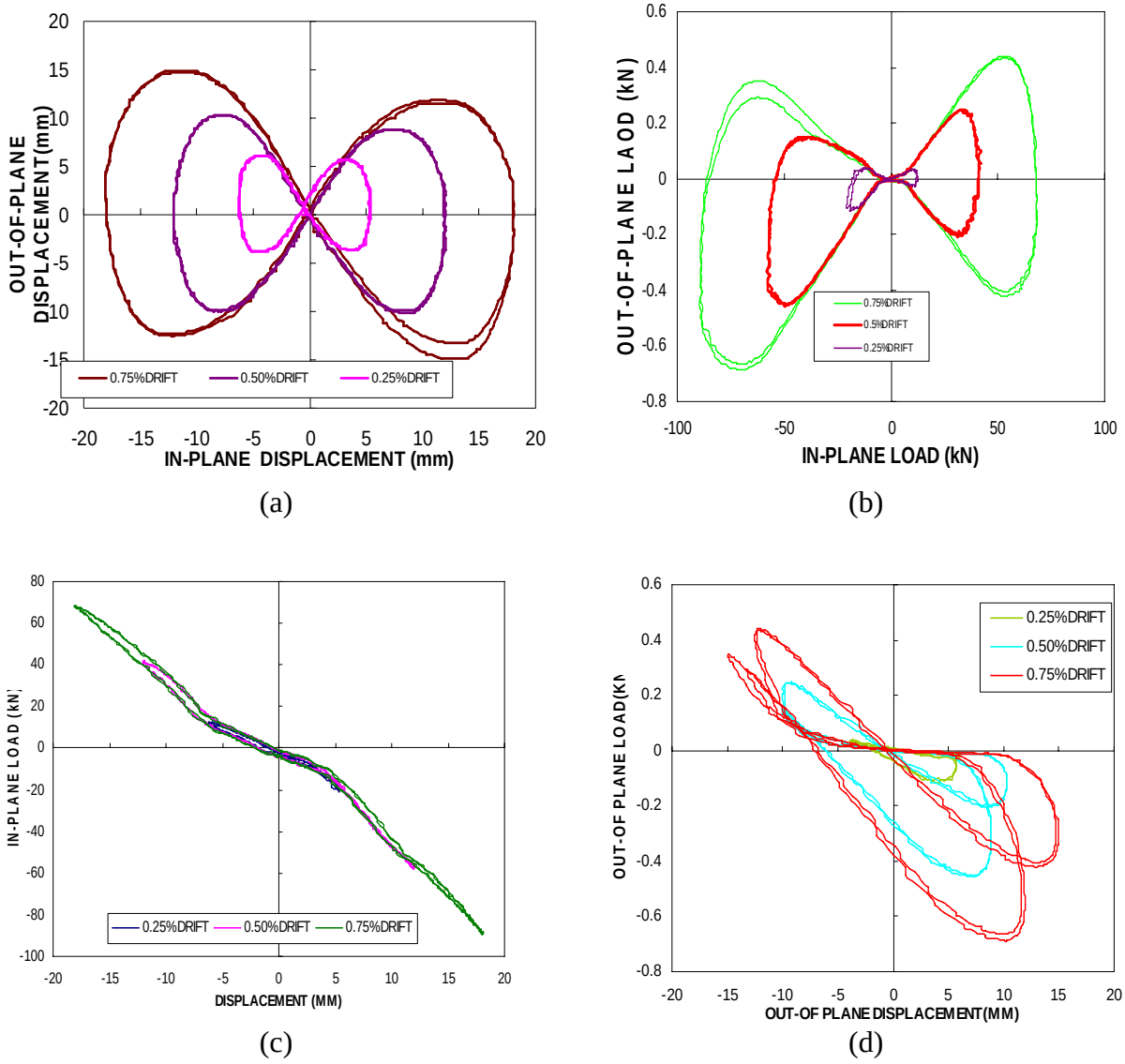


Figure A2.10: Experimental results of Wall 1-P+A on shaking table subjected to "2-leaf clover" loading pattern; (a) out-of-plane displacement vs in-plane displacement; (b) out-of-plane load vs in-plane load; (c) in-plane load vs in-plane displacement; and (d) out of plane load vs out-of-plane displacement.

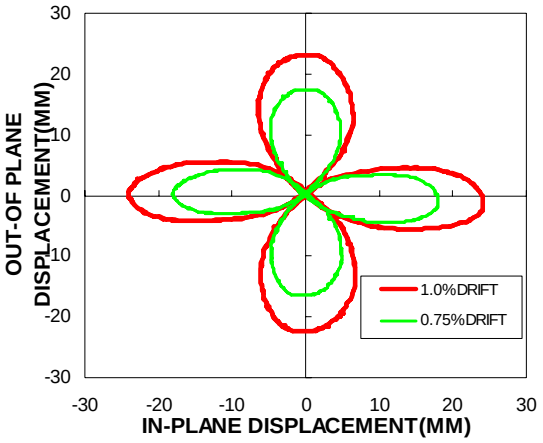


(a)

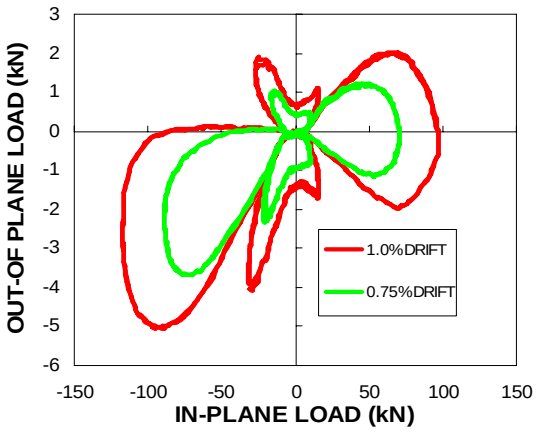


(b)

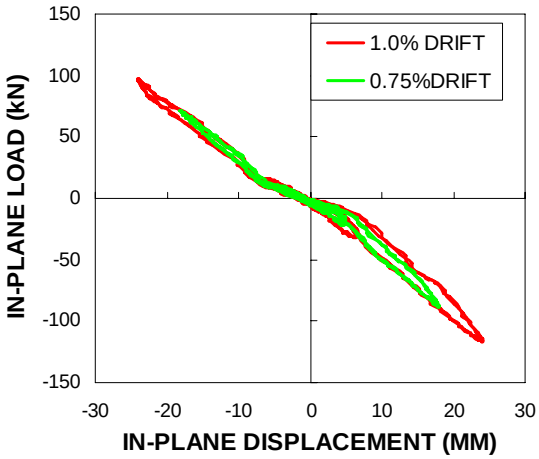


(c)

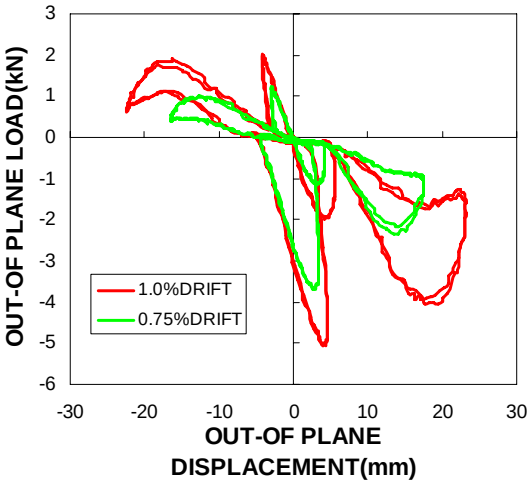


(d)

Figure A2.11: Experimental results of Wall 1-P+A on shaking table subjected to "4-leaf clover" loading pattern; (a) out-of-plane displacement vs in-plane displacement; (b) out-of-plane load vs in-plane load; (c) in-plane load vs in-plane displacement; and (d) out-of-plane load vs out-of-plane displacement.

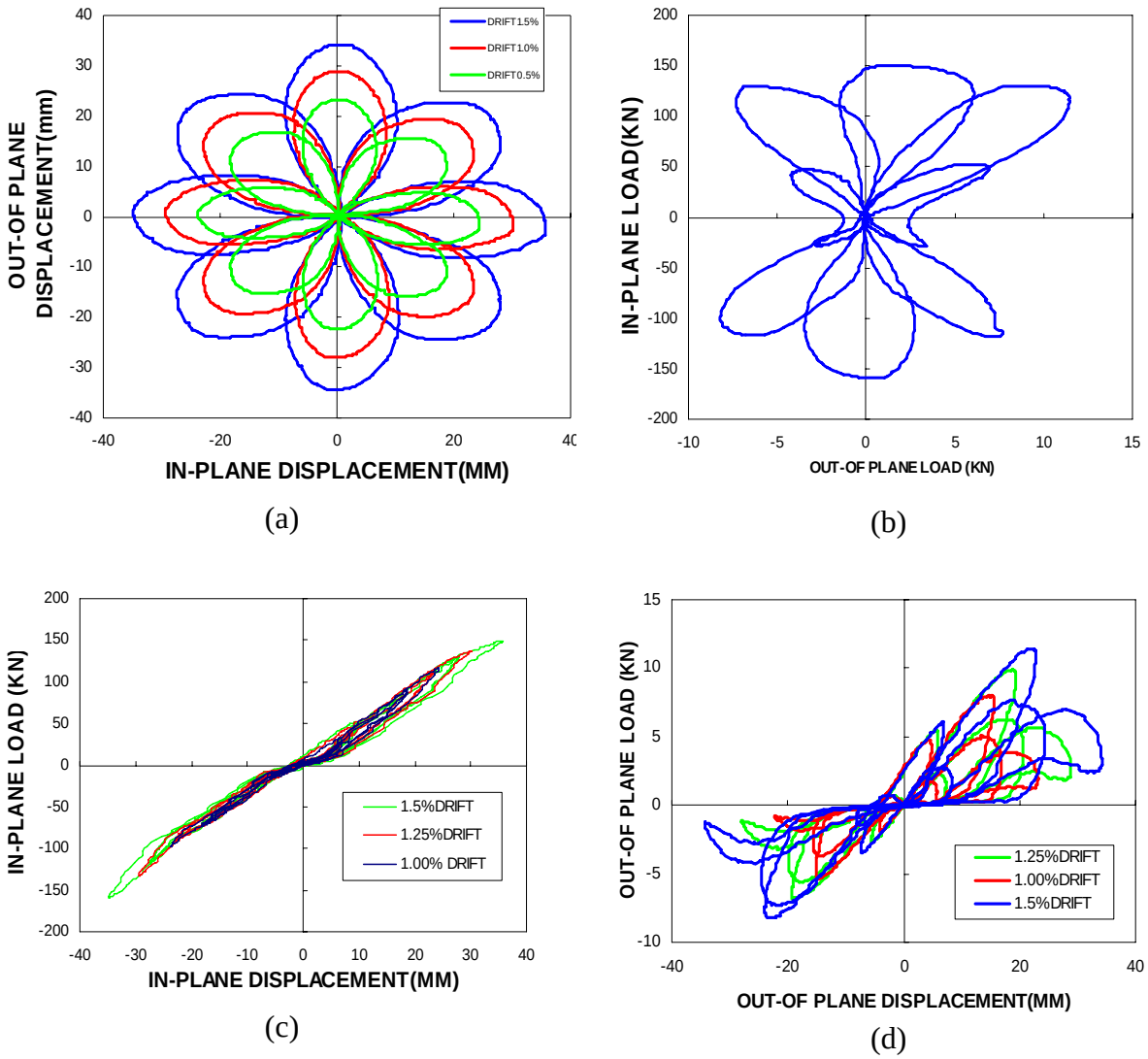


Figure A2.12: Experimental results of Wall 1-P+A tested on shaking table subjected to " double 4-leaf clover" loading pattern; (a) out-of-plane displacement vs in-plane displacement; (b) in-plane load vs out-of-plane load at +1.5% drift; (c) in-plane load vs in-plane displacement; and (d) out-of-plane load vs out-of-plane displacement.


(a)


(b)


(c)

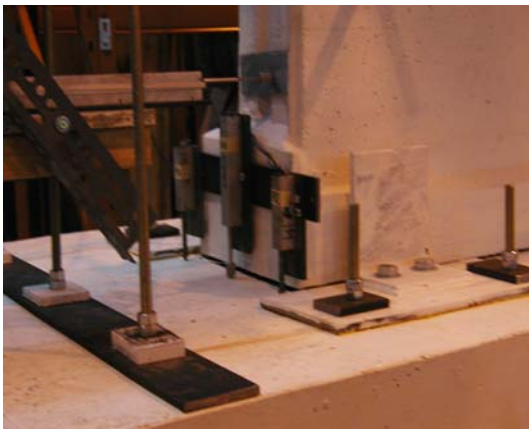

(d)

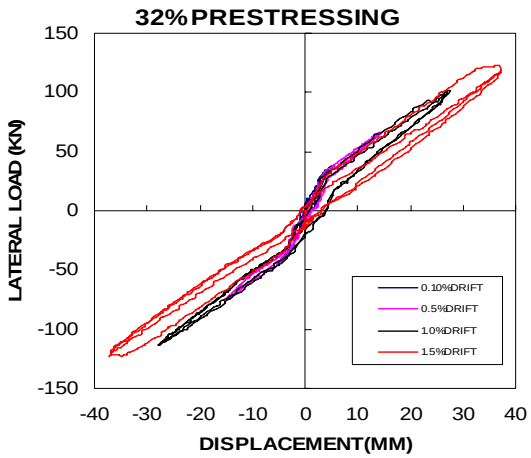


(e)

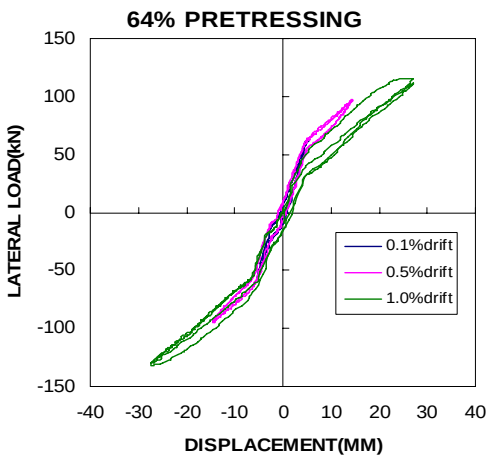


(f)

Figure A2.13: Visual observations and experimental results of Wall 2-P+O: (a) in-plane displacement at 0% prestressing at 2% drift; (b) in-plane displacement (32% prestressing) at 1.5% drift; (c) biaxial (64% prestressing) at 1.5% drift; (d) out-of-plane directions; (e) lateral load vs displacement graph at 32% prestressing of unbonded tendons; and (f) lateral load vs displacement graph at 64% prestressing of unbonded tendons.

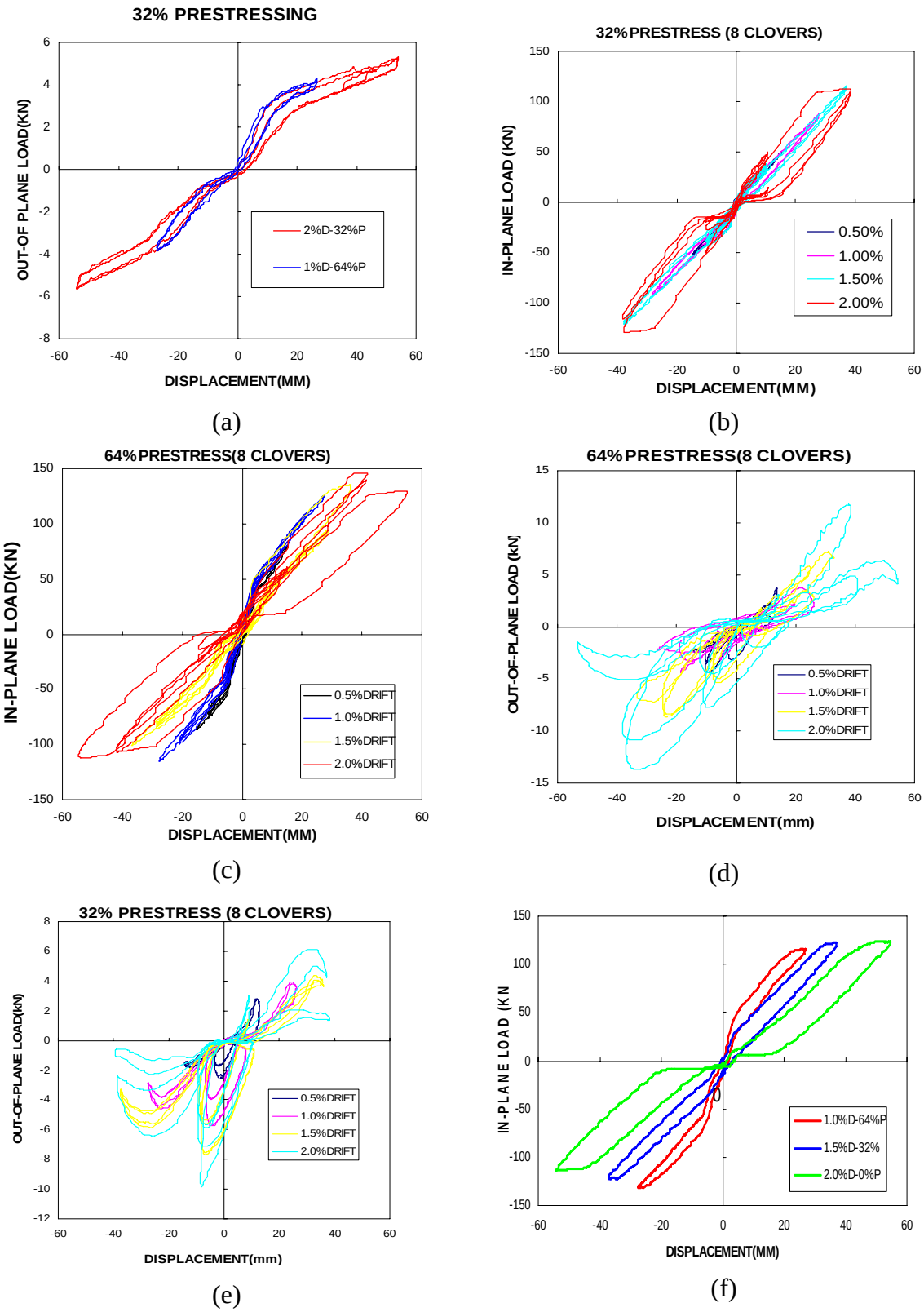


Figure A2.14: Experimental results of Wall 2-P+O; (a) out-of-plane vs displacement at 32% prestressing; (b) 32% prestressing using “double 4-leaf clover” pattern; (c) 64% prestressing of unbonded tendons; (d) 64% prestressing using “double 4-leaf clover” pattern; (e) 32% prestressing using “double 4-leaf clover” pattern; and (f) flag shape behaviour at snug tight, 32% and 64% prestressing unbonded tendons.

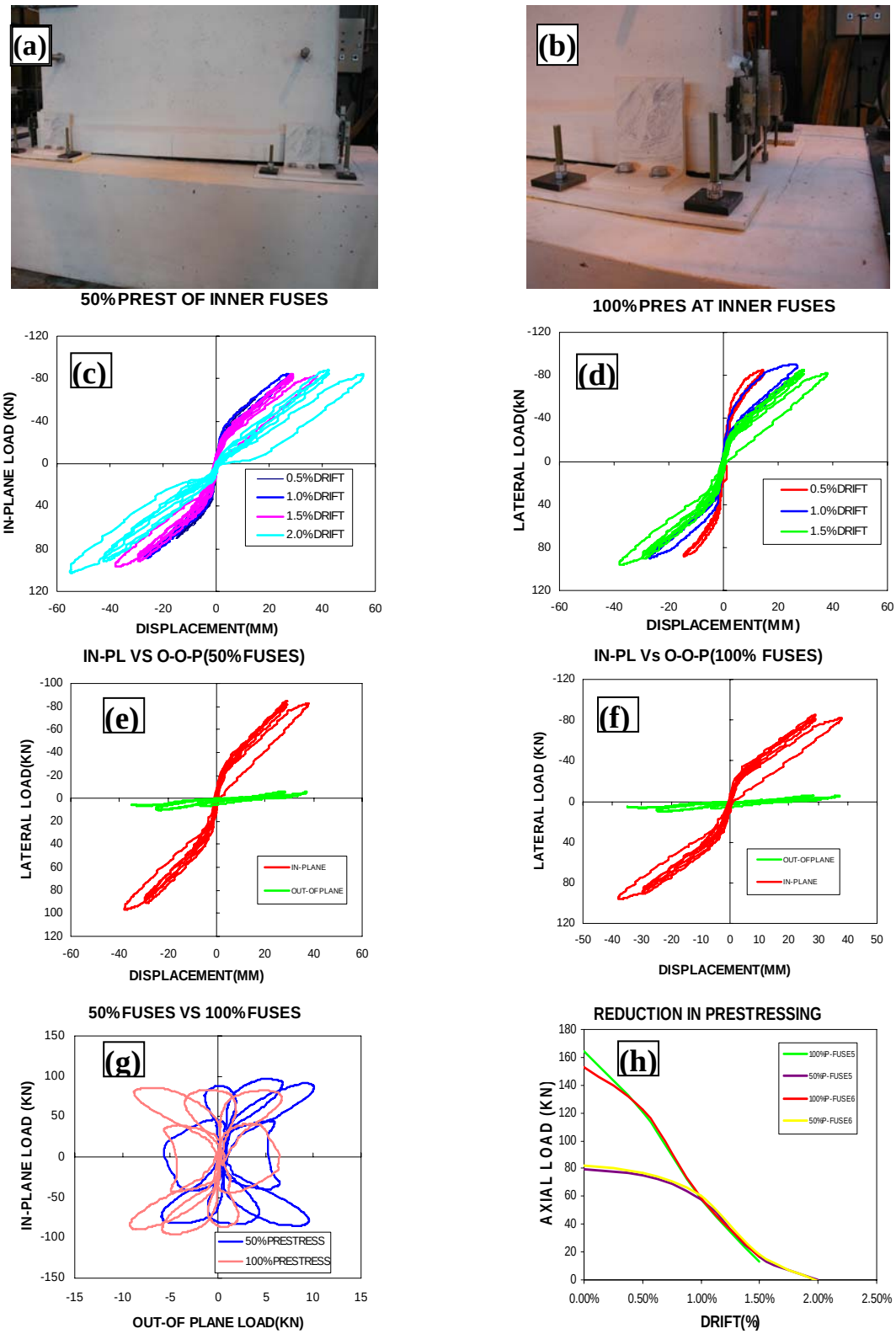


Figure A2.15: Visual observations and experimental results of Wall 2-P+B; (a) uplifting bottom wall (50% prestressing unbonded fuse-bars); (b) uplifting bottom wall (100% prestressing); (c) in-plane load vs displacement (50% prestressing); (d) in-plane load vs displacement (100% prestressing); (e) comparison between in-plane and out-of-plane load (50% prestressing); (f) comparison between in-plane and out-of-plane (100% prestressing); (g) comparison between 50% and 100% prestressing under " double 4-leaf clover" pattern; and (h) loss of prestressing in fuse-bars for 50% and 100% prestressing fuse-bars.

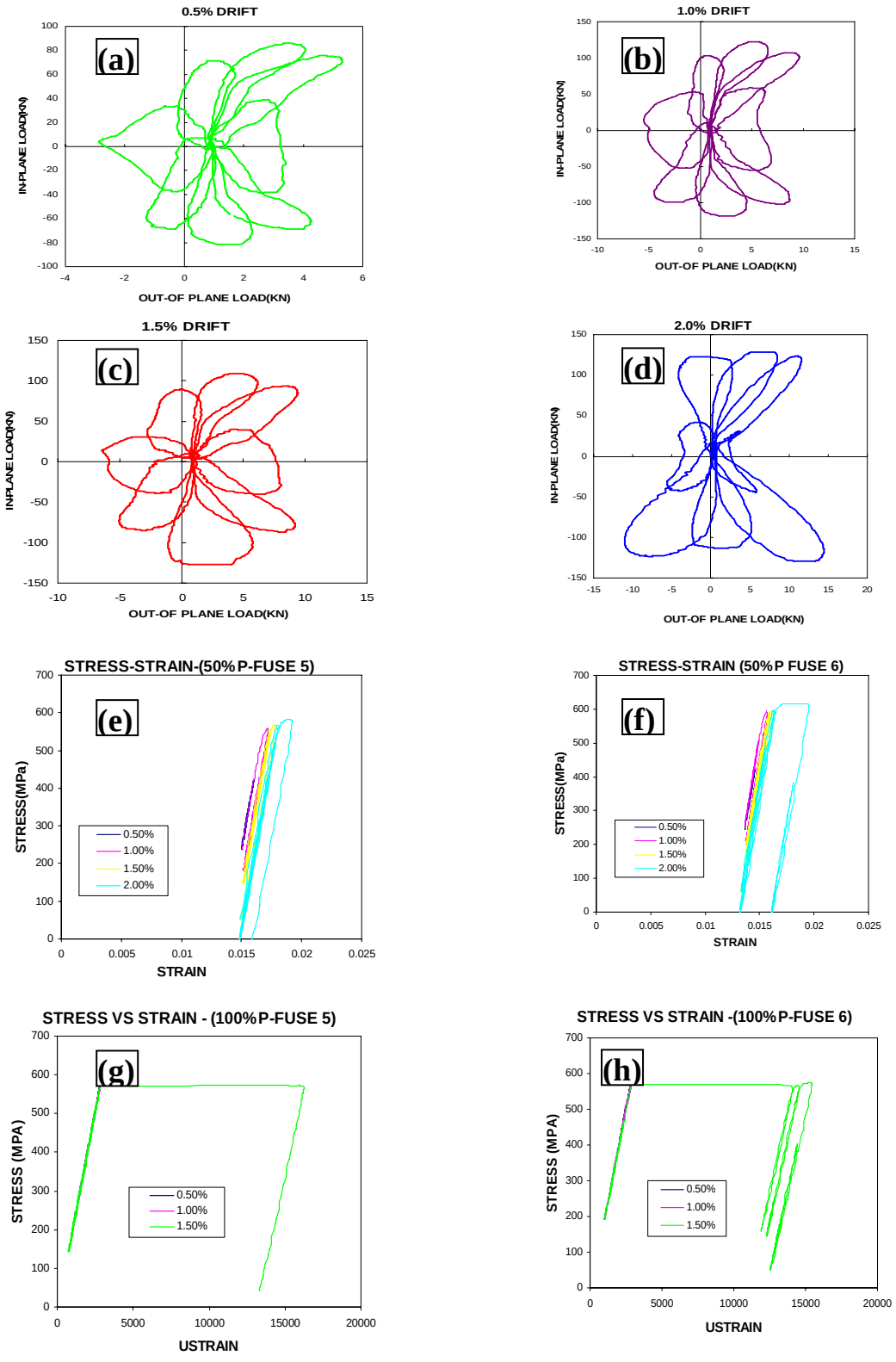


Figure A2.16: Experimental results of Wall 2-O+B; (a) “double 4-leaf clover” pattern at 0.5% drift; (b) 1.0% drift; (c) 1.5% drift; (d) 2.0% drift; (e) stress-strain relationship when 50% prestressed Fuse 5; (f) 50% prestressed Fuse 6; (g) 100% prestressed Fuse 5; and (h) 100% prestressed Fuse 6.

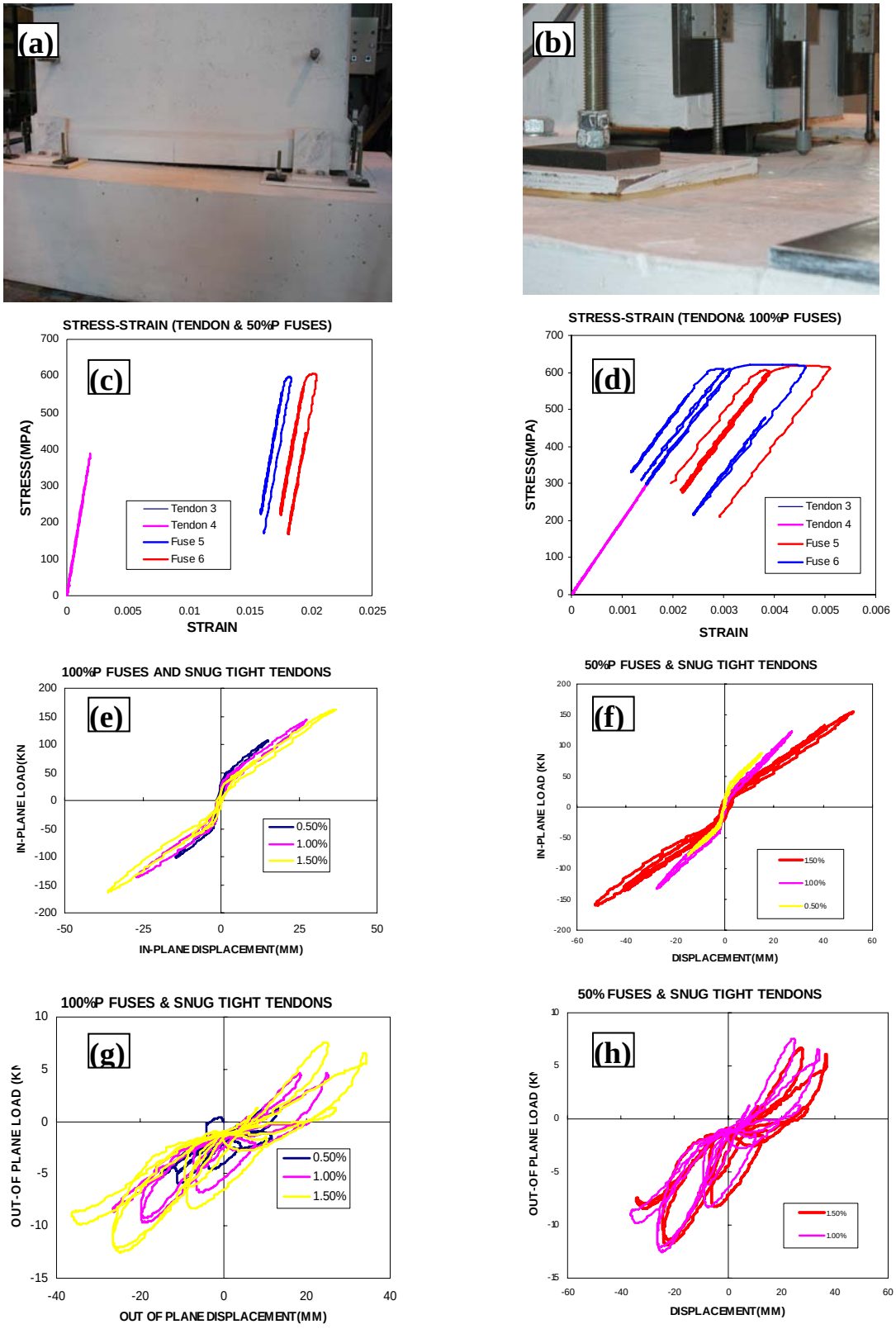


Figure A2.17: Visual observations and experimental results of Wall 2-P+B; (a) uplifting bottom wall at 2.0% drift; (b) linear potentiometers use to measure vertical displacement; (c) stress-strain curve (50 % prestressing fuse-bar); (d) stress-strain curve (100% prestressing fuse-bar); (e) 100% prestressing fuse-bar and snug-tight tendons; (f) 50% prestressing fuse-bar and snug-tight tendons; (g) 100% prestressing fuse-bars and snug-tight tendons; and (h) 50% prestressing fuse-bar and snug-tight tendons.

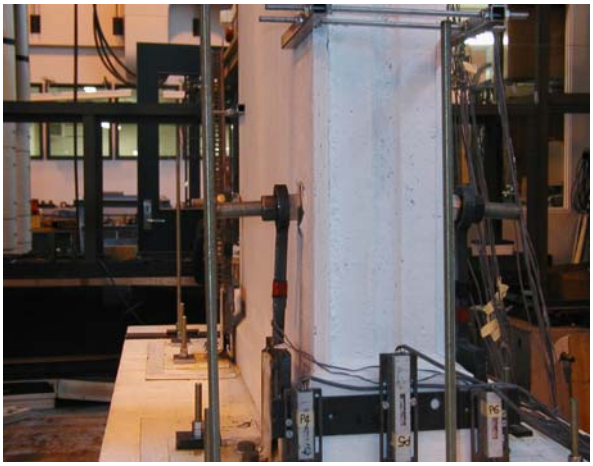

(a)

(b)

(c)

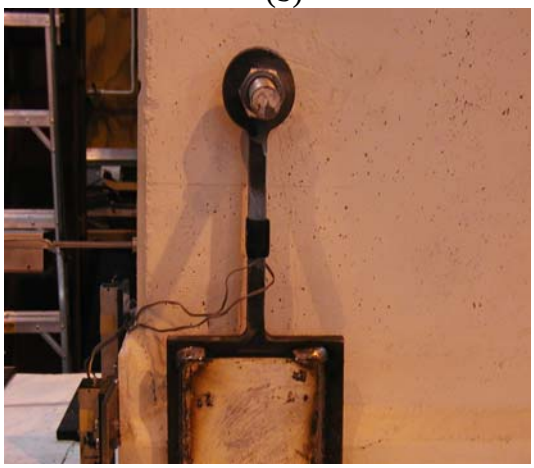

(d)

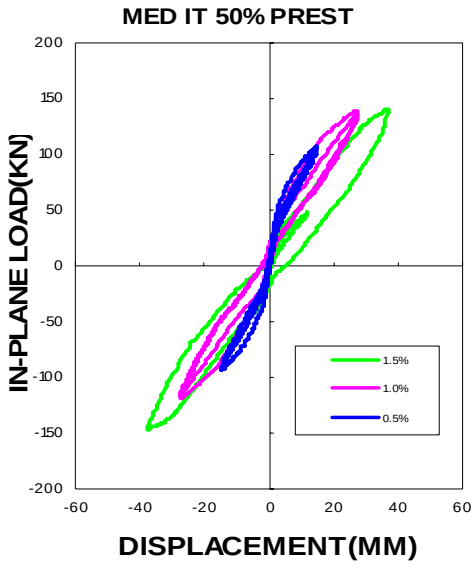


(e)

Figure A2.18: Visual observations and performance of Wall 2-P+C; (a) side elevation of mechanical energy dissipator at +2.0% drift; (b) bending of threaded rod when the wall uplifts; (c) spalling of concrete around the bolt; (d) mechanical energy dissipator welded to steel angle and strain gauge attached at the middle of gauge length; and (e) in-plane behaviour of wall panel under cyclic loading.

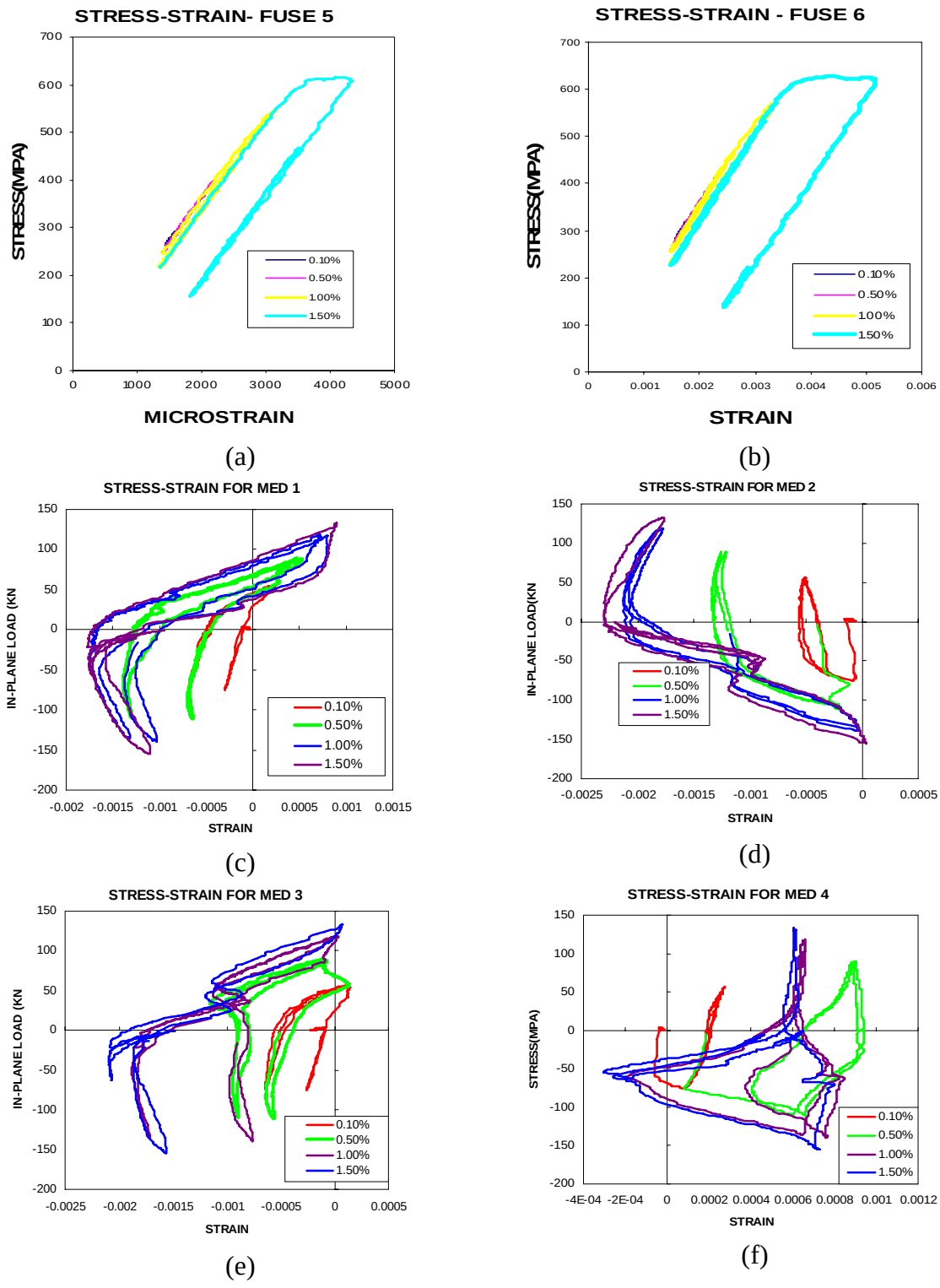


Figure A2.19: Experimental results of Wall 2-P+C; (a) stress-strain curve for Fuse 5; (b) stress-strain curve for Fuse 6; (c) stress-strain curve for the first mechanical energy dissipator; (d) stress-strain curve for the second mechanical energy dissipator; (e) stress-strain curve for the third mechanical energy dissipator; and (f) stress-strain curve for the fourth energy dissipator.

Table A3.1: Compression force and strain of rubber block spacers located between wall panels

Hardness of rubber block, IRHD 5.5
Young Modulus of rubber block 3.25MPa
Shear Modulus of rubber block 0.81MPa
Constant 0.64

| Drift | Location | Interface | Rubber thickness(mm) | Initial Distance(mm) | Distance travel | Compression Thickness | Cross-Area A($mm^2$) | Compression Force(kN) | Compression Or tension | Strain ε |
|---|---|---|---|---|---|---|---|---|---|---|
| 0.5%drift (push) | Top | Wall 1-Wall 2 | 24.55 | 100.39 | 94.6 | 5.79 | 4450.48 | 3.411279324 | compession | -0.05767507 |
| | Bottom | Wall 1-Wall 2 | 22.65 | 191.00 | 190.00 | 1.00 | 4294.25 | 0.616172737 | compession | -0.0052356 |
| | Top | Wall 2- Wall 3 | 20.86 | 100.62 | 96.98 | 3.64 | 4320.23 | 2.450063322 | compession | -0.03617571 |
| | Bottom | Wall 2- Wall 3 | 37.85 | 101.4 | 100.35 | 1.05 | 4788.83 | 0.431753828 | compession | -0.01035503 |
| | Top | Wall 3-Wall 4 | 25.15 | 100.33 | 98.61 | 1.72 | 4600.23 | 1.022476569 | compession | -0.01714343 |
| | Bottom | Wall 3-Wall 4 | 32.16 | 100.81 | 100.38 | 0.43 | 4500.21 | 0.195554834 | compession | -0.00426545 |
| | Top | Wall 4-Wall 5 | 29.47 | 100.56 | 99.78 | 0.78 | 4321.12 | 0.371701364 | compession | -0.00775656 |
| | Bottom | Wall 4-Wall 5 | 28.25 | 100.92 | 100.65 | 0.27 | 4839.66 | 0.150329262 | compession | -0.00267539 |
| | Top | Wall 5-Wall 6 | 33.95 | 101.27 | 111.81 | -10.54 | 4700.21 | -4.74243575 | gap | 0.104078207 |
| | Bottom | Wall 5-Wall 6 | 30.12 | 100.81 | 103.28 | -2.47 | 4834.07 | -1.28836311 | gap | 0.024501538 |
| 0.5%drift (pull) | Top | Wall 1-Wall 2 | 24.55 | 100.39 | 112.63 | -12.24 | 4450.48 | -7.21140914 | gap | 0.121924494 |
| | Bottom | Wall 1-Wall 2 | 22.65 | 191.00 | 194.00 | -3.00 | 4294.25 | -1.84851821 | gap | 0.015706806 |
| | Top | Wall 2- Wall 3 | 20.86 | 100.62 | 98.83 | 1.79 | 4320.23 | 1.204838831 | compession | -0.0177897 |
| | Bottom | Wall 2- Wall 3 | 37.85 | 101.40 | 101.05 | 0.35 | 4788.83 | 0.143917943 | compession | -0.00345168 |
| | Top | Wall 3-Wall 4 | 25.15 | 100.33 | 98.28 | 2.05 | 4600.23 | 1.218649399 | compession | -0.02043257 |
| | Bottom | Wall 3-Wall 4 | 32.16 | 100.81 | 100.26 | 0.55 | 4500.21 | 0.250128277 | compession | -0.00545581 |
| | Top | Wall 4-Wall 5 | 29.47 | 100.56 | 98.86 | 1.70 | 4321.12 | 0.810118358 | compession | -0.01690533 |
| | Bottom | Wall 4-Wall 5 | 28.25 | 100.92 | 99.95 | 0.97 | 4839.66 | 0.540071793 | compession | -0.00961157 |
| | Top | Wall 5-Wall 6 | 33.95 | 101.27 | 96.05 | 5.22 | 4700.21 | 2.348720549 | compession | -0.05154537 |
| | Bottom | Wall 5-Wall 6 | 30.12 | 100.81 | 99.68 | 1.13 | 4834.07 | 0.589413083 | compession | -0.01120921 |

| | | | | | | | | | | |
|---|---|---|---|---|---|---|---|---|---|---|
| 1%drift (push) | Top | Wall 1-Wall 2 | 24.55 | 100.39 | 92.90 | 7.49 | 4450.48 | 4.412863927 | compession | -0.07460902 |
| | Bottom | Wall 1-Wall 2 | 22.65 | 191.00 | 190.50 | 0.50 | 4294.25 | 0.308086369 | compession | -0.0026178 |
| | Top | Wall 2- Wall 3 | 20.86 | 100.62 | 96.07 | 4.55 | 4320.23 | 3.062579153 | compession | -0.04521964 |
| | Bottom | Wall 2- Wall 3 | 37.85 | 101.40 | 100.31 | 1.09 | 4788.83 | 0.448201592 | compession | -0.01074951 |
| | Top | Wall 3-Wall 4 | 25.15 | 100.33 | 97.76 | 2.57 | 4600.23 | 1.527770222 | compession | -0.02561547 |
| | Bottom | Wall 3-Wall 4 | 32.16 | 100.81 | 100.21 | 0.60 | 4500.21 | 0.272867211 | compession | -0.00595179 |
| | Top | Wall 4-Wall 5 | 29.47 | 100.56 | 99.12 | 1.44 | 4321.12 | 0.686217903 | compession | -0.01431981 |
| | Bottom | Wall 4-Wall 5 | 28.25 | 100.92 | 100.55 | 0.37 | 4839.66 | 0.206006766 | compession | -0.00366627 |
| | Top | Wall 5-Wall 6 | 33.95 | 101.27 | 115.83 | -14.56 | 4700.21 | -6.55122054 | gap | 0.143774069 |
| | Bottom | Wall 5-Wall 6 | 30.12 | 100.81 | 103.46 | -2.65 | 4834.07 | -1.38225192 | gap | 0.026287075 |
| 1%drift (pull) | Top | Wall 1-Wall 2 | 24.55 | 100.39 | 119.53 | -19.14 | 4450.48 | -11.2766643 | gap | 0.19065644 |
| | Bottom | Wall 1-Wall 2 | 22.65 | 191.00 | 195.00 | -4.00 | 4294.25 | -2.46469095 | gap | 0.020942408 |
| | Top | Wall 2- Wall 3 | 20.86 | 100.62 | 98.07 | 2.55 | 4320.23 | 1.716390514 | compession | -0.02534287 |
| | Bottom | Wall 2- Wall 3 | 37.85 | 101.40 | 100.91 | 0.49 | 4788.83 | 0.20148512 | compession | -0.00483235 |
| | Top | Wall 3-Wall 4 | 25.15 | 100.33 | 98.12 | 2.21 | 4600.23 | 1.313763498 | compession | -0.02202731 |
| | Bottom | Wall 3-Wall 4 | 32.16 | 100.81 | 99.71 | 1.10 | 4500.21 | 0.500256553 | compession | -0.01091162 |
| | Top | Wall 4-Wall 5 | 29.47 | 100.56 | 94.64 | 5.92 | 4321.12 | 2.821118045 | compession | -0.05887033 |
| | Bottom | Wall 4-Wall 5 | 28.25 | 100.92 | 99.41 | 1.51 | 4839.66 | 0.840730317 | compession | -0.01496235 |
| | Top | Wall 5-Wall 6 | 33.95 | 101.27 | 94.83 | 6.44 | 4700.21 | 2.897655237 | compession | -0.06359238 |
| | Bottom | Wall 5-Wall 6 | 30.12 | 100.81 | 99.37 | 1.44 | 4834.07 | 0.751110478 | compession | -0.0142843 |
| 1.5%drift (push) | Top | Wall 1-Wall 2 | 24.55 | 100.39 | 91.99 | 8.40 | 4450.48 | 4.949006273 | compession | -0.08367367 |
| | Bottom | Wall 1-Wall 2 | 22.65 | 191.00 | 190.00 | 1.00 | 4294.25 | 0.616172737 | compession | -0.0052356 |
| | Top | Wall 2- Wall 3 | 20.86 | 100.62 | 95.55 | 5.07 | 4320.23 | 3.412588199 | compession | -0.0503876 |
| | Bottom | Wall 2- Wall 3 | 37.85 | 101.4 | 100.73 | 0.67 | 4788.83 | 0.275500061 | compession | -0.0066075 |
| | Top | Wall 3-Wall 4 | 25.15 | 100.33 | 97.55 | 2.78 | 4600.23 | 1.652607477 | compession | -0.02770856 |
| | Bottom | Wall 3-Wall 4 | 32.16 | 100.81 | 99.97 | 0.84 | 4500.21 | 0.382014095 | compession | -0.00833251 |
| | Top | Wall 4-Wall 5 | 29.47 | 100.56 | 98.64 | 1.92 | 4321.12 | 0.914957204 | compession | -0.01909308 |
| | Bottom | Wall 4-Wall 5 | 28.25 | 100.92 | 99.92 | 1.00 | 4839.66 | 0.556775044 | compession | -0.00990884 |
| | Top | Wall 5-Wall 6 | 33.95 | 101.27 | 119.23 | -17.96 | 4700.21 | -8.08103852 | gap | 0.177347684 |
| | Bottom | Wall 5-Wall 6 | 30.12 | 100.81 | 105.75 | -4.94 | 4834.07 | -2.57672622 | gap | 0.049003075 |

| | | | | | | | | | | |
|---|---|---|---|---|---|---|---|---|---|---|
| 2.0%drift (push) | Top | Wall 1-Wall 2 | 24.55 | 100.39 | 91.37 | 9.02 | 4450.48 | 5.314290069 | compression | -0.08984959 |
| | Bottom | Wall 1-Wall 2 | 22.65 | 191.00 | 192.00 | -1.00 | 4294.25 | -0.61617274 | gap | 0.005235602 |
| | Top | Wall 2- Wall 3 | 20.86 | 100.62 | 95.26 | 5.36 | 4320.23 | 3.607785551 | compression | -0.05326973 |
| | Bottom | Wall 2- Wall 3 | 37.85 | 101.40 | 100.77 | 0.63 | 4788.83 | 0.259052297 | compression | -0.00621302 |
| | Top | Wall 3-Wall 4 | 25.15 | 100.33 | 97.29 | 3.04 | 4600.23 | 1.807167889 | compression | -0.03030001 |
| | Bottom | Wall 3-Wall 4 | 32.16 | 100.81 | 99.83 | 0.98 | 4500.21 | 0.445683111 | compression | -0.00972126 |
| | Top | Wall 4-Wall 5 | 29.47 | 100.56 | 98.38 | 2.18 | 4321.12 | 1.038857659 | compression | -0.0216786 |
| | Bottom | Wall 4-Wall 5 | 28.25 | 100.92 | 99.69 | 1.23 | 4839.66 | 0.684833304 | compression | -0.01218787 |
| | Top | Wall 5-Wall 6 | 33.95 | 101.27 | 121.55 | -20.28 | 4700.21 | -9.12491432 | gap | 0.200256739 |
| | Bottom | Wall 5-Wall 6 | 30.12 | 100.81 | 106.2 | -5.39 | 4834.07 | -2.81144825 | gap | 0.053466918 |
| 2.0%drift (pull) | Top | Wall 1-Wall 2 | 24.55 | 100.39 | 129.26 | -28.87 | 4450.48 | -17.0092632 | gap | 0.287578444 |
| | Bottom | Wall 1-Wall 2 | 22.65 | 191.00 | 199.00 | -8.00 | 4294.25 | -4.9293819 | gap | 0.041884817 |
| | Top | Wall 2- Wall 3 | 20.86 | 100.62 | 97.48 | 3.14 | 4320.23 | 2.113516163 | compression | -0.03120652 |
| | Bottom | Wall 2- Wall 3 | 37.85 | 101.40 | 107.30 | -5.90 | 4788.83 | -2.42604532 | gap | 0.058185404 |
| | Top | Wall 3-Wall 4 | 25.15 | 100.33 | 97.31 | 3.02 | 4600.23 | 1.795278626 | compression | -0.03010067 |
| | Bottom | Wall 3-Wall 4 | 32.16 | 100.81 | 99.05 | 1.76 | 4500.21 | 0.800410485 | compression | -0.01745859 |
| | Top | Wall 4-Wall 5 | 29.47 | 100.56 | 92.73 | 7.83 | 4321.12 | 3.731309847 | compression | -0.07786396 |
| | Bottom | Wall 4-Wall 5 | 28.25 | 100.92 | 99.75 | 1.17 | 4839.66 | 0.651426802 | compression | -0.01159334 |
| | Top | Wall 5-Wall 6 | 33.95 | 101.27 | 91.65 | 9.62 | 4700.21 | 4.328484997 | compression | -0.09499358 |
| | Bottom | Wall 5-Wall 6 | 30.12 | 100.81 | 100.23 | 0.58 | 4834.07 | 0.302530609 | compression | -0.0057534 |

Table A3.2: Strain, compression and tension force of rubber block spacers and silicone sealant between wall panels

| | |
|---|---|
| Hardness of rubber block, IRHD | 5.5 |
| Young Modulus of rubber block | 3.25MPa |
| Shear Modulus of rubber block | 0.81MPa |
| Shear Modulus of silicone sealant | 12kPa |
| Constant | 0.64 |

| Drift | Location | Interface | Thickness of rubber (mm) | Initial Distance(mm) | Distance travel | Compression Thickness | Cross-Area A($mm^2$) | Compression Force(kN) | Tension and compression zone | Strain ε |
|---|---|---|---|---|---|---|---|---|---|---|
| 0.5%drift (push) | Top | Wall 1-Wall 2 | 24.55 | 101.44 | 97.25 | 4.19 | 4450.48 | 3.304141496 | compession | -0.04131 |
| | Bottom | Wall 1-Wall 2 | 22.65 | 191.05 | 191.00 | 0.05 | 4294.25 | 0.041236175 | compession | -0.00026 |
| | Top | Wall 2- Wall 3 | 20.86 | 99.92 | 98.25 | 1.67 | 4320.23 | 1.504521133 | compession | -0.01671 |
| | Bottom | Wall 2- Wall 3 | 37.85 | 100.97 | 100.51 | 0.46 | 4788.83 | 0.253169058 | compession | -0.00456 |
| | Top | Wall 3-Wall 4 | 25.15 | 100.20 | 99.33 | 0.87 | 4600.23 | 0.692229441 | compession | -0.00868 |
| | Bottom | Wall 3-Wall 4 | 32.16 | 99.65 | 100.18 | -0.53 | 4500.21 | -0.322613 | tension | 0.005319 |
| | Top | Wall 4-Wall 5 | 29.47 | 100.56 | 99.78 | 0.78 | 4321.12 | 0.49750798 | compession | -0.00776 |
| | Bottom | Wall 4-Wall 5 | 28.25 | 100.97 | 100.87 | 0.10 | 4839.66 | 0.074522198 | compession | -0.00099 |
| | Top | Wall 5-Wall 6 | 33.95 | 100.43 | 105.47 | -5.04 | 4700.21 | -3.03526963 | tension | 0.050184 |
| | Bottom | Wall 5-Wall 6 | 30.12 | 103.05 | 102.70 | 0.35 | 4834.07 | 0.244351646 | compression | -0.0034 |
| 1.0% drift (push) | Top | Wall 1-Wall 2 | 24.55 | 101.44 | 95.51 | 5.93 | 4450.48 | 4.676267081 | compression | -0.05846 |
| | Bottom | Wall 1-Wall 2 | 22.65 | 191.05 | 191.00 | 0.05 | 4294.25 | 0.041236175 | compression | -0.00026 |
| | Top | Wall 2- Wall 3 | 20.86 | 99.92 | 97.13 | 2.79 | 4320.23 | 2.513541294 | compession | -0.02792 |
| | Bottom | Wall 2- Wall 3 | 37.85 | 100.97 | 100.50 | 0.47 | 4788.83 | 0.258672733 | compession | -0.00465 |
| | Top | Wall 3-Wall 4 | 25.15 | 100.2 | 98.88 | 1.32 | 4600.23 | 1.050279151 | compession | -0.01317 |
| | Bottom | Wall 3-Wall 4 | 32.16 | 99.65 | 99.90 | -0.25 | 4500.21 | -0.15217594 | tension | 0.002509 |
| | Top | Wall 4-Wall 5 | 29.47 | 100.56 | 102.79 | -2.23 | 4321.12 | -1.42236256 | tension | 0.022176 |
| | Bottom | Wall 4-Wall 5 | 28.25 | 100.97 | 100.75 | 0.22 | 4839.66 | 0.163948836 | compession | -0.00218 |
| | Top | Wall 5-Wall 6 | 33.95 | 100.43 | 96.05 | 4.38 | 4700.21 | 2.637793848 | compession | -0.04361 |

| | | | | | | | | | | |
|---|---|---|---|---|---|---|---|---|---|---|
| | Bottom | Wall 5-Wall 6 | 30.12 | 103.05 | 108.51 | -5.46 | 4834.07 | -3.81188568 | tension | 0.052984 |
| 2.0%drift | Top | Wall 1-Wall 2 | 24.55 | 101.44 | 92.82 | 8.62 | 4450.48 | 6.797541693 | compession | -0.08498 |
| (push) | Bottom | Wall 1-Wall 2 | 22.65 | 191.05 | 194.00 | -2.95 | 4294.25 | -2.43293435 | tension | 0.015441 |
| | Top | Wall 2- Wall 3 | 20.86 | 99.92 | 96.15 | 3.77 | 4320.23 | 3.396433935 | compession | -0.03773 |
| | Bottom | Wall 2- Wall 3 | 37.85 | 100.97 | 101.00 | -0.03 | 4788.83 | -0.01651103 | tension | 0.000297 |
| | Top | Wall 3-Wall 4 | 25.15 | 100.20 | 98.00 | 2.20 | 4600.23 | 1.750465252 | compession | -0.02196 |
| | Bottom | Wall 3-Wall 4 | 32.16 | 99.65 | 99.36 | 0.29 | 4500.21 | 0.176524096 | compession | -0.00291 |
| | Top | Wall 4-Wall 5 | 29.47 | 100.56 | 102.29 | -1.73 | 4321.12 | -1.10344719 | tension | 0.017204 |
| | Bottom | Wall 4-Wall 5 | 28.25 | 100.97 | 100.63 | 0.34 | 4839.66 | 0.253375474 | compession | -0.00337 |
| | Top | Wall 5-Wall 6 | 33.95 | 100.43 | 114.66 | -14.23 | 4700.21 | -8.56981882 | tension | 0.141691 |
| | Bottom | Wall 5-Wall 6 | 30.12 | 103.05 | 100.56 | 2.49 | 4834.07 | 1.738387424 | compression | -0.02416 |
| 3.0%drift | Top | Wall 1-Wall 2 | 24.55 | 101.44 | 91.46 | 9.98 | 4450.48 | 7.870007668 | compession | -0.09838 |
| (push) | Bottom | Wall 1-Wall 2 | 22.65 | 191.05 | 195 | -3.95 | 4294.25 | -3.25765786 | tension | 0.020675 |
| | Top | Wall 2- Wall 3 | 20.86 | 99.92 | 95.04 | 4.88 | 4320.23 | 4.396444988 | compession | -0.04884 |
| | Bottom | Wall 2- Wall 3 | 37.85 | 100.97 | 103.11 | -2.14 | 4788.83 | -1.17778649 | tension | 0.021194 |
| | Top | Wall 3-Wall 4 | 25.15 | 100.20 | 97.19 | 3.01 | 4600.23 | 2.394954732 | compession | -0.03004 |
| | Bottom | Wall 3-Wall 4 | 32.16 | 99.65 | 99.71 | -0.06 | 4500.21 | -0.03652223 | tension | 0.000602 |
| | Top | Wall 4-Wall 5 | 29.47 | 100.56 | 101.59 | -1.03 | 4321.12 | -0.65696567 | tension | 0.010243 |
| | Bottom | Wall 4-Wall 5 | 28.25 | 100.97 | 100 | 0.97 | 4839.66 | 0.722865323 | compession | -0.00961 |
| | Top | Wall 5-Wall 6 | 33.95 | 100.43 | 121.34 | -20.91 | 4700.21 | -12.5927556 | tension | 0.208205 |
| | Bottom | Wall 5-Wall 6 | 30.12 | 103.05 | 100.85 | 2.20 | 4834.07 | 1.535924631 | compession | -0.02135 |
| 4.0%drift | Top | Wall 1-Wall 2 | 24.55 | 101.44 | 136.18 | -34.74 | 4450.48 | -27.395197 | tension | 0.342468 |
| (push) | Bottom | Wall 1-Wall 2 | 22.65 | 191.05 | 196.00 | -4.95 | 4294.25 | -4.08238137 | tension | 0.025909 |
| | Top | Wall 2- Wall 3 | 20.86 | 99.92 | 99.63 | 0.29 | 4320.23 | 0.261264149 | compession | -0.0029 |
| | Bottom | Wall 2- Wall 3 | 37.85 | 100.97 | 105.23 | -4.26 | 4788.83 | -2.34456562 | tension | 0.042191 |
| | Top | Wall 3-Wall 4 | 25.15 | 100.2 | 96.71 | 3.49 | 4600.23 | 2.776874423 | compession | -0.03483 |
| | Bottom | Wall 3-Wall 4 | 32.16 | 99.65 | 99.91 | -0.26 | 4500.21 | -0.15826298 | tension | 0.002609 |
| | Top | Wall 4-Wall 5 | 29.47 | 100.56 | 95.83 | 4.73 | 4321.12 | 3.016939415 | compession | -0.04704 |
| | Bottom | Wall 4-Wall 5 | 28.25 | 100.97 | 100.21 | 0.76 | 4839.66 | 0.566368707 | compession | -0.00753 |
| | Top | Wall 5-Wall 6 | 33.95 | 100.43 | 91.71 | 8.72 | 4700.21 | 5.251498254 | compression | -0.08683 |

| | | | | | | | | | | |
|---|---|---|---|---|---|---|---|---|---|---|
| | Bottom | Wall 5-Wall 6 | 30.12 | 103.05 | 103.71 | -0.66 | 4834.07 | -0.46077739 | tension | 0.006405 |
| 4.0%drift (pull) | Top | Wall 1-Wall 2 | 24.55 | 101.44 | 89.47 | 11.97 | 4450.48 | 9.439277734 | compression | -0.118 |
| | Bottom | Wall 1-Wall 2 | 22.65 | 191.05 | 199.00 | -7.95 | 4294.25 | -6.5565519 | tension | 0.041612 |
| | Top | Wall 2- Wall 3 | 20.86 | 99.92 | 92.66 | 7.26 | 4320.23 | 6.54061283 | compression | -0.07266 |
| | Bottom | Wall 2- Wall 3 | 37.85 | 100.97 | 99.39 | 1.58 | 4788.83 | 0.869580676 | compression | -0.01565 |
| | Top | Wall 3-Wall 4 | 25.15 | 100.2 | 96.66 | 3.54 | 4600.23 | 2.816657724 | compression | -0.03533 |
| | Bottom | Wall 3-Wall 4 | 32.16 | 99.65 | 98.03 | 1.62 | 4500.21 | 0.98610012 | compression | -0.01626 |
| | Top | Wall 4-Wall 5 | 29.47 | 100.56 | 98.00 | 2.56 | 4321.12 | 1.632846702 | compression | -0.02546 |
| | Bottom | Wall 4-Wall 5 | 28.25 | 100.97 | 102.08 | -1.11 | 4839.66 | -0.8271964 | tension | 0.010993 |
| | Top | Wall 5-Wall 6 | 33.95 | 100.43 | 165 | -64.57 | 4700.21 | -38.886381 | tension | 0.642935 |
| | Bottom | Wall 5-Wall 6 | 30.12 | 103.05 | 114.36 | -11.31 | 4834.07 | -7.8960489 | tension | 0.109753 |

# APPENDIX A3

(a)

(b)

(c)

(d)

(e)

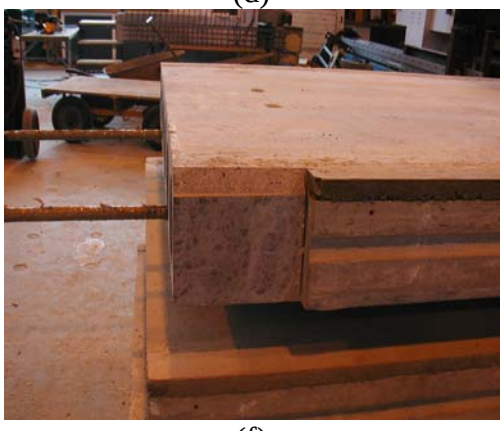

(f)

Figure A3.1: Preparation of foundation beam and non-seismic wall panels;
(a) RHS placed across the foundation beam to prevent from sliding; (b) vibrating concrete in the formwork; (c) formwork was fill with concrete; (d) a stack of precast hollow core walls used for the construction of multi-panel walls; (e) pouring mortar on one side of seismic wall panel; and (f) cutting off 200x200x30mm from bottom edge of non-seismic wall panel.

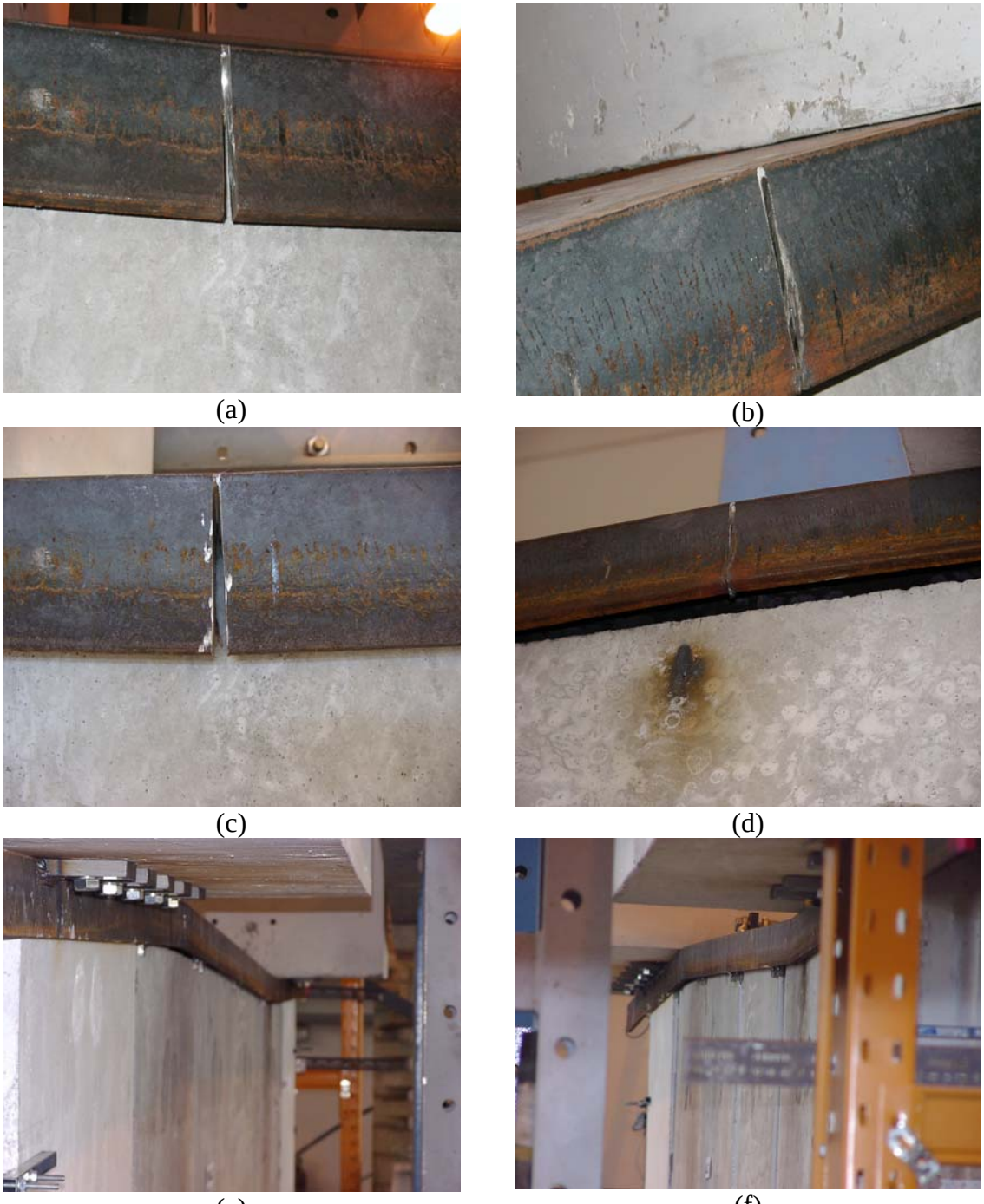

Figure A3.2: Cutting V-shape on top of steel channel (plastic hinge mechanism);
(a) both side of flange were cut; (b) closing gap between flange at when applied lateral load ; (c) opening gap between flange when steel channel under tension; (d) closing gap and buckling occurred at hinge when steel channel under compression; (e) plastic hinge mechanism at +2.0% drift; and (f) plastic hinge mechanism at +3.0% drift.

(a)

(b)

(c)

(d)

(e)

(f)

Figure A3.3: Assembling multi-panel wall on strong floor; (a) placing concrete block and bolted to the top of steel channel; (b) positioning steel channel on middle of precast hollow core walls; (c) lifting non-seismic wall using crane; (d) placing non-seismic walls on non-seismic foundation beam; (e) make sure the gap between wall panels is 25mm for installation of silicone sealant; and (f) make sure the non-seismic wall is parallel to seismic wall.


(a)


(b)

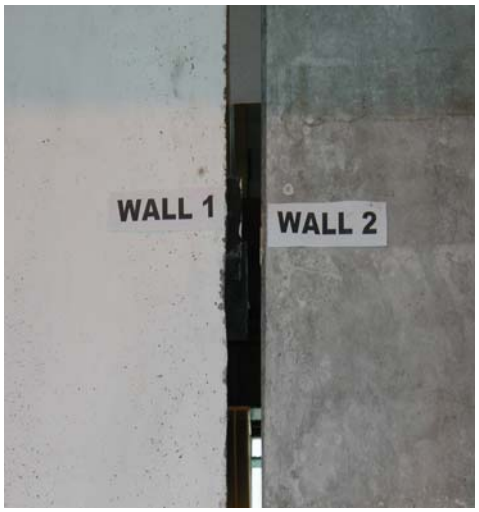


(c)


(d)

Figure A3.4: Placing rubber block between wall panels; (a) inserting rubber block between non-seismic wall panels; (b) inserting rubber block between seismic and non-seismic wall panels; (c) rubber block experienced compression zone between seismic and non-seismic wall; and (d) shearing mechanism occurred between non-seismic and seismic wall panels.

(a)

(b)

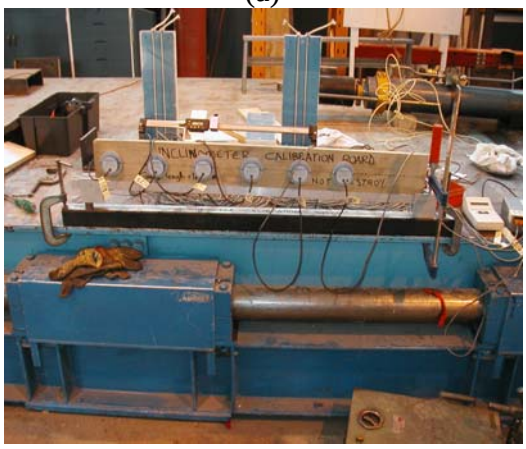


(c)

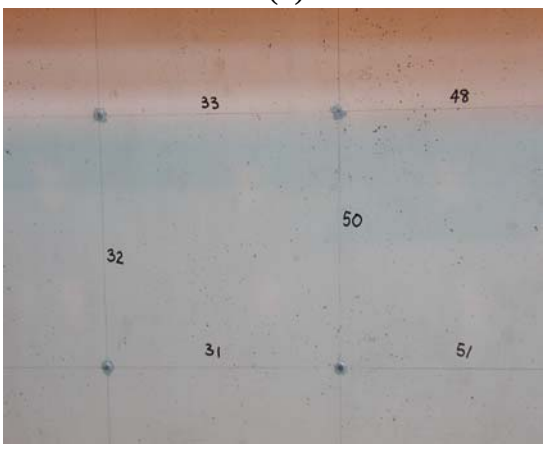


(d)

(e)

Figure A3.5: Instrumentation of multi-panel wall system; (a) linear potentiometer to measure uplifting of concrete block; (b) rotary potentiometer to measure in-plane displacement; (c) inclinometer to measure rotation on each wall; (d) “demac” points to measure strain in concrete; and (e) overall view of superassemblage of multi-panel which is ready for testing.


(a)


(b)

(c)


(d)

(e)


(f)

Figure A3.6: Installation of silicone sealants on multi-panel wall; (a) inserting backing rod in between gap of PHCW using wooden block; (b) make sure all the gap are filled with backing rod before putting sealant; (c) use triggered gun and nozzle to fill in the gaps between wall; (d) use spatula for smoothing the surface of sealant; (e) tear-off the masking tape between the gap when sealant surface is smooth; and (f) silicone sealant takes about one week to be completely dry before testing take place.

(a)

(b)

(c)

(d)

Figure A3.7: Visual observation during experimental work for Phase 1(20mm diameter of fuse-bars and rubber block spacers); (a) uplifting end corner of foundation beam at 1.0% drift; (b) two linear potentiometer used to measure sliding and uplifting of foundation block; (c) uplifting bottom corner of seismic wall at 1.0% drift; (d) slight lifting of non-seismic wall which seated on rubber pad.

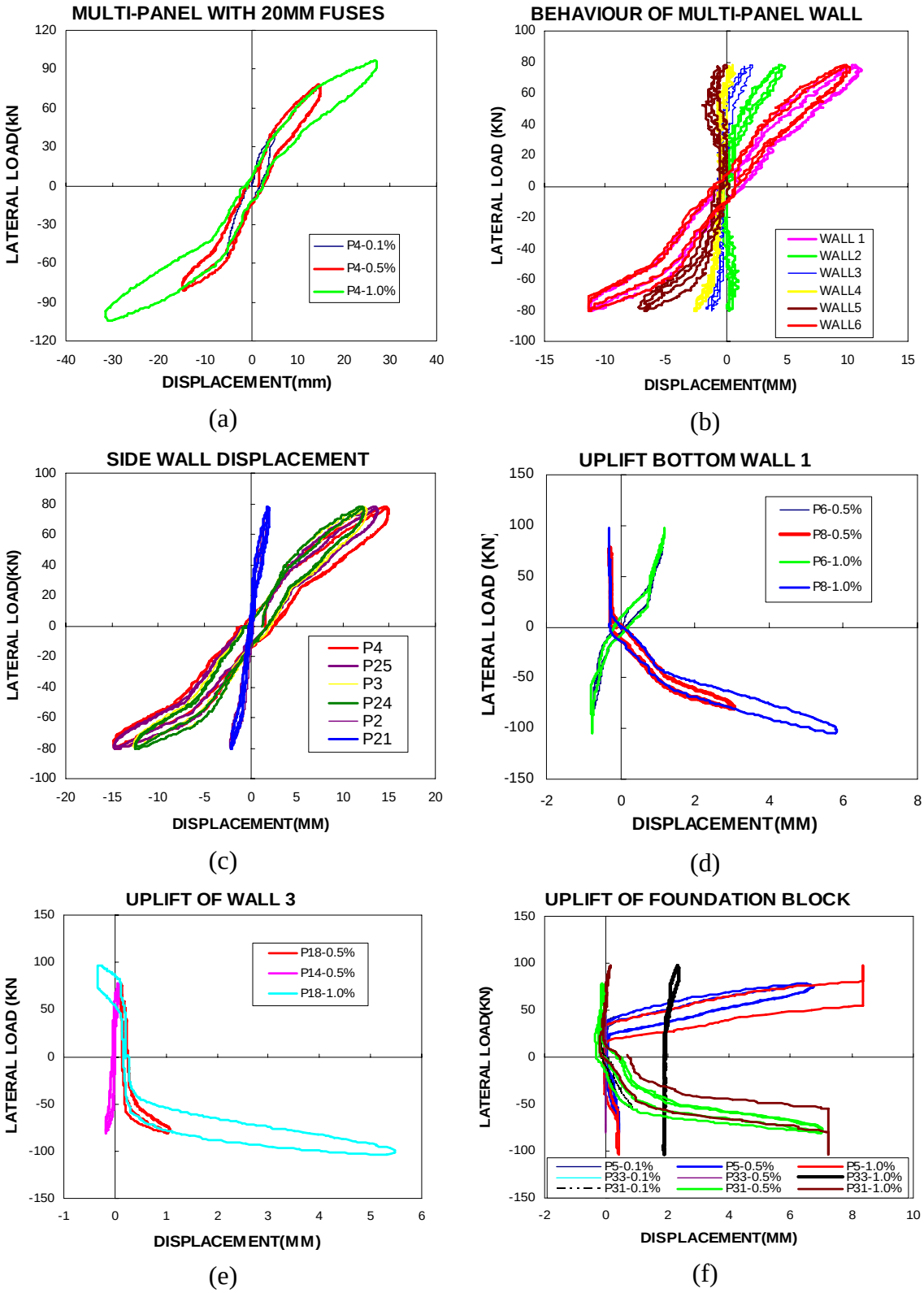


Figure A3.8: Experimental results for Phase 1; (a) overall cyclic behaviour at ±0.1%,± 0.5% and ±1.0% drift; (b) individual's wall behaviour at ±0.5% drift; (c) cyclic lateral displacement of far end wall at 0.5% drift; (d) uplift at bottom corner of seismic Wall 1; (e) uplift of non-seismic Wall 3; and (f) uplift of foundation block.

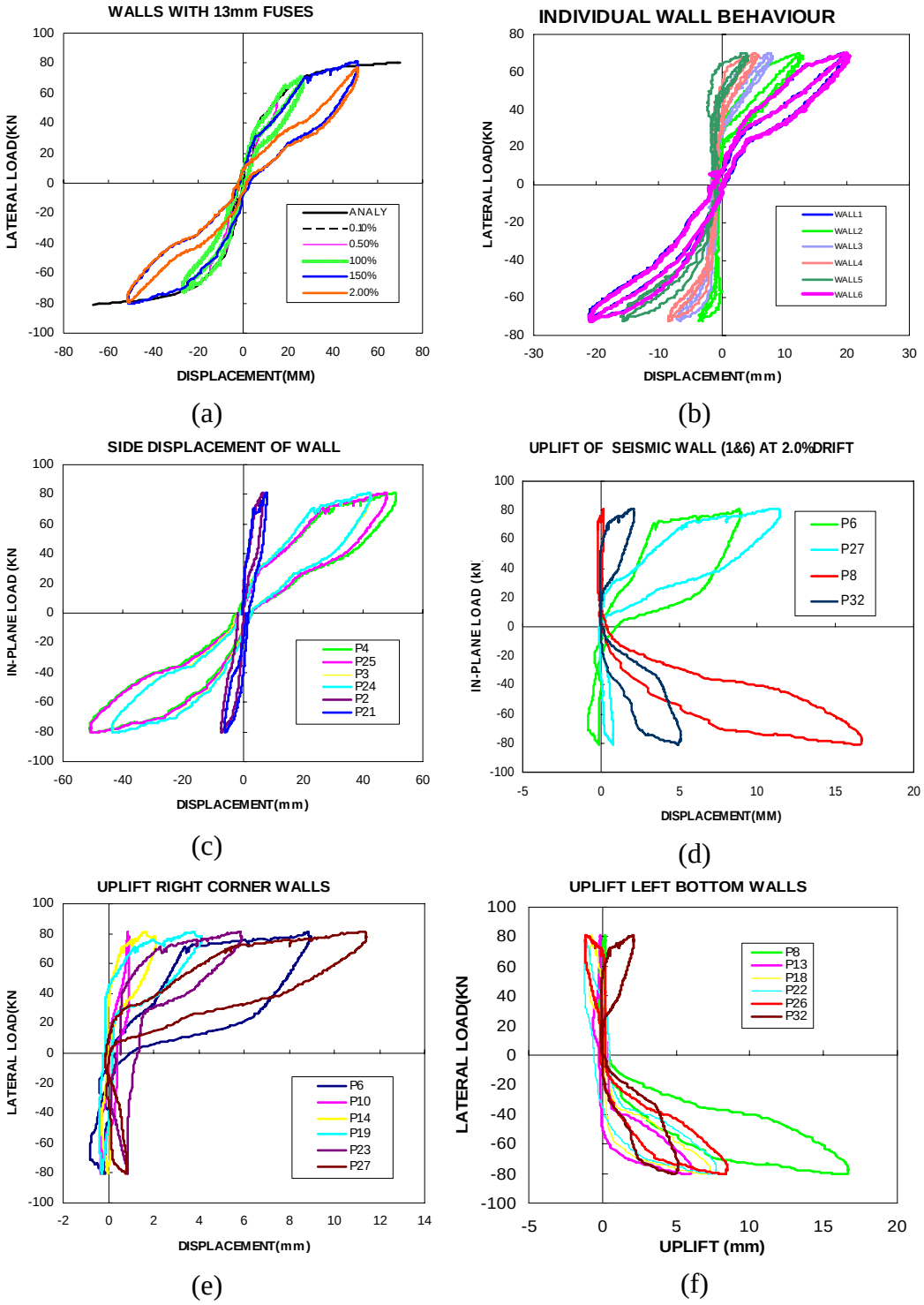


Figure A3.9: Experimental results during testing Phase 2 (13mm diameter of fuse-bars and rubber block spacers); (a) overall behaviour of multi-panel wall up to 2.0% drift; (b) individual behaviour of seismic wall at ± 2.0% drift; (c) lateral displacement of seismic wall; (d) uplifting bottom corner of the seismic wall; (e) uplifting of bottom right corner of non-seismic walls; and (f) uplifting bottom left corner of non-seismic wall.

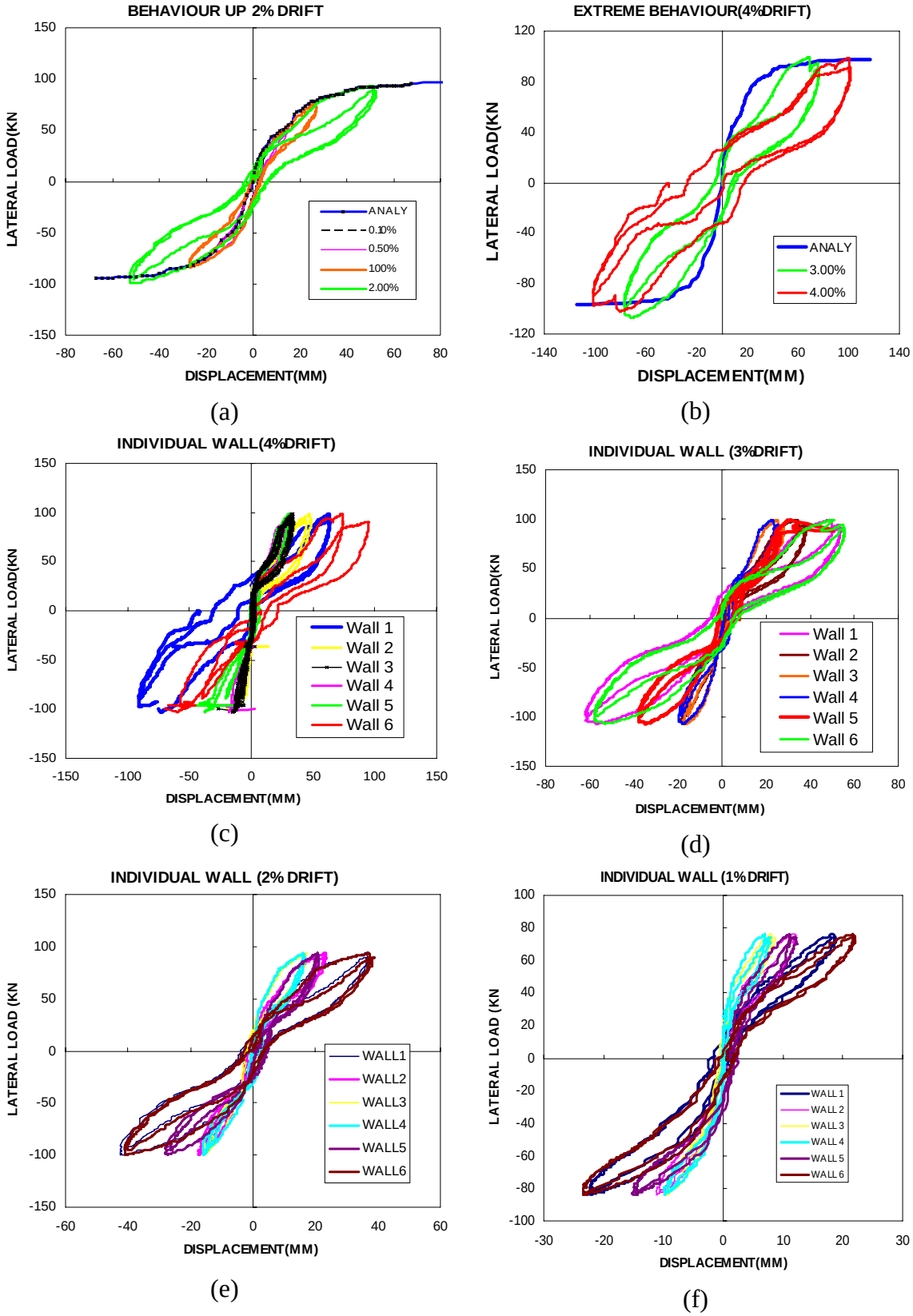


Figure A3.10: Experimental results for Phase 3 (13mm fuse-bars, rubber blocks and sealant); (a) overall behaviour up to ± 2% drift; (b) extreme behaviour at ± 3% and ± 4% drift); (c) individual behaviour at ± 4% drift; (d) individual behaviour at ± 3% drift; (e) individual behaviour at ± 2% drift; and (f) individual behaviour at ± 1% drift.

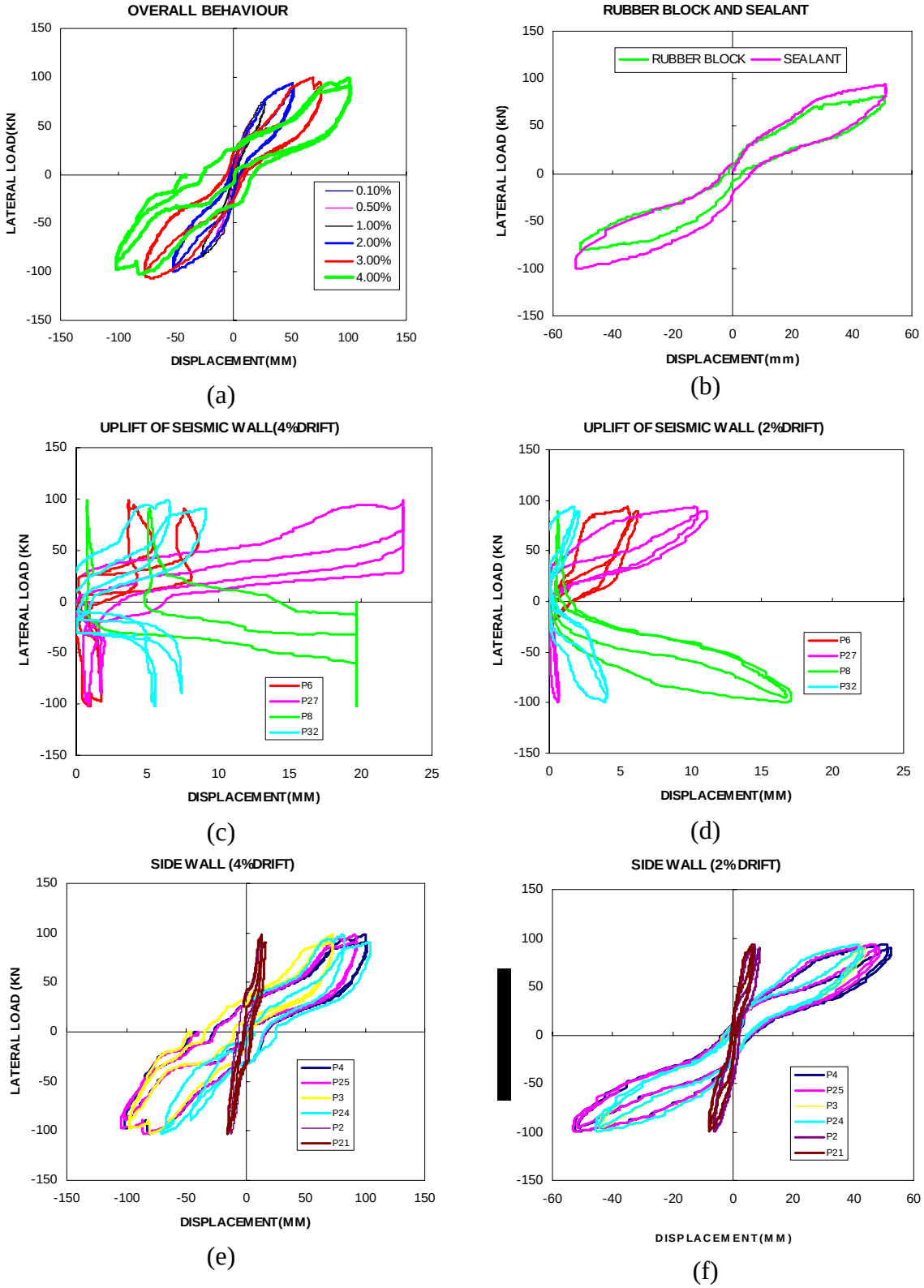


Figure A3.11: Experimental results for Phase 3; (a) overall behaviour up to 4% drift; (b) a comparison of Wall1 between sealant and rubber block spacers; (c) uplifting bottom corner of seismic wall at 4% drift; (d) uplifting bottom corner of seismic wall at 2% drift; (e) in-plane displacement of seismic wall at 4% drift; and (f) in-plane displacement of seismic wall at 2% drift.


(a)


(b)

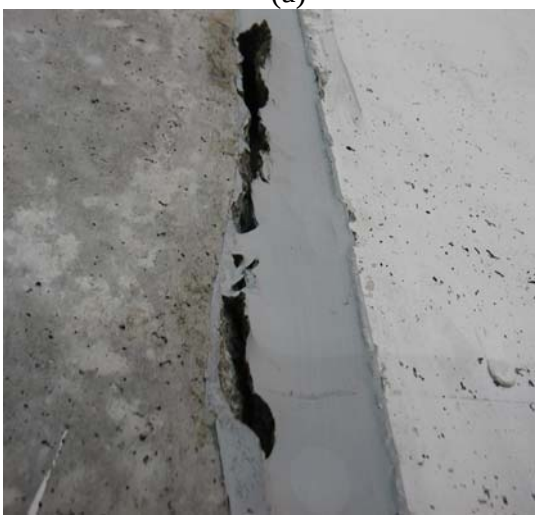

(c)

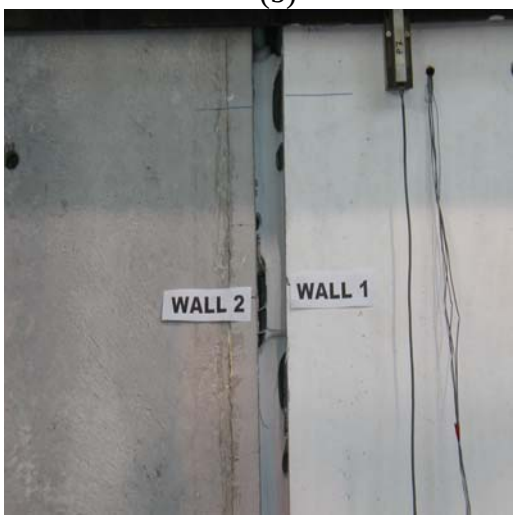


(d)


(e)

(f)

Figure A3.12: Visual observation of silicone sealant under cyclic loading; (a) no damage occurred at 1.0% drift; (b) small holes at 2.0% drift; (c) adhesive failure occurred at 3.0% drift; (d) spalling failure occurred at 4.0% drift; (e) interaction between sealant and rubber block spacers; and (f) silicone sealant behaves well between non-seismic walls.


(a)


(b)


(c)


(d)


(e)


(f)

Figure A3.13: Visual observation on shearing mechanism of silicone sealant ;
(a) at + 0.1% drift, (b) at + 1.0% drift; (c) at + 2.0% drift; (d) at + 3.0% drift; (e) at + 2.0% drift; and (f) at + 4.0% drift.

(a)


(b)


(c)


(d)

(e)

(f)

Figure A3.14: Visual observation on types of failure in sealant; (a) adhesion failure; (b) adhesion failure; (c) spalling failure; (d) spalling failure; (e) folding failure; and (f) folding failure.

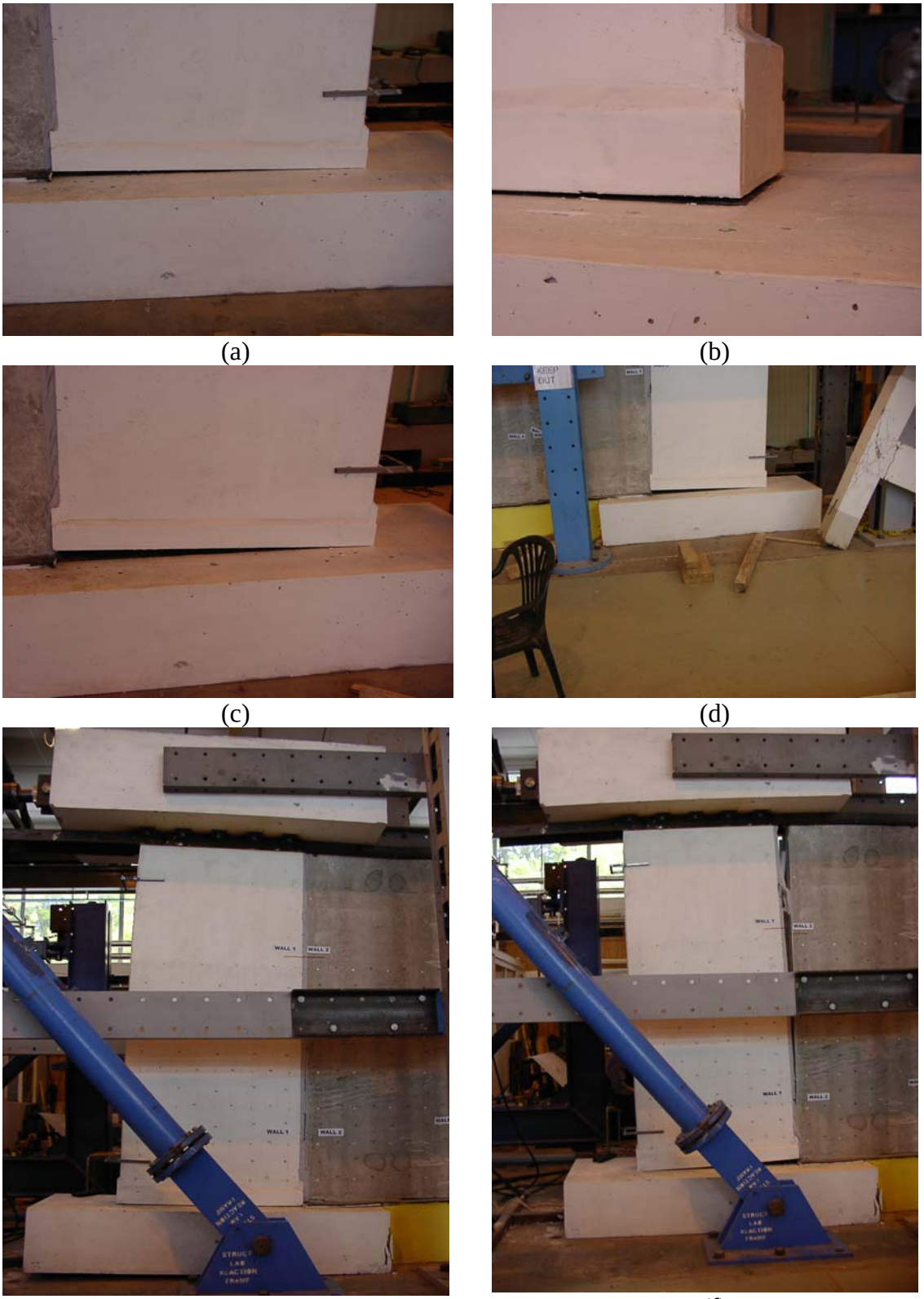

Figure A3.15: Rocking mechanism of multi-panel wall on foundation beam; (a) uplifting of seismic wall at 2.0% without any damage; (b) rocking toe of seismic wall; (c)uplifting of seismic wall at 4.0% drift; (d)uplifting of seismic wall at 3.0% drift; (e) overall behaviour of seismic wall at + 4.0% drift; and (f) overall behaviour of seismic wall at - 4.0% drift.

## A3.1 IN-PLANE RESPONSE OF PRECAST HOLLOW CORE WALL

Derivation of in-plane lateral force in precast hollow core wall using rectangular simplified stress concrete block and Direct Displacement Design approach is employed. This approach is modified using the method used by Pampanin (2000). The design parameters for this type of panel are wall thickness ($b_w$), wall height (H), wall width (B), diameter of fuse-bars and unbonded tendons, initial prestressing of unbonded tendons and amount of axial load (N) representing cladding and roof loading. The dimension variables of unbonded tendons and fuse-bars such as length, cross-sectional area and location from pivot point will be analysed using this approach.

The mechanism of opening and closing the gap between precast hollow core wall (PHCW) and foundation interface plays an important role in determining the lateral force to resist ground motion. In-plane and out-of plane lateral load are restrained by positioning energy dissipator and unbonded tendons at middle of the wall. The elongation of energy dissipators and unbonded tendons attribute to drift level and strength of the wall. Stress-strain relationship in unbonded tendons and energy dissipators can be calculated using Restrepo-Dodd steel model (1995). Mander's model (1988) for unconfined concrete is used to determine stress-strain curve for concrete in wall panel. Strain compatibility between steel and concrete are used to determine the depth of neutral axis under equivalent simplified stress block. By equating fixed-base monolithic wall with precast wall panel approaches, the plastic rotation can be evaluated. The integration of one strip layer along the wall thickness ($b_w$) under concrete compression zone had been utilized. St Venant's theorem (uncracked section)

states that yielding will occur when the largest principal strains equal to strain corresponding to yield strength. Thus, compression strength in concrete is equal to the total tension strength in steel would applicable in this situation. The depth to neutral axis under simplified stress block can be determined by using equilibrium equation where the compression forces of concrete is equal to tension forces in unbonded tendons and energy dissipator. Finally, the in-plane lateral force versus displacement can be plotted and use this result to predict the in-plane behaviour of PHCW. The following topic described eight steps in producing in-plane response for precast hollow core wall panel.

## A3.2 PROCEDURE FOR IN-PLANE RESPONSE

Step by step explanation is involved in this procedure followed by a schematic illustration of diagram are presented herein.

**Step 1: Set the target drift for end rotation of wall panel**

The rotation (θ) between wall-foundation interfaces is related to a simple geometric considerations. The geometry diagram for opening gap between wall-foundation interfaces and lateral displacement of the wall is given in Figure A3.16. By assuming the wall is perfectly rigid and adjacent ends are perpendicular to each other, then the effective rotation (θ) can be expressed as:

$$\theta = \frac{h_b}{B} = \frac{\Delta_l}{H} \qquad \text{(A3.1)}$$

where $h_b$ = height of opening gap between wall-foundation interface, $B$ = width of the wall, $\Delta_1$ = lateral displacement and $H$ = wall height. The drift limit can be calculated by multiplying the effective rotation by one hundred percent. Based on direct displacement design, a target drift is estimated by considering Design Basis Earthquake (DBE) and Maximum Considered Earthquake (MCE) requirement.

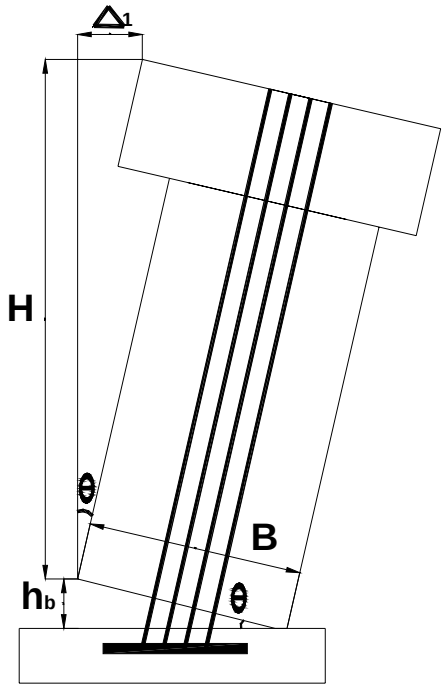


Figure A3.16: Effective rotation between wall-foundation interfaces.

**Step 2 : Calculate the strain in unbonded tendons**

The lateral restraint of wall panel largely depends on the cross-area of unbonded tendons and angle of rotation. Drift levels increase linearly with respect to elongation of unbonded tendons under elastic regions and non-linear after exceeding yield limit. Figure A3.17 illustrated the elongation of unbonded tendons during opening gap mechanism between wall-foundation interfaces. In order to maintain self-centering characteristic, the strain in unbonded tendons keep remain elastic by using higher

tensile strength and utilizing longer unbonded tendons. Hence, the strain for both of unbonded post-tensioned tendons remain elastic as derived below.

$$\varepsilon_{pt1} = \frac{\Delta_{pt1}}{l_{ub}} \quad \text{and} \quad \varepsilon_{pt2} = \frac{\Delta_{pt2}}{l_{ub}} \tag{A3.2}$$

in which $\Delta_{pt1} = \theta(d_{pt1} - c), \Delta_{pt2} = \theta(d_{pt2} - c)$, $\Delta_{pt1}$ = gap opening at first tendons, $\Delta_{pt2}$ = gap opening at second tendon, $\varepsilon_{pt1}$ = strain in first tendon, $\varepsilon_{pt2}$ = strain in second tendon, $l_{ub}$ = unbonded length of the post-tensioned bars, $d_{pt1}$ = depth from end corner of wall to first tendon, $d_{pt2}$ = depth from end corner of wall to second tendon and $c$ = the distance from end wall to neutral axis under compression zone.

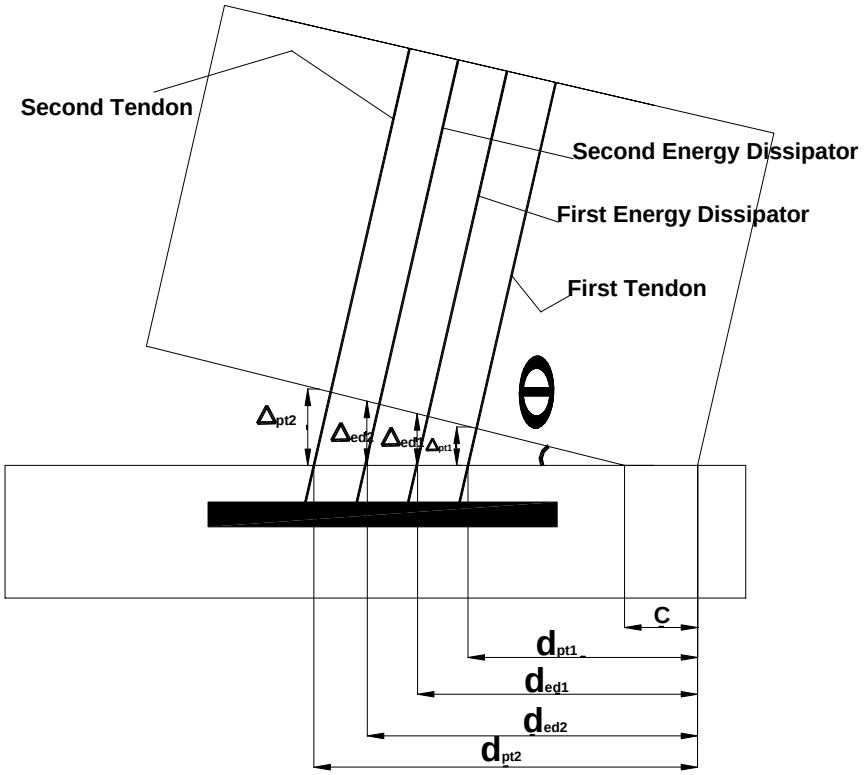


Figure A3.17: Elongation of tendons due to opening gap between wall-foundation interfaces.

**Step 3: Calculate the strain in the energy dissipators**

Two energy dissipators are utilized by locating them at the third and fourth void section of precast hollow core wall as illustrated in Figure A3.17. Thus, the steel strain for both energy of dissipator is given by the following equation which is allowed yielding.

$$\varepsilon_{ed1} = \frac{\left(\Delta_{ed1} - 2\Delta_{sp}\right)}{\left(L'_{ub}\right)} \text{ and } \qquad \varepsilon_{ed2} = \frac{\left(\Delta_{ed2} - 2\Delta_{sp}\right)}{\left(L'_{ub}\right)} \tag{A3.3}$$

in which $\Delta_{ed1}$ = elongation of first energy dissipator due to gap opening, $\Delta_{ed2}$ = elongation of second energy dissipator, $L'_{ub}$ = the length of energy dissipator under tension and compression. The displacement due to strain penetration is given by

$$\Delta_{sp} = \frac{2}{3} l_{sp}\varepsilon_e + l_{sp}\varepsilon_p \tag{A3.4}$$

where $l_{sp}$ = strain penetration taken as $0.15 f_y d_{bl}$, $d_{bl}$ = diameter of reinforcement bar, $f_y$ = yield strength of energy dissipator, $\varepsilon_e = \varepsilon_s - \varepsilon_p$ = elastic strain for energy dissipator and $\varepsilon_p = \alpha\varepsilon_y$ = plastic strain in energy dissipator. The relationship between $\varepsilon_e$ and $\varepsilon_p$ can be obtained by using stress-strain curve for mild steel as shown in Figure A3.18.

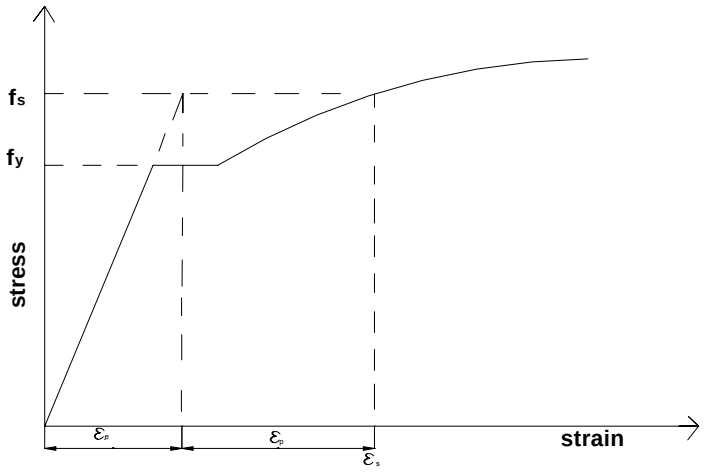


Figure A3.18 : Stress-strain curve for energy dissipator (steel)

Thus, equation A2.3 becomes

$$\varepsilon_{ed1} = \frac{\left(\Delta_{ed1} + 2/3 l_{sp} \alpha \varepsilon_y\right)}{\left(L'_{ub} + 2 l_{sp}\right)} \text{ and } \varepsilon_{ed2} = \frac{\left(\Delta_{ed2} + 2/3 l_{sp} \alpha \varepsilon_y\right)}{\left(L'_{ub} + 2 l_{sp}\right)} \qquad \text{A2.5}$$

where $\Delta_{ed1} = \theta(d_{ed1} - c)$, $\Delta_{ed2} = \theta(d_{ed2} - c)$, $\alpha$ = the ratio of elastic strain over yielding strain, $\varepsilon_y$ = yield strain of energy dissipator, $d_{ed1}$ = distance between end wall to first energy dissipator and $d_{ed1}$ = distance between end wall to second energy dissipator.

**Step 4: Estimate the strain of concrete using fixed-base monolithic wall panel**

According to the monolithic beam analogy where the total deformation of monolithic cantilever wall is equal to total deformation of precast hollow core wall panel as shown in Figure A3.19. Thus, equation becomes

$$\Delta_{totalprecast} = \Delta_{totalmonolithic} \qquad \text{A2-6}$$

$$\Delta_{pre} + \Delta_{el} = \Delta_p + \Delta_{el} \qquad \text{A2-7}$$

$$\Delta_p = \theta_p L_{cant} \qquad \text{A2-8}$$

By utilizing the monolithic case of ultimate and yielding curvature concepts by Paulay and Priestley (1992):

$$\Delta_p = \theta_p\left(L_{cant} - \frac{L_p}{2}\right) = (\phi_u - \phi_y) L_p \left[L_{cant} - \frac{L_p}{2}\right] \qquad \text{A2-9}$$

where $L_p = 0.08L + 4400\varepsilon_y d_b$

By equating Equation A2-8 and Equation A2-9

$$\theta_p L_{cant} = (\phi_u - \phi_y) L_p \left[ L_{cant} - \frac{L_p}{2} \right] \qquad \text{A2-10}$$

$$(\phi_u - \phi_y) = \frac{\theta_p L_{cant}}{L_p \left[ L_{cant} - \frac{L_p}{2} \right]} \qquad \text{A2-12}$$

$$\phi_u = \frac{\varepsilon_c}{c} = \frac{\left(\theta L_{cant}\right)}{\left( L_{cant} - \frac{L_p}{2} \right) L_p} + \theta_y \qquad \text{A2-13}$$

$$\varepsilon_c = \left( \frac{\left(\theta_b L_{cant}\right)}{\left( L_{cant} - \frac{L_p}{2} \right) L_p} + \theta_y \right) c \qquad \text{A2-14}$$

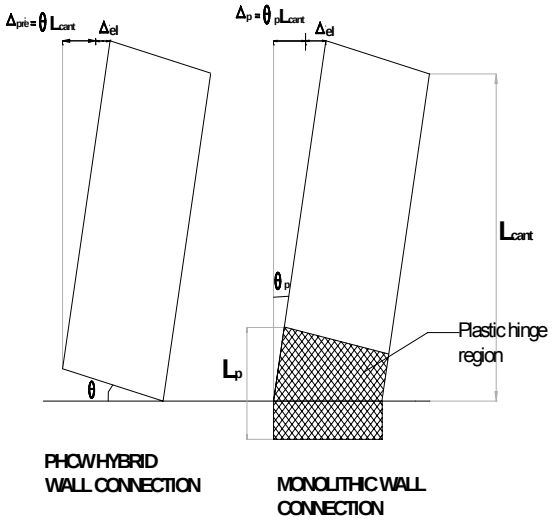


Figure A3.19: Monolithic beam analogy

**Step 5: Section equilibrium with new value of neutral axis**

Under equilibrium situation, the external forces which are due to initial prestressing, elongation of unbonded tendons and energy dissipator must equal to compression force in concrete and axial load (gravity load). Thus, the equilibrium is as follows:

$$C_c - T_{ed1} - T_{ed2} = T_{pt} - N \qquad \text{A2-15}$$

where $T_{pt} = T_{pt1} + T_{in1} + T_{pt2} + T_{in2}$, $T_{pt1} = f(\varepsilon_{pt1})A_{pt1}$, $T_{pt2} = f(\varepsilon_{pt2})A_{pt2}$, $T_{in1} =$ the initial prestressing of first tendon, $T_{in2} =$ the initial prestressing of second tendon, $T_{ed1} = f(\varepsilon_{ed1})A_{ed1}$, $T_{ed2} = f(\varepsilon_{ed2})A_{ed2}$, $N =$ axial force which come from roofing and cladding and $C_c =$ the compression force in concrete. The value of neutral axis, c in the compression force of concrete can be determined by assuming an equivalent stress block to represent the stress distribution in the concrete.

**Step 6: Iterative procedure until converge**

The iteration of the equation will be carried out until the value *c* is convergence where the compression force is equal to tension force in precast wall panels. The depth to neutral axis can be calculated by setting the summation of forces equal to zero. As the level of drift increases, the value of *c* is reduce until it become plateau.

## Step 7: Evaluate the Moment Capacity

From the above iteration, the total value of moment capacity with respect with rotation can be calculating using spreadsheet. Table A3.3 shows the program which calculates the moment capacity versus rotation and lateral force versus displacement. The theoretical in-plane moment capacity versus rotation is plotted based on the value obtained from the iteration.

Table A3.3: Theoretical in-plane response for precast hollow core wall panel.

| GEOMETRY OF THE WALL | | | | | REINFORCEMENT | | | | | 25 |
|---|---|---|---|---|---|---|---|---|---|---|
| Width(mm) | Thickness(mm) | H/2 | d'(mm) | d(mm) | As1 | As2 | dbl | dpt1 | dpt2 | Apt(mm2) |
| 1200 | 200 | 600 | 505 | 695 | 201 | 201 | 25 | 315 | 885 | 490.9 |
| Drift | Depth to N.A | Δ1 | lsp | l'ub(steel) | lub(tendon) | n(opening) | Δpt1 | Δpt2 | N,axil(kN) | Msteel |
| 0.02 | 146.7092 | 10.9658163 | 291.5 | 50 | 4500 | 1 | 14.7658 | 3.3658 | 50 | 98.11 |
| 2 | STEP | Δ2 | Mander | 811.8727 | GOAL SEEK | -0.000745 | Δsp | | Moment | 419.4 |
| STRAIN | 4 | 7.16581629 | TENSION | COMPRESSION | Cat. Cov | -62.850951 | 5.02455 | | Mtotal | 460.2 |
| εS1 | fs | fplastic | Ts1(kN) | Cc(kN) | a | c,neutral axis | Moment (kNm) | Capacity | a | a/2 |
| 0.01814 | 541.6122 | 541.612161 | 108.86404 | 811.8735 | 71.279499 | 83.8582342 | 481.905 | | 124.7 | 62.35 |
| εpt1 | fpt | fplastic | Tpt1(kN) | Tin1(kN) | Ttot(kN) | SUM OF FORCE | | | | |
| 0.00434 | 530 | 522.771148 | 260.16314 | 104.0653 | 645.78963 | 0.00000E+00 | | | | |
| εpt2 | fpt | fplastic | Tpt2(kN) | Tin2(kN) | Ttot1(kN) | | | | | |
| 0.00181 | 361.5918 | 519.202435 | 177.49598 | 104.0653 | 364.2284 | | | | | |
| εs2 | f's | fplastic | Ts2(kN) | εo (Prestress) | Ttot2(kN) | | | | | |
| 0.01214 | 533.4319 | 533.431933 | 107.21982 | 0.00106 | 281.56123 | | | | | |
| εc | Lp | effective height | Lcant | | | | | | | |
| 0.00744 | 416 | 4000 | 4000 | | | | | | | |

## Step 8: Derive lateral load versus displacement with different drift

The in-plane lateral force versus lateral displacement can be plotted based on moment capacity versus rotation as obtained from step 7. It can be done by dividing the moment with height of the wall to get in-plane lateral force and the displacement can be calculated by the product of rotation and height of wall.

# APPENDIX A4

## A4.1 DESIGN EXAMPLE

A typical single storey warehouse buildings (Type II) using precast hollow core walls is designed and to be constructed in the highest seismic hazard region in Wellington, New Zealand with zone intensity of VII. No external column is provided. Seismic wall acting as load-bearing wall and non-seismic walls carry the cladding. The Basic Design Earthquake (DBE) is 0.4g and Maximum Considered Earthquake (MCE) is 0.8g. The layout of the plan is shown in Figure A4.3 with 60m long, 40m wide and spacing between rafters is 6m. The dimension of Dycore unit is 8mx1.2mx0.2m. Three longitudinal prestressing strands, 13.5mm is located at bottom of void section and two strands with 11.5mm are placed at top of the void section. A multi-panel wall consists of 2 seismic walls and four non-seismic walls. The warehouse building is situated on intermediate soil, type b according to soil classification (NZS 4203:1992). The following assumptions are made for design purposes:

(i) Self-weight of the roof, $W_r = 1.5kN/m^2$

(ii) Unit weight of reinforced concrete, $W_w = 24kN/m^3$

(iii) The soil type factor, S=1.0

(iv) Compressive strength of concrete, $f'_c=50MPa$

(v) Acceleration of gravity, $g = 9.81m/s^2$

(vi) For unbonded post-tensioned tendons, $f_y=530MPa$, $f_{su}=680MPa$ and $E_s=200kPa$

## A4.2 DESIGN SOLUTION FOR WAREHOUSE BUILDING USING DAMAGE AVOIDANCE DESIGN

### A4.2.1 DESIGN SEISMIC PRECAST HOLLOW CORE WALL

(a) Structural geometry of seismic wall

Number of panel, n= $\frac{\text{spacing between rafter}}{\text{width of the wall}}$ + 1

$$n = \frac{6m}{1.2m} + 1 = 6$$

Choose six numbers of panels consist of two seismic walls and four infill non-seismic walls. Assume each seismic wall carries a gravity load of $0.1 f_c^{'} A_g$.

Total gravity load from roof, $W_r$ = 1.5kN/m$^2$x40mx6m = 360kN
Amount of loading carried by one seismic wall = 360/2 = 180kN
The cross-sectional area required of seismic wall to carry this loading

$$A_g > \frac{W_r}{0.1 f_c^{'}} = \frac{180000}{0.1(50)x10^6} = 0.036m^2$$

Check the cross-sectional area provided by precast hollow core units where $A_{g,provided}$=0.2mX1.2m= 0.24m$^2$. This section is satisfied under compression load from the roof.

(b) Calculate the seismic weight of wall panels and roof loading

Self-weight of the wall, $W_w$ = 24kN/m$^3$x1.2mx0.2mx8m=46kN
Total weight of wall, $W_s$=n$W_w$= 6x46kN =276kN
Seismic mass of the wall, $m_w$=276kN/9.81=28.18 tonnes
Self-weight of the roof, $W_r$ = 1.5kN/m$^2$x6mx20m=180kN
Seismic mass of the roof, $m_r$=180kN/9.81= 18.3 tonnes

(c) Dynamic properties of rocking precast hollow core wall

The critical overturning angle for wall is given by

$$\alpha = \tan^{-1}\left(\frac{B}{H}\right) = \tan^{-1}\left(\frac{1.2}{8}\right) = 8.53^o$$

When the wall uplift, the distance from top corner of the wall to the diagonal bottom toe is

$$R = \sqrt{H^2 + B^2} = \sqrt{1.2^2 + 8^2} = 8.09m$$

The effective mass of the rocking system is calculated using equation 4-38

$$m_{eff} = m_r + \frac{4m_w}{3}\left(\frac{H^2 + B^2}{4H^2 + B^2}\right)$$

$$m_{eff} = 18.3t + \frac{4 \times 28.18t}{3}\left(\frac{8^2 + 1.2^2}{4 \times 8^2 + 1.2^2}\right) = 27.90t$$

The kinetic energy reduction factor is calculated using equation 4-39

$$r = \left[1 - \frac{m_{eff}B^2}{m_{eff}(H^2 + B^2/4)}\right]$$

$$r = \left[1 - \frac{27.90t(1.2)^2}{27.90t(8^2 + 1.2^2/4)}\right] = 0.9776$$

$$1 - r = 1 - 0.9776 = 0.0224$$

(d) Base shear capacity for multi-panel wall system

Total seismic weight of wall = $nW_w$ = 6x46kN=276kN
Seismic roof loading, $W_r$ = 180kN
Use 4 reidbar with 25mm and $f_y$ =530kN/mm$^2$
Therefore, T = 4x$A_f$ x $f_y$ = 4x490x530=1040kN

Calculate lateral seismic loading using equation 4-15

$$F_H = \frac{1.2}{2 \times 8}(276 + 180 + 1040) = 112.2kN$$

Base shear capacity of wall system is determined using equation 4-16,

$$Cc = \frac{B}{2H}\left(1 + \frac{T}{W_s}\right)$$

where $W_s$=$W_r$+$nW_w$= 180kN + 276kN = 456kN. Thus

$$Cc = \frac{1.2}{2(8)}\left(1 + \frac{1040}{456}\right) = 0.24$$

(e) Estimate effective damping ($\xi_{eff}$) using equation 4-31 where

$$\xi_{eff} = \xi_{inst} + \xi_{rock} + \xi_{hyst}$$

The radiation damping can be calculated using equation 4-34

$$\xi_{rock} = \frac{(1-r)}{\pi C_c}\frac{B}{2H}$$

$$\xi_{rock} = \frac{0.0224 \times 1.2}{\pi \times 0.119 \times 2 \times 8} \times 100 = 0.45\%$$

Hysteretic energy dissipation can be calculated using equation 4-43

$$\xi_{hyst} = \frac{2\eta}{\pi}\left(\frac{1}{1-\alpha(\mu-1)} - \frac{1}{\mu}\right)$$

where $\eta = 0.2,\ \mu = 3.5,$ and $\alpha = 0.0071$

$$\xi_{hyst} = \frac{2 \times 0.2}{\pi}\left(\frac{1}{1-0.0071(3.5-1)} - \frac{1}{3.5}\right) \times 100 = 9.3\%$$

and $\xi_{inst} = 2\%$ (for reinforced concrete structures)

Therefore, total effective damping is

$$\xi_{eff} = \xi_{inst} + \xi_{rock} + \xi_{hyst} = 2\% + 0.45\% + 9.3\% = 11.75\%$$

(f) Determine the maximum response displacement for DBE and MCE

Set target drift for DBE, $\theta_{\max}^{DBE}$ = 1.5%
Set target drift for MCE, $\theta_{\max}^{MCE}$ = 3.0%

Target design displacement is can be calculated using equation 4-44

$\Delta_{\max}^{DBE} = 1.5 \times 8000/100 = 120mm$
$\Delta_{\max}^{MCE} = 3.0 \times 8000/100 = 240mm$

(g) Calculate the natural period of vibration using equation 4-4

T(DBE) = 2x3.14(120/(0.119x9.81)^0.5 =2.011second
T(MCE) = 2x 3.14(340/(0.119x9.81)^0.5= 2.845second

(h) Determine reduction damping factor, $B_v$ since it lies within medium period.

Calculate reduction damping factor for short period using equation 4-12

$$B_a = \sqrt{\frac{2+\xi}{7}} = \sqrt{\frac{2+11.75}{7}} = 1.40$$

Calculate reduction damping factor for long period using equation 4-13

$$B_d = \sqrt{\frac{8+\xi}{13}} = \sqrt{\frac{8+11.75}{13}} = 1.23$$

From the plotted DBE and MCE curves as shown in Figure 4.7:

The values $S_{da}$=0.03975m, $S_{dv}$=0.2484m and $S_{dd}$=0.120m

Thus, the reduction factor for constant velocity of DBE is given by equation 4-14

$$B_v = \frac{B_d(S_{dv} - S_{da}) - B_a(S_{dv} - S_{dd})}{S_{dd} - S_{da}}$$

$$B_v = \frac{1.23(0.2484 - 0.03975) - 1.4(0.2484 - 0.120)}{0.12 - 0.03975} = 1.337$$

The entire damped capacity-spectrum is calculated using equation 4-5, 4-6 and 4-7 as derived in Chapter Four.

Thus, the entire damped capacity-spectrum of DBE can be thus taken as greater of:

$F_vS_1 = T_vB_aC_c$=0.4x1.40x0.24=0.1344 equation 4-5
$F_vS_1$=2x3.14x((0.24x0.12)/9.81)^0.5x1.337=0.455 equation 4-6
$F_vS_1$ = 4x3.14x3.14x1.23x0.12/(9.81x3)=0.198 equation 4-7

Choose the greatest value of DBE from equation 4-5 to equation 4-7 as
$F_vS_1$ =0.455g > 0.4g (ok)

For the entire damped capacity-spectrum of MCE is calculated below

$F_vS_1 = T_vB_aC_c = 0.4x1.40x0.119 = 0.06664$
$F_vS_1 = 2x3.14x((0.24x0.24)/9.81)^{0.5}x1.337 = 0.91g$
$F_vS_1 = 4x3.14^2x1.23x0.24/(9.81x3) = 0.396g$

Choose the greatest value of MCE from the above calculation, thus
$F_vS_1 = 0.91g > 0.8g$ (ok)

From the above calculations, it shows that the base shear capacities of the structures are bigger than spectral demand for both DBE and MCE. Therefore both of them satisfied equation 4-11.

## A4.4.2 STRIP FOOTING DESIGN

The foundation beam is designed to carry $n$ number of panels and self-weight of the roof. The dimension of foundation beam is 7.2mx0.5mx1.0m which is designed to support seismic weight and gravity load without uplifting it during ground shaking.

(a) Calculate the tension force in fuse-bars and the lateral strength limits of precast hollow core walls under seismic loading.

self-weight of the roof, $W_r$ = 180kN
self-weight of one panel, $W_w$ = 46kN
self- weight of foundation beam,Wf =24x7.2x0.5x1.0=86kN
seismic-weight of rocking system ,$W_s = W_r + nW_w$ = 180kN+6(46kN)=456kN
$n =$ number of panels

Determine the minimum number of wall panels with light foundation block by using equation 4-24.

$$n > \frac{3}{1 + W_f / W_s} = 3 \text{ when } W_f \to 0$$

Therefore, adopt $n = 6$ number of panels

The tension force in fuse-bars can be determined using equation 4-23 without uplifting the foundation block.

$$T < \frac{n}{3}(W_s + W_f) - W_s = \frac{6}{3}(456kN + 86kN) - 456kN = 628kN$$

Base shear capacity of the PHCW can be computed using equation 4-26

$$C_c = \frac{B}{H}\left(1+\frac{W_f}{W_s}\right) = \frac{1.2}{8}\left(1+\frac{86}{456}\right) = 0.1783$$

(b) Determine the eccentricity on foundation beam so that there is no tension uplift on the strip footing.

The lateral load capacity of multi-panel wall is calculated using equation 4-15 where

$$F = \frac{1.2}{2\times 8}(180+276+628) = 81.3kN$$

The eccentricity of soil pressure is calculated using equation 4-20

$$\frac{e}{B} = \frac{1}{2}\left(\frac{1+628/456}{1+86/456}\right) = 1.00$$

$$e = 1.00B = 1.0\times 1.2m = 1.2m \le Ls/6 = 7.5/6 = 1.25m$$

Therefore, eccentricity under foundation beam is satisfactory under soil pressure.

(c) Rocking base

- In order to accommodate high contact point on rocking toe, steel-steel rocking interface is designed.
- A 1.35x0.4x0.03m steel plate is positioned on top of foundation beam where seismic precast hollow core wall is located.
- Seismic wall is inserted into steel channel 254x89x37.74kg/m and acting as rocking toe for the wall.
- To prevent the wall from sliding during ground motion, two 140x100x10mm steel plate are welded to steel channel closed to rocking toes. These steel plate or pintles will prevent the wall from in-plane sliding and avoid out-of-plane toppling.

The shear capacity of two pintles is given by

$$\Phi V_s = \Phi\frac{f_y}{\sqrt{3}}A_s = 0.65x\frac{250}{\sqrt{3}}x(2x10x100) = 187kN > F_{lateral} = 150kN$$

The drawings of warehouse building are shown in Appendix A4-8 to A4-23.

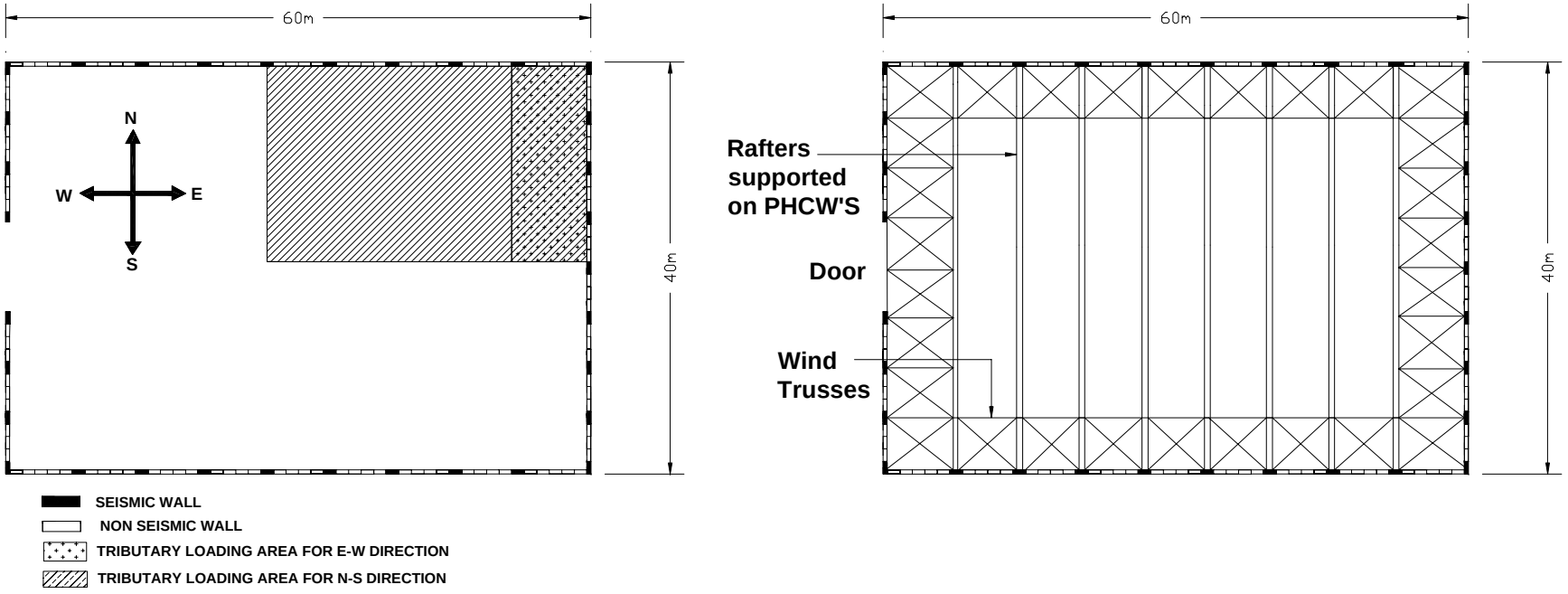


| | | |
|---|---|---|
| **DESIGN ENGINEER: NOR HAYATI ABDUL HAMID**<br>**DEPARTMENT OF CIVIL ENGINEERING**<br>**UNIVERSITY OF CANTERBURY**<br>**CHRISTCHURCH, NEW ZEALAND** | **STRUCTURE: SINGLE STOREY WAREHOUSE BUILDING**<br>**LOCATION: PLAN VIEW**<br>**DATE: 23.7.2003**<br>**SCALE: NOT TO SCALE** | DRAWING NO:<br>PLATE 1 |

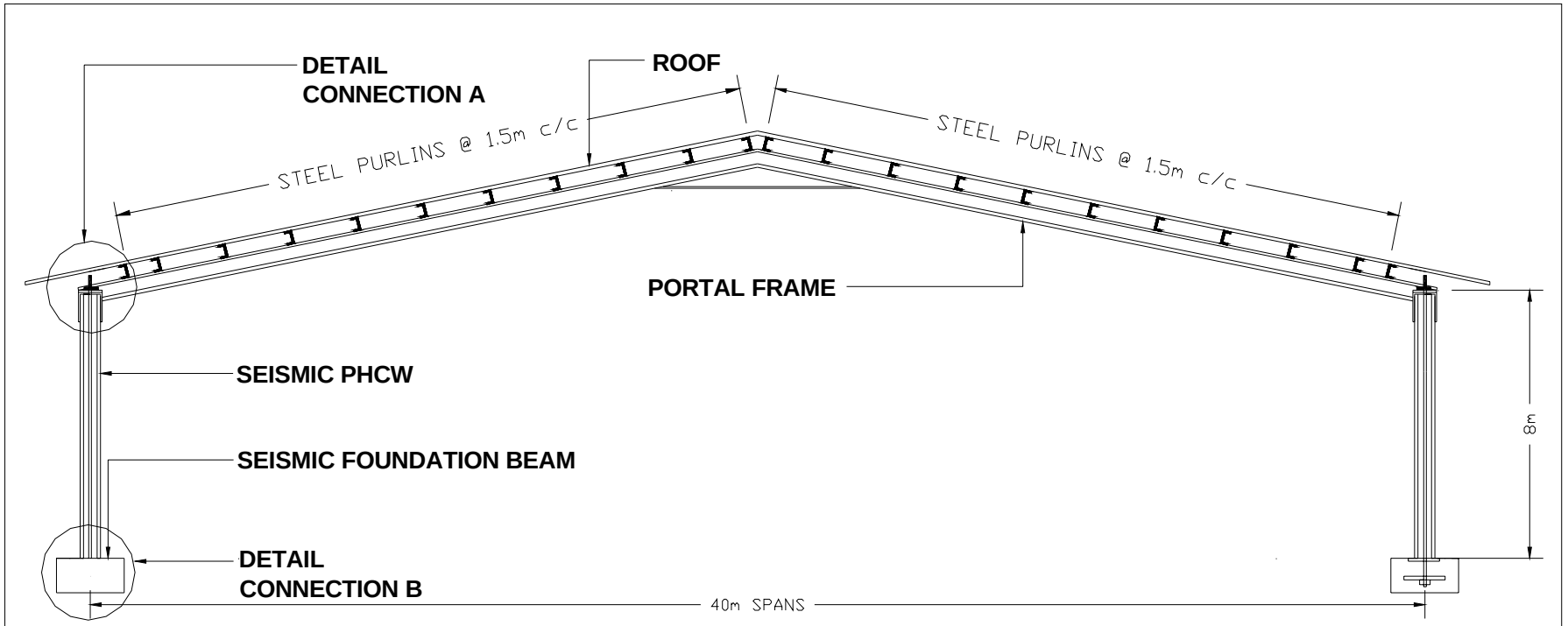


| | | |
|---|---|---|
| **DESIGN ENGINEER: NOR HAYATI ABDUL HAMID**<br>**DEPARTMENT OF CIVIL ENGINEERING**<br>**UNIVERSITY OF CANTERBURY**<br>**CHRISTCHURCH, NEW ZEALAND** | **STRUCTURE: STEEL PORTAL FRAME**<br>**VIEW: TRANSVERSE CROSS-SECTION**<br>**DATE: 23.7.2003**<br>**SCALE: NOT TO SCALE** | DRAWING NO:<br>PLATE 2 |

## DETAIL CONNECTION A

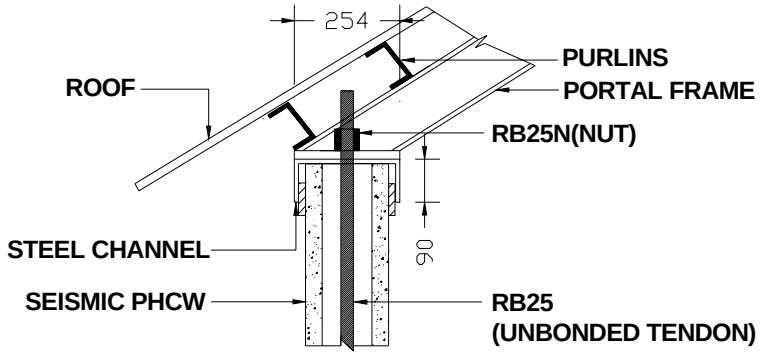


## DETAIL CONNECTION B

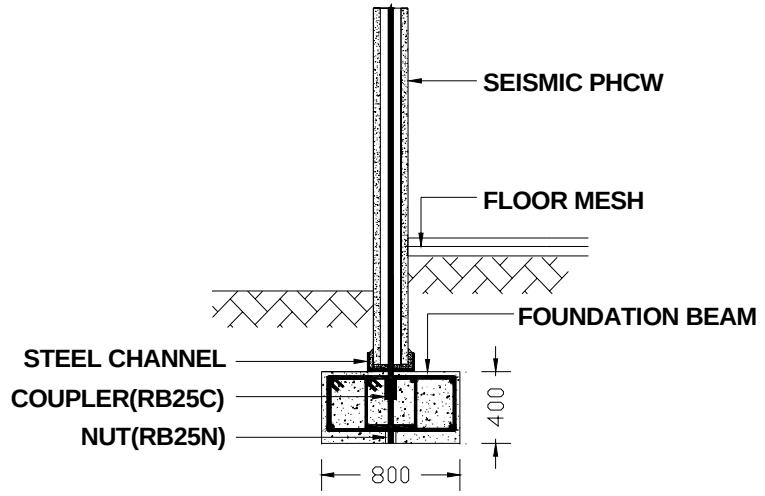


| | | |
|---|---|---|
| **DESIGN ENGINEER: NOR HAYATI ABDUL HAMID**<br>**DEPARTMENT OF CIVIL ENGINEERING**<br>**UNIVERSITY OF CANTERBURY**<br>**CHRISTCHURCH, NEW ZEALAND** | **STRUCTURE: DETAIL CONNECTION OF A AND B**<br>**VIEW:SIDE ELEVATION**<br>**DATE: 23.7.2003**<br>**SCALE: NOT TO SCALE** | DRAWING NO:<br>PLATE 3 |

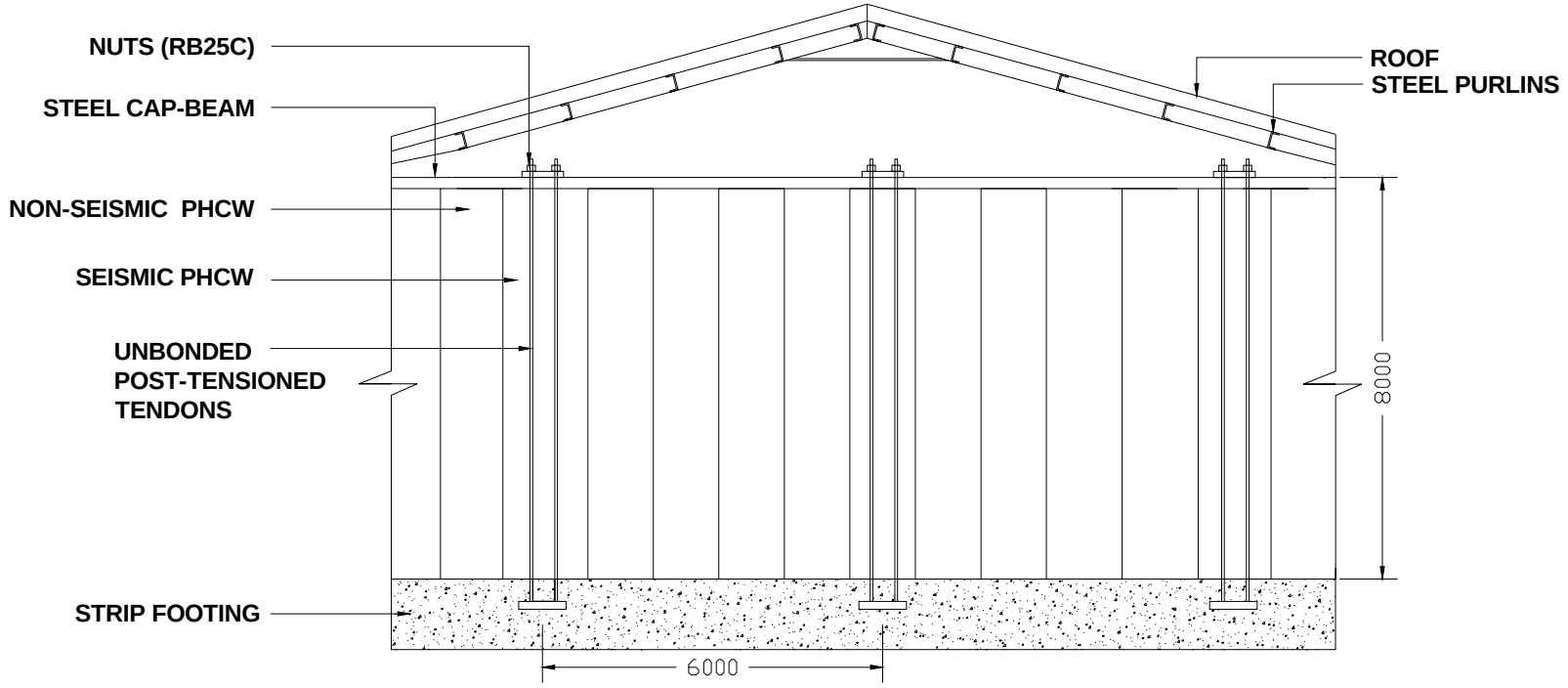


| | | |
|---|---|---|
| **DESIGN ENGINEER: NOR HAYATI ABDUL HAMID**<br>**DEPARTMENT OF CIVIL ENGINEERING**<br>**UNIVERSITY OF CANTERBURY**<br>**CHRISTCHURCH, NEW ZEALAND** | **STRUCTURE: SCHEMATIC ARRANGEMENT OF PHC**<br>**LOCATION : TRANSVERSE CROSS-SECTION**<br>**DATE: 23.7.2003**<br>**SCALE: NOT TO SCALE** | DRAWING NO:<br>PLATE 4 |

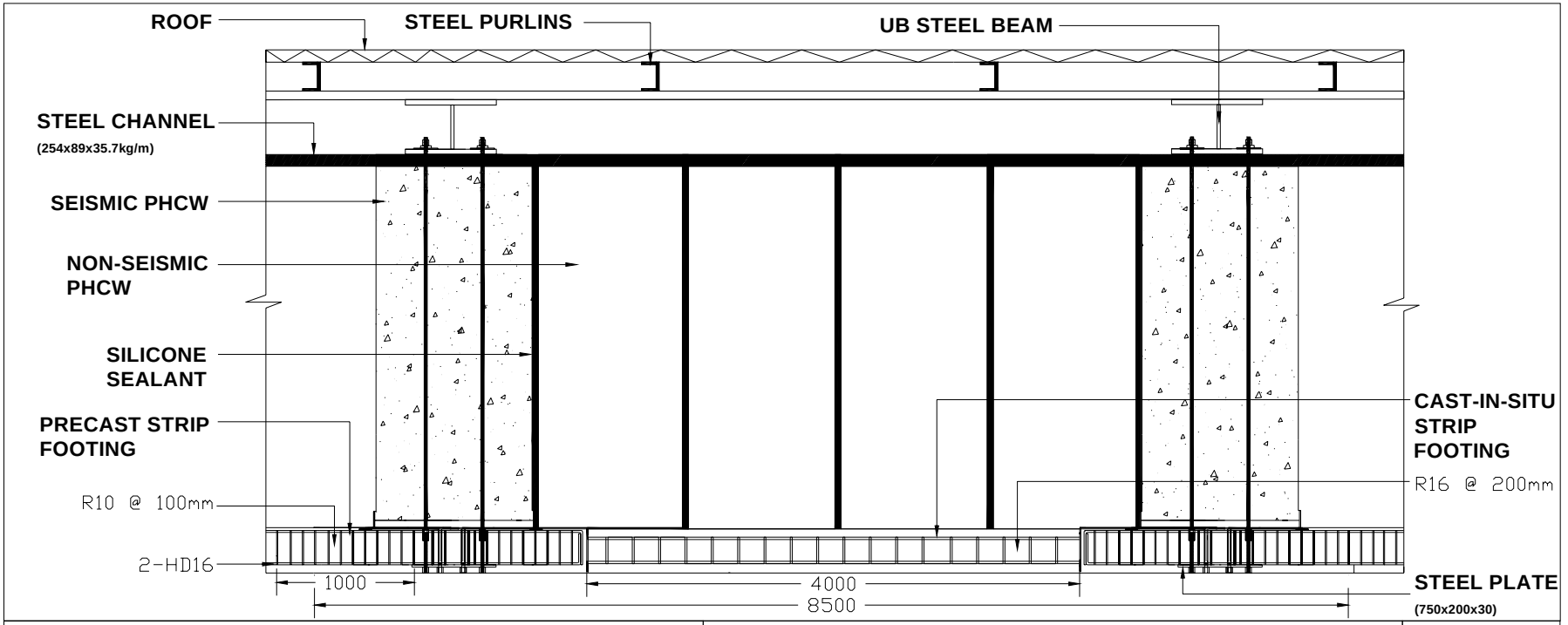


| | | |
|---|---|---|
| **DESIGN ENGINEER: NOR HAYATI ABDUL HAMID**<br>**DEPARTMENT OF CIVIL ENGINEERING**<br>**UNIVERSITY OF CANTERBURY**<br>**CHRISTCHURCH, NEW ZEALAND** | **STRUCTURE: SCHEMATIC ARRANGEMENT OF PHCW**<br>**LOCATION : LONGITUDINAL CROSS-SECTION**<br>**DATE: 23.7.2003**<br>**SCALE: NOT TO SCALE** | DRAWING NO:<br>PLATE 5 |

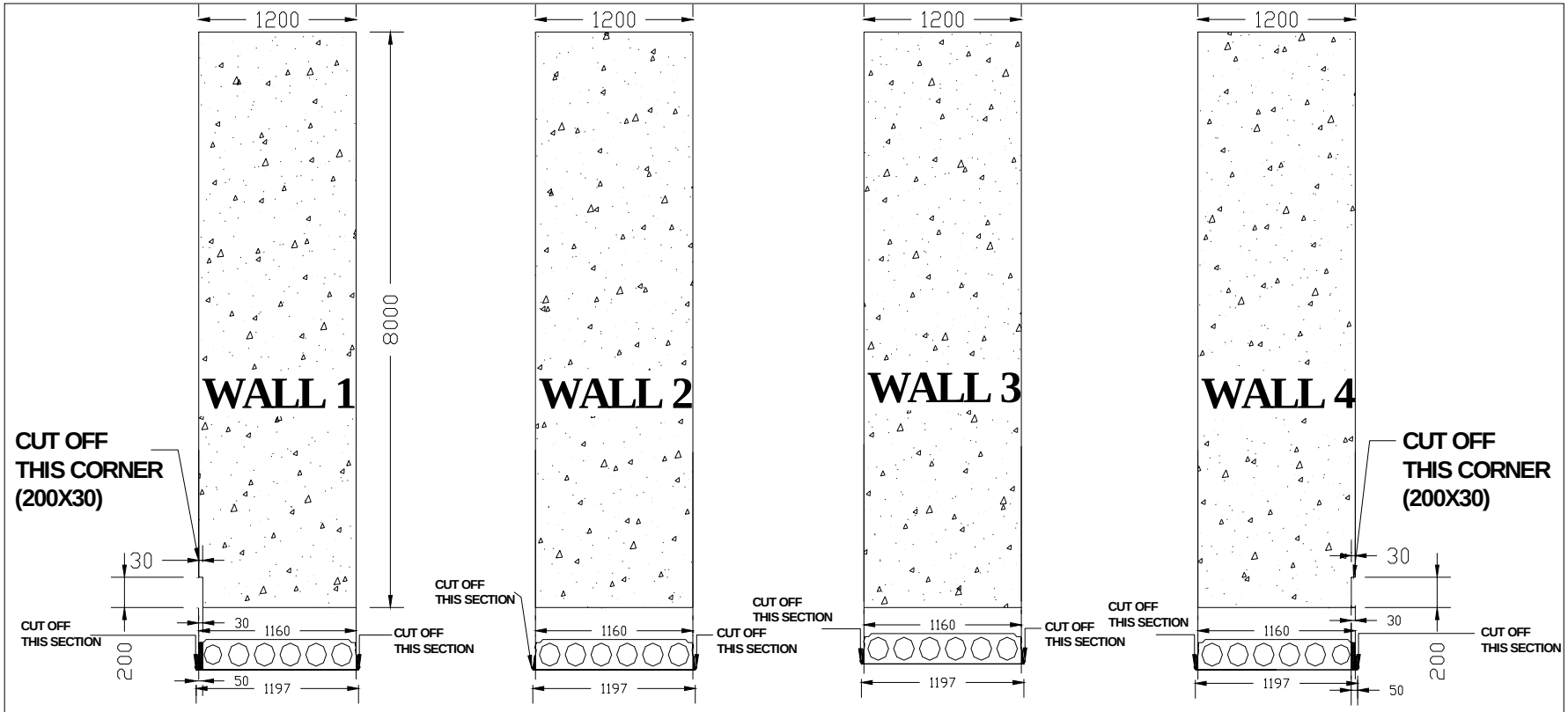


**DESIGN ENGINEER: NOR HAYATI ABDUL HAMID**
**DEPARTMENT OF CIVIL ENGINEERING**
**UNIVERSITY OF CANTERBURY**
**CHRISTCHURCH, NEW ZEALAND**

**STRUCTURE: NON SEISMIC WALL (IN-FILL)**
**VIEW : FRONT ELEVATION**
**DATE: 23.7.2003**
**SCALE: NOT TO SCALE**

DRAWING NO:
PLATE 6

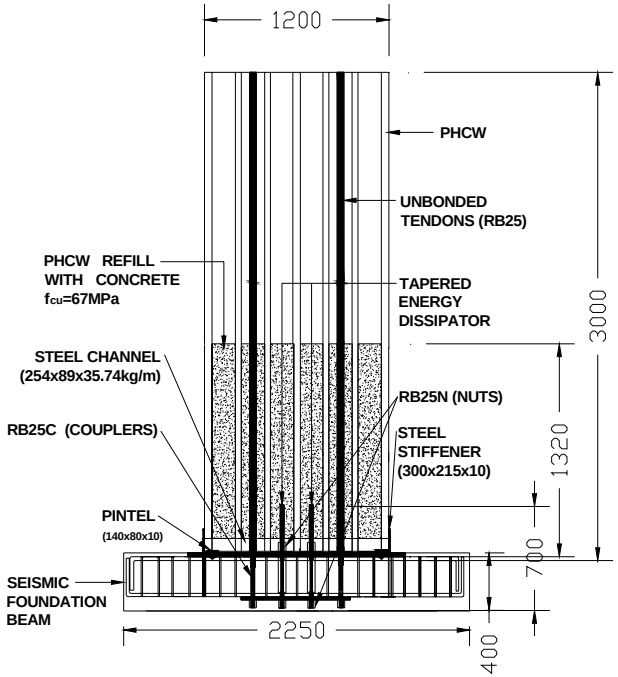


## CROSS-SECTION A-A

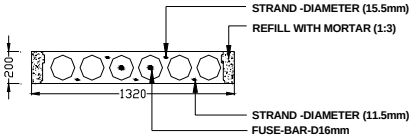


## CROSS-SECTION B-B

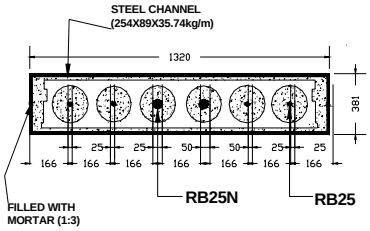


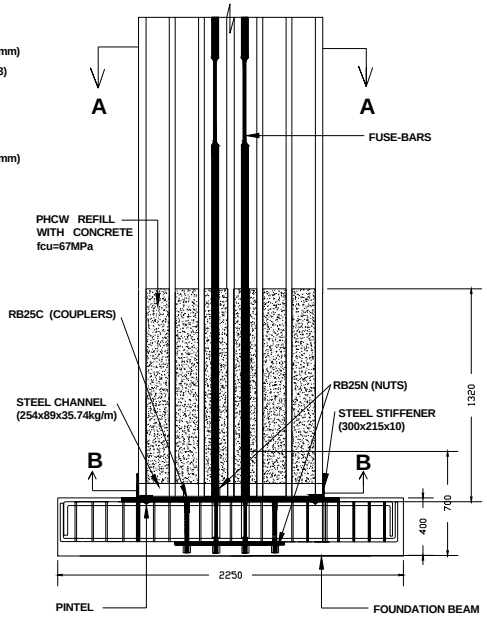


**DESIGN ENGINEER: NOR HAYATI ABDUL HAMID**
**DEPARTMENT OF CIVIL ENGINEERING**
**UNIVERSITY OF CANTERBURY**
**CHRISTCHURCH, NEW ZEALAND**

**STRUCTURE: DETAIL OF SEISMIC WALLS**
**VIEW: FRONT VIEW & CROSS-SECTIONAL AREA**
**DATE: 23.7.2003**
**SCALE: NOT TO SCALE**

DRAWING NO:
PLATE 7

## STIFFENER

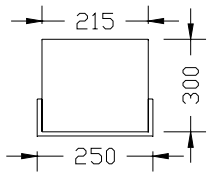


## SIDE ELEVATION OF ROCKING TOE (STEEL CHANNEL)

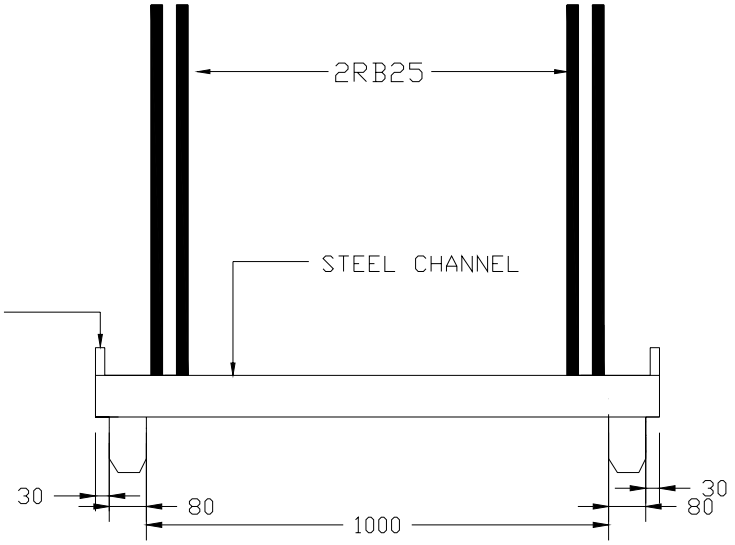


## CROSS-SECTION ROCKING TOE OF PHCW

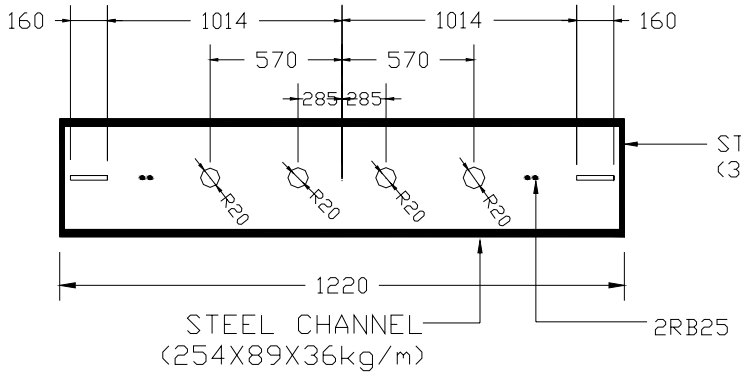


| | | |
|---|---|---|
| **DESIGN ENGINEER: NOR HAYATI ABDUL HAMID**<br>**DEPARTMENT OF CIVIL ENGINEERING**<br>**UNIVERSITY OF CANTERBURY**<br>**CHRISTCHURCH, NEW ZEALAND** | **STRUCTURE: ROCKING TOE (STEEL CHANNEL)**<br>**VIEW: CROSS-SECTION AND FRONT ELEVATION**<br>**DATE: 23.7.2003**<br>**SCALE: NOT TO SCALE** | DRAWING NO:<br>PLATE 8 |

# BASE PLATE

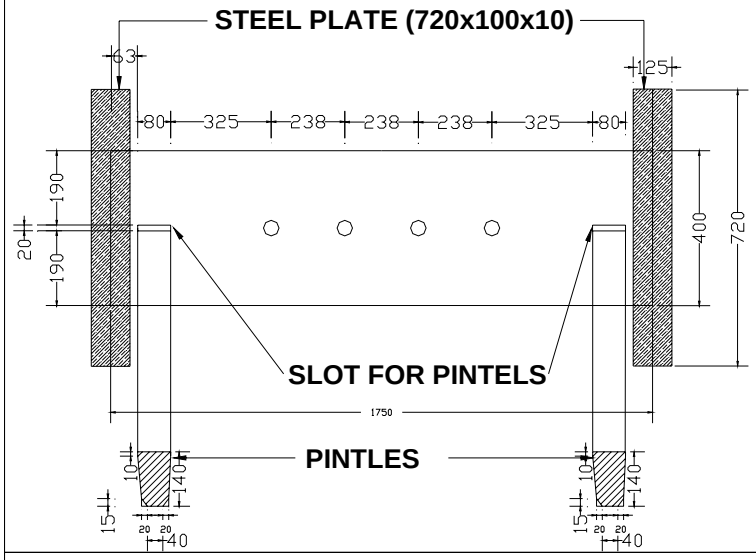


**END OF FOUNDATION BEAM**

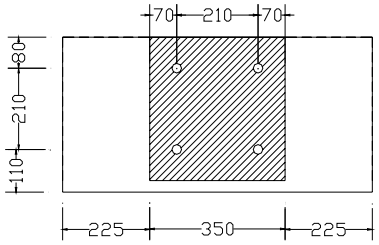


**SP1(SIDE)**

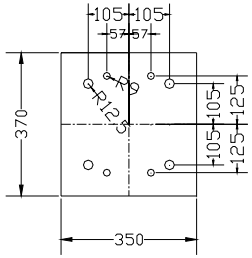


**SP2(FRONT)**

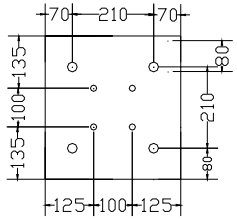


**DESIGN ENGINEER: NOR HAYATI ABDUL HAMID**
**DEPARTMENT OF CIVIL ENGINEERING**
**UNIVERSITY OF CANTERBURY**
**CHRISTCHURCH, NEW ZEALAND**

**STRUCTURE: BASE PLATE AND PINTLES**
**VIEW: CROSS-SECTIONAL AREA**
**DATE: 23.7.2003**
**SCALE: NOT TO SCALE**

DRAWING NO:
PLATE 9

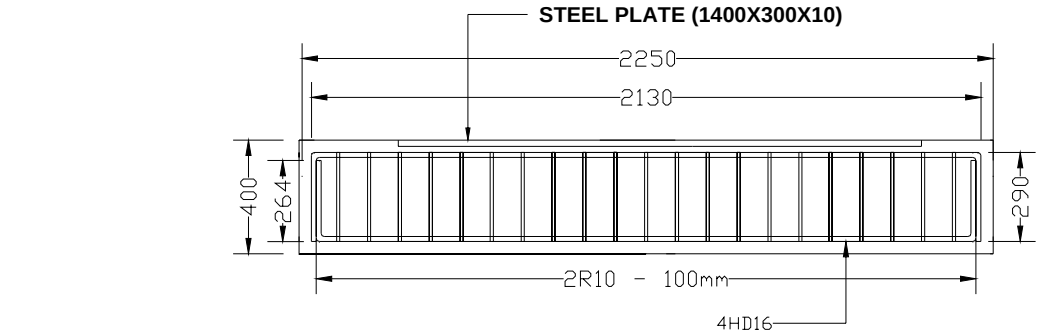


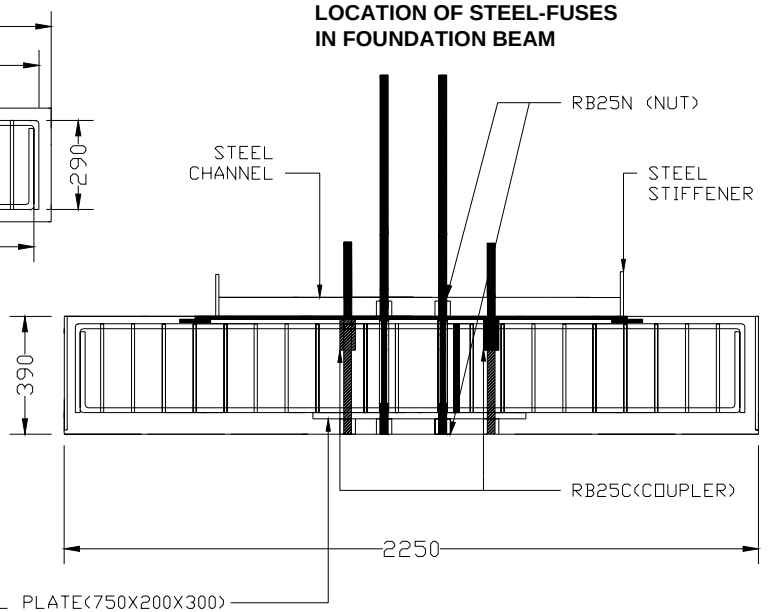


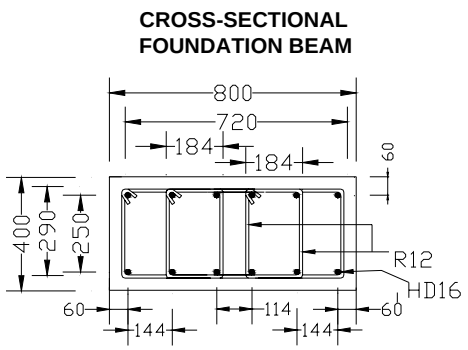


| | | |
|---|---|---|
| **DESIGN ENGINEER: NOR HAYATI ABDUL HAMID**<br>**DEPARTMENT OF CIVIL ENGINEERING**<br>**UNIVERSITY OF CANTERBURY**<br>**CHRISTCHURCH, NEW ZEALAND** | **STRUCTURE: SEISMIC PRECAST FOUNDATION**<br>**ELEMENT: ARRANGEMENT REINFORCEMENT BARS**<br>**DATE: 23.7.2003**<br>**SCALE: NOT TO SCALE** | DRAWING NO:<br>PLATE 10 |

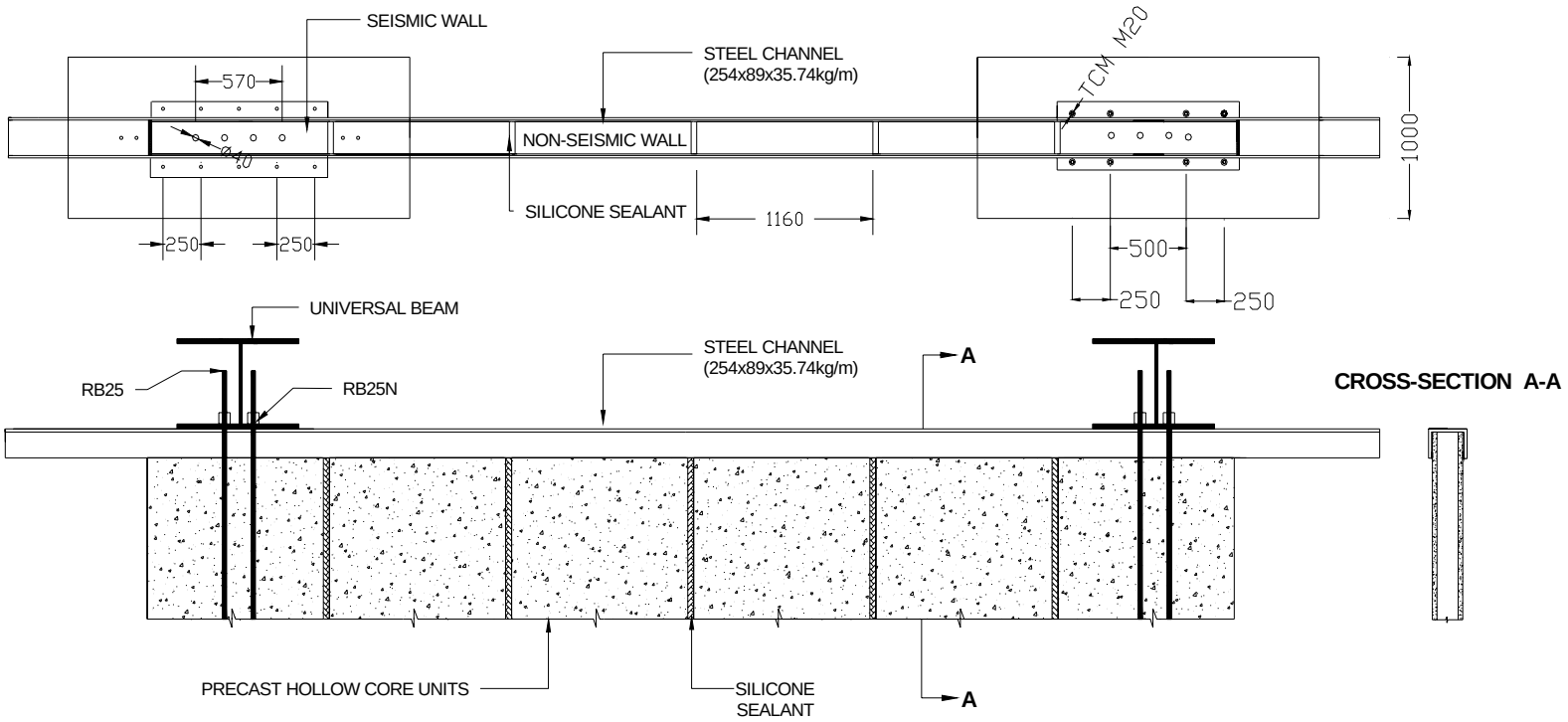


| | | |
|---|---|---|
| **DESIGN ENGINEER: NOR HAYATI ABDUL HAMID**<br>**DEPARTMENT OF CIVIL ENGINEERING**<br>**UNIVERSITY OF CANTERBURY**<br>**CHRISTCHURCH, NEW ZEALAND** | **STRUCTURE: WALL-ROOF INTERFACE**<br>**VIEW: LONGITUDINAL CROSS-SECTION**<br>**DATE: 23.7.2003**<br>**SCALE: 1 :15** | DRAWING NO:<br>PLATE 11 |

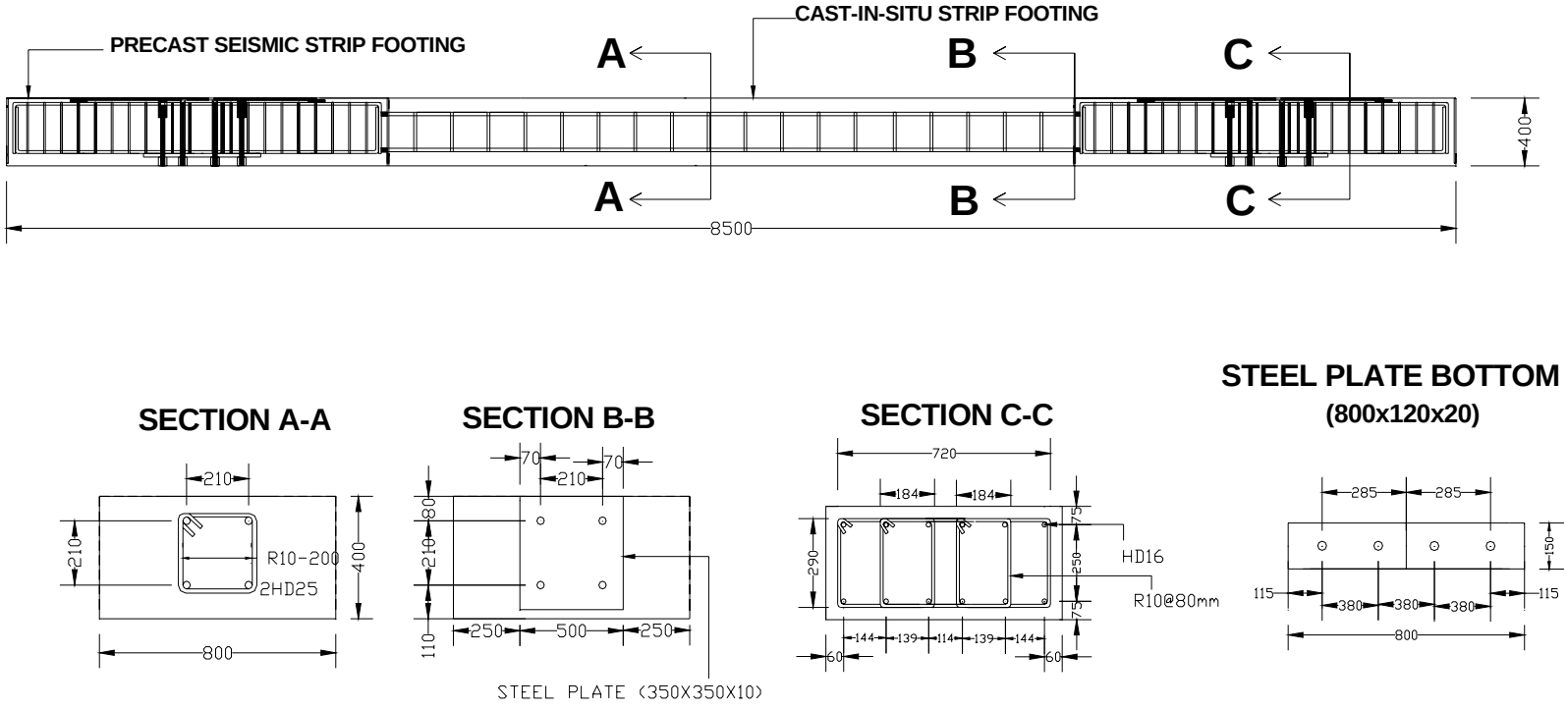


| | | |
|---|---|---|
| **DESIGN ENGINEER: NOR HAYATI ABDUL HAMID**<br>**DEPARTMENT OF CIVIL ENGINEERING**<br>**UNIVERSITY OF CANTERBURY**<br>**CHRISTCHURCH, NEW ZEALAND** | **STRUCTURE: STRIP FOOTING AND ROCKING BASE**<br>**VIEW: CROSS-SECTIONAL AREA**<br>**DATE: 23.7.2003**<br>**SCALE: 1 :15** | DRAWING NO:<br>PLATE 12 |

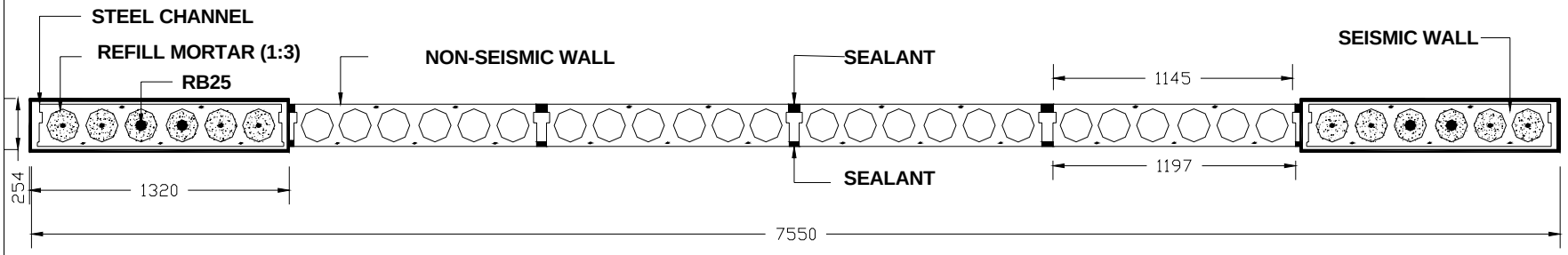


# DETAIL CONNECTION BETWEEN TWO WALLS

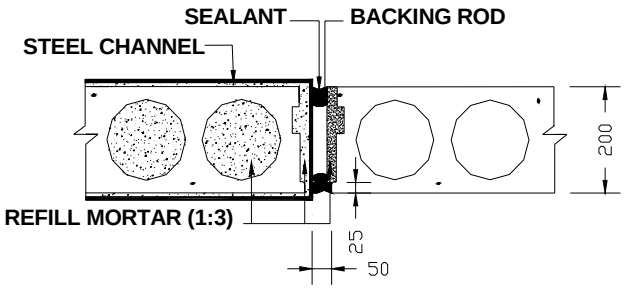


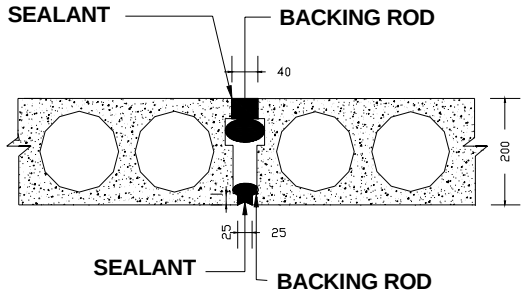


| | | |
|---|---|---|
| **DESIGN ENGINEER: NOR HAYATI ABDUL HAMID**<br>**DEPARTMENT OF CIVIL ENGINEERING**<br>**UNIVERSITY OF CANTERBURY**<br>**CHRISTCHURCH, NEW ZEALAND** | **STRUCTURE: MULTI-PANEL WALL WITH SEALANT**<br>**VIEW: CROSS-SECTIONAL AREA**<br>**DATE: 23.7.2003**<br>**SCALE: NOT TO SCALE** | DRAWING NO:<br>PLATE 13 |

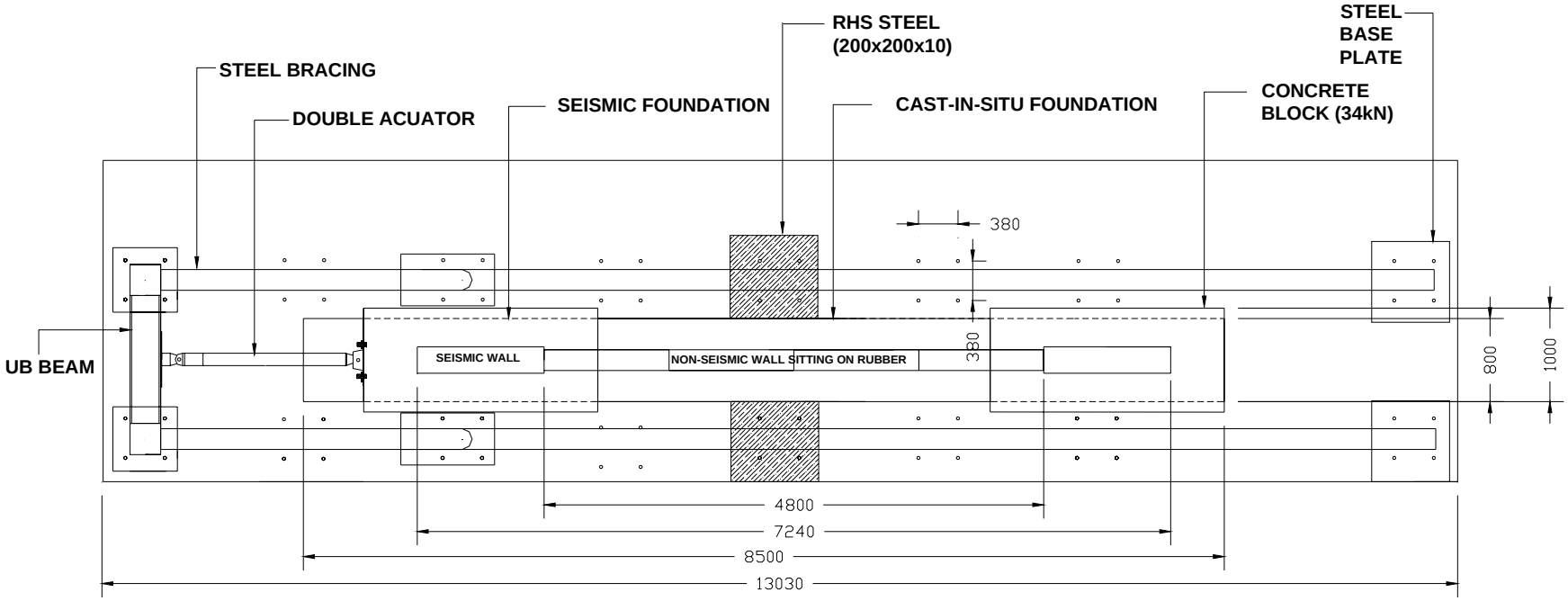


| | | |
|---|---|---|
| **DESIGN ENGINEER: NOR HAYATI ABDUL HAMID**<br>**DEPARTMENT OF CIVIL ENGINEERING**<br>**UNIVERSITY OF CANTERBURY**<br>**CHRISTCHURCH, NEW ZEALAND** | **STRUCTURE: MULTI-PANEL WALL ON STRONG FLOOR**<br>**LOCATION: PLAN VIEW**<br>**DATE: 23.7.2003**<br>**SCALE: NOT TO SCALE** | DRAWING NO:<br>PLATE 14 |

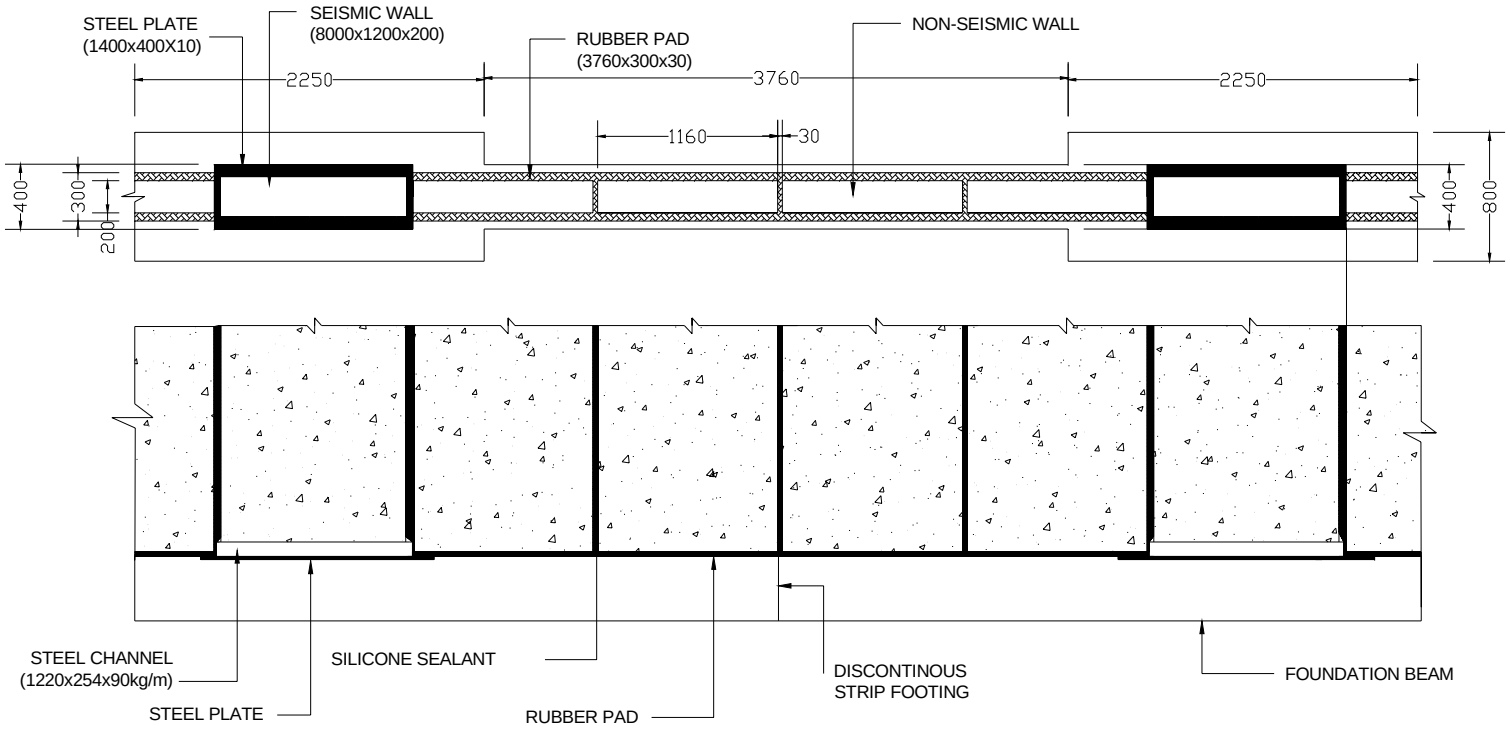


| | | |
|---|---|---|
| **DESIGN ENGINEER: NOR HAYATI ABDUL HAMID**<br>**DEPARTMENT OF CIVIL ENGINEERING**<br>**UNIVERSITY OF CANTERBURY**<br>**CHRISTCHURCH, NEW ZEALAND** | **STRUCTURE: WALL-FOUNDATION INTERFACE**<br>**VIEW: SIDE ELEVATION**<br>**DATE: 23.7.2003**<br>**SCALE: 1 :15** | DRAWING NO:<br>PLATE 15 |

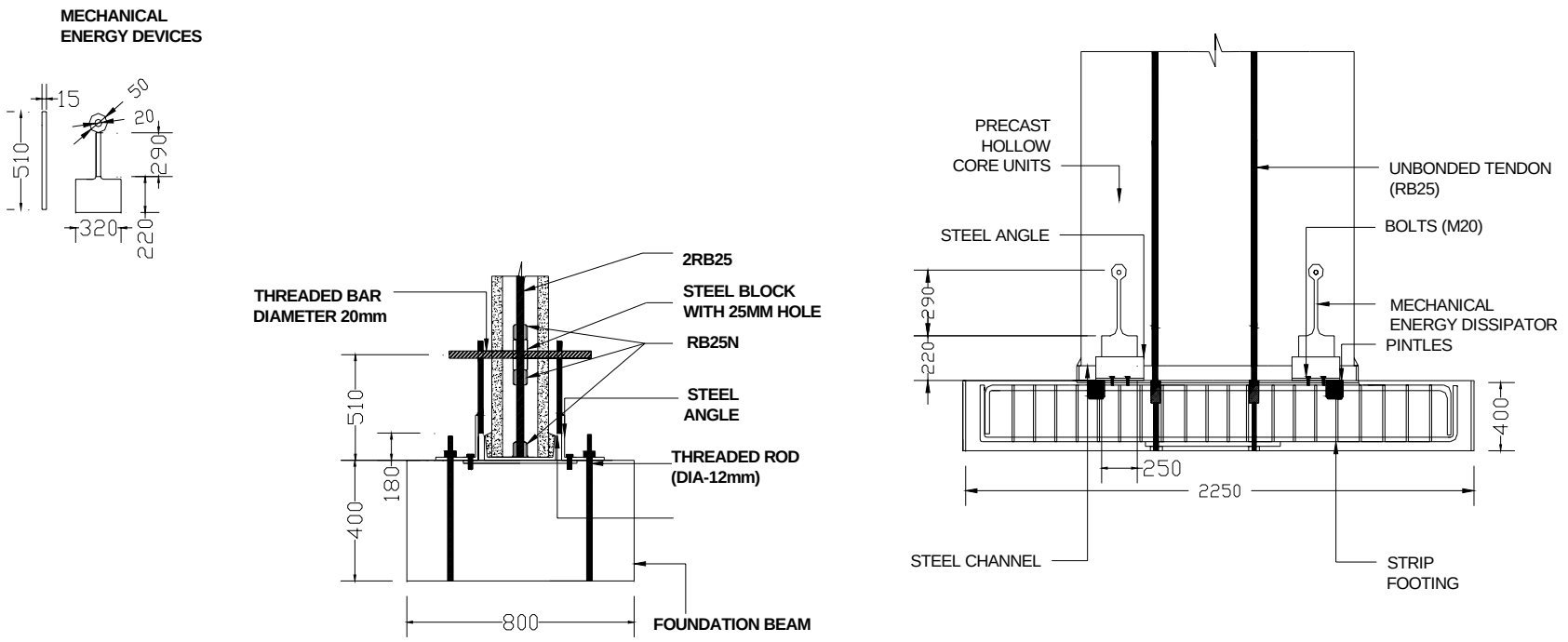


| | | |
|---|---|---|
| **DESIGN ENGINEER: NOR HAYATI ABDUL HAMID**<br>**DEPARTMENT OF CIVIL ENGINEERING**<br>**UNIVERSITY OF CANTERBURY**<br>**CHRISTCHURCH, NEW ZEALAND** | **STRUCTURE: MECHANICAL ENERGY DISSIPATOR**<br>**VIEW: CROSS-SECTIONAL AREA**<br>**DATE: 23.7.2003**<br>**SCALE: 1 :15** | DRAWING NO:<br>PLATE 16 |

# APPENDIX A5

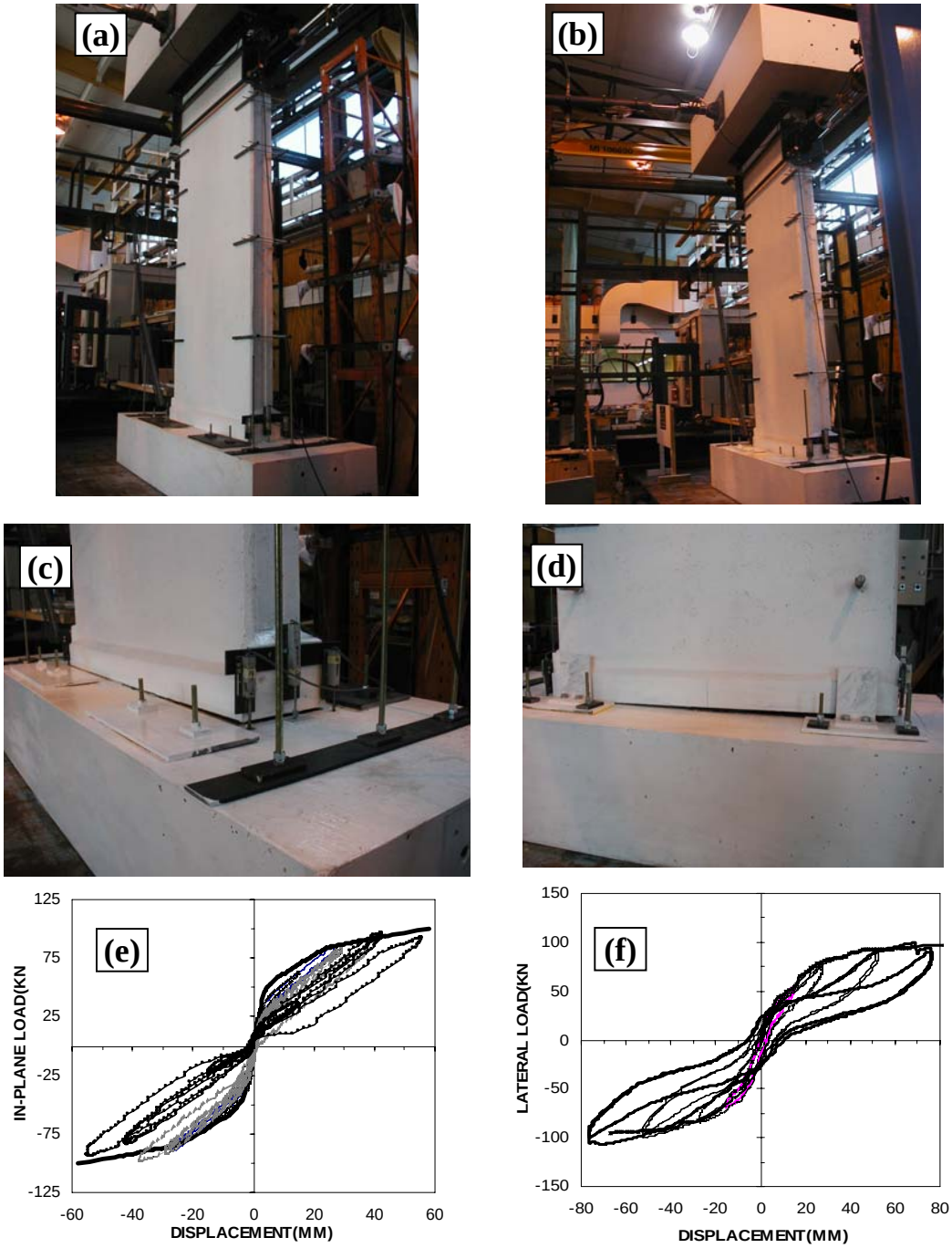


Figure A5.1: The seismic performance of precast hollow core walls designed according to damage avoidance design philosophy subjected to biaxial loading; (a) the biaxial behaviour of wall at 1.0% drift; (b) overall behaviour of wall at 2.0% drift; (c) no visible damage at 1.5% drift; and (d) the uplift of the eastern corner of wall did not cause any cracking, crushing and spalling of concrete; (e) the hysteresis loop at 2.0% drift; and (f) the hysteresis loop at 3.0% drift.

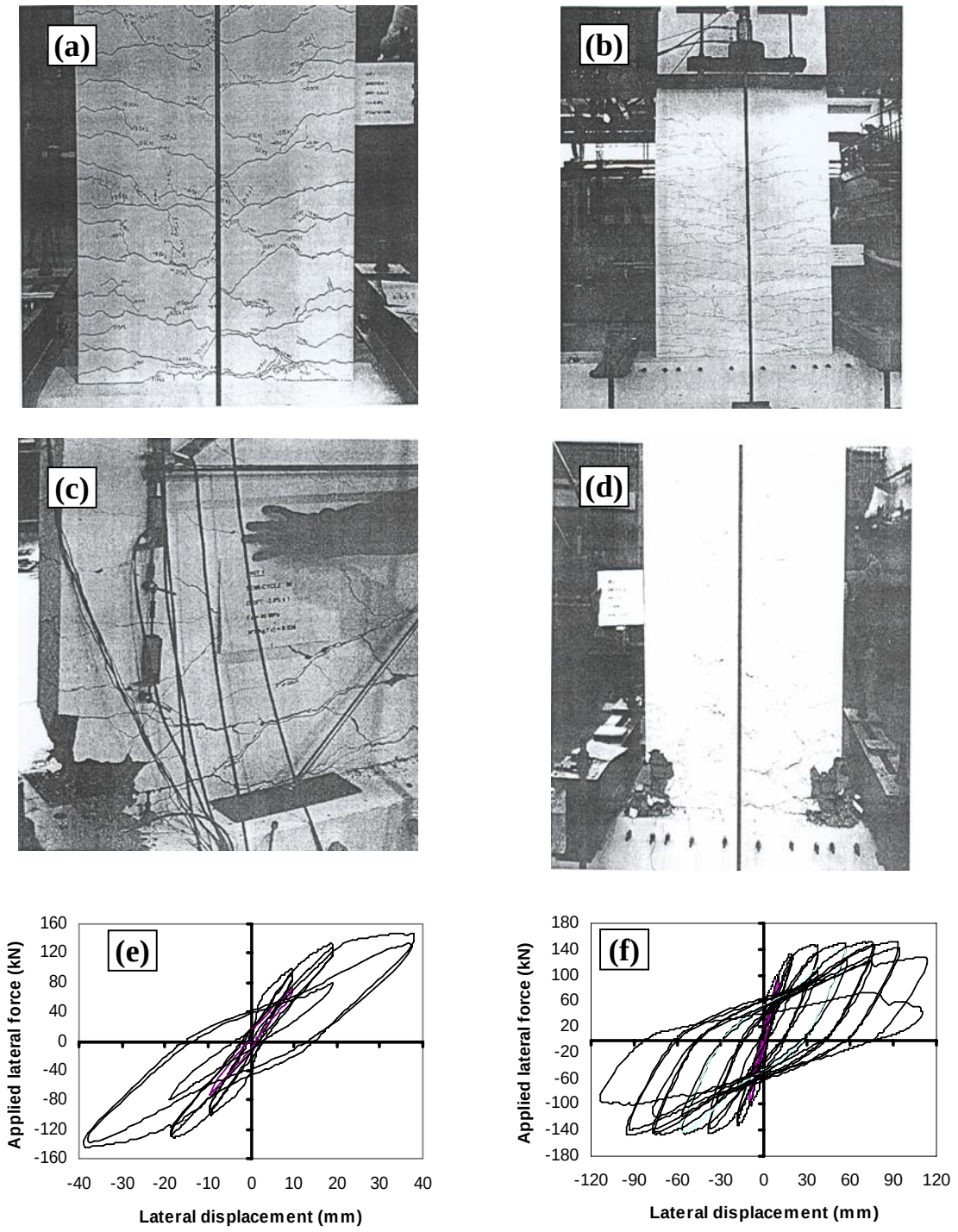


Figure A5.2:The seismic performance of conventional reinforced concrete walls according to the standard code of NZ3101 tested under quasi-static in-plane loading: (a) the cracks on the north face of the wall at 0.5% drift; (b) wider cracks at 1.0% drift; (c) spalling and crushing on both bottom corners of the wall at 2.0% drift; (d) fractured longitudinal bars at 3.0% drift; (e) the hysteresis loop at 1.0% drift; and (f) the hysteresis loop at 3.0% drift.(courtesy (Holden, (2001)).

Table A5.1: Definition of colour coding used to classify warehouse damage using precast hollow core wall.

| Tag Colour | Description of damage level | Drift level | Ductility Factor |
|---|---|---|---|
| Green | Pre-uplift of walls, no cosmetic damage, warehouse occupiable. | 0.5% | 1 |
| Yellow | The external fuses are yielding, no damage, warehouse occupiable. | 1.5% | 3 |
| Orange | Rocking response with minor cracks at the corners, no structural damage, P-delta effect for taller walls, and loss of prestressing of tendons/fuses. The building can be entered to remove belongings. | 2.0% | 4 |
| Red | Fractures of tendons or external fuses, no clamping forces,<br>Warehouse might collapse. Buildings cannot be entered. | 4.0% | 8 |

Table A5.2: Definition of colour coding and performance level using conventional reinforced concrete wall.

| Tag Colour | Performance Level | Description of damage level | Drift level | Ductility Factor |
|---|---|---|---|---|
| Green | Operational | Minor cracks, no damage, warehouse occupiable. | 0.5% | 1.0 |
| Yellow | Functional | Wider cracks, initial spalling at corner of walls with moderate level of damage. The warehouses can be entered to remove belongings. | 1.0% | 1.5 |
| Orange | Life Safety | Extensive spalling along bottom walls, longitudinal bars buckling with heavy damage on the walls. Warehouse can be entered for short periods for removing important items. | 2.0% | 3.0 |
| Red | Near Collapse | Fracturing of longitudinal bars, no stability of structures, near collapse. The building cannot be entered. | 3.0% | 4.5 |

```
SINGLE DEGREE OF FREEDOM FOR PRECAST HOLLOW CORE WALL SYSTEM
8 0 1 0 0 0 0 0 0                          ! Control Parameters
3 2 2 4 1 4 9.81 5.0 5.0 0.005 40 1.0          ! Frame and Time-history
0 4 1 1 3 10 0.7 0.1                           ! Output and Plotting Options
10 0 0.01                                  ! Iteration Control

NODES
1  0.0     0.0         1 1 1   0   0  0   0     ! bottom of wall
2  0.0     0.0002      0 1 0   0   0  0   0          ! middle of wall
3  0.0     3.0002      0 1 0  -1   0  0   0    ! top of column

ELEMENTS
1   1  2  3                                    ! top wall
2   2  1  2                                    ! bottom wall

PROPS
1 FRAME                                        ! wall properties
  1 0 0 0 0 0 0 0                              ! Paramaters for wall member
  2.96E10  1.14E10 0.13025 0 6.579E-04  0.126  0.0 0.0    ! Elastic properties

2 SPRING                                       ! Joint rotational spring
  1 50 0 0 8.27E7 8.27E7  8.2E2 0 0.05  0.05 0 0 0 0  ! control parameters –flag shape
  0 0 0 0  170  -170                             ! yield surface
  0.5 0.6  0.8                                 ! slope coefficient


WEIGHTS 0
1  0    0      0.0
2  0.0  0      0.0
3  0.0  34500  0.0

LOADS
1   0.0 0.0 0.0
3   0.0 0.0 0.0
```

```
SINGLE DEGREE OF FREEDOM FOR FIXED-END MONOLITHIC PRECAST WALL
8 0 1 0 0 0 0 0 0                                   ! Control Parameters
3 2 2 4 1 4 9.81 5.0 5.0 0.005 19 1.0               ! Frame and Time-history
0 4 1 1 3 10 0.7 0.1                                ! Output and Plotting Options
10 0 0.01                                           ! Iteration Control

NODES
1  0.0     0.0        1 1 1   0   0  0   0         ! bottom of wall
2  0.0     0.0002      0 1 0   0   0  0   0         ! middle of wall
3  0.0     3.0002      0 1 0  -1   0  0   0         ! top of column

ELEMENTS
1   1  2  3                                 ! top wall
2   2  1  2                                 ! bottom wall

PROPS
1 FRAME                                                                 ! wall properties
  1 0 0 0 0 0 0 0                                                       ! Parameters Takeda Hysteresis
  2.96E10  1.14E10 0.13025 0 6.579E-04  0.126  0.0 0.0   ! Elastic properties of wall

2 SPRING                                                                  ! Joint rotational spring
  1 4 0 0 8.27E7 8.27E7  8.2E2 0 0.05  0.05 0 0 0 0                       ! control parameters
  0 0 0 0  200  -200                                                    ! yield surface
  1.56 1.66 2.88

WEIGHTS 0
1  0    0      0.0
2  0.0  0      0.0
3  0.0  34500  0.0

LOADS
1   0.0 0.0 0.0
3   0.0 0.0 0.0
```